Molecular Mechanosensing Mechanisms of the Carnivorous Plant *Dionaea muscipula*

Molekulare Mechanismen der Mechanoperzeption in der fleischfressenden Pflanze *Dionaea muscipula*

Anda-Larisa Iosip
from Cluj-Napoca

Thesis Submitted for the Degree of Doctor of Philosophy At
Julius-Maximilian University of Würzburg
Natural Sciences

Würzburg, 2022
Germany

Molecular Mechanosensing Mechanisms of the Carnivorous Plant *Dionaea muscipula*

Molekulare Mechanismen der Mechanoperzeption in der fleischfressenden Pflanze *Dionaea muscipula*

Anda-Larisa Iosip
from Cluj-Napoca

Thesis Submitted for the Degree of Doctor of Philosophy At
Julius-Maximilian University of Würzburg
Natural Sciences

Würzburg, 2022
Germany

Submitted on:

Members of the Thesis Committee

Chairperson:

Primary Supervisor: **Prof. Dr. Rainer Hedrich**
Department of Botany I
Julius-von-Sachs-Institute of Biosciences
University of Würzburg

Second Supervisor: **Prof. Dr. Jörg Schultz**
Center for Computational and Theoretical Biology
University of Würzburg

Date of Public Defence:

Date of Receipt of Certificates:

Affidavit

I hereby declare that my thesis entitled: „Molecular Mechanosensing Mechanisms of the Carnivorous Plant *Dionaea muscipula*" is the result of my own work. I did not receive any help or support from commercial consultants. All sources and / or materials applied are listed and specified in the thesis.

Furthermore I verify that the thesis has not been submitted as part of another examination process neither in identical nor in similar form.

Besides I declare that if I do not hold the copyright for figures and paragraphs, I obtained it from the rights holder and that paragraphs and figures have been marked according to law or for figures taken from the internet the hyperlink has been added accordingly.

Anda-Larisa Iosip
Würzburg, February 28, 2022

Eidesstattliche Erklärung

Hiermit erkläre ich an Eides statt, die Dissertation: „Molekulare Mechanismen der Mechanoperzeption in der fleischfressenden Pflanze *Dionaea muscipula*", eigenständig, d. h. insbesondere selbständig und ohne Hilfe eines kommerziellen Promotionsberaters, angefertigt und keine anderen, als die von mir angegebenen Quellen und Hilfsmittel verwendet zu haben.

Ich erkläre außerdem, dass die Dissertation weder in gleicher noch in ähnlicher Form bereits in einem anderen Prüfungsverfahren vorgelegen hat.

Weiterhin erkläre ich, dass bei allen Abbildungen und Texten bei denen die Verwer-tungsrechte (Copyright) nicht bei mir liegen, diese von den Rechtsinhabern eingeholt wurden und die Textstellen bzw. Abbildungen entsprechend den rechtlichen Vorgaben gekennzeichnet sind sowie bei Abbbildungen, die dem Internet entnommen wurden, der entsprechende Hypertextlink angegeben wurde.

Anda-Larisa Iosip
Würzburg, 28 Februar, 2022

To my mother,
and all the nature lovers who fight biodiversity loss,
climate change and animal cruelty.

Acknowledgements

Knowledge is in the end based on acknowledgement.

Ludwig Wittgenstein

During my PhD journey I have been accompanied by many people whose support made my research and finally this thesis possible.

Foremost, I would like to thank **Prof. Dr. Rainer Hedrich** for accepting me to work in his group on one of his favorite topics of green hunters and for his support and orchestration of my project. I would like to extend my sincere thanks to **Dr. Ines Kreuzer** for being a wholehearted "Doktormutter", for being caring and highly supportive and protective, for always being there for me, for accepting my research ideas, for keeping me on track when I wanted to accomplish more than I could handle and for all the help and guidance she provided throughout the years. I am also deeply grateful for the unceasing mentorship I have received from my co-supervisor, **Prof. Dr. Jörg Schultz**. I immensely appreciate his everlasting positivity which has always transformed tough scientific discussions into a lot of fun, and I cannot state enough how much his positive feedback (and all the virtual cookies) have meant to me. I am extremely grateful to all of my supervisors for enabling me to present my work to conferences and for initiating and supporting my lab visit to our collaborator group in Japan.

Without financial support, my work would have not been possible. So I would like to thank **KAAD** (Katholischer Akademischer Ausländer-Dienst) for helping me commence my journey in Germany by offering me a scholarship during my master degree for an internship in this group - which was the building block for my PhD - and for further sponsoring the first one and a half years of my PhD I also appreciate their effort in organising meetings with all the scholars, which gave me the opportunity to get to know people all around the world. Next, I would also like to thank the **University of Würzburg** for offering me a three-year "Brückendoktorand" position between two departments: CCTB and Botany I (thanks to my supervisors who wrote the proposal). For the last stage of my PhD, I am so grateful and feel so lucky for receiving a **DAAD** (Deutscher Akademischer Austauschdienst) STIBET scholarship for “Abschlußbeihilfen” (also thanks to Prof. Dr. Jörg Schultz for writing the application and to Prof. Dr. Dirk Becker for the recommendation letter). I am grateful for having had the opportunity to visit our collaborator lab in Japan thanks to **BayIntAn Grant** (Bavarian Funding Programme for the Initiation of International Projects) - for this I would like to thank again all my supervisors for making this knowledge exchange possible.

I would like to recognize the invaluable assistance of all the "carni-team" members. Maybe not officially part of the "cani-team", but also caught up in the mysteries of carnivorous plants, I would like to thank **Prof. Dr. Dirk Becker** who has always taken a bit of his super-busy schedule to talk about my results and data interpretation and whose great expertise in molecular biology has been of great value for my project. I also wish to thank **Dr. Kenji Fukushima** for sharing his knowledge, bioinformatic tools and passion for carnivorous plants. Next, I would like to thank **Dr. Jennifer Scherzer** and **Dr. Sönke Scherzer** for introducing me to plant electrophysiology techniques and for the great discussions and collaboration. I would like to express my super-special regards to **Brigitte Neumann** and **Sarah Zehnter** for technical assistance in the lab. Brigitte’s cheerfulness, openness and special spirit brought a lot of fun to the team. It was a pleasure to have **Sonja Bauer** as a great colleague and supportive friend,

joining me throughout almost all my research time and I wholeheartedly appreciate her help with my experiments as well as lab work throughout the years.

I would also like to thank my close colleagues and friends that have given me an amazing time and lovely memories, especially to **Ramona Börner, Dr. Hanna Faist** and **Dr. Khushbu Kumari**, and all the colleagues from Botany I.

I would like to thank **Dr. Markus Krischke** from Pharmaceutical Biology for running the UPLC measurements.

I wish to show my gratitude to the former Computational Evolutionary Biology team who introduced me to the world of bioinformatics, especially to **Dr. Niklas Terhoeven** and **Franziska Saul**. I would also like to thank **Dr. Markus Ankenbrand** for maintaining our transcriptome browser and for always giving a helping hand with any technical issue. I am forever indebted to **Matthias Freund** for assisting me throughout my early stages of bioinformatic endeavours, for his patience, for sharing all the amazing and intriguing scientific discussions, debates, brainstorms, epiphanies and for always helping me in any possible way (from technical and moral support to critically but sweetly reading my thesis or manuscripts). During my time at the CCTB, besides the "compevolbiol" team, it was also lovely to share the office with **Andreas Kuhn** and **Martin Hochheimer** and to have insightful discussions during our breaks. Many thanks to all my colleagues and PIs for creating the special CCTB-specific atmosphere (a.k.a "unicorn world").

I would also like to thank our collaborator group from Japan conducted by **Prof. Dr. Mitsuyasu Hasebe** for being open to share knowledge. I show my regards to **Dr. Hiraku Suda** for taking the time to share his protocol on *Dionaea* transformation and to **Dr. Gergő Pálfalvi** for showing me the best tips and tricks in ONT sequencing library prep and for making sure that I have an amazing time in Japan.

I also want to thank my former master thesis supervisor **Dr. Dorina Podar** from my home university (UBB) for always putting me forward.

Contributing to my well-being by helping me maintain a healthy mind and body was my amazing capoeira group (big shout to the girls - **Prina, Franzi, Shrimati, Rosa, Sonja**). I must thank our trainer **Naô** for being a magnet of beautiful spirits and for organising our trip to Brazil. I will never forget the surprise I felt finding a *Mimosa pudica* in its natural habitat and all the awe-inspiring landscapes with bewildering plants from bromeliads to sundews. Many thanks go to my former and actual capoeirista flatmates **Stas, Thati, Dalina, Caro** and **Annika** who have been like a family to me during my time in Würzburg. I very much appreciate that besides playing a huge role in the capo family, **Dr. Annika Kreikenbohm** was always thrilled to share her big data visualisation passion with me.

Last but not least, I cannot begin to express my thanks to my **family** (*Mulțumesc mama, tata, buni, bengoasele!*) and all of my friends, especially to **Lăcră**, for their infinite emotional support and love. Immeasurable gratitude goes to my **mother**, for whom it has been very hard to have me away from home for so long. I couldn't thank her enough for accepting, allowing, supporting, encouraging and sustaining my ambitions, passions and dreams.

At last, I would like to express my remorse for sacrificing the life of ants and crickets in the name of science.

Abstract

Plants are able to sense mechanical forces in order to defend themselves against predators, for instance by synthesizing repellent compounds. Very few plants evolved extremely sensitive tactile abilities that allow them to perceive, interpret and respond by rapid movement in the milliseconds range. One such rarity is the charismatic Venus flytrap (*Dionaea muscipula*) - a carnivorous plant which relies on its spectacular active trapping strategy to catch its prey. The snapping traps are equipped with touch-specialised trigger hairs, that upon bending elicit an action potential (AP). This electrical signal originates within the trigger hairs' mechanosensory cells and further propagates throughout the whole trap, alerting the plant of potential prey. Two APs triggered within thirty seconds will set off the trap and more than five APs will initiate the green stomach formation for prey decomposition and nutrient uptake. Neither the molecular components of the plant's AP nor the Venus flytrap's fast closure mechanism have been fully elucidated yet. Therefore, the general objective of this study is to expound on the molecular basis of touch perception: from AP initiation to trap closure and finally to stomach formation.

The typical electrical signal in plants lasts for minutes and its shape is determined by the intensity of the mechanical force applied. In contrast, the Venus flytrap's one-second AP is of all-or-nothing type, similar in shape to the animal AP. In order to gain more insight into the molecular components that give rise to the Venus flytrap's emblematic AP, the transcriptomic landscape of its unique mechanotransducer - the trigger hair – was compared to the rest of the non-specialised tissues and organs. Additionally, the transcriptome of the electrically excitable fully-developed adult trap was compared to non-excitable juvenile traps that are unable to produce sharp APs. Together, the two strategies helped with the identification of electrogenic channels and pumps for each step of the AP as follows: *(1)* the most specific to the trigger hair was the mechanosensitive channel *DmMSL10*, making up the best candidate for the initial AP depolarization phase, *(2)* the K^+ outward rectifier *DmSKOR* could be responsible for repolarisation, *(3)* further, the proton pump *DmAHA4*, might kick in during repolarisation and go on with hyperpolarisation and *(4)* the hyperpolarization- and acid-activated K^+ inward rectifier *KDM1* might contribute to the re-establishment of electrochemical gradient and the resting potential. Responsible for the AP-associated Ca^{2+} wave and electrical signal propagation, the glutamate-like receptor *DmGLR3.6* was also enriched in the trigger hairs. Together, these findings suggest that the reuse of genes involved in electrical signalling in ordinary plants can give rise to the Venus flytrap's trademark AP.

The Venus flytrap has been cultivated ever since its discovery, generating more than one hundred cultivars over the years. Among them, indistinguishable from a normal Venus flytrap at first sight, the 'ERROR' cultivar exhibits a peculiar behaviour: it is unable to snap its traps upon two APs. Nevertheless, it is still able to elicit normal APs. To get a better understanding of the key molecular mechanisms and pathways that are essential for a successful trap closure, the 'ERROR' mutant was compared to the functional wild type.

Timelapse photography led to the observation that the 'ERROR' mutants were able to leisurely half close their traps when repeated mechanostimulation was applied (10 minutes after 20 APs, 0.03 Hz). As a result of touch or wounding in non-carnivorous plants, jasmonic acid (JA) is synthesized, alerting the plants of potential predators. Curiously, the JA levels were

reduced upon mechanostimulation and completely impaired upon wounding in the 'ERROR' mutant. In search of genes accountable for the 'ERROR' mutant's defects, the transcriptomes of the two phenotypes were compared before and after mechanostimulation (1h after 10 APs, 0.01 Hz). The overall dampened response of the mutant compared to the wild type, was reflected at transcriptomic level as well. Only about 50% of wild type's upregulated genes after touch stimulation were differentially expressed in 'ERROR' and they manifested only half of the wild type's expression amplitude. Among unresponsive functional categories of genes in 'ERROR' phenotype, there were: cell wall integrity surveilling system, auxin biosynthesis and stress-related transcription factors from the ethylene-responsive AP2/ERF and C2H2-ZF families. Deregulated Ca^{2+}-decoding as well as redox-related elements together with JA-pathway components might also contribute to the malfunctioning of the 'ERROR' mutant. As the mutant does not undergo full stomach formation after mechanical treatment, these missing processes represent key milestones that might mediate growth-defence trade-offs under JA signalling. This confirms the idea that carnivory has evolved by recycling the already available molecular machineries of the ubiquitous plant immune system.

To better understand the mutant's defect in the trap snapping mechanism, the ground states (unstimulated traps) of the two phenotypes were compared. In this case, many cell wall-related genes (*e.g.* expansins) were downregulated in the 'ERROR' mutant. For the first time, these data point to the importance of a special cell wall architecture of the trap, that might confer the mechanical properties needed for a functional buckling system - which amplifies the speed of the trap closure.

This study provides candidate channels for each of the AP phases that give rise to and shape the sharp Venus flytrap-specific AP. It further underlines the possible contribution of the cell wall architecture to the metastable ready-to-snap configuration of the trap before stimulation - which might be crucial for the buckling-dependent snapping. And finally, it highlights molecular milestones linked to defence responses that ensure trap morphing into a green stomach after mechanostimulation. Altogether, these processes prove to be interdependent and essential for a successful carnivorous lifestyle.

Zusammenfassung

Pflanzen sind in der Lage, mechanische Einflüsse zu spüren, um sich gegen Fressfeinde zu verteidigen, indem sie zum Beispiel abweisende Verbindungen synthetisieren. Nur sehr wenige Pflanzen haben extrem sensible taktile Fähigkeiten entwickelt, die es ihnen ermöglichen, schnelle Bewegungen im Millisekundenbereich wahrzunehmen, zu interpretieren und darauf zu reagieren. Eine solche Rarität ist die charismatische Venusfliegenfalle (*Dionaea muscipula*) - eine fleischfressende Pflanze, die sich auf ihre spektakuläre aktive Fallenstrategie verlässt, um ihre Beute zu fangen. Die Schnappfallen sind mit berührungssensitiven Auslösehaaren ausgestattet, die beim Biegen ein Aktionspotenzial (AP) auslösen. Dieses elektrische Signal entsteht in den mechanosensorischen Zellen der Auslösehaare und breitet sich in der gesamten Falle aus, wodurch die Pflanze auf potenzielle Beute aufmerksam gemacht wird. Zwei APs, die innerhalb von dreißig Sekunden ausgelöst werden, lösen die Falle aus, und mehr als fünf APs leiten die Bildung des grünen Magens ein, der die Beute zersetzt und die Nährstoffe aufnimmt. Weder die molekularen Komponenten des AP der Pflanze noch der Schnellverschlussmechanismus der Venusfliegenfalle sind bisher vollständig geklärt. Daher besteht das allgemeine Ziel dieser Studie darin, die molekularen Grundlagen der Berührungswahrnehmung zu erforschen: von der Initiierung des AP bis zum Schließen der Falle und schließlich zur Magenbildung.

Das typische elektrische Signal in Pflanzen dauert Minuten und seine Form wird durch die Intensität der angewandten mechanischen Kraft bestimmt. Im Gegensatz dazu ist das einsekündige AP der Venusfliegenfalle vom Alles-oder-Nichts-Typ und ähnelt in seiner Form dem tierischen AP. Um mehr Einblick in die molekularen Komponenten zu erhalten, die das emblematische AP der Venusfliegenfalle hervorbringen, wurde das Transkriptom ihres einzigartigen Mechanosensors - des Triggerhaars - mit den übrigen nicht spezialisierten Geweben und Organen verglichen. Darüber hinaus wurde das Transkriptom der elektrisch erregbaren, voll entwickelten adulten Falle mit nicht erregbaren juvenilen Fallen verglichen, die keine scharfen APs erzeugen können. Beide Strategien zusammen halfen bei der Identifizierung von elektrogenen Kanälen und Pumpen für jeden Schritt des AP: *(1)* Am spezifischsten für die Triggerhaare war der mechanosensitive Kanal *DmMSL10*, der der beste Kandidat für die anfängliche AP-Depolarisationsphase war, *(2)* der K^+-Auswärtsgleichrichter *DmSKOR* könnte für die Repolarisation verantwortlich sein, *(3)* ferner, die H^+-Pumpe *DmAHA4*, könnte während der Repolarisation einsetzen und mit der Hyperpolarisation fortfahren und *(4)* der durch Hyperpolarisation und Säure aktivierte K^+-Einwärtsgleichrichter *KDM1* könnte zur Wiederherstellung des elektrochemischen Gradienten und des Ruhepotentials beitragen. Der möglicherweise für die AP-assoziierte Ca^{2+}-Welle und die elektrische Signalausbreitung verantwortliche Glutamatrezeptor *DmGLR3.6* war ebenfalls in den Triggerhaaren angereichert. Zusammengenommen deuten diese Ergebnisse darauf hin, dass die Wiederverwendung von Genen, die an der elektrischen Signalübertragung in gewöhnlichen Pflanzen beteiligt sind, zu dem für die Venusfliegenfalle typischen AP führen kann.

Die Venusfliegenfalle wird seit ihrer Entdeckung kultiviert und hat im Laufe der Jahre mehr als hundert Kultivare hervorgebracht. Die Sorte "ERROR", die auf den ersten Blick nicht von einer normalen Venusfliegenfalle zu unterscheiden ist, weist ein besonderes Verhalten auf: Sie ist nicht in der Lage, ihre Fallen nach dem Auslösen von 2 APs zu schließen. Dennoch

ist sie in der Lage, normale APs auszulösen. Um ein besseres Verständnis der molekularen Schlüsselmechanismen und -wege zu erhalten, die für ein erfolgreiches Schließen der Fallen notwendig sind, wurde die "ERROR"-Mutante mit dem funktionalen Wildtyp verglichen.

Zeitrafferaufnahmen führten zu der Beobachtung, dass die 'ERROR'-Mutanten in der Lage waren, ihre Fallen bei wiederholter mechanischer Stimulation (10 Minuten nach 20 APs, 0,03 Hz) sehr langsam etwa zur Hälfte zu schließen. Bei nicht karnivoren Pflanzen wird infolge von Berührungen oder Verletzungen Jasmonsäure (JA) synthetisiert, die die Pflanzen vor potenziellen Fressfeinden warnt. Merkwürdigerweise waren die JA-Spiegel bei mechanischer Stimulation reduziert und bei Verwundung in der "ERROR"-Mutante im Gegensatz zum WT überhaupt nicht erhöht. Auf der Suche nach Genen, die für die Defekte der "ERROR"-Mutante verantwortlich sind, wurden die Transkriptome der beiden Phänotypen vor und nach der Mechanostimulation (1 Stunde nach 10 APs, 0,01 Hz) verglichen. Die insgesamt gedämpfte Reaktion der Mutante im Vergleich zum Wildtyp spiegelte sich auch auf transkriptomischer Ebene wider. Nur etwa 50 % der nach Berührungsstimulation hochregulierten Gene des Wildtyps wurden in "ERROR" unterschiedlich exprimiert, und sie wiesen nur die Hälfte der Expressionsamplitude des Wildtyps auf. Zu den nicht reagierenden funktionellen Genkategorien gehörten: das System zur Überwachung der Zellwandintegrität, die Auxin-Biosynthese und stressbezogene Transkriptionsfaktoren aus den auf Ethylen reagierenden AP2/ERF- und C2H2-ZF-Familien. Deregulierte Ca^{2+}-decodierende sowie redoxbezogene Elemente könnten zusammen mit Komponenten des JA-Signalwegs ebenfalls zur Fehlfunktion der "ERROR"-Mutante beitragen. Da die Mutante nach mechanischer Behandlung keine vollständige Magenbildung durchläuft, stellen diese fehlenden Prozesse wichtige Meilensteine dar, die bei der JA-Signalübertragung einen Kompromiss zwischen Wachstum und Verteidigung vermitteln könnten. Dies bestätigt die Idee, dass sich Karnivorie durch die Wiederverwertung bereits vorhandener Signalwege und -komponenten entwickelt hat.

Um den Defekt der Mutante im Fallenschnappmechanismus besser zu verstehen, wurden die Grundzustände (unstimulierte Fallen) der beiden Phänotypen verglichen. In diesem Fall waren viele zellwandbezogene Gene (z. B. Expansine) in der "ERROR"-Mutante herunterreguliert. Diese Daten weisen zum ersten Mal auf die Bedeutung einer speziellen Zellwandarchitektur der Falle hin, die möglicherweise die mechanischen Eigenschaften für ein Umklappen der Fallenhälften verleiht, was wiederum die Geschwindigkeit des Fallenschlusses erhöht.

Diese Studie liefert Kandidatenkanäle für jede der AP-Phasen, die das scharfe Venusfliegenfallen-spezifische AP hervorbringen und formen. Sie unterstreicht außerdem den möglichen Beitrag der Zellwandarchitektur zur metastabilen, schnappbereiten Konfiguration der Falle vor der Stimulation - die für das durch das Umklappen der Fallenhälften bedingte Zuschnappen der Falle entscheidend sein könnte. Und schließlich werden molekulare Meilensteine hervorgehoben, die mit Abwehrreaktionen verbunden sind und dafür sorgen, dass sich die Falle nach mechanischer Stimulation in einen grünen Magen verwandelt. Insgesamt erweisen sich diese Prozesse als voneinander abhängig und wesentlich für eine erfolgreiche fleischfressende Lebens-weise.

Contents

List of Figures

List of Tables

List of Abbreviations

AA	Amino Acid
ABA	Abscisic Acid
AFM	Atomic Force Microscopy
AMT	Ammonium Channel Transporter
AP	Action Potential
APC	Amino acid/Polyamine/organo-Cation
Ara	Arabinose
ArAE	The Aromatic Acid Exporter
AUX	Auxin
BH	Benjamini-Hochberg
BR	Brassinosteroidsÿ
CaCA	Cation Carrier Groups
Ca-ClC	Calcium-dependent Chloride Channel
CDF	Cation Diffusion Facilitator
CEI	Cell Elongation Inhibition
cGMP	Cyclic Guanosine Monophosphate
ChIP-seq	Chromoatin Imunnoprecipitation sequencing
cNMP	Cyclic Nucleotide Monophosphate
COR	Coronatine
CP	Catabolic Processes
CT	Cytokinin
CWI	Cell Wall Integrity
dd-water	Double distilled water
DEG	Differentially Expressed Gene
Dm	*Dionaea muscipula*
epiBL	Epibrassinolide
ER	Endoplasmic Reticulum
ERR	*Dionaea muscipula* 'ERROR' cultivar
ET	Ethylene
FC	Fold Change
FPKM	Fragments Per Kilobase of transcript per Million mapped reads
Fuc	Fucose
Gal	Galactose
GalA	Galacturonic Acid
GIC	Glutamate-gated Ion Channel
Glc	Glucose
GO	Gene Ontology
GO	Gene Ontology
ID	Identifier
indels	insertion-deletions
JA	Jasmonic Acid
KO	Knock Out
MeJA	Methyl-Jasmonate
MFS	Major Facilitator Superfamily
MGL	Massive Gene Loss

MP	Metabolic Processes
Mya	Milions of years before present
NA	Not Assigned
NMR	Nuclear Magnetic Resonance
NS	Non-Significant
OE	Over Expression
OPDA	12-Oxophytodienoic Acid
PCA	Principle Component Analysis
PRR	Pattern Recognition Receptors
PTR	Proton-dependent Oligopeptide Transporter
QC	Quality check
Rha	Rhamnose
SE	Standard Error
SNPs	Single nucleotide polymorfism
SRA	Sequence read archive
SulP	Sulfate Permease
TE	Transposable Element
TF	Transcription Factor
TGD	Tandem Gene Duplications
TH	Trigger Hair
VIC	Voltage-gated Ion Channel
VOC	Volatile Organic Compounds
VP	Variation Potential
WGD	Whole Genome Duplication
WT	Wild Type
Xyl	Xylose

1 Introduction

1.1 Plant Carnivory

1.1.1 Defining Carnivory in the Plant Kingdom

Plants are marvellous: they can make their food out of thin air (through photosynthesis), they can live for thousands of years making up the oldest (up to 5000 years old *Pinus longaeva* [1]) or the tallest (*Sequoia sempervirens* [2]) organisms on Earth, they can endlessly elongate their leaves (*Welwitschia mirabilis*), they can emanate the most enchanting fragrances (*Jasminum officinale*) or the most repelling ones (*Amorphophallus titanum*), they can mimic bee pheromones and trick them into reward-free pollination (*Ophris sp.*), they can turn shabby-looking by touch (*Mimosa pudica*), they can even parasitize and survive without photosynthesis (*Rafflesia sp.*), but maybe most fascinating of all, they can hunt animals.

The word "carnivory" comes from the Latin *carnis* meaning "meat" and *vorare* meaning "to swallow" [3]. Even if they are able to digest flesh, their prey consists mainly of small arthropods: from ants to bees, from moths to spiders, from flies to wasps and very seldom slugs [4] or even salamanders [5]. Darwin, who was one of the first to thoroughly study them, preferred the term *insectivorous plants* [6], making them sound less menacing.

So what makes a plant carnivorous (or insectivorous)? In order to be called carnivorous, plants should be able to get hold of all of the following traits: **(i)** capturing, **(ii)** killing, **(iii)** digesting the prey and **(iv)** absorbing, as well as **(v)** making use of the resulting nutrients [3]. However, other researchers also include attraction and retention of prey to the list of attributes [7, 8].

Completely crushing their killer reputation, some of them went vegan. Mainly relying on plant material to sustain their growth, they could be rather called herbivorous (such as some *Utricularia* species whose diet consists of 80% algae [9, 10], *Pinguicula* species digesting pine pollen [11, 12]) or detritivorous (such as *Nepenthes ampullaria* which depend on leaf litter for their nitrogen acquisition [13, 14]). Even more innocent is the coprophagous *Nepenthes hemsleyana* which evolved to attract *Kerivoula hardwickii* bats and makes use of their droppings [15]. Taking it further, *Nepenthes bicalcarata* is using the carnivory syndrome to form a symbiotic myrmecotrophic relationship with *Camponotus schmitzi* ants. Benefiting from a protected area within the domatium (provided by the swollen tendril of the pitcher plant) and fed with nectar, the ants throw dead remains of insects and other waste into the pitcher, providing 42-76% of the nitrogen [16]. Hence, we see that there are various degrees of carnivory.

At the end of the spectrum, there are so-called borderline carnivores or protocarnivores. These plants can trap and kill small insects but lack the ability to completely digest them or absorb the resulting nutrients directly. For example, some *Stylidium* species can entrap small insects using their inflorescence glandular hairs that have been linked with protease activity [17, 18] and there are studies showing nutrient uptake too [19]. One study detected 15 plant species (among which *Geranium, Potentilla, Solanum, Stellaria, Mimulus* species) showing surface proteinase activity of their glandular leaves, stems or flowers [20]. These observations support

the idea that carnivory has evolved from simple plant defence mechanisms. Starting from an anatomical level, plants use sticky glandular hairs for entrapping possible arthropod herbivores in order to defend themselves. At molecular level, hydrolase activity is a well-known weapon against pathogen attacks, such as chitinase for breaking down invading fungal cell walls [21].

1.1.2 The Evolution of Plant Carnivory

1.1.2.1 Plant Carnivory Has at Least Eleven Roots

In his book "*Insectivorous Plants*", Darwin (1875) infers that there are at least three lineages of carnivorous plants, while later, Croizat (1960) proposed a single common origin for all carnivorous plants [22]. To date, we know that carnivory evolved independently at least eleven times within angiosperms, with more than 800 species distributed across five orders: Lamiales, Ericales, Nepenthales (= non-core Caryophyllales), Oxalidales and Poales (Figure 1A) [3]. The newest carnivorous species *Triantha occidentalis*, discovered in 2021, adds another order to the list: Alismatales [23]. This definitely shows that there are many "hidden" carnivorous plant species still awaiting to be discovered if we take the chance to do so.

Independent of their phylogenetic classification, there are five main types of traps (Figure 1B): **(i) flypaper traps** (or adhesive traps, with sticky glandular hairs), **(ii) pitcher traps** (consisting of tubular leaves or a rosette of leaves filled with liquid), **(iii) lobster-pot traps** (formed by tubular leaves with retrorse hairs guiding small prey toward a stomach-pouch and preventing them to go back), **(iv) suction-traps** (which are modified bladder-like leaves which form a vacuum inside) and last but not least **(v) snap trap** (formed by a rapidly closing bilobed leaf). More recently, a new type of hybrid trap with catapulting (or snapping) tentacles have been discovered in the flypaper traps of *Drosera glanduligera*. Fascinating as it sounds, small arthropods that get in contact with such long marginal tentacles are glued to the tentacle's head and catapulted within 75 ms to the middle of the flypaper trap where digestion can occur more efficiently [24].

Some trapping mechanisms evolved convergently in several different lineages, while others evolved only once. For example pitcher traps formed by tubular leaves are found in: Oxalidales (Cephalotaceae), Nepenthales (Nepenthaceae) and Ericales (Saraceniaceae). The same way, flypaper traps are found in: Nepenthales (Droseraceae, Drosophyllaceae, Dioncopyllaceae), Ericales (Roridulaceae) and Lamiales (Lentibulariaceae). The snap traps of *Dionaea* and *Aldrovanda* evolved only once [25].

A Focus on Nepenthales

The subject of this study, *Dionaea muscipula*, is part of Droseraceae family, Caryophyllales order. Some authors consider the Nepenthales as the non-core carnivorous branch of Caryophyllales [26]. Nepenthales is the oldest lineage of carnivorous plants, estimated to have emerged before the mass extinction of dinosaurs: with an estimated phylogenetic age of 95.1 Mya (millions of years before present) [3]. This means, that dispersion via continental drift before Gondwana completely broke up is plausible. Nowadays, members of Nepenthales are found all over the globe: the species-rich *Drosera* ($\sim$ 250) is cosmopolitan, while *Nepenthes* ($\sim$ 130-160) is found in Australia and south-east Asia.

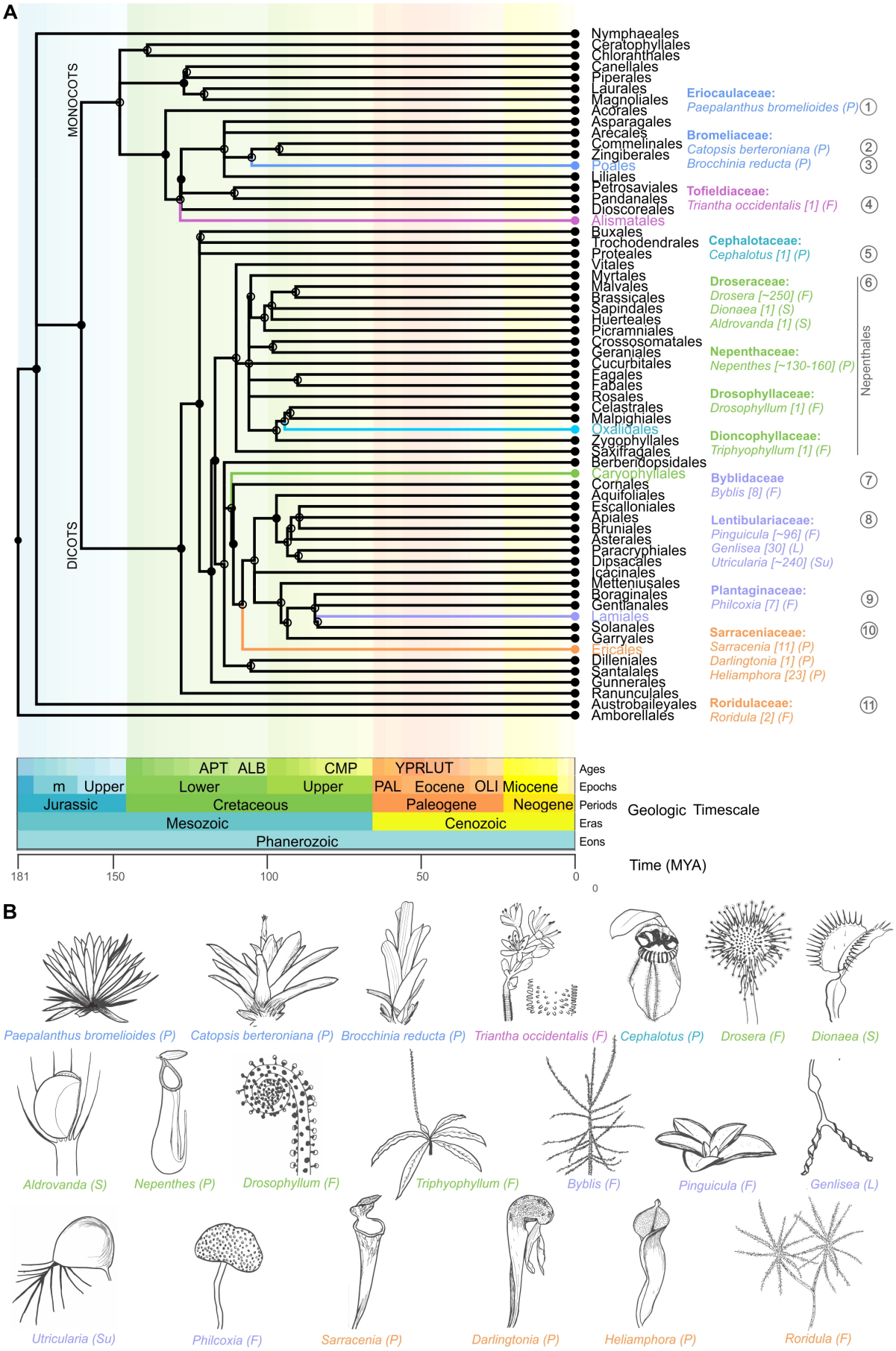

Figure 1: (A) Carnivory evolved at least 11 times in 6 orders, 13 families and 20 genera. Phylogenetic tree produced with Timetree. In square brackets = the number of species for each genus. P = pitcher, F = flypaper, Su = suction trap, S = snap trap, L = lobster-pot traps. (B) Drawings of each of the 20 carnivorous genera (by the author).

Interestingly, today, the remaining species are monotypic: *Aldrovanda vesiculosa* (widespread), *Dionaea muscipula* (eastern USA), *Drosophyllum lusitanicum* (western Mediterranean region), *Triphyophyllum peltatum* (tropical western Africa). The sister core group of Caryophylalles contains non-carnivorous species from Polygonaceaea, Plumbaginaceae, Tamaricaceaea and Frankeniaceae families. Interestingly, the majority possess glandular hairs or other secretory tissues. Living in extreme saline or calcareous soils, within the Frankeniaceae family, plants have evolved vascularized glands that excrete salt or chalk. These glands could have provided the first building blocks in the evolution of carnivory [26].

However, the newly discovered *Triantha occidentalis* [23], makes the monocotyledons Alismatales the oldest order containing carnivorous plant species (originating in Lower Cretaceous according to Timetree). Further phylogenetic studies are needed in order to better understand the deepest roots of plant carnivory.

Genomes of Droseraceae

The clustering of Nepenthaceae together with Droseraceae is supported by morphological synapomorphy such as the echinate pollen tetrads, as well as chemical synapomorphy given by the presence of the yellow toxic naphthoquinone 7-methyljuglone. Meanwhile, the non-carnivorous branches of the Caryophyllales together with the Drosophyllaceae, Dioncophyllaceae and Acistrocladaceae have pollen as monads and the naphthoquinone plumbagin. Since *Nepenthes* species live in wet tropical rainforests, transition from a possible water-based adhesive flypaper trap ancestor (that would be ineffective during heavy rain) into a pitcher, might be a good adaptation. For similar reason, *Triphyophyllum peltatum* might take an evolutionary path to non-carnivory. *Triphyophyllum* is an outstanding example of "facultative carnivore", with carnivorous flypaper leaves (very similar to that of *Drosophyllum*) only during the less rainy season, while its closest relatives *Habropetalum* and *Dioncophyllum* are completely non-carnivorous [3, 26].

The stem age of Droseraceae family is thought to date from Late Cretaceous (84.8 Mya) with a later split of *Dionaea* and *Aldrovanda* from *Drosera* (53.5 Mya) [3]. The fossil evidence for Droseraceae is mainly based on *Aldrovanda* seeds and the highly family-specific pollen tetrads of *Aldrovanda* and *Drosera*. The oldest remains of a carnivorous plant were the *Paleoaldrovanda splendens* fossilised seeds found in the Czech Republic dated from the Senonian epoch (85-75 Mya) [27]. However, other researchers claim that these fossil seeds do not resemble any extant members of Droseraceae and they may rather be insect eggs, proposing that the family did not evolve until the Tertiary [28]. Nevertheless, compared to other carnivorous species, *Aldrovanda* paleontological material is very rich. Based on this, at least 17 now extinct *Aldrovanda* species are estimated to have lived starting from Eocene (54 Mya) up until Pleistocene (2.5 Mya) [27]. *Drosera* pollen has been found in New Zealand from the Miocene [29]. *Dionaea*-like pollen belonging to an extinct genus of Droseraceae (*Fischeripollis sp.*) has been found in Australia dating from middle to late Eocene (48-34 Mya), as well as in Miocene sediments from Germany [30]. Other Droseraceae extinct genera have been found as well: *Droseridites parvus* found in Assam dating from Paleocene (65-55 Mya) and *Saxonipollis* sp. (which is *Aldrovanda*-like) from Eocene sediments (55-38 Mya). However, up to now, the most unique and well preserved, entrapped in Eocene Baltic amber, is the first fossilised *Roridula* trap, bringing evidence of plant carnivory from 35-47 Mya [31].

Nevertheless, in order to understand how carnivory evolved within Droseraceae, new technologies like genome sequencing can be used instead of fossils. This approach might bring more information to fill the gap between non-carnivorous ancestors and extant carnivorous species [32].

Recently, the genomes of three representative Droseraceae species: *Dionaea muscipula, Aldrovanda vesiculosa* and *Drosera spatulata* were sequenced, assembled and annotated. In search of family- and species-specific adaptations, given the different trapping strategies, Palfalvi and colleagues from our group, compared and analysed the three genomes with other closely related species [25]. The main findings were that: **(i)** a whole-genome duplication (WGD) event happened at the base of the family, providing enough gene material, out of which carnivory-related processes could be selected. This event was paralleled with **(ii)** massive gene losses (MGL) (Figure 2A). The majority of lost genes were involved in kinetochore formation and ubiquitination, as well as root development in *Aldrovanda*. On the contrary to gene losses, gene family expansions occurred for carnivory-related genes involved in: prey attraction, signal transduction, hormonal signalling, digestion and nutrient uptake (Figure 2B). *Drosera spatulata* showed a high number of tandem gene duplications (TGD), while *Dionaea* exhibited an incredible amount of transposable elements (TE, mainly LTRs) making up half of its genome (and creating many challenges for the genome assembly procedures). Curiously, *Aldrovanda* has undergone another WGD, meaning that most of the genes are quadruplicated. Another interesting observation that is unique to the snap trap, is the expansion of genes involved in leaf formation and cell wall (CW) biogenesis as well as modification. This will prove to be important and strongly reflected in the present study (Figure 2A). The authors also searched for tissue-specific processes in *Dionaea*, based on available transcriptomic data. Photosynthesis-related GO-terms were enriched in petiole and rim, while CW-related processes were specific to the rim only. In activated trap and glands GO-terms such as redox processes signalling stress, proteolysis that may help with prey digestion and other catabolic processes were enriched (Figure 2C) [25].

Other carnivorous species, such as *Utricularia gibba* [33, 34] and *Genlisea aurea* [35] are part of the top smallest genomes sequenced so far. In general, all three Droseraceae have a very low number of genes (Table 2) and fall into the small genome size end of the spectrum, except for *Dionaea* which has a bigger genome size due to an extremely high proportion of repetitive elements.

Table 2: Genome sizes and number of genes in each of the three representative Droseraceae species based on [25], chromosome number based on [36]. According to the same source, all three species are diploid.

Species	Genome (Mbp)	Assembly (Mbp)	Predicted Genes	Annotated Genes	Chromosomes
Di. muscipula	3 187	1 500	21 135	19 873	2n=32
A. vesiculosa	509	420	25 123	24 450	2n=48
Dr. spatulata	293	238	18 111	17 645	2n=20

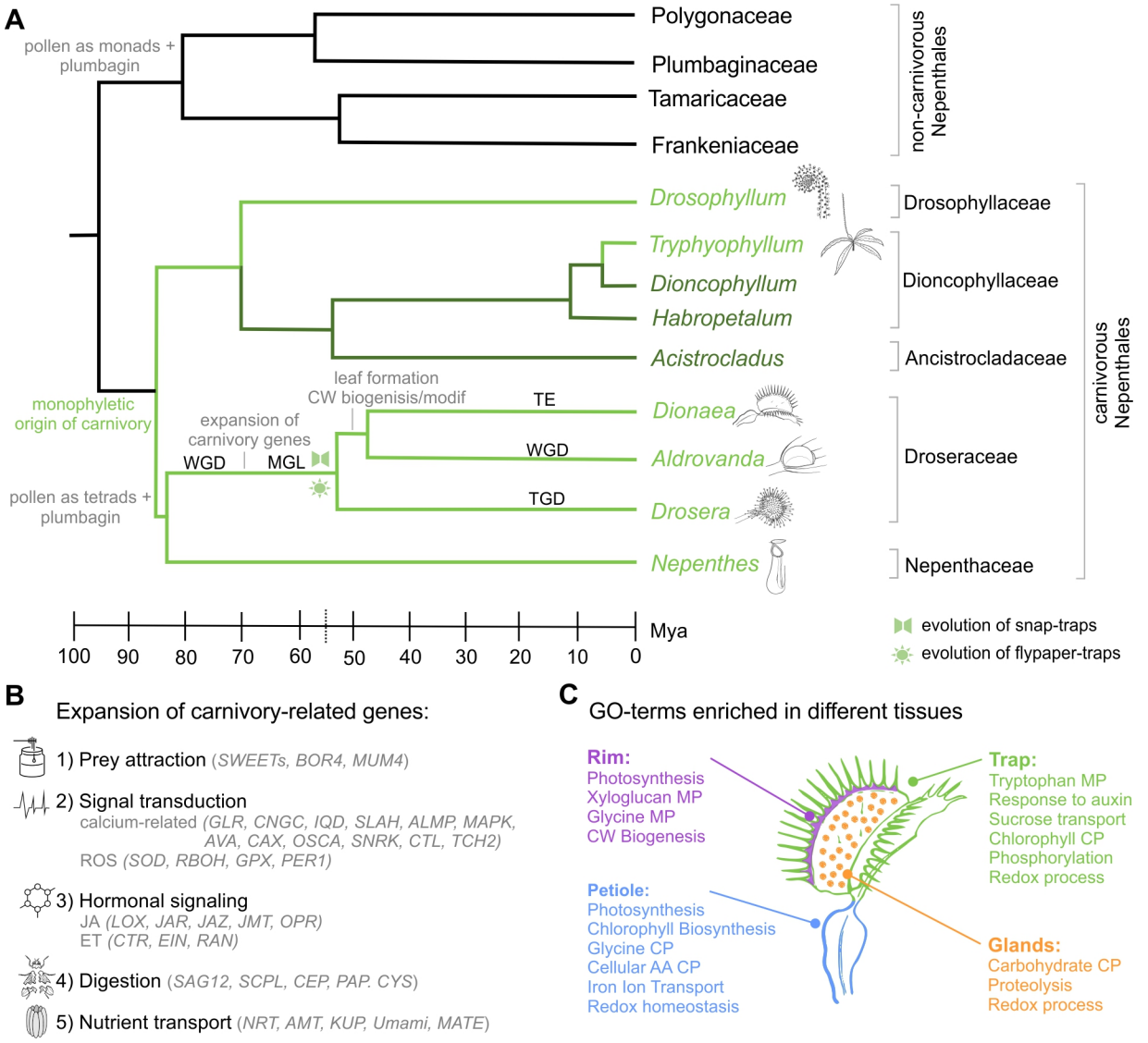

Figure 2: (A) Nepenthales phylogenetic tree based on APG (2016) [26]. Carnivorous lineages are shown in light green accompanied by representative drawings. Lineages where carnivory was lost are shown in dark green, and the rest non-carnivorous are shown in black. Annotations on tree contains information from [26] and [25]. WGD = whole genome duplication, TE = transposable elements expansion, MGL = massive gene loss, TGD = tandem gene duplications. (B) Carnivory-related genes that were expanded in all three Droseraceae based on [25]. (C) Processes specific to each of *Dionaea*'s tissues (based on GO-term enrichment) as shown by [25]. MP = metabolic processes, CP = catabolic processes, AA = amino acid, CW = cell wall.

1.1.2.2 How Adhesive Traps Became Snap Traps

The sisterhood of *Dionaea* and *Aldrovanda* is indisputable [3, 37, 25, 38, 39] therefore snap trap evolved only once in the tree of life. Since there are no intermediate forms, it is very hard to answer the question of how snap trap evolved from flypaper traps. There are different disputable and opposing theories. Most researchers suggest that the common ancestor was terrestrial [37, 6, 40] while others suggest that it was aquatic [3, 41, 42]. Snap-traps evolving from flypaper-trap as an adaptation to an aquatic environment is supported by the observation that *Dionaea* traps snap with the same speed and are capable of digestion underwater, making them suitable to grow in seasonally inundated habitats [42]. Why would *Dionaea* need to hermetically seal its trap if the teeth prevent prey from escaping anyways? Maybe the common ancestor was not completely aquatic but indeed highly adapted to flooded conditions in which carnivory might have been an advantage.

Juniper and colleagues draw a step-by-step evolutionary scenario from flypaper-trap to snap trap which implies: **(i)** bilobed leaf blade modifications, **(ii)** loss of stalked glands and selection of sessile glands, **(iii)** transition from marginal glandular tentacles to marginal teeth, **(iv)** the retention of at least six non-glandular sensitive tentacles to become the trigger hairs of *Dionaea* [8]. This last idea is supported by the presence of the endodermoid layer in *Drosera* stalked glands which is also recognisable but non-functional, rather like a relict, in *Dionaea* trigger hairs [43].

Poppinga and Hartmeyer together with their colleagues build on this hypothesis, further proposing that the special *Drosera glanduligera* catapult/snap tentacles could be a good precursor candidate of snap trap due to their fast mechanical responses. They propose that a hypothetical predecessor *Dionaea*-like trap had all the prerequisites needed, including a mechanosensory system and sessile glands to form a bilobed trap. A double surface curvature was the final touch needed for a snap-buckling speed boosting system [44].

The numerous *Drosera* clade is sister to *Dionaea*+*Aldrovanda* clade. Moreover, the earliest branching species in the *Drosera* clade, is *Drosera regia* [38, 39, 40]. Interestingly, this species has long leaves with a very pronounced midrib resembling that of *Dionaea*. Other studies that do not include *Drosera regia* in the analysis, show that *Drosera glanduligera* is the earliest branching species [45].

Another personal observation, that brings more evidence to the similarity of flypaper and snap trap, is the curious rolling of *Dionaea* traps when in contact with wet meat (that does not touch the trigger hairs) (see Appendix Figure 61). Besides the digestive fluid secretion in response to meat, which was well studied by Darwin [6], *Dionaea* did not lose the ability to slowly move by rolling its lobes around the meat, in the same way, *Drosera* slowly engulfs its prey when forming the outer stomach, getting as many tentacular glands in contact with the prey as possible. This proves that (besides the mechanosensitivity), a common chemotaxis exists between the two trapping strategies.

1.1.2.3 Carnivory Evolved From Defence Mechanisms

As sessile organisms, plants have to fight back herbivores and phytopathogens. Besides possessing thorns (like roses do), stinging trichomes (such as nettles) or glandular trichomes (like tobacco plants) or pretending to be invisible (like *Mimosa pudica* does), plants defend themselves in ways humans cannot perceive at first glance. Plants have evolved intricate molecular defence mechanisms that integrate different layers of networks [46]: **(i)** perception network: comprising receptors for damage or invasion recognition of the cell wall integrity (CWI) surveillance system (RLRs, RLKs, NLRs, CaMs) [47], **(ii)** signalling network: from fast electrical signalling (APs, VPs) [48], together with ROS and Ca^{2+} signalling [49], to activation of kinases (MAPKs, CDPKs, and others), and modulation of growth-defence trade-off by multi-hormonal networks (defence - JA, SA, ET, ABA; growth - AUX, BR, CT), **(iii)** massive transcriptome reprogramming network (TFs: AP2/ERF, bHLH, WRKYs, bZIP, NAC) [50], **(iv)** response of secondary metabolism network (biosynthesis of alkaloids, flavonoids and phenolics) [51] as well as accumulation of pathogenesis-related (PR) proteins (chitinases, peroxidase, β-1,3-glucanases, defensins, polyphenol oxidase, phenylalanine ammonia lyase) [52], which in the end repel herbivores or slow down disease spreading.

When a pathogen, such as a fungus, attacks a plant, it develops specialized hyphal structures (called haustoria) that penetrate inside the host [53]. Among others, fungal CW comprises chitin-oligomers, such as the ones found in insect exoskeleton. Plant lysin-motif (LysM) RLK CERK1 is a pattern recognition receptors (PRRs), and more specifically, a chitin receptor required for recognition of fungal chitin-oligomers [54]. PRR signalling immediately triggers subsequent signalling networks mentioned above. In *Dionaea*, upon insect feeding, *CERK1* is upregulated together with one of the main digestive hydrolases: the chitinase VfChitinase I (from Venus flytrap chitinase) [55], referred to as *DmCHIB* in [56] and throughout this manuscript. This is a clear example that carnivorous plants are able to use the basic defence strategies for feeding purposes, such as perceiving and degrading the main component of the insect exoskeleton.

Electrical signals were first discovered over 200 years ago, and described in both plants and animals [57]. Pierre Bertholon de Saint-Lazare was a pioneer in the field, writing about plant electricity first (*De l'électricité des végétaux*) [58]) in 1783, and only three years later about human electricity (*De l'électricité du corps humain dans l'état de santé et de maladie*) in 1786. Only after about 100 years (1873), thanks to Darwin's request, Burdon-Sanderson measured the first electrical signals in plants: the APs of *Dionaea muscipula* [59, 60]. However, the existence of electrical signals in "normal" plants was still questioned. It was not until another 100 years later, when Barbara Pickard's review on *Action potentials in higher plants* (1973) [61] forged ahead the fact that APs are not restricted to the so-called "sensitive plants" (such as *Dionaea* and *Mimosa pudica*) [62]. Nowadays, we know that electrical signals are one of the first and fastest mechanisms present in the majority of plants that get triggered upon touch and wounding [63].

There are different types of electrical signals: action potentials (APs), system potentials (SP) and variation potentials (VP, also known as slow-wave potentials SWP). APs are all-or-nothing signals, preserving the same amplitude and shape no matter the type of stimulus, with a duration between 0.6 to 3 seconds and an amplitude of $\sim$100 mV [64]. Usually succeeding

the APs, SPs are systemically propagated hyperpolarizations (∼50 mV), with a long duration (up to 30 minutes)[63]. SWP are easily induced by wounding and are transmitted from organ to organ. Similar to SWP, they have a lower amplitude and longer duration which is changing according to the intensity and type of the stimulus. Interestingly, until very recently the function of these electrical signals was unknown [63]. Mousavi and colleagues showed for the first time that in *Arabidopsis thaliana* SWPs are important for JA-genes activation (such as *JAZ10*) and that glutamate-like receptors GLRs are essential for the SWP systemic propagation [65]. Even more recently, Marhavy and colleagues showed that single-cell wounding in roots of *Arabidopsis thaliana*, results in non-systemic, therefore local surface potential changes accompanied by Ca^{2+} and ROS waves which activate ET production and signalling. Curiously, in their study, no robust JA responses were initiated [66].

In carnivorous plants with active trapping mechanisms, APs are needed for fast prey capture response. While the presence of AP is certain in *Dionaea, Aldrovanda* and *Drosera*, it remains poorly understood in *Utricularia* (Table 3). So far, there is more evidence that the fast suction trap of *Utricularia* works mechanically [3].

Table 3: Jasmonic acid (JA) accumulation, action potential (AP) and enzyme secretion upon prey feeding, touch stimulus, wound stimulus or external JA application in various carnivorous plants. sys = systemic, nonsys = non-systemic, ? = not clear, . = no data

	JA accumulation			Action potential			Enzyme secretion				
	prey	touch	wound	prey	touch	wound	prey	touch	wound	JA	bib
Dionaea	yes	yes	yes(nonsys)	yes	yes	yes	yes	yes	yes	yes	[67][68]
Drosera	yes	yes	yes(sys)	yes	yes	yes	yes	yes	yes	yes	[69][70][71][72]
Aldrovanda	yes	.	.	yes	yes	.	yes	.	.	yes	[73][74]
Nepenthes	yes	.	.	no	no	no	yes	.	.	.	[75][76]
Utricularia	no	.	.	.	.	no/?	yes	.	.	.	[77][74]
Pinguicula	no	.	yes	no	.	no	yes	.	.	no	[78]
Sarracenia	.	.	.	no	no	no	yes	no	.	.	[79][76]

Curiously, upon mechanostimulation, the elicited AP originating from the trigger hairs, spreads throughout the trap of *Dionaea* but does not travel to the connected petiole, while that of *Drosera* is initiated in the head of the tentacle, spreading through the stalk, but does not reach the leaf-blade of the trap [72]. As in non-carnivorous plants, the electrical signalling has been linked to the activation of the JA pathway. It is well known that different numbers of APs trigger different processes in *Dionaea*: two APs are needed for trap closure, more than two APs are inducing the activation of JA-related genes and more than five APs activate the expression of genes encoding for digestive fluid hydrolases [67].

Interestingly, upon wounding, the JA signalling is still restricted to the trap of *Dionaea*, while in *Drosera*, the signal is systemically spread to other traps, similar to *Arabidopsis* [65, 70, 68, 80]. In all Droseraceae (including *Nepenthes*) it has been shown that JA accumulation occurs after prey capture. On the contrary, there are carnivorous species which work in a JA-independent fashion, such as *Utricularia* [74] and *Pinguicula* [78], where no JA accumulation occurred after insect feeding (Table 3). As it was very recently discovered, even in *Arabidopsis* roots there are JA-independent defence mechanisms [66], suggesting that this could be the case in some carnivorous plants as well. Therefore, studying the carnivorous syndrome in as many species as possible could answer defence-related physiological questions.

After the induction of the complex hormonal network, like "normal" plants, carnivores also produce defence compounds. Indeed, in many carnivorous species, pathogen-related

(PR) proteins are common in the digestive fluid [80]. More than 170 secondary metabolites have been found across all (so far studied) carnivorous species, out of which 26 compounds are common in all genera. Secondary metabolites play important roles in prey attraction (anthocyanins giving red pigmentation to *Drosera*, phenolics and quinones in the UV-fluorescent peristome of *Nepenthes*, VOCs in the rim of *Dionaea*). Additionally, they assure antifungal and antibacterial properties during prey decomposition (such as plumbagin and juglone found in Nephenthales) [81].

While Ca^{2+} waves could be recently beautifully visualised upon trigger hair bending and wounding of transgenic gCaMP *Dionaea* traps [82], there are still many open questions. One of the least studied aspects is the ROS signalling (as well as CWI-system) involvement in the carnivory syndrome.

1.2 Anatomy, Physiology and Ecology

1.2.1 Botanical History

Dionaea muscipula became known to the Europeans thanks to Arthur Dobbs, who was a wealthy landowner with an interest in botany and nature. With Irish origins, he moved to America in 1754 and became the Governor of North Carolina. After one of his explorations of swamps in the region, he wrote to the horticulturalist Peter Collinson, who was a Fellow of the Royal Society [4, 83]:

> *We have a kind of Catch Fly Sensitive which closes upon anything that touches it.* [84]

Living specimens were finally brought to England in 1768 by William Young, the "Queen's Botanist", and John Ellis, a passionate naturalist laid hands on one of Young's specimens. He was not the first to carefully study the plant, but he was the first to publish the plant's description in *St. James's Chronicle* right away. In his letter to the editor of the journal, he does acknowledge that Doctor Solander was the first to dissect the plant. Here is a fragment of that letter [4, 83, 85]:

> *At the request of Mr. Collinson, the ingenious Doctor Solander, now on his Voyage to the South Seas, in Search of rarer Productions of Nature, dissected the Plant before some of his Friends; and from the beautiful Appearance of its Milk-white Flowers, and the Elegance of its Leaves, thought it well deserved one of the Names of the Goddess of Beauty, and therefore call it Dionaea. As this Name was generally approved of, and so well adapted by the eminent Botanist, I shall only add a specific Name to distinguish it from others of this Genus, that may possibly be discovered hereafter. From the Structure then and particular moving Quality of its Leaves when irritated, I shall call it Dionaea muscipula, which may be construed into English, with humble Submission both to Critics and foreign Commentators, either Venus's Flytrap, or Venus's Mousetrap.* [86]

John Ellis was in touch with many naturalists and nature lovers at the time, including Linnaeus. However, an astonishing question came from Lord Moreton [4, 83]:

> *Do you think Sr that the plant receives any nourishment from the Insects it catches?* [87]

In a later edition (1770) of Ellison's "*Botanical Description of the Dionaea muscipula or Venus's Fly-Trap. A Newly-discovered Sensitive Plant.*", his speculation of the plant being carnivorous is reflected in the way he described it [4, 83, 85]:

> *Nature may have a view towards nourishment, in forming the upper joint of the leaf like a machine to catch food; upon the middle of this lies the bait for the unhappy insect that becomes its prey.* [88]

Linnaeus, however, did not agree, regarding *Dionaea*'s sensitivity as a defence mechanism like in the case of *Mimosa pudica* and argued that the capture of insects was rather accidental. Due to his influential authority at that time, many botanists did not question his assumption. The first known experiment was done by the amateur naturalist Thomas Andrew Knight who placed raw beef meat on the traps and noticed that the fed plants grew larger than the unfed ones. This experiment was not sufficient to prove the Venus flytrap's carnivory. Other more detailed experiments were carried out independently around 1875 by other naturalists such as William Canby, Asa Grey and Charles Darwin and they all strongly agreed that trapped insects

are digested for nourishment [4].

1.2.2 Distribution, Ecology and Status

Dionaea muscipula is endemic to North and South Carolina. Nowadays it is present only in 12 countries, being extirpated from 9 other. Beyond their native habitat, naturalised populations of *Dionaea* are found in other states of the USA (California, Florida, New Jersey) and even in southern England and New Zealand [4].

Dionaea grows in a very unique habitat with a narrow ecotone: between wet *Sphagnum* peat moss swamps with acidic and nutrient-poor soils and dry open *Pinus* woodlands with sandy soils. Because of this, it is adapted to both floodings, due to seasonal rains (being able to catch aquatic animals), and seasonal wildfires. This is possible thanks to its rhizome where nutrients can be stored underground. Its hemicryptophytic (or bulbous geophytic) nature, with a rosette of leaves protecting the shoot, allows it to enter winter dormancy and survive frost as well [3, 8]. Since *Dionaea* grows slowly, reaching maturity after 4-7 years, it is also a weak competitor. In this case, wildfires which inhibit competing vegetation, might be actually beneficial [4].

Unfortunately, due to habitat destruction for agricultural and human habitation usage, pollution and poaching [8, 89] as well as wetland drainage, fire suppression and massive seed collection [4], *Dionaea* is listed as vulnerable in the IUCN red list, while its other Droseraceae sisters are endangered (*Aldrovanda* and 12 *Drosera* species) and critically endangered (30 *Nepenthes* species and 9 *Drosera* species) [89]. In 2016 there was a petition to list *Dionaea* as endangered under the 1973 endangered species act.

It has been estimated that more than 4 million *Dionaea* individual plants were present in 1980, dropping to only 86 thousand by 2012 distributed across a total of 179 sites [4]. The majority of sites comprise non-viable populations (with less than one hundred individuals). While 25 viable *Dionaea* populations are protected, 42 remain unprotected. Even the protected population sites management objectives does not necessarily benefit *Dionaea*. Bailey and McPherson propose four conservation recommendations: **(i)** exigent penalties for poaching, **(ii)** annual prescribed fires, **(iii)** management of land purchases where unprotected populations occur, **(iv)** development of more funding conservation programs [4].

1.2.3 Morphology and Anatomy

1.2.3.1 General Description

Dionaea muscipula is a herbaceous perennial hemicryptophyte, with a bulb-like rhizome from which the rosette of leaves emerges above the ground and weakly branched **roots** underground [4, 22]. The leaves are around 7 cm long and are divided into two parts: the base, which forms the primary photosynthetic organ - **the petiole** with a prominent midvein, while the upper part forms a special prey capture organ - **the snap trap** [4, 22, 90]. The so-called "linker" part merges the petiole's midvein with the trap's midrib. The trap is made up of two lobes that are separated by the midrib, forming an angle of 60-80° [91]. The trap margin, also called **the rim**, bears ∼ 20 bristle-like **teeth** which upon trap closure intercalate. At the base of these teeth, the so-called **trap rim** part fosters transparent **nectary glands** that might release VOCs in order to allure potential prey [92]. The rest of the adaxial (upper / inner) trap side is covered in red-pigmented **digestive glands** that are responsible for both digestive fluid secretion and nutrient uptake. Another special structure of the trap, are the **trigger hairs** which are responsible for prey perception. When the trigger hairs are touched and therefore bent, the mechanostimulus gets transformed into an electrical signal that alerts the plant of potential prey. When the plants reach maturity, flowers develop from the middle of the leaf rosette. As described by Ellis, the delicate white **flowers** are produced on a < 40 cm tall stalk forming a cymose inflorescence [3].
All the above-mentioned organs, tissues and special structures can be seen in Figure 3.

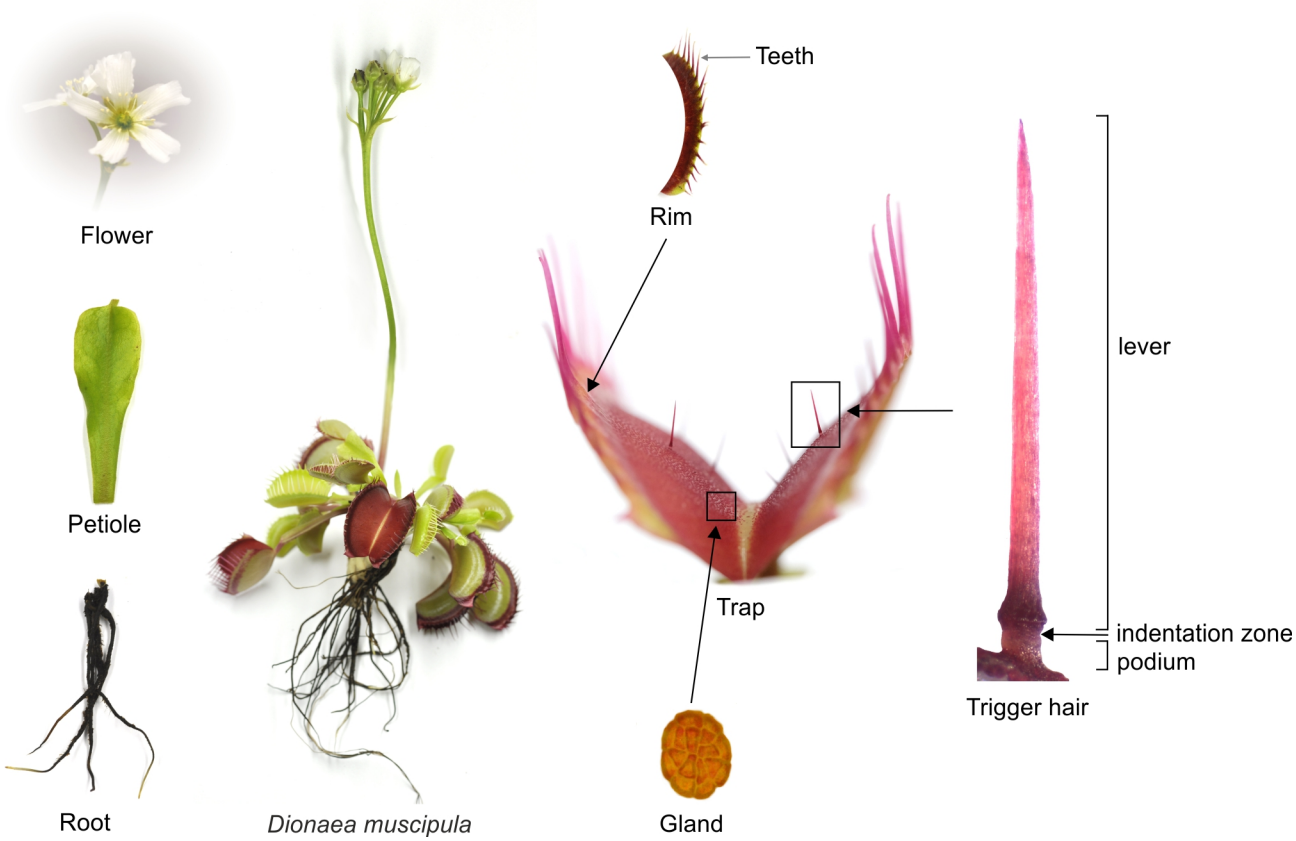

Figure 3: *Dionaea*'s main organs (left) and special carnivory-adapted structures of the snap trap (right). (Photos taken by the author).

1.2.3.2 Carnivory-Related Features

The Trap

The snap trap of *Dionaea muscipula* is unique in the plant kingdom. Even if the closest sister species, the aquatic *Aldrovanda vesiculosa* shares the same trap type, the mechanism behind the snapping strategy is different. *Aldrovanda*'s fast snapping mechanism relies on the deformation of the midrib (and neighbour cells) which bends inwards, inviting the trap lobes to come together, while in *Dionaea* the deformation occurs in the trap lobes themselves. However, for both strategies, the hydraulic turgor-change together with the stored prestress release are necessary [93, 94].

In the ready-to-hunt mode, *Dionaea*'s traps are open, the upper part of the lobes is strongly bent in a convex shape. To reach the closed state, the trap lobes have to invert their curvature into a concave state, with a sudden release of stored elastic energy in a nonlinear dynamic fashion. This can be achieved by a change in turgor status of two (or three [91]) cell layers. The adaxial (upper or inner) layer of cells is highly turgid during the open ready-to-snap state, while the abaxial (lower or outer) cell layer is less turgid. The shrinkage and loss of turgor in the adaxial layer, together with water uptake and therefore expansion of abaxial layer cells, results in the trap closure. The buckling instability is a key element that amplifies the speed of the trap closure resulting in a 100 ms fast snapping [91, 95, 96, 97].

The Nectary Glands

A band of transparent nectary glands are found as part of the rim's inner surface. Each sessile gland is deepened in a small dent so that they are not damaged when the trap lobes press forcefully on each other. They are known to secrete carbohydrates that might help in trap sealing [8]. The nectary glands may play a role in prey attraction, but compared to other carnivorous plants, it is weak. There are studies showing that VOCs are indeed emitted, most of which are normally found in flowers and fruits [92, 98]. This leads to the subject of pollinator-prey conflict. It seems that *Dionaea* is well adapted to not eat its pollinators. One study shows that, at taxonomic level, very little overlap exists between species that were flower-visitors and species that were entrapped by the capture organ. While *Dionaea*'s pollinators mainly consist of bees and beetles (such as *Augochlorella gratiosa, Lasioglossum creberrimum, Typocerus sinuatus, Trichodes apivorus*), among the most common prey were spiders, beetles and ants (such as *Camponotus castaneus, Disonycha admirabilis*, Salticidae, Lycosidae) [99].

The Digestive Glands

The inner surface of the trap is covered with digestive glands, which play an important role in the carnivory syndrome. They are responsible for the digestive fluid secretion and nutrient uptake after prey decomposition has taken place. Most of the time the glands become red due to anthocyanins accumulation [8], making them resemble tiny raspberries. As the nectaries, the digestive glands are also sessile, but conversely, they are not sunken but rather protruding from the upper epidermis. They are also covered by a thick cuticle that forms gaps during digestion. Early morphological studies already showen that they are composed of 46 cells arranged in three distinguishable layers: the outer layer, the inner layer and the

endodermoid layer [8]. Recent studies show the ultrastructure of the three-layered gland cells [56]. The innermost, endodermoid layer (comprising only two cells [8]) is packed with lots of oleosomes indicating that triacylglycerol (TAG) is the primary source of energy for the highly consumptive digestion process. Supporting this idea, transcripts involved in TAG breakdown have been found in glands [56]. The inner layer is highly supplied with mitochondria, suggesting that the ATP generation from the fatty acids occurs at this site. The outer layer is considered to be responsible for protein biosynthesis and translocation machinery as it presents an expanded rough endoplasmic reticulum (ER) and high transcriptional activity of genes encoding hydrolases, the prime components of the digestive fluid. A high volume of fluid can be released at once via exocytosis, speeding up the secretion process [100]. Between the outer layer and the inner layer, pronounced plasma membrane invaginations indicate a high nutrient transport capacity [56]. Upon stimulation, the glands swell, increasing their surface by more than 30%, enabling them to perform an effective digestion [101].

The Mechanosensitive Trigger Hairs

Three (or more) strategically positioned mechanosensitive hairs are found on each trap lobe [8]. These special structures are responsible for prey detection and perception. When they are touched, the mechanosensation is translated into an electrical signal [102]. Therefore, the trigger hairs are the site of action potential (AP) origin, which further propagates throughout the entire trap. Thanks to a successful transformation protocol, Suda and colleagues were able to visualise the cytoplasmic Ca^{2+} waves for the first time in a transgenic *Dionaea* line harbouring GCaMP Ca^{2+} indicator. They could clearly show that the wave starts at the base of the trigger hair, spreading with an average propagation velocity of 53 $\pm 8.2 mms^{-1}$ in the lateral (from midrib to rim) direction, and slightly slower in the other directions [82].
One trigger hair consists of three main parts: **(i)** the upper slender cone called the lever, **(ii)** the lower part called the podium and **(iii)** the indentation zone which strangulates the trigger hair, separating the upper part from the lower part (Figure 3) [102, 103, 104]. When the trigger hair is bent, the upper part amplifies the signal, acting as a pressure transducer. Recently, Scherzer and colleagues have measured the force needed to elicit an AP. It seems that as little as 29 µN is enough to fire an AP, a threshold that ants easily exceed [105]. The bulged base of the lever consists of anticlinal cells with thin cell wall (CW), containing numerous mitochondria [103]. On top, making up the main part of the lever, are elongated cells with thick CWs, giving the trigger hair a stiff structure. The indentation zone (or constriction zone) is the site where the bending of the trigger hair occurs, acting as a hinge. It comprises around 50 mechanoreceptor cells that are arranged concentrically in one layer [104]. The CWs of these cells are highly thickened, enabling them to stand the repeated shear stress that takes place once an insect is trapped inside the trap, continuously flexing the hairs. The ultrastructure of the mechanoreceptor cells shows a polar arrangement of a well developed endoplasmic reticulum (ER) system, making up a perfect Ca^{2+} storage site [104, 106]. The podium zone which connects the trigger hair to the trap mesophyll accommodates cells containing large vacuoles as well as plastids with starch grains [103].
Even though APs can be elicited by applying strong pressure on the trap lobes, it seems that the trigger hairs are highly sensitive structures designed to perceive 1000 times lighter forces, such as those induced by small arthropods [105].

1.3 The Hunting Cycle

Digestion is an expensive metabolic process that requires a high quantity of *de novo* synthesized proteins (such as: peroxidases, nucleases, phosphatases, phospholipases, chitinases, cysteine proteases and serine carboxypeptidase [107]), which is also reflected in the high expression of genes encoding these proteins [56]. In order to wisely use its energy, *Dionaea* has to distinguish between the touch of a juicy prey and other accidental touches induced by raindrops, falling leaves or very small prey which would not exceed the cost vs benefit ratio. To solve this problem, the hunting behaviour of *Dionaea* includes several "checkpoints" that enables it to come back to the resting state if "false alarms" are triggered.
The hunting cycle with underlying activated molecular layers are presented in Figure 4.

Di Palma and colleagues were the first to demonstrate that two consecutive trigger hair touches that elicit two action potentials (APs) are needed for **the fast trap closure (/snapping)** [108]. Recent studies show that under one sustained hair displacement with constant speed and an intermediate angular velocity (between 0.03 to 4 rad s^{-1}), two APs can be generated resulting in trap closure [109].
Curiously, so-called "touch receptors" or stellate trichomes found on the outer trap surface (as well as petioles) can also generate APs, independently of the trigger hairs, leading to trap closure [110]. Also from personal observations, under special circumstances when these stellate trichomes are brushed, a pre-depolarization can help to build up the AP, and the trap closure can indeed occur with only one touch. Maybe these curious stellate hairs are involved in priming the trap so that the predator crawling on the petiole can easily become prey.

Once an AP has been fired, the electrical and Ca^{2+} memory of the trap starts to fade. Consequently, a second AP should be fired within about 30 seconds so that the threshold can be reached in order for the trap to snap [82]. If the prey would be too small, a second "checkpoint" lets the small prey escape through the small gaps between the interlocking teeth. If no additional stimulation is applied, the trap reopens in around 24h.

Böhm and colleagues have shown that two APs already start the transcriptional activation of JA-pathway genes (such as *JAZ1*), while five APs are needed for the activation of genes encoding marker hydrolases (such as *CHIB, SAG12, SCPL49*) [67, 90]. By this step, the prey-dependent **slow closure** begins. When a small arthropod is encaged, usually it starts to panic and struggle, touching the trigger hairs multiple times. The highest number of fired APs were recorded within the first hour, with an average of 63 APs after prey capture (such as a struggling cricket *Acheta domesticus*) [67]. Therefore, further mechanostimulation is accompanied by further trap closure until it is completely sealed, and **the green stomach fully formed**. The force exhibited between the two trap rims pressed against each other has been measured as 73 mN at the beginning of the closure [109], reaching up to 149 mN in later digestion stages [111]. Such a force can definitely "*squeeze to death*" the poor prey as already expressed by Ellis in *St. James's Chronicle* [4].

The secretory process can be induced by pure chemostimulation. In his early experiments, Darwin placed a small piece of meat on the open traps which led to secretion [6] (Appendix Figure 61). However, in nature, chemosensing might be needed to adjust the composition of the digestive enzyme cocktail [90].

Along with secretion, gene expression of nutrient transporters such as *AMT1, HAK5, HKT1* is induced within 2-4h, reaching a peak after 12h [56]. Indeed, DmAMT1 has been electrophysiologically characterised as an ammonium-selective channel found in the glands, and thus responsible for prey-derived nitrogen compounds absorption [112]. Similarly, DmHKT1 has been shown to mediate prey-derived sodium uptake [67]. As for K^+ acquisition, DmKT1 is responsible for high-capacity and DmHAK5 for H^+-driven high-affinity K^+ uptake, both of which are activated by Ca^{2+}-dependent kinases (CBL-CIPK) [113].
Besides this, endocytosis is also essential for the uptake of other nutrients, such as bigger molecules (peptides, amino acids) [114].

At the end of digestion, the digestive secretion along with the nutrients is reabsorbed. After 5-14 days, depending on the prey size, **the trap reopens** exposing the dry empty and light exoskeleton of the small arthropod which can be easily brushed off by the wind, and the trap is ready for the next capture [90].

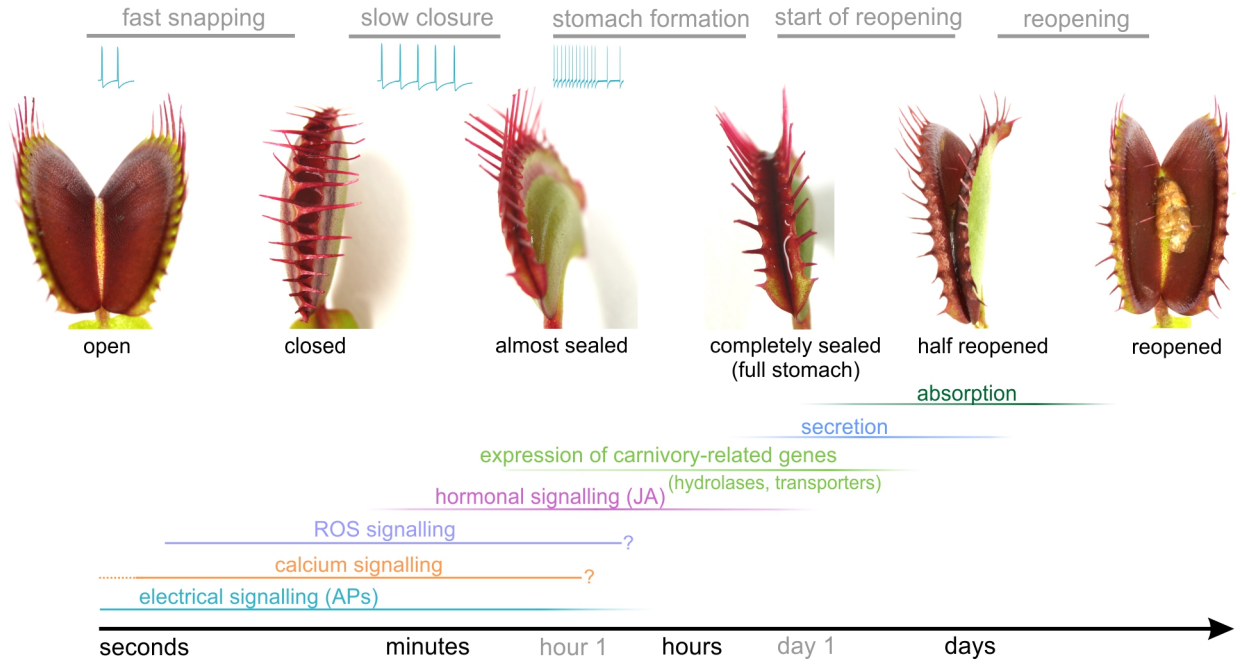

Figure 4: *Dionaea*'s hunting cycle with underlying molecular signalling pathways and their relative active period throughout the cycle [115]. The fast APs are the first to alarm the plant of possible prey capture, accompanied by Ca^{2+} signalling. It is not clear yet how Ca^{2+} is involved in later steps of the digestion. ROS may play an important part in signalling as well (as it has been shown in other carnivores [116, 117]), but very little is known up to know. These fast responses trigger JA signalling, from JA biosynthesis to JA-dependent activation of TFs. This leads to the expression of carnivory-related genes (such as: hydrolases for prey digestion, transporters for nutrient absorption and secondary metabolites with antiseptic properties). The acidic digestive fluid is secreted via exocytosis and the resulting nutrients are absorbed via transporters/channels and endocytosis. When all the liquid is resorbed, the trap is ready to reopen and start the cycle again. The whole cycle can take between 3 days up to 4 weeks depending on prey size, time of the year and fitness of the plants. (Photos taken by the author.)

1.4 Snap Trap Closure Mechanism

For more than 200 years, the spectacular mechanism that made humankind think differently about plants - the fast thigmonastic motion of the Venus flytrap - is still intriguing. There is no clear answer that describes and proves how the underlying mechanism works, leaving the mystery still unsolved.

Darwin was one of the first to study the closure mechanism, by marking the upper and lower trap surface with ink dots and observing how the distance between the dots changes after closure. He proposed that the "contraction" of the upper surface of the trap is important for the fast movement [6]. Other naturalists at that time built up on this idea, adding that an expansion of the lower surface is also needed [118] and that changes in turgescence of the lower parenchyma layer are contributing to the movement [119]. Some interesting experiments done by Brown, made him conclude that the increase of the abaxial cell size is due to a sudden increase in osmotic pressure that stretches the cell walls which become "fixed" by growth (irreversible cell expansion). In these experiments, he observed how closed traps that were boiled in water reopened after transferring them into xylene (through alcohol) and closed again when transferred back to the water. He explains that this phenomenon is due to the precipitation of sugars, and therefore a loss in osmotic pressure in xylene solution, while the osmotic pressure of the lower layer of cells is regained when transferred back to water. Brown argues that it is unlikely that sufficient water could enter the lower cells, thus causing an effect, without other "helping" mechanisms [118]. Others have taken the idea of cell growth further, arguing that this cell expansion is only possible due to cell wall acidification. Their experiments showing rapid closure of traps infiltrated in acid buffers (with the best response for cell wall pH 4.5) and no closure in neutral buffers, made them propose that the fast closure is due to a very fast proton pump that can induce a very fast acid-stimulated growth response [120].

Therefore two main theories were born: **(i)** the hydraulic model (swelling and shrinking mechanisms) and **(ii)** the fast acid growth theory.

Hodick and Sievers doubt both theories, objecting against the loss of turgor pressure in the upper epidermis as well as the acid-induced rapid cell wall loosening explanation, giving the following reasons: **(i)** a rise in apoplastic K^+ concentration from 1 to 10 mM should reduce the AP by 35%, which does not happen, **(ii)** the upper epidermal cells retain an osmolality which is similar to that of mesophyll cells based on their measurement, **(iii)** and apoplastic pH change from 6 to 4 should also reduce the APs by 33%, which does not happen, **(iv)** buffering the apoplast at pH 6 does not prevent trap movement from their experiments. The authors argue that: "*it is very likely that mesophyll cells are already extensible but are kept compressed in the open trap, thus developing tissue tension*". They also account for the shape of the trap lobes. They correlate the orientation and a large number of microfibrils in the anticlinal cell walls of the upper epidermis as well as mesophyll cells with the turgor-driven extension of mesophyll cells in the direction of their axes (from midrib to rim), while an increase in cell diameter is prevented by the hoop-like cellulose alignment [121]. This is one of the very few studies that proposes the mesophyll tissue as a driving force for the trap movement, while the epidermal cells control the "expression" of the movement through their extensibility [122].

More recent models support the idea that the fast motion is hydraulically driven [91, 123]. The most accepted model so far, by Forterre and colleagues, assert the importance of snap-buckling instability for amplifying the speed, considering that water transport alone, across 0.5 mm trap lobe thickness, cannot account for such a fast snapping mechanism [124]. Using the old ink-dot method, they calculated the strain field due to closure. Interestingly, the maximum strain of 9% was on the outer layer in the direction perpendicular to the midrib and only 1% strain on the inner layer [97]. Therefore the shell-like geometry of the trap lobes plays an important role in the snapping mechanism by allowing for hydraulically driven lobe deformation. Further on, the same team measured the pressure and poroelastic properties of the cells using a microfluidic pressure probe in the open state. The results suggest that the poroelastic time is much too slow (20-150 seconds) for the 0.1-second trap closure even including the buckling system, questioning the main theory of the hydraulic model of osmotically driven water transport between the cells [125].
Alternative models that do not rely on snap buckling have also been put forward. Markin and colleagues propose a new hydroelastic curvature model, in which different hydrostatic pressure can build up between the outer and inner layer of cells thanks to the trap's curvature elasticity. They suggest that aquaporins between the two main layers allow water to rush from one hydraulic layer to the other until the equilibrium configuration is reached - which is the closed state [126]. Considering that the opening of the trap is an irreversible growth mechanism [8], Joyeux proposes an elastic model in which the open state is the minimum elastic energy and where the strain field is highly anisotropic [127].

Other authors propose a very different closing mechanism that is based on the accumulation of so-called "trap-closing factors" (TCF) in a step-wise accumulation manner. They hypothesise that bioactive metabolites are released after each trigger hair stimulation until the threshold is reached, triggering ion channel opening responsible for the action potentials. Even though this hypothesis is the most different from the other more acceptable ones, their experiments are still intriguing. They isolated *Dionaea* extracts with so-called bioactive compounds from recently closed traps and inactive compounds from open / unstimulated traps. Afterwards, they fed these extracts to other traps via the petiole. The cut petiole with the connected adjacent trap was placed in a solution containing the bioactive or inactive *Dionaea* extract. Curiously, the traps fed with bioactive extract closed within 96 hours, while no leaf closure was observed for the plants fed with inactive extract [128].

Other unusual experiments, such as parabolic flight experiments, suggest that the closure is dependent on gravity. They show that traps respond faster in hypergravity and slower in microgravity [129]. This could be explained by a gravity-dependent open state probability of ion channels that are responsible for the APs [130]. However, further electrophysiological studies during parabolic flight experiments would be needed to confirm this.

1.5 The Action Potential of *Dionaea muscipula*

There are very few plants that can produce an all-or-nothing self-propagating fast and sharp action potential (AP) (Table 4). The first plant electrical signal was measured in *Dionaea muscipula* traps in 1873 by Burdon-Sanderson upon Darwin's request [59, 60]. The high robustness and reproducibility of *Dionaea*'s trap AP, makes it a perfect model organism for electrophysiological studies.

Table 4: The approx. AP duration and propagation velocities in different excitable plant species compared to non-excitable *Arabidopsis thaliana*.

Species	AP duration [s]	AP velocity [cm/s]	Bib
Dionaea muscipula	1	1-6	[131]
Aldrovanda vesiculosa	1	7.4	[73]
Drosera rotundifolia	10	0.5	[72]
Mimosa pudica	5	2-3	[132]
Arabidopsis thaliana	80	0.04	[65]

The resting potential in the Venus flytrap cells is around -140 to -120 mV, which might be maintained at such negative levels, like in other plant systems, by the H^+-ATPase. When trigger hairs (THs) are bent, and mechanosensory cells deformed, the AP originating at the base of the trigger hair, fires with an amplitude of about 100 mV. Thus, the depolarization reaches -20 to 0 mV, with an AP duration of 1-2 seconds [90] and a propagation velocity of 5-25 cm / second reported by older studies [64], and 1-6 cm / second (depending on the temperature) reported by the latest studies [131].

The very first step in AP generation is still unknown. However, very recently, the Venus flytrap mechanosensitive channel MscS-Like MSL, called by the authors FLYC1 (Flycatcher1), has been electrophysiologically characterised as a chloride-permeable stretch-activated channel, which might contribute to membrane depolarization [133].

Besides the electrical signalling, Ca^{2+} signalling goes hand in hand with the AP. For the first time, the AP together with the Ca^{2+} wave could be measured simultaneously in Ca^{2+} reporter GCaMP *Dionaea muscipula* transformed plants. Observing a very similar propagation velocity, Scherzer and colleagues propose that the two signalling types are synchronous, adding to the general belief that Ca^{2+} initiates the APs [131]. Unfortunately, the origin of Ca^{2+} influx is still unknown. There are several candidates, however, such as: the glutamate-receptors GLRs [65, 134], cyclic nucleotide-gated channels CNGCs [135, 136] and the hyperosmolality-gated Ca^{2+}-permeable channel OSCAs [137]. Besides OSCA, another mechanosensitive Ca^{2+}-channel candidate would be the Piezo channels[138].

An initial small depolarization caused by Ca^{2+} influx is thought to further activate Ca^{2+}-dependent anion channels / Cl^- channels, resulting in maximum depolarization of the membrane. This in turn activates voltage-gated K^+ efflux channels for repolarization of the membrane. Furthermore, a H^+ efflux via the AHA H^+-ATP-ase is thought to contribute to the AP repolarization and even hyperpolarization of the plasma membrane [32, 90, 131]. The membrane potential can be restored through an interplay between K^+ and H^+ influx [32, 131].

Even though there is a general idea on how the AP is generated (as described above), there is little evidence that proves these hypotheses, letting the AP-responsible channels / transporters / pumps undetermined thus far.

1.6 *Dionaea* 'ERROR' - A Cultivar That Lost the Ability to Snap

Dionaea has been cultivated ever since its discovery. Nowadays there are many carnivorous plant fanatic horticulturalists who sometimes deliberately expose plants (or seeds) to mutagenic chemicals (such as colchicine) [4]. Alternatively, mutations can occur randomly but might be enhanced or triggered by mass vegetative propagation. *Dionaea*'s genome is rich in transposable elements (TEs) [25], which upon activation might result in gene silencing or enhancement by getting inserted in the promotor region or even exonic region of a gene. This might give birth to a different phenotype than the original wild type (WT). This gave rise to as many as over one hundred *Dionaea* cultivars.

A cultivated variety, in short cultivar, is defined as a specific strain (or group of strains) of a plant species that can be perpetuated and sustained over time (through vegetative propagation or seed cultivation) [4]. In their book "*Dionaea - The Venus's Flytrap*", Bailey and McPherson bring together a collection of all known *Dionaea* cultivars. They describe all sorts of odd appearances: from fused teeth (*Dionaea* "Cross Teeth"), to fused trap-lobes (*Dionaea* "Triton"), from curled teeth (*Dionaea* "Umgekrempelt") to traps without teeth (*Dionaea* "Microdent"). There are even varieties with "gigantic" traps (up to 5.7 cm *Dionaea* "B52", "DC XL") or no traps at all (*Dionaea* "Rose").

The *Dionaea* "ERROR" mutant is another extraordinary cultivated variety, that at first glance, however, looks like the WT. It has, thus, a functional rather than morphological impairment: it is not able to snap its trap upon trigger hair mechanostimulation. This characteristic was discovered by chance, by the horticulturalist Mathias Maier in 2011. Since then, it has been officially registered in the ICPS (International Carnivorous Plant Society). ICPS is the International Cultivar Registration Authority (ICRA) for cultivated carnivorous plants, appointed by the International Society for Horticultural Science (ISHS) in order to maintain the order and avoid duplicated cultivars.
Here, the "ERROR" cultivar, or as I am going to refer to it throughout the thesis - the ERR mutant, is described as follows:

> *The inside of the traps and the marginal lashes of Dionaea 'ERROR' M. Maier develop pure reddish-purple colouration when exposed to direct sunlight. The exterior surfaces of the trap lobes are reddish and often bear a prominent red line below the margins of the lobes. The leaf bases and petioles are pure yellowish green.*

Also, the overall plant size is comparable with the WT, having an 8 cm long petiole and up to 3.2 cm long traps [4]. The plants are able to produce normal-looking flowers, but the seed viability hasn't been checked yet.
Its incapacity to snap can be used in contrast to a functional WT for studying key features that are necessary for a successful fast buckled closure. Since producing stable transgenic *Dionaea* lines has proven to be unsuccessful throughout the previous years, an inverse approach, by searching for transcriptomic differences in the ERR mutant's phenotype, might help us elucidate the molecular mechanosensing mechanisms of the charismatic Venus flytrap.

1.7 Study Objectives

With a fast reaction upon mechanostimulation and a sharp animal-like action potential (AP), *Dionaea muscipula* makes up the perfect organism to study plant sensitivity to touch. Additionally, it might give us insights into how plants have repurposed defence functions into carnivorous traits during their evolution in the plant kingdom.

The general objective of the present study is, thus, to expound upon the molecular basis of touch perception from AP initiation to stomach formation. In order to study *Dionaea*'s mechanosensing mechanisms together with their downstream components, two main ideas were followed:

1) Dissecting the emblematic AP of *Dionaea muscipula* in search of key molecular players (chapter 3.1) by:

   a) Analyzing the transcriptomic landscape that empowers the touch-sensitive trigger hairs to fire APs, in comparison to other non-specialised tissues and organs of *Dionaea muscipula* (chapter 3.1.2).

   b) Gathering more evidence for the molecular components that make up *Dionaea*'s AP by comparing electrogenic adult traps with juvenile traps that are not able to produce sharp APs (chapter 3.1.3).

2) Get a better understanding of the essential molecular mechanisms and pathways needed for a successful response upon mechanostimulation by comparing the transcriptomes of *Dionaea muscipula* functional wild-type traps with a non-functional *Dionaea muscipula* cultivar that is impaired in fast trap closure, such as the 'ERROR' phenotype (chapter 3.2).

2 Materials and Methods

2.1 Materials

2.1.1 Plant Material

2.1.1.1 Wild Type

Dionaea muscipula wild-type material was used for RNA-seq experiments as well as qPCR experiments and observational experiments.
Wild type *Dionaea muscipula* cultivated by Crescova Carnivora V.O.F (Netherlands) were purchased for all of the experiments. The plants were further grown under greenhouse conditions as follows: minimum 22°C during daytime and 18°C during nighttime, in a 16:8h light-dark photoperiod with a minimal light intensity of 130 µmol/m^2/s (SON-T Agro 400W, Phillips). The air humidity was maintained high with an automatic water spraying system.
All the analysed tissues (traps, petioles, roots and flowers) were cut and immediately frozen in liquid nitrogen. The plant material was then ground in liquid nitrogen until a very fine powder was obtained using mortar and pestle.

2.1.1.2 Trigger Hair Material

Trigger hair material was used for RNA-seq as well as qPCR.
Trigger hairs were harvested under the binocular by gently picking them up, being careful to include the podium cells, using tweezers. Three hundred trigger hairs were needed for one replicate coming from 50 different traps. In total three replicates were used for RNA-seq, making it almost 1000 hairs from 150 traps. Therefore, many people were needed to collect such a tremendous amount of hairs. The lab technicians Brigitte Neumann and Kerstin Neuwinger were helped by assistants, principal investigators and students at that time: Dr. Ines Kreuzer, Dr. Katharina von Meyer, Maria Albrecht, Julia Köber, Dr. Franziska Karl, Alicja Dembsky. Because of their small size and because of the time needed to collect them, the hairs were stored in RNAlater (Sigma-Aldrich, Taufkirchen, Germany, R0901-100ML) solution until RNA was extracted.

2.1.1.3 Juvenile Traps

Juvenile traps were used in comparison to fully grown adult traps for RNA-seq, qPCR and electrophysiological experiments. Different stages of juvenile traps, emerging from the centre of the rosette, were described by Casser in her PhD thesis, therefore we followed the existing nomenclature [106, 139] (Figure 5).
In order to identify traps that were not able to produce sharp action potentials (APs), different developmental stages were electrophysiologically analysed. The APs were induced by gently squeezing the unopened traps with tweezers. The tip of the tweezers was made out of a non conducting material (such as bone). In order to be consistent throughout the experiments, one representative juvenile stage which was not able to produce sharp APs and which was easily

identifiable throughout many intermediate developmental stages were chosen. Fulfilling these criteria and additionally being the closest stage to the adult traps (stage 6), were the juvenile (stage 5) traps. As it can be seen in Figure 5, the traps are easily recognisable by the zipper-like teeth and the position of the trap relative to the petiole (which is almost 180°).

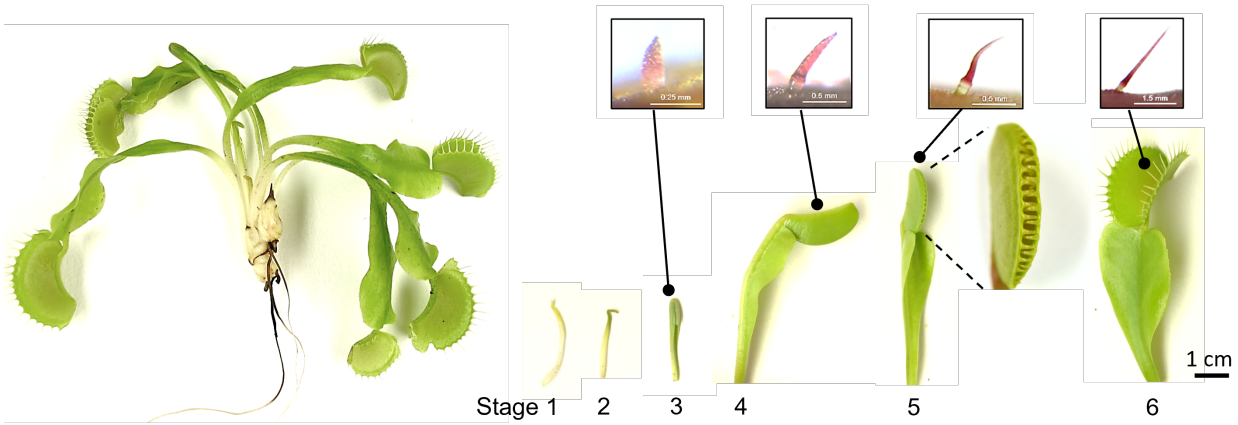

Figure 5: Trap developmental stages according to Casser [139] including trigger hairs for stages 3, 4, 5 and 6.

2.1.1.4 Trigger Hairs from Juvenile Traps

Trigger hairs from juvenile stage 5 were compared to adult (stage 6) throughout qPCR experiments (Figure 5). A glass pipette tip with 1 mm Ø was used in order to cut discs within the trap containing the trigger hairs for both juvenile (stage 5) and adult (stage 6) traps. For one replicate, 30 discs with trigger hairs (from 5 traps) were collected in screw cap tubes containing four metal balls which were placed in liquid nitrogen. The plant material was ground in the tissue-lyser for two minutes at a frequency of 30 Hz, while keeping the samples frozen by constantly adding liquid nitrogen to the cooling blocks. The RNA was then extracted from the frozen ground material.

2.1.1.5 The 'ERROR' Mutant Cultivar

Three 'ERROR' mutant cultivar plants were purchased from an amateur horticulturalist. The plants were further micropropagated by our collaborator, Prof. Dr. Traud Winkelmann from Leibniz Universität Hannover. Our technician, Brigitte Neumann, continued the micropropagation in sterile medium (1/2 MS with vitamins, 20% sucrose, 10 mg/l = 0,0465 mM kinetin, 0,6% agar, pH 5.6). The plants were transferred to soil (Patzer Erden, Blue Substrate, 12-00900) and were later acclimatised by keeping them in the greenhouse, in a transparent box chamber (for about 3 months), and gradually exposing them to the greenhouse air by opening the small window of the chamber. It normally takes between 3-5 years to obtain fully grown plants, in a sufficient number for the following experiments.

2.1.2 Chemicals, Reagents and Devices

In the following table (Table 5), all chemicals, reagents and devices that have been used during this study are listed.

Table 5: Reagents and devices used in this study

Reagent or device	Company
2-Propanol	BioChemica, AppliChem, Darmstadt, Germany
DEPC	Sigma-Aldrich, München, Germany
DNase I, RNase-free 1000 units 1u/ul	Thermo Fisher Scientific, Darmstadt, Germany
Ethanol	Carl Roth, Karlsruhe, Germany
Etyl acetate	Carl Roth, Karlsruhe, Germany
Experion RNA high sense analysis kit	Bio-Rad Laboratories, München, Germany
Formic acid	Carl Roth, Karlsruhe, Germany
Fruit Mate Solution	Takara, Saint-Germain-en-Laye, France
glycogen (RNA-Grade, 20mg/ml)	Thermo Fisher Scientific, Darmstadt, Germany
HH water (Wasser ROTISOLV HPLC Gradient Grade)	Carl Roth, Karlsruhe, Germany
M-MLV Reverse Transcriptase (RNase H-Point Mutant)	Promega, Walldorf, Germany
M-MVL RT 5x Buffer	Thermo Fisher Scientific, Darmstadt, Germany
NucleoSpin Plant RNA extraction kit	Macherey-Nagel, Düren, Germany
oligo-dT	Thermo Fisher Scientific, Darmstadt, Germany
RiboLock RNase Inhibitor 40 U/ul	Darmstadt, Germany
SYBER Green Enzyme Mix (AbsoluteSYBR Capillary Mix)	Thermo Fisher Scientific, Darmstadt, Germany
TCEP	Sigma-Aldrich, Taufkirchen, Germany
MiniSpin Plus microcentrifuge	Eppendorf, Hamburg, Germany
Nanodrop 2000c Spectrophotometer	Thermo Fisher Scientific, Dreieich, Germany
Centrifuge 5180R	Eppendorf, Hamburg, Germany
Centrifuge 5424	Eppendorf, Hamburg, Germany
Eppendorf Realplex Mastercycler system	Eppendorf, Hamburg, Germany
Experion automated electrophoresis system	Bio-Rad Laboratories, München, Germany
Mastercycler (PCR cycler)	Eppendorf, Hamburg, Germany
SpeedVac Vacuum	Martin Christ, Osterode am Harz, Germany

2.1.3 Bioinformatic Tools, Software and Programs

Computational demanding tasks were performed on the CCTB's (Center for Computational and Theoretical Biology) high-performance compute cluster (HPC) which contains seven compute nodes, 360 cores and storage systems (116TB + 232TB). The HPC runs on Linux (20.04.3 LTS Focal Fossa) and jobs can be submitted to Slurm Workload Manager (version 19.05.5).

Table 6: Main software used in this study

Software	Version	Ref
FastQC	0.11.5	[140]
multiQC	1.5	[141]
STAR Aligner	2.5.0a	[142]
HTseq	0.11.0	[143]
DEseq2	1.30.1	[144, 145]
Ontologizer	2.1	[146]
Mercator/MapMan	3.6 and 4	[147, 148]
FIMO (from MEME suite)	5.0.2	[149]
Cytoscape	3.8.2	[150]

2.2 Methods

2.2.1 Wet Lab Methods

2.2.1.1 Action Potential Measurements

Surface electrodes were used for measuring action potentials (APs). One silver electrode was inserted into and intact healthy trap (usually into the midrib) and another one was grounded into the soil of the pot. The electrical signal was amplified (100x) and recorded with PatchMaster software (from HEKA).

2.2.1.2 Timelapse of Trap Closure and Trap Opening Angle Measurements

Timelapse photography was used for detecting small and slow trap movements after trigger hair stimulation in 'ERROR' mutant traps. For the wild type, normal speed videos were recorded. For the 'ERROR' mutant hyperlapse videos (8x faster) were recorded using Samsung Galaxy A71 camera. The traps were positioned (in a lightbox for photography) with the distal part facing the camera in such a way that the trap angle was clearly visible. The videos were further loaded in ImageJ (version 1.53f51) from Fiji, and the trap opening angle was measured manually. In order to be consistent throughout the measurements, three reference points were used: the left lobe rim (outer part), the midrib (lower part) and the right lobe rim (outer part). The angles were measured for each sample every minute.

For curvature of trap lobes, ImageJ Kappa-plugin was used. The trace was set manually and average values were used.

2.2.1.3 RNA Extraction

For RNA isolation, NucleoSpin Plant RNA extraction kit (Macherey-Nagel, Düren, Germany) was used. Additionally, the Fruit Mate Solution for RNA purification (Takara Bio Eurore, SAS, Saint-Germain-en-Laye, France) was used to reduce the large amounts of polysaccharides and polyphenols that are usually found in *Dionaea* traps.
The plant material was ground in liquid nitrogen using a mortar and pestle (which were previously cleaned and incubated in a dry oven at 220° in order to destroy any RNases before use).

As a preparation step, 350 µl of Fruit Mate Solution was added to the powdered plant material and vortexed immediately for 20 seconds, then centrifuged for 10 minutes at 4° at 14000 x g. The supernatant was transferred in a 1.5 ml Eppendorf tube together with 350 µl RAP lysis buffer provided by the kit. In plus, 3.5 µl TCEP (Tris(2-carboxyethyl)phosphine hydrochloride, 0.5M, pH7, Sigma-Aldrich) was added for preventing RNA degradation. The total volume of about 700 µl was applied to the NucleoSpin Filters provided by the kit and centrifuged for one minute at room temperature (11000 x g) for homogenization and reduction of lysate viscosity. The flow-trough was mixed with 700 µl 70% Ethanol (Carl Roth, Karlsruhe) in a new Eppendorf tube and 350 µl of the volume was applied to the NucleoSpin RNA Plant Columns for

binding the RNA to the membrane, and further centrifuged for 30 seconds at room temperature (11000 x g). The flow-through was discarded and the column was washed as described in the kit's protocol. For the first wash, 200 µl of RAW2 kit's wash buffer was added to the NucleoSpin RNA Plant Column and centrifuged for 30 seconds at room temperature (11000 x g). Afterwards, the flow-through was discarded. For the second wash, 600 µl of RA3 kit's wash buffer was added to the column and centrifuged for 30 seconds at room temperature (11000 x g). Finally, for the third wash, 250 µl of RA3 wash buffer was added to the column and centrifuged for 30 seconds. The 2 ml collection tube was changed and the empty column was centrifuged for another two minutes to completely dry the membrane. In the end, the NucleoSpin RNA Plant Column was placed in a new 1.5 ml Eppendorf tube. For elution, 30 µl of DEPC-treated water (Diethyl pyrocarbonate 0.1 % (v/v), Sigma-Aldrich, München, treated and autoclaved water) was applied to the membrane and left at room temperature for one minute. Afterwards, the samples were centrifuged for 1 minute at 11000 x g. For a higher yield and higher concentration, the elute was applied once more to the column for re-elution.

RNA quantity and quality were determined by either Nanodrop 2000c Spectrophotometer (Thermo Fisher Scientific, Dreieich) measurements or by capillary electrophoresis (Experion automated electrophoresis system and Experion RNA high sense analysis kit, Bio-Rad Laboratories, München). A dilution of 1:20 of each sample was loaded into the chip wells according to the kit's protocol.

The samples with a high RNA quality were further processed and treated with DNase in order to remove the DNA contamination. Each sample was adjusted to the final volume of 30 µl using: 3 µl of DNase Buffer (10x Reaction Buffer with $MgCl_2$ for DNase, Thermo Fisher Scientific, Darmstadt, Germany), 0.5 µl RNase inhibitor (RiboLock RNase Inhibitor 40 U/ul, Thermo Fisher Scientific, Darmstadt, Germany), 1µl of DNase (DNase I, RNase-free 1000 units 1u/ul, Thermo Fisher Scientific, Darmstadt, Germany) and for each sample, the volume of RNA needed for a concentration of 1µg / 30µl was calculated. The dilution was done by adding DEPC-water up to the final volume of 30 µl and left for the reaction to take place at 37°C for 30 minutes. Afterwards, the RNA was precipitated with isopropanol on ice by adding: DEPC-water up to 100 µl, 0.1 volume of NH_4-Acetate (5mM in EDTA), 0.6 volume of isopropanol (2-Propanol BioChemica, AppliChem, Darmstadt, Germany) and 1 µl glycogen (RNA-Grade, 20mg/ml, Thermo Fisher Scientific). The samples were gently mixed and let to precipitate overnight at -20°C. The next day, RNA was pelleted, washed with 70% EtOH and dried as described above. The pellet was re-dissolved in 7 µl of DEPC-water and kept at -20°C until use.

2.2.1.4 qPCR

In order to study gene expression, quantitative PCR (qPCR) was performed using Eppendorf Realplex Mastercycler system or Mastercycler (Eppendorf, Hamburg, Germany) for different experiments.

The extracted RNA, was further transcribed into cDNA. For the reverse transcription reaction, the following master mix was added to the 7 µl of RNA: 2 µl Buffer (M-MVL RT 5x Buffer, Thermo Fisher Scientific), 0.5 µl of dNTPs (dNTP Set, 100 mM Solutions, Thermo Fisher Scientific), 0.4 µl of oligo-dT (Thermo Fisher Scientific). The samples were incubated at 70°C

for two minutes, and only afterwards the M-MLV Reverse Transcriptase (RNase H-Point Mutant, Promega, Walldorf, Germany) was added: 0.4 µl for each sample and incubated at 42°C for one hour. The samples were kept at -20°C until use. Or used right-away for qPCR.

For the qPCR, a dilution of 1:20 of the cDNA samples was used. 2 µl of the diluted samples were added into 18 µl master mix placed in each plate well. The master mix consisted of: 8 µl of the primer mix and 10 µl of SYBER Green Enzyme Mix (AbsoluteSYBR Capillary Mix, Thermo Fisher Scientific).The primer mix consisted of: 6 µl forward primer, 6 µl reverse primer, HPLC-water up to 400 µl (HH water: Wasser ROTISOLV HPLC Gradient Grade, Carl Roth). For each gene of interest, one qPCR run was performed in a 96 PCR plate, using the following PCR programme steps: **(i)** 15 minutes at 95°C for the initial denaturation step, **(ii)** 15 minutes at 95°C for the denaturation step, **(iii)** 30 seconds at the specific annealing tempreture of each primer pair, **(iv)** 30 seconds at 72°C directly followed by **(v)** 20 seconds at 79°C for the extension step. The stpes (ii), (iii), (iv) and (v) were repeated 40-45 times. For the melting curve, the following steps were followed: 15 seconds at 95°C, 15 seconds at 70°C, five seconds at 95°C and two minutes at 40°C.
The sequences of all the primers pairs used throughout this study are listed in Appendix Table 14.

In order to find out the best annealing temperature for each primer pair, a temperature gradient (from 48°C to 67°C) PCR was run. The PCR product quantity and length was quickly checked via gel electrophoresis for each temperature. A high quantity would mean a better amplification, indicating which annealing temperature is the best. The obtained PCR products were cleaned using Qiagen MinElute kit and sequenced by LGC Genomics (Berlin, Germany) to make sure that the right transcript had been investigated.
For the qPCR, a standard series dilution in which the amount of PCR product is known was used as a reference. The PCR product sample was brought to a volume of 20 µl and a concentration of 10 ng/µl, and it was used as a stock solution to start the standard series dilution. Each standard had a final volume of 200 µl and the following concentrations: Std 1 = 10 ng/µl, Std 3 = 100 pg/µl , Std 5 = 1 pg/µl, Std 7 = 10 fg/µl, Std 8 = 1 fg/µl, Std 9 = 0.1 fg/µl, Std 10 = 0.01 fg/µl. The dilution was made using HPLC-water (HH water: Wasser ROTISOLV HPLC Gradient Grade - Carl Roth).

Knowing that:

$$1\ \mu g \text{ of } 1000 \text{ bp DNA} = 1.52 \text{ pmol} = 9.1 \text{ X } 10^{11} \text{ molecules [151]}$$

$$1 \text{ fg of } 1000 \text{ bp DNA} = 910 \text{ molecules}$$

The relative number of molecules in each well plate was calculated by transforming the SYBR Green I [fg] concentration (given by Realplex Mastercycler system program after the PCR run) into number of molecules, using the following formula:

$$\frac{910}{PCR\_product\_length[kbp]} SYBR\_GreenI[fg]$$

In all experiments, actin (*DmACT1*, GenBank:KC285589, Dm_00017292-RA) was used as a housekeeping gene. The number of relative transcripts of a gene of interest was normalised to 10 000 molecules of actin.

2.2.1.5 UPLC Measurements

The plant material was ground manually in liquid nitrogen using mortar and pestle. 200 mg of powdered plant material was then vortexed together with 960 µl ethyl acetate:formic acid (99:1) and 50 µl internal standard (IS) in a 2ml screw-cap tube. IS contained 1 ng/µl in acetonitrile: [$^{18}O_2$]OPDA, JA-Norvaline, [D_4]SA and [D_6]ABA). Ceramic beads were added to the samples and shaken in the tissue lyser machine for 3 minutes at a frequency of 30 Hz, followed by 2 minutes sonication and 10 minutes centrifugation at 20 000 x g at room temperature. The resulting supernatant was transferred to a new tube and evaporated in SpeedVac Vacuum concentrator (Christ, RVC 2-25 CD plus) at 40-50°C until completely dry. 960 µl ethyl acetate:formic acid (99:1) was added again to the dried pellet and the whole procedure was repeated 3 times. The final pellet was dissolved in 60 µl acetonitrile:water (1:1) and transferred into UPLC glass vial. The samples were stored at -20°C until processing. The UPLC measurements were done by Dr. Markus Krischke (Pharmaceutical Biology Department, University of Würzburg).

2.2.2 RNA-Sequencing Data Analysis

High-quality RNA was sent to GATC Biotech (nowadays Eurofins Scientific) where cDNA libraries were generated and sequenced on an Illumina HighSeq2000 platform using paired-end sequencing. Already published RNA-seq data includes *Dionea*'s tissues: petiole, flower, root, rim, trap, gland [25, 56] and trigger hair [102], which are deposited in GenBank's Sequence Read Archive (SRA).

2.2.2.1 Mapping and Quantifying Reads

After the quality check (FastQC High Throughput Sequence Quality Check Report version 0.11.5) [140] (see FastQC summary for all RNA-seq experiments Appendix Table 15, Appendix Table 16, Appendix Table 17), the paired-end reads (containing three replicates for each sample group) were mapped to the available *Dionaea muscipula* draft genome [25]. The mapping was done using STAR Aligner (version 2.5.0a [142]) with the basic options, following the manual instructions. For all the replicates more than 80% of the reads were mapped to the genome (see Appendix Table 18). Next, the quantification of the mapped reads was done using HTseq (version 0.11.0) [143] with the following options: `-f bam -r pos -s no -i transcript_id`.

2.2.2.2 Expression Analysis

RNA-seq data was further analysed using R-studio's DEseq2 package (version 1.30.1). The HTseq-generated raw counts were imported using the `DEseqDataSetFromHTSeqCount` function. Regularized log transformation, using the `rlog` function, transforms the raw count data (from HTseq) to a $\log_2$ scale in such a way that it minimizes differences between samples for genes with small counts, and additionally normalizes with respect to library size (or sequencing depth). The generated rlog data was used for PCA plots and sometimes genes expression plots. However, in order to further normalise for gene length, the `fpkm` function included in the DEseq2 package was used to calculated the FPKM (Fragments Per Kilobase of

transcript per Million mapped reads) values, which were also used for expression charts and heatmaps.

2.2.2.3 Differential Expression Analysis

For pairwise differential expression analysis, DEseq2 R package authors recommend un-normalized counts as input, since DEseq2 model internally corrects for library size. Pairwise comparison, usually comparing treatment group (Condition A) versus control group (Condition B), was done by differential expression analysis using `DESeq` function which is dependent on `estimateSizeFactors` function for "median ratio method" normalisation. In short: counts are divided by sample-specific size factors (calculated using Equation 5 in [144]) determined by the median of ratios of gene counts relative to the geometric means across samples for each gene. Differentially expressed genes (DEGs) were considered genes that passed the following filter thresholds: **(i)** for upregulated genes: $\log_2$FC value > 1, adjusted p-value < 0.05, base mean values of Condition A > 50 counts, **(ii)** for the downregulated genes: $\log_2$FC values $<$ -1, adjusted p-value < 0.05, base mean of Condition B > 50 counts. DEseq2 uses Wald test for p-value and BH (Benjamini-Hochberg) adjusted p-values for padj. The $\log_2$FC values indicate how much the gene's expression has changed between the pairwise comparison groups, on a logarithmic scale (with positive values showing upregulation and negative values showing downregulation). The base mean represents the average of the normalized count values (of the three replicates) divided by size factors, taken over all samples. Log_2FC values of DEGs were most of the time visualised as heatmaps.

For the trigger hair transcriptomic data analysis (Exp_TH), a stricter adjusted p-value was used (adjusted p-value < 0.001).

All the $\log_2$FC values for each pairwise comparison as well as average FPKM expression values for each condition for all the genes mentioned in the text or figures of Exp_ERR are shown in Appendix Table 20.

Please note that $\log_2$FC values were calculated from normalised counts. While the normalised counts only correct for sequencing depth, it is always indicated to look at other types of normalised expression, such as FPKM - which accounts for the gene length besides the sequencing depth.

2.2.2.4 Shannon Entropy Method for Tissue Specificity

The Shannon entropy method, described in the context of tissue specificity by Schug and colleagues [152], calculates two values: **(i)** the H_{gene}-value indicating the overall genes' specificity across all tissues - this value indicates if a gene is expressed strictly in only one tissue (H_{gene}-value < 0), or if a gene is expressed in multiple tissues (if the gene is highly expressed in all analysed tissue, it indicates a ubiquitous gene with a very high H_{gene}-value), **(ii)** the $Q_{gene|tissue}$-value - this value is attributed to each gene in each tissue (a low $Q_{gene|tissue}$-value would indicate a high specificity of that gene to that tissue and a very high value would indicate less specificity of that gene to that particular tissue). The tissue specificity was calculated as described in [25] running the R-studio script provided by Franziska Saul and Gergő Pálfalvi.

2.2.2.5 GO-Term Annotation and GO-Term Enrichment Analysis

The GO (Gene Ontology) terms were assigned by Niklas Terhoeven using Interproscan (version 5.25-64.0) on the reference genome of *Dionaea muscipula* [25] using the `-goterms` parameter [153]. The GO term enrichment analysis was done using Ontologizer (version 2.1) with Parent-Child-Union calculation method and Benjamini-Hochberg method for *p*-value correction. Genes with BH-corrected *p*-value < 0.05 were considered significantly enriched and subjected to ReviGO online tool [154] which summarizes the GO-term enrichment by clustering similar GO-terms in a treemap, thus reducing redundancy.

2.2.2.6 MapMan Bin Annotation and Bin Enrichment Analysis

Using the available *Dionaea muscipula* reference genome [25], the predicted assembled transcriptome was annotated using Mercator4 [148], a tool for plant functional annotation and classification. For the bin enrichment analysis, the MapMan 3.6.0RC1 [147] software was used, which allows for an *Overview Pathway Analysis* using Mercator4 annotated genes as mapping file. As an input, each list of Differentially Expressed Genes (DEGs) belonging to each of the Venn subsets, together with their $\log_2$FC values and the corresponding background (for which a zero value was attributed) were used.
The corresponding background consisted of genes not passing the established thresholds for DEGs (as explained in previous chapter 2.2.2.3). For the upregulated genes, the background genes were considered: **(i)** upregulated genes that don't have a significant adjusted *p*-value ($\log_2$FC > 0, padj > 0.05) + **(ii)** upregulated genes that have a significant adjusted *p*-value but are bellow the desired $\log_2$FC threshold of 1 ($\log_2$FC > 0, $\log_2$FC < 1, padj < 0.05) + **(iii)** upregulated genes that have a significant adjusted *p*-value but are bellow the desired expression value of 50 counts (*i.e*: Condition A (treatment group) < 50, padj < 0.05). For the downregulated genes, the background genes were considered: **(i)** downregulated genes that don't have a significant adjusted *p*-value ($\log_2$FC < 0, padj > 0.05) + **(ii)** downregulated genes that have a significant adjusted *p*-value but are above the desired $\log_2$FC threshold of -1 ($\log_2$FC < 0, $\log_2$FC $>$ -1, padj < 0.05) + **(iii)** downregulated genes that have a significant adjusted *p*-value but are bellow the desired expression value of 50 counts (*i.e*: Condition B (control group) < 50, padj < 0.05).

For the bin enrichment analysis, the BH-corrected *p*-value of Wilcoxon Rank Sum test calculated within MapMan 3.6.0RC1 software was used, which compares the $\log_2$FC value of one bin against all the other bins, and it does so for each bin. This is why, for the enrichment, the number of genes in one bin, as well as the $\log_2$FC values of the genes belonging to that bin, are both important. Taking into consideration that some of the genes belonging to the background have a considerable high $\log_2$FC value while having a statistically insignificant adjusted *p*-value (*e.g.*: $\log_2$FC $= 7$, padj $= 0.1$), might result in enriched bins due to highly expressed genes in the background rather than true DEGs. In order to prevent this, I attributed to all the genes belonging to the background a value of zero.

By performing an enrichment analysis of the MapMan bins for each of the double Venn diagram subsets, we could later carefully look at bins that are enriched (Wilcoxon Rank Sum Test BH-corrected *p*-value < 0.05) in the WT phenotype upon mechanostimulation (*e.g.*: AP_WT_only double Venn diagram subset) while the same bins were not enriched

(Wilcoxon Rank Sum Test BH-corrected p-value > 0.05) in the ERR mutant phenotype upon mechanostimulation (*e.g.*: AP_ERR_shared double Venn diagram subset) (Figure 50), due to the fact that in the ERR mutant those genes belonging to such a bin contains very few DEGs, and the DEGs that are present don't have extreme $\log_2$FC values (such as very high values for the upregulated or very low values for the downregulated genes). In this way, we wanted to check if there are major functional categories (or bins) of genes unresponsive to touch in the ERR mutant, therefore underrepresented (= not enriched) while being highly responsive in the WT, therefore strongly represented (= enriched).

2.2.2.7 Hypergeometric Distribution Test on MapMan Bins of Interest

In order to check if there is a significant difference between the number of Differentially Expressed Genes (DEGs) in each of the MapMan bins of interest (bins that are significantly enriched in the WT upon mechanostimulation while not being enriched in the ERR mutant upon mechanostimulation), a Hypergeometric Distribution Test was applied for each bin of interest. The hypergeometric distribution is used for sampling without replacement and it's characterized by the following formula: $\frac{k \cdot m}{m+n}$

Where m = number of DEGs in a bin of interest, n = total number of upregulated DEGs in one phenotype without m, k = total number of upregulated shared DEGs in both phenotypes. If we would consider DEGs as marbles, m would represent the number of total red marbles, (*i.e.*: for the upregulated subsets of the Venn diagram, number of genes in AP_WT_only subset in the bin of interest 12.1.3 = 3), n = number of green marbles (= total number of marbles – m) (*i.e.*: all the upregulated genes in WT – m = 1614 - m = 1611), k = how many times we draw marbles (*i.e.*: total number of upregulated shared DEGs = 752)(Figure 50).

For probability calculation, we wanted to answer the question: What is the probability of selecting $x = 1$ marbles from a sample of $k = 752$, taking from a bowl containing $m = 3$ red marbles and $n = 1611$ green marbles? For this, the `phyper` function of R studio (version 4.0.4) was used. A p-value < 0.2 was considered significant enough to show a tendency of having different number of DEGs than expected. In the same way, the expected number of DEGs together with its probability for the ERR mutant downregulated DEGs was calculated.

In this way, we could see if the difference in number of DEGs attributes to a bin of interest (*i.e.* enriched in WT, but not in ERR) is statistically significant.

2.2.2.8 Aramemnon Database for Permeome Annotation

Aramemnon - Plant Membrane Protein Database nomenclature and classification of transporters, channels and pumps which make up the plants' permoeome (or transportome) - was used to identify genes belonging to this category. The whole *Dionaea muscipula* transcriptome was blasted against the database by Dr. Rainer Schwacke.

2.2.2.9 Transcription Factor Network Analysis

Transcription factors (TFs) were selected based on Mercator4 annotation ("transcriptional regulation" bin). In total 846 TFs were upregulated in WT (which were not upregulated in ERR). The binding motif of each TF was searched within the Plant Transcription Factor Database (planttfdb.gao-lab.org). Since no TF database includes *Dionaea muscipula*, but only model plants, *Arabidopsis thaliana* orthologs were used instead. The *Arabidopsis thaliana* orthologs were identified by Mercator3.4 annotation tool based on best BLAST hit. In total 70 TFs had a known binding motif within the database. The motifs were scanned within the -2000 bp promoter region of each gene of *Dionaea*'s draft genome [25]. The upstream sequences were extracted from the draft genome by Matthias Freund during his master thesis [155]. The scan was done using FIMO tool (Find Individual Motif Occurrences, which is part of MEME suite, version 5.0.2) [149] on the command line with default parameters. The output contained the calculated *p*-values for each motif occurrence which were further converted to q-values following the Benjamini-Hochberg method. A filter of q-value < 0.05 was defined as the minimal false discovery rate at which a given motif occurrence was considered significant. Additionally, only genes that were upregulated DEGs upon mechanostimulation in WT and at the same time not DEGs in ERR upon mechanostimulation were selected. The network was visualised using Cytoscape (version 3.8.2) [150].

In this way, a TF-network which was "missing" (or not expressed) in the ERR upon mechanostimulation was obtained.

2.2.2.10 Jasmonic Acid Network

The JA network was built using different literature sources [156, 157, 158]. For visualisation, Cytoscape (version 3.8.2) was used together with the "Omics Data" visualizer plugin [159] for drawing heatmaps representing $\log_2$FC values in all five pairwise comparisons.

2.2.3 Experimental Procedure Description

2.2.3.1 Experimental Design for RNA-Seq

• **Name**: Exp_TH; **Date**: 12.2012 - 04.2013;
Treatment: None; **Material**: Petiole, flower, roots, rim, traps, glands, trigger hairs; **Description**: The experiment was done by our technician, Brigitte Neumann, as described in [56] and [102], while the data was analysed by the author; **Sample number**: 3 replicates per tissue group; **Methods**: RNA-seq; **Figures**: Figure 8, Appendix Figure 62, Figure 10.

• **Name**: Exp_ERR **Date**: 10.2017;
Treatment: mechanostimulation (10 APs, 1 AP/min); COR (100 µl 0.1 mM coronatine) **Material**: WT and ERR traps; **Description**: The experiment was done by our technician, Brigitte Neumann, while the data was analysed by the author. The mechanostimulation was done by touching the trigger hairs 10 times every minute. The first two APs were elicited consecutively (in a less than 30-second interval), while the rest were elicited every minute. For the WT, after the trap closure, the traps were gently squeezed for firing APs. The COR (100 µl 0.1 mM coronatine) treatment was applied by spaying untouched open traps. **Sample**

number: 3 samples per group (for one sample, 3 traps from 3 different plants were mixed together to get enough RNA); **Methods**: RNA-seq, qPCR; **Figures**: All figures from chapter 3.2.2

• **Name**: Exp_Juv (E06); **Date**: 23.08.2017;
Treatment: none; **Material**: WT juvenile (stage 5) and adult (stage 6) traps **Description**: Healthy and intact traps at the right stages were identified and harvested (not more than two days apart) by cutting them at the linker site and directly freezing them in liquid nitrogen. One pair of juvenile and adult traps were always collected from the same plant; **Sample number**: 3 samples (for one sample, 5 traps were needed, in order to get enough RNA, which were harvested from different plants); **Methods**: RNA-seq, qPCR; **Figures**: Figure 13; Figure 14, Appendix Figure 20.

2.2.3.2 Experimental Design of Various Experiments

• **Name**: E01; **Date**: 02.02.2017;
Treatment: mechanostimulation (10 APs, 1 AP/min); **Material**: WT traps, ERR traps; **Description**: For WT the mechanostimulation was done using a plastic stick which was placed inside the trap. After touching the trigger hairs two times, the trap closed, and half of the stick remained inside. The other half which was hanging outside, was used to gently move the stick in order to simulate the trigger hairs one time per minute, for 10 minutes, without hurting the glands. For ERR, because the trap of the ERR mutant didn't close after the induction of two APs, the plastic stick was used to brush the three trigger hairs of one lobe at once (which induces only one AP). One AP per minute was elicited, with the exception of the first two APs which were applied one after the other within 30 sec. **Time points**: 0 minutes (control), 30 minutes, 1 hour, 2 hours, 4 hours and 6 hours (after treatment); **Sample number**: 6 traps for each time point (2 traps/ plant); **Methods**: qPCR; **Figures**: Figure 29, Figure 30, Figure 33, Figure 47.

• **Name**: E02; **Date**: 23.03.2017;
Treatment: mechanostimulation, wounding; **Material**: WT traps, ERR traps; **Description**: For WT and ERR the mechanostimulation was done as described in E01. The wounding was done by crushing/hardly squeezing, one time, one trap lobe with sharp tweezers so that the tissue was destroyed and visible holes were made in the trap lobes. The experimental procedure was done with the help of Brigitte Neumann. The sample processing for UPLC measurements was done with the help of Ramona Börner; **Time points**: 0 minutes (control), 15 minutes, 30 minutes, 1 hour, 3 hours, and 24 hours (after treatment); **Sample number**: 6 traps for each time point (3 traps / plant); **Methods**: UPLC, qPCR; **Figures**: Figure 31, Appendix Figure 66.

• **Name**: E03; **Date**: 02.06.2017;
Treatment: Wounding; **Material**: WT traps and petioles, ERR traps and petioles; **Description**: For both WT and ERR traps, the wounding was done as described in E02. The petioles of both WT and ERR were wounded with the same sharp tweezers as used for traps, crushing the petiole in the middle (including the midvein); **Time points**: 0 minutes (control), 3 hours (after treatment); **Sample number**: 6 samples per time point (for WT and ERR traps: 3 traps / plant, for WT and ERR petioles: 2 petioles (from 2 plants) for WT and 3 petioles (from 3 plants) for ERR were sampled together in order to get enough plant material; **Methods**: UPLC,

qPCR (not shown); **Figures**: Figure 32.

• **Name**: E05; **Date**: 14.08.2017;
Treatment: none; **Material**: WT juvenile (stage 5) and adult (stage 6) trigger hairs; **Description**: The experimental procedure was done with the help of Dr. Sönke Scherzer and Dr. Jennifer Scherzer. The trigger hairs of both juvenile and adult traps were collected using a 1 mm Ø sharp glass pipette tip, in order to cut small discs containing the trigger hairs. **Sample number**: 3 samples for adult and 4 samples for juvenile trigger hairs (for one sample, 30 discs with trigger hairs from five traps were needed) **Methods**: qPCR **Figures**: Figure 14

• **Name**: E07; **Date**: 31.01.2018;
Treatment: COR (400 µl 0.1 mM coronatine); **Material**: WT traps; **Description**: The experiment was done with the help of Sonja Bauer. In total, 30 traps were placed in a Faraday Cage and impaled with surface electrodes in the midrib (3 traps per plant), inducing trap closure. The surface electrodes were left in the midrib throughout the whole experiment. After the impalement and labeling, the plants were left to recover for one hour and the APs were measured in order to be sure that all of them were healthy before applying the cornonatine treatment. The APs were elicited by gently squeezing the traps with plastic tweezers, which made the trigger hairs within the closed trap to bend. Next, the plants were left untouched for at least 20 hours when they fully reopened. The first APs measured for the mock group (before treatment), were elicited after 24 hours (after impalement) and they looked very sharp, indicating full recovery. Then, the COR treatment was applied by gently opening the traps and pipetting inside 400 µl of 0.1 mM coronatine (diluted in dd-water). For the control group, the same procedure was done using 400 µl of dd-water. The APs were elicited and measured each day for five days. After each measurement, five traps were harvested for RNA extraction and qPCR. In addition, for the qPCR, the control group consisted of intact untreated open traps (that haven't been impaled); NOTE: previous experiments have been done (such as water (instead of COR) vs impaled traps and water vs non-impaled traps) in order to check if the way the treatment was applied as well as if the impalement procedure had an effect on the expression of genes of interest. The results showed that the impalement, had very little effect on the expression. **Time points**: 0 days (control), 1 day, 2 days, 3 days, 4 days and 5 days (after treatment); **Sample number**: 5 samples per time point (from 5 different plants); **Methods**: AP measurements, qPCR; **Figures**: Figure 16, Figure 17.

• **Name**: E09; **Date**: 21.03.2018;
Treatment: Insect (*Acromyrmex sp.* ant); **Material**: WT traps; **Description**: The experiment was done with the help of Sonja Bauer (who besides helping during the experiment, she also continued further sample processing such as RNA extraction and qPCR). The same procedure was followed as described for E07, but instead of COR, one ant was placed in each trap. The ants were previously kept at 4°C for no more than 10 minutes, in order to slow them down for easier manipulation. They restarted their activity shortly after being brought at room temperature. The experiment was designed for a longer period. The APs were measured every day, until the traps started to reopen, finishing the digestion; **Time points**: 0 days (control), 3 day, 5 days, 7 days, 9 days, 11 days, 13 days (after treatment); **Sample number**: 7 samples per time point (from 7 different plants). Some traps did not reopen and dried out after the digestion, leaving 4-3 traps per time point in the later time points; **Methods**: AP measurements, qPCR; **Figures**: Figure 18, Figure 19.

• **Name**: E10; **Date**: 20.06.2018;
Treatment: None; **Material**: WT juvenile trap (stage 5), intermediate steps (5.1, 5.2) and adult traps (stage 6); **Description**: The four different developmental stages were identified and described as follows: stage 5 - closed traps with teeth pointing inside the trap looking like a zipper, stage 5.1 - straps with teeth emerging outside of the still-closed trap, stage 5.2 - semi-open trap with teeth intercalated, stage 6 - fully open adult trap. The colour is also a good indication for the developmental stages, especially for the semi-open traps that open for the first time, as they are always light green (or even green chartreuse) compared to the adult traps which are either darker green or many times red (inside). Six traps for each of the described stages were impaled with surface electrodes and left to recover for 24 hours. For the elicitation of an AP, the closed traps were squeezed very gently with a boned tip tweezers three times (1 AP per minute, maximum 4 times), and for open (including semi-open) traps the trigger hair was touched with a plastic pipette tip. Right after the third AP, each trap was harvested and frozen in liquid nitrogen, one by one. Additionally, another control group consisting of adult unimpaled traps were also harvested; **Sample number**: 6 samples per group; **Methods**: AP measurements, qPCR; **Figures**: Figure 12, Figure 15.

• **Name**: E16; **Date**: 29.09.2020;
Treatment: Different numbers of APs (10 and 20) at different frequencies (1 AP / 15 seconds, 1 AP/ 30 seconds and 1 AP / 60 seconds); **Material**: WT and ERR traps; **Description**: Around each trap sample, a round white paper was attached like a collar around the linker (between the trap and the petiole), without touching the trigger hairs. This assured a white background in order to easily distinguish the trap angle. The paper collar was attached at least 20 minutes prior to starting the experiment. Each plant pot was placed in a photo box in front of the camera in the same position (in which the trap angle was clearly visible). Hyperlapse (x8 times faster) videos were recorded with Samsung Galaxy A71 camera. For the ERR, the trigger hairs were touched in order to induce the APs with different numbers and frequencies and the recording was run for at least 20 minutes. Each sample was measured individually. Since the purpose of the experiment was to see how many APs and under which interval would the ERR mutant traps close, for the WT (which is closed after two APs) only two APs were applied (for each of the mentioned frequencies). **Time points**: 0-20 and 0-30 minutes; **Sample number**: 12 samples for ERR and 6 samples for WT, per group; **Methods**: Timelapse and trap opening measurement; **Figures**: Figure 25, Figure 26.

• **Name**: E17; **Date**: 24.11.2020;
Treatment: 2 APs (1 AP / 30 seconds); **Material**: WT and ERR traps; **Description**: The experiment procedure was the same as described for E16, with the exception that the white paper collar was applied 24 hours prior to starting the experiment; **Time points**: 0-20 minutes; **Sample number**: 9 samples for ERR and 3 samples for WT; **Methods**: Timelapse and trap opening measurement; **Figures**: Figure 24

• **Name**: E18; **Date**: 15.01.2021;
Treatment: COR (400 µl 0.1 mM coronatine); **Material**: WT and ERR traps; **Description**: The experiment procedure was the same as described for E16. However, instead of mechanostimulation, COR was sprayed on the open traps. Each trap was recorded individually for 48 hours. The timelapse recording was done a with Cannon camera (1 frame per minute). **Time points**: 0-48 hours; **Sample number**: 10 samples per group; **Methods**: Timelapse and

trap opening measurement; **Figures**: Figure 27.

• **Name**: E22; **Date**: 01.06.2021;
Treatment: Different number of APs (20, 120 continuously or 120 interrupted) with a frequency of 1 AP / 30 seconds; **Material**: WT and ERR traps; **Description**: The AP induction was done as described in E01. The elicitation of 20 APs with a frequency of one AP every 30 seconds takes 10 minutes. 120 APs were induced continuously for one hour (1 AP / 30 seconds) or interrupted, in 20 APs blocks (repeated 6 times) as follows: 10 minutes of 20 APs induction were followed by 50 minutes without any mechanostimulation, every hour for 6 hours; **Sample number**: 6 samples per group; **Methods**: The secretion of the mechanostimulated traps was measured using a filter paper which was placed inside the trap at the end of the experiment in order to absorb all the liquid. The filter paper was weighed before and after absorbing the liquid in order to identify the amount of secreted fluid; **Figures**: Figure 35.

Throughout the thesis, a consistent colour code was used for different treatments and tissues, in order to easily distinguish between charts of different experiments (Figure 6).

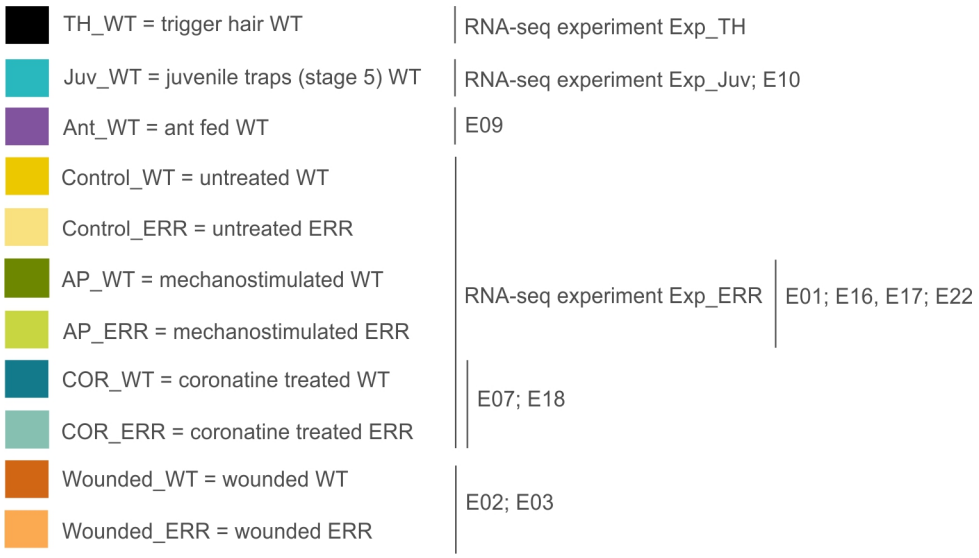

Figure 6: Colour code used throughout the thesis for the applied treatments in different tissues of WT or ERR cultivar, together with the experiments' names in which they were used.

3 Results and Discussion

3.1 *Dionaea muscipula* - A Model Organism for Plant AP Study

3.1.1 Short Introduction

In search of the molecular markers of the plant action potential (AP), *Dionaea muscipula* can be used as a model organism thanks to its iconic AP. As described in chapter 3.1.3, *Dionaea*'s AP is an all-or-nothing, sharp and robust electrical signal. This makes every experiment highly reproducible. Moreover, it is very easy to work with *Dionaea*, as it is a medium-sized plant which makes the electrodes impalement much easier (compared to *Aldrovanda* or *Drosera*).

Just like the animal AP, *Dionaea*'s AP also consists of distinct phases (Figure 7) : **(i)** depolarization - the membrane potential becomes less negative, **(ii)** repolarization - the membrane potential drops back to more negative values, **(iii)** hyperpolarization - is an overshoot of the repolarization, the membrane potential becoming even more negative than the initial resting potential, **(iv)** the recovery phase - the membrane potential is restored back to initial resting potential [90, 160].

Since the channels/transporters/pumps responsible for plant AP generation haven't been fully elucidated yet, we set up to investigate *Dionaea*'s emblematic AP. For this, we used two approaches: **(i)** we looked for trigger hair-specific genes (chapter 3.1.2) and **(ii)** we compared the non-excitable juvenile traps with excitable adult traps (chapter 3.1.3)).

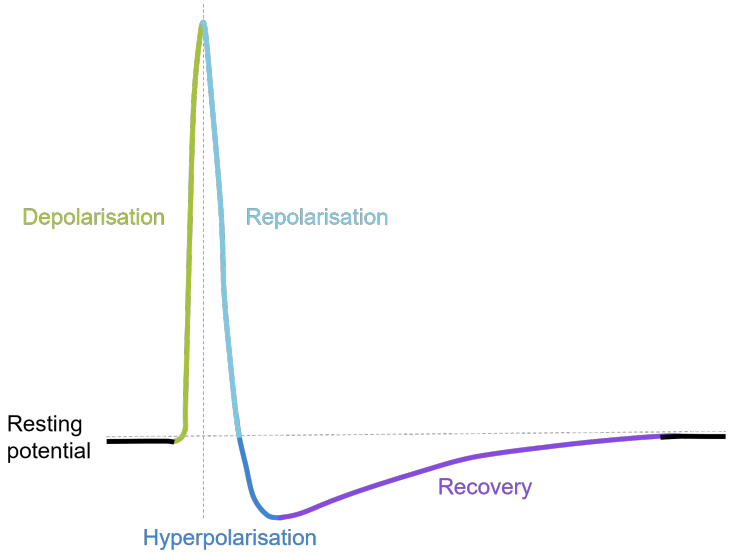

Figure 7: The action potential (AP) of *Dionaea muscipula*. Different AP phases are represented with different colours.

3.1.2 The Trigger Hair's Transcriptomic Landscape Reveals Highly Specific Electrogenic Channels

The results presented in this chapter (3.1.2) have been published as part of [102].

In order to better understand the molecular basis of *Dionaea*'s action potential (AP), we first looked at the transcriptomic landscape of its distinctive mechanoresponsive trigger hairs.

To decipher the unique molecular repertoire of the trigger hair (TH), we compared it to all the other *Dionaea* tissues. For this, RNA-seq data that was already available from flower, root, petiole, whole trap, trap rim, and glands [56] was used in addition to the trigger hair RNA-seq data (with three replicates for each tissue group).

The PCA-plot (Figure 8A) already gives us an overview of which tissues are more similar to one another since they would cluster closer together. We can therefore see, that the flower and root tissues are separated away from the rest of the tissue (based on the x-axes that give 59% of the variance) and that the trigger hair clusters closer to glands and trap tissues. To corroborate this assumption, we zoomed into the rest of the tissues excluding the flower and root. For this, I performed a correlation analysis (Figure 8B), which indeed shows that the trigger hair is most similar to the trap (0.76) and glands (0.59). This might be explained by the fact that trap is also an excitable tissue, capable of AP-generation upon wounding or upon strong mechanostimulation and highly specialised in AP propagation, while the trigger hair is designed to commence the AP and amplify the signal by reducing the force needed for AP-elicitation [105]. The similarity with glands can be explained by the possibility of a common evolutionary origin. As explained in chapter 1.1.2.2 and chapter 1.2.3.2, THs might have evolved from glandular structures, as they present a relict of an endodermoid layer which is prominent in digestive glands [43]. However, it could also be explained by a technical issue: gland-tissue contamination within the trigger hair tissue, since THs were collected at the base, ensuring that podium cells are included, several glands close to the trigger hair base might have been included as well.

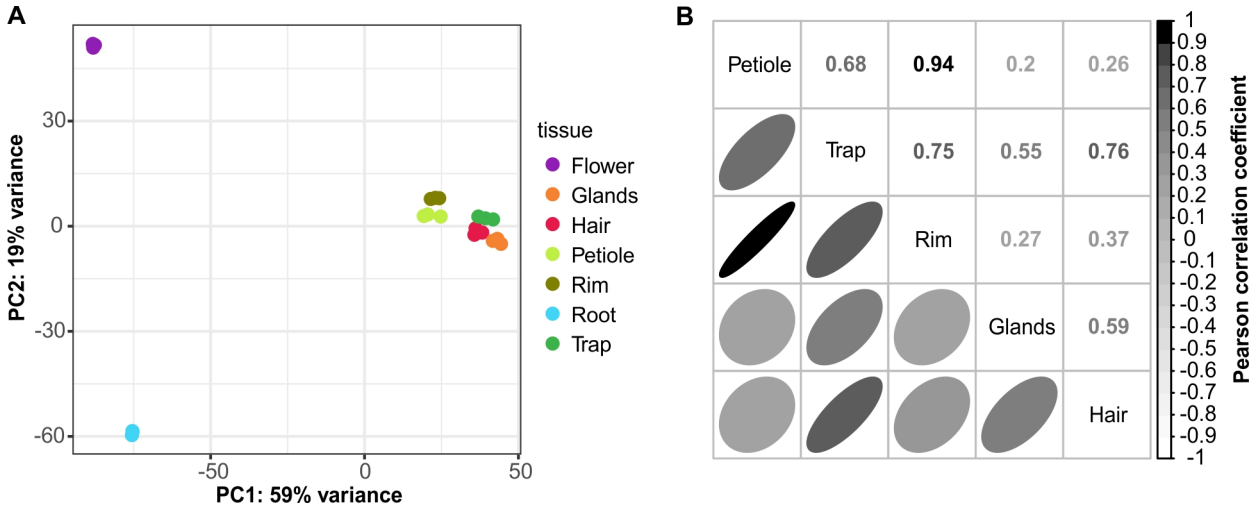

Figure 8: (A) PCA plot of all replicates of the analysed tissues (B) Pearson correlation analysis between analysed tissues

In order to identify the molecular elements that make the trigger hair so remarkable, we first had a look at genes that are upregulated in the hair compared to all the other tissues. For this, I performed a pairwise differential expression analysis and analysed the intersection of overlapping DEGs. In Figure 9 (subset 02), we can see that 810 genes are upregulated in the trigger hair by a factor of at least two against all the other tissues. I further carried out a GO-enrichment analysis for this particular subset, in order to have an overview of the function of this set of genes. Transcription- , ER- and CW-related GO-terms have been identified. This is not surprising, since the mechanoreceptor cells of the trigger hair have been reported to possess a highly developed ER and thick CW, which might both be essential as Ca^{2+}-storage sites [104, 106].
Sorting out the top highly upregulated DEGs in the trigger hair taking into account six pairwise comparisons would not be the best approach. Therefore, in order to have a better understanding of the top trigger hair-specific genes, another method was used: the Shannon entropy for tissue specificity.

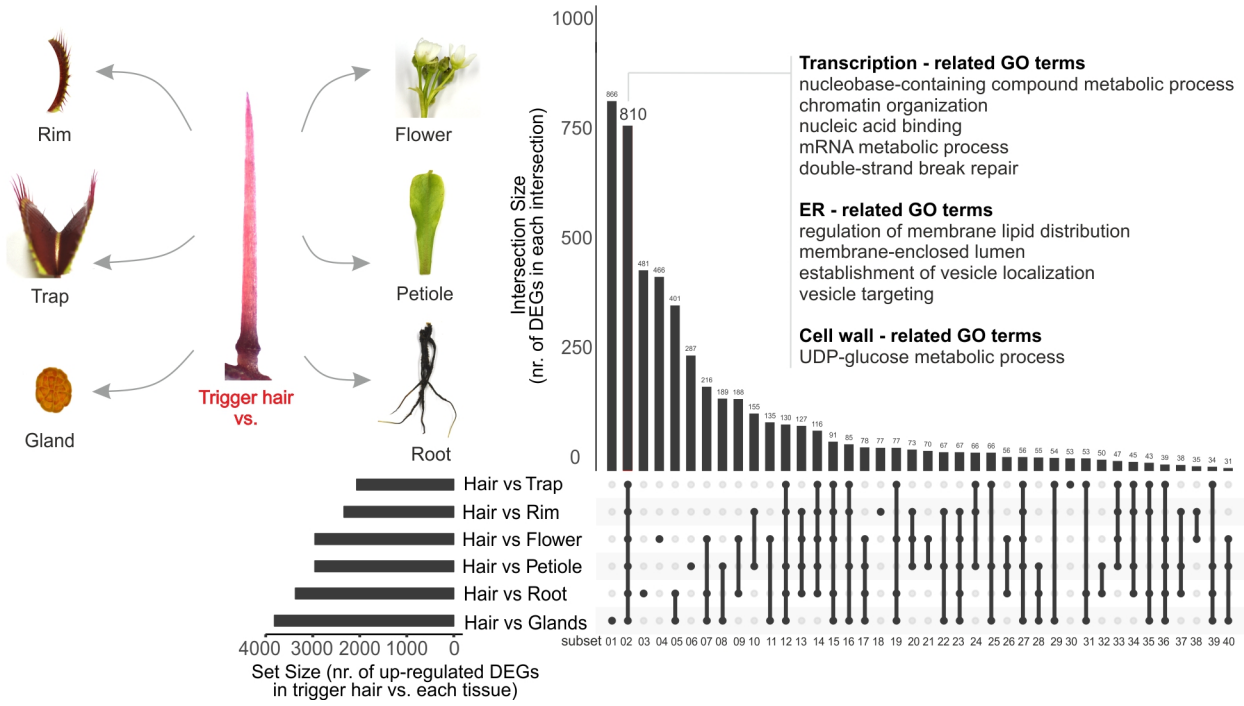

Figure 9: Intersection analysis of upregulated DEGs in the trigger hair. Trigger hair upregulated DEGs were considered genes with $\log_2$FC > 1 against all the other tissues (trap, rim, flower, petiole, root, and gland), BH adjusted p-value < 0.001, trigger hair normalized counts > 50. Enriched GO-terms for the subset 02 containing upregulated DEGs in the trigger hair vs all the other tissues are summarised.

The Shannon entropy method, calculates an overall tissue specificity (so-called H_{gene}-value) and a tissue-specific one, the so-called $Q_{gene|hair}$-value for each gene [152]. In this way, I was able to classify and order the genes according to their $Q_{gene|hair}$-value. The smaller the $Q_{gene|hair}$-value, the more specific that gene is to that particular tissue. That means, it has a high expression value in that particular tissue and very low expression values in the rest of the tissues.
As it turns out, the mechanosensitive channel *MSL10* is the most trigger hair-specific gene, with the lowest $Q_{MSL10|hair}$-value (1.13 bits) (Figure 10).

On the second place, the *Arabidopsis thaliana* KAT ortholog, a Shaker-type K^+ channel, that we named KDM1 (from $\underline{K^+}$ *Dionaea muscipula* 1) is also highly specific ($Q_{KDM1|hair}$-value = 1.70 bits). Remarkably, from the top five most specific trigger hair genes, four of them were channels. This aligns with the trigger hair's special function in AP-generation. The other two channels from top five are also electrogenic channels with a possible role in shaping the AP: the glutamate-receptor *GLR3.6.1* ($Q_{GLR3.6|hair}$ = 1.92 bits) and the K^+ outward rectifier *SKOR* ($Q_{SKOR|hair}$ = 2.15 bits). The GLRs have been shown to be important for the electrical signal and Ca^{2+} wave propagation in *Arabidopsis thaliana* [65, 134], while GORK (SKOR's ortholog) is involved in stomatal closure by the release of K^+ which leads to loss of turgor pressure in the guard cells [161, 162].
Of note, even though these genes are highly specific to the trigger hair, they are also expressed, though to a much lower extent, in the trap tissue, which is also electrically excitable.

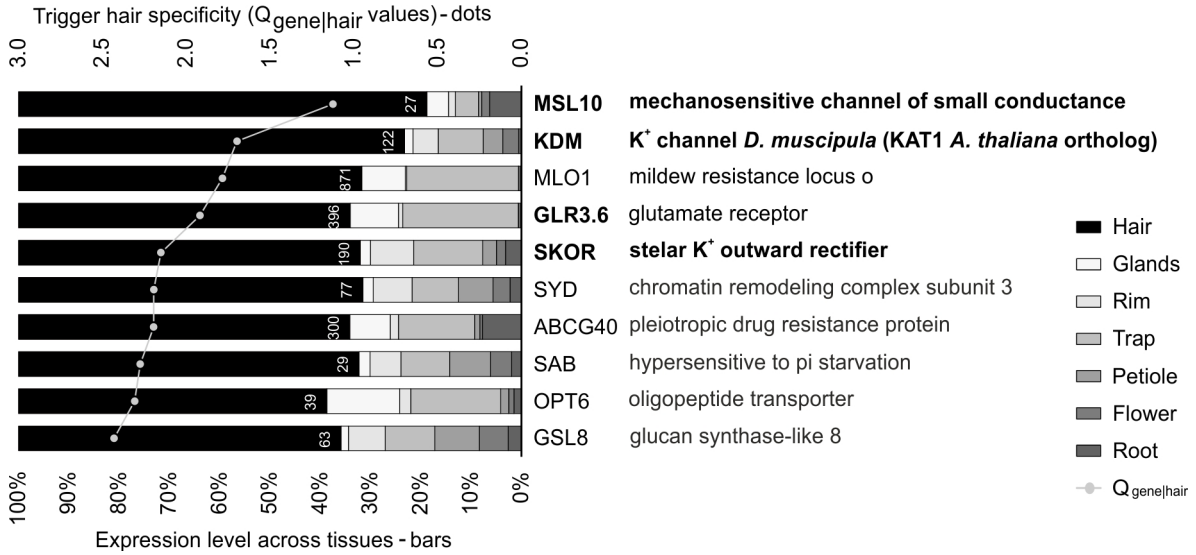

Figure 10: Top 10 highly trigger hair-specific genes. The bars represent the proportion of expression in each analysed tissue. The numbers on the bars represent the FPKM expression values in the trigger hair. The Shannon entropy Q-value for tissue specificity is represented with dots for each gene.

In search of other AP candidates, we next had a look at the whole trigger hair permeome (comprising all the channels, transporters and pumps). For this, all the transcripts were annotated using Aramemnon - Plant Membrane Protein Database [163]. Using a threshold of 1% (which corresponded to a $Q_{gene|hair}$-value of 3.9) [25], the whole trigger hair-specific permeome was identified. Besides the already mentioned channels, the H^+ pump *AHA4* ($Q_{AHA4|hair}$ = 3.19 bits) was also part of the trigger hair-specific list, along with other pumps such as the Ca^{2+} pump *ACA2* ($Q_{ACA2|hair}$ = 3.21 bits) and the Ca^{2+} exchanger *CAX9* ($Q_{CAX9|hair}$ = 3.74 bits). Additionally, the K^+ transporter *KUP8* ($Q_{KUP8|hair}$ = 3.64 bits) and other ABC-transporters were also identified (Appendix Figure 62).

To sum up, from this analysis we found out that the most remarkable genes with high expression values in the trigger hair compared to the rest of the analysed tissues were all electrogenic channels (*MSL10, KDM, GLR3.6, SKOR*), which might be involved in the generation and shaping of *Dionaea*'s AP.

3.1.3 Dissecting *Dionaea muscipula*'s Action Potential

3.1.3.1 Transcriptomes of Different Trap Developmental Stages Shed Light on Possible Candidates for Repolarization and Hyperpolarization

In order to gain more insight into the molecular components that give rise to *Dionaea*'s AP, we further carried out another comparison. This time, we did the comparison within the same tissue.

As one might expect, *Dionaea* traps are not always electrically-excitable throughout their entire life cycle. During their developmental journey, they only gain full excitability very late, as they become adult ready-to-snap traps. We took advantage of this observation and compared the transcriptome of juvenile traps with that of fully-developed adult traps.

For this, I had to identify the perfect juvenile developmental stage having two criteria in mind: **(i)** it should be easily distinguishable in the vast range of intermediate steps between newly emerged and fully mature trap, **(ii)** it should not be able to fire sharp all-or-nothing type APs. By measuring the APs of many juvenile stages, I came to the conclusion that stage 5 would be the most appropriate: easy to recognise with its zipper-like intercalated teeth and unable to fire sharp APs (Figure 11). It was also one of the closest stages to the adult traps (stage 6), which would narrow the differences in developmental-related genes. Casser [139] already described 6 developmental stages in *Dionaea*, therefore we followed the existing nomenclature (see Figure 5).

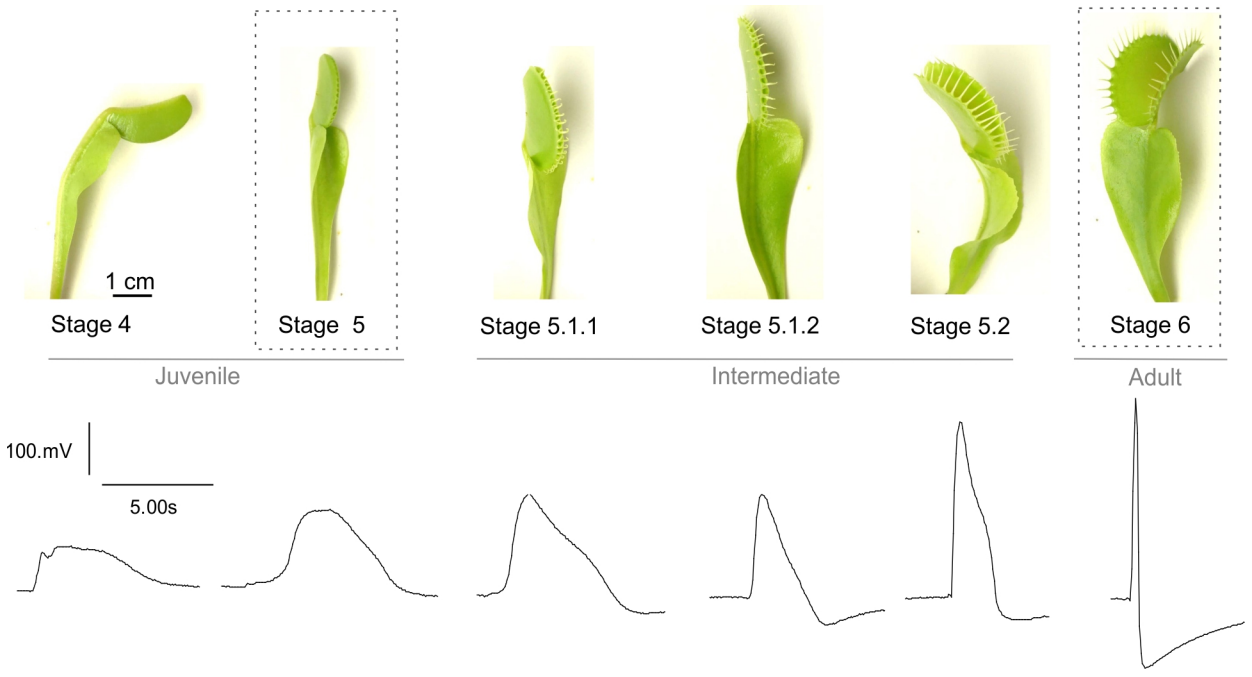

Figure 11: Trap developmental stages according to Casser [139]. Stages 4 and 5 (including intermediate stages) represent juvenile stages, while stage 6 is the final adult stage. Representative APs can be seen for each stage. Marked with dotted rectangle are stages used for RNA-seq (stage 5 and stage 6).

Since the shapes of the APs look very different in each of the developmental stages (Figure 11), I next quantified the entire AP duration, the depolarization and repolarization duration, and the hyperpolarization amplitude. It is easy to remark the strong discrepancy regarding the AP duration between stage 5 (with an average of 15 seconds) and stage 6 (with an average of less than one second) (Figure 12A). If we dissect the AP duration in its two major phases (depolarization and repolarization, Figure 7) which are divided by its peak, we can see that the repolarization duration is much larger (and more consistent) in juvenile stage 5 (on average 11 seconds) than the depolarization phase (on average three seconds) (Figure 12B,C). Therefore, the major player in a prolonged AP in juvenile stage 5, is rather a widened repolarization (and not so much the depolarization) phase of the AP. The hyperpolarization also plays an important role in shaping the AP, as it is almost completely missing from the juvenile stage 5 (Figure 12D).

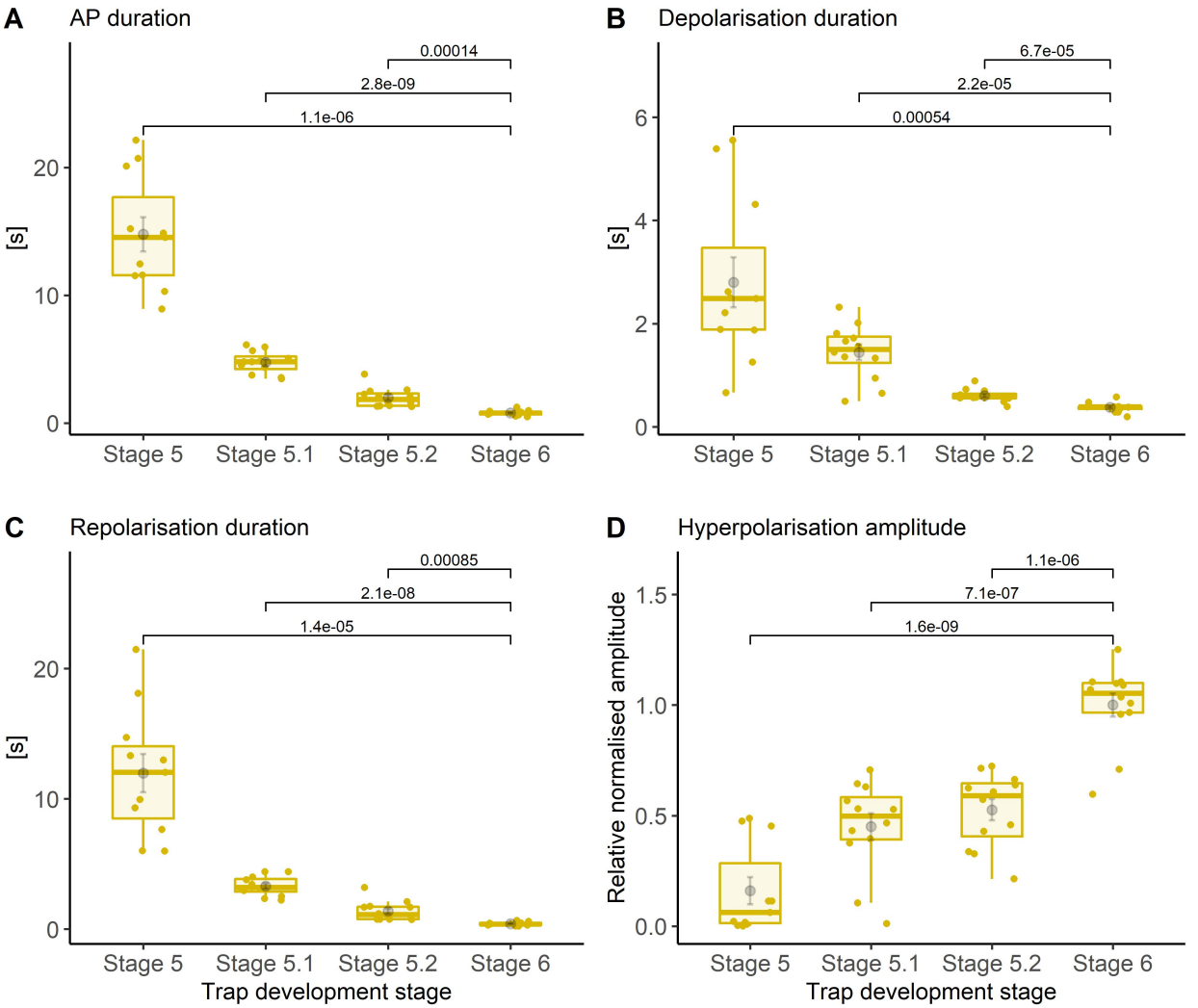

Figure 12: The whole AP duration (A), AP depolarization duration (B), AP repolarization duration (C) and AP hyperpolarization amplitude (D) in juvenile stage 5, intermediate stages 5.1 and 5.2 and adult stage 6. T-test p value can be seen for each group compared against the adult stage 6 group. The hyperpolarization normalisation was done by dividing each sample to the average value of the reference adult stage 6 group. Average value of each group can be seen as grey dot +/- SE. p value of Shapiro-Wilk normality test for each group > 0.05, indicating a normal distribution. $n = 12$

Knowing that there are differences regarding the electrical signalling capabilities, I next looked at differences at the whole transcriptomic level. Within the PCA analysis, the three replicates of each group are closely clustered together indicating small variance within groups (Appendix Figure 63A). The top 10 most variable genes, gives us an overview of the most prominent genes that have a large contribution to the differences between the two compared groups. Curiously, *XTH6* and *EXPA11* were highly expressed in the adult trap and not in the juvenile trap. This is interesting because both of them - having a cell wall modifying function - would be expected to play a role in cell growth and therefore have a higher expression in earlier developmental stages, as is the case for other species [164, 165]. This might point to a special carnivory-related role of these two genes in *Dionaea*'s adult traps. Another gene that might also be important for the carnivorous lifestyle, is *TCH2*, as it is highly expressed in the adult trap (with a very low expression in the juvenile traps) (Appendix Figure 63B).

In search of the underlying active genes, I performed a differential expression analysis between the adult trap (stage 6) and juvenile trap (stage 5), and selected only the genes annotated as part of the permeome (using Aramemnon - Plant Membrane Protein Database Classification). The term 'Permeome' refers to the sum of all permeable molecular structures embedded in membranes, such as: channels, porins, carriers/transporters and pumps [163].

Permeome annotated differentially expressed genes (DEGs) can be visualised as part of the Sunburst chart showing their classification into Aramemnon database nomenclature system, together with their $\log_2$FC values represented as a heatmap (Figure 13). Here we can spot, three glutame-receptor paralogs as part of the "Glutamate-gated Ion Channel" family, out of which *GLR3.6.1* has the highest $\log_2$FC value (*GLR3.6.1* / Dm_00002270-RA $\log_2$FC = 6.4 , *GLR3.6.2* / Dm_00012322-RA $\log_2$FC = 2.2 and *GLR3.4* / Dm_00004609-RA $\log_2$FC = 3.5). Next we can see *AHA4/HA4* H^+ pump (Dm_00013634-RA, $\log_2$FC = 5.8) together with other two H^+ pumps (*HA3* / Dm_00000738-RA $\log_2$FC = 3.1, *HA5* / Dm_00004749-RA, $\log_2$FC = 2.6). As part of the "Proton-dependent Oligopeptide Transporter" family within the "Major Facilitator" superfamily we can see: the multi-functional transporter *GTR2* (Dm_00010563-RA, $\log_2$FC = 4.7), the nitrate anion transporter *NPF6.2* (Dm_00000083-RA, $\log_2$FC = 4.15), the plant hormone transporter *NRT1.2* (Dm_00010884-RA, $\log_2$FC = 2.3) and the nitrate transporter *NRT2.5* (Dm_00019854-RA, $\log_2$FC = 2.3). Besides *GLR3.6*, we re-encounter the other trigger hair-specific channels *KDM1* (Dm_00004067-RA, $\log_2$FC = 3) and *SKOR* (Dm_00007946-RA, $\log_2$FC = 3.27). As a mechanosensitive channel [166], also worth mentioning is the hyperosmolality-gated Ca^{2+}-permeable channel OSCA1.7 (Dm_00005287-RA, $\log_2$FC = 2.82).

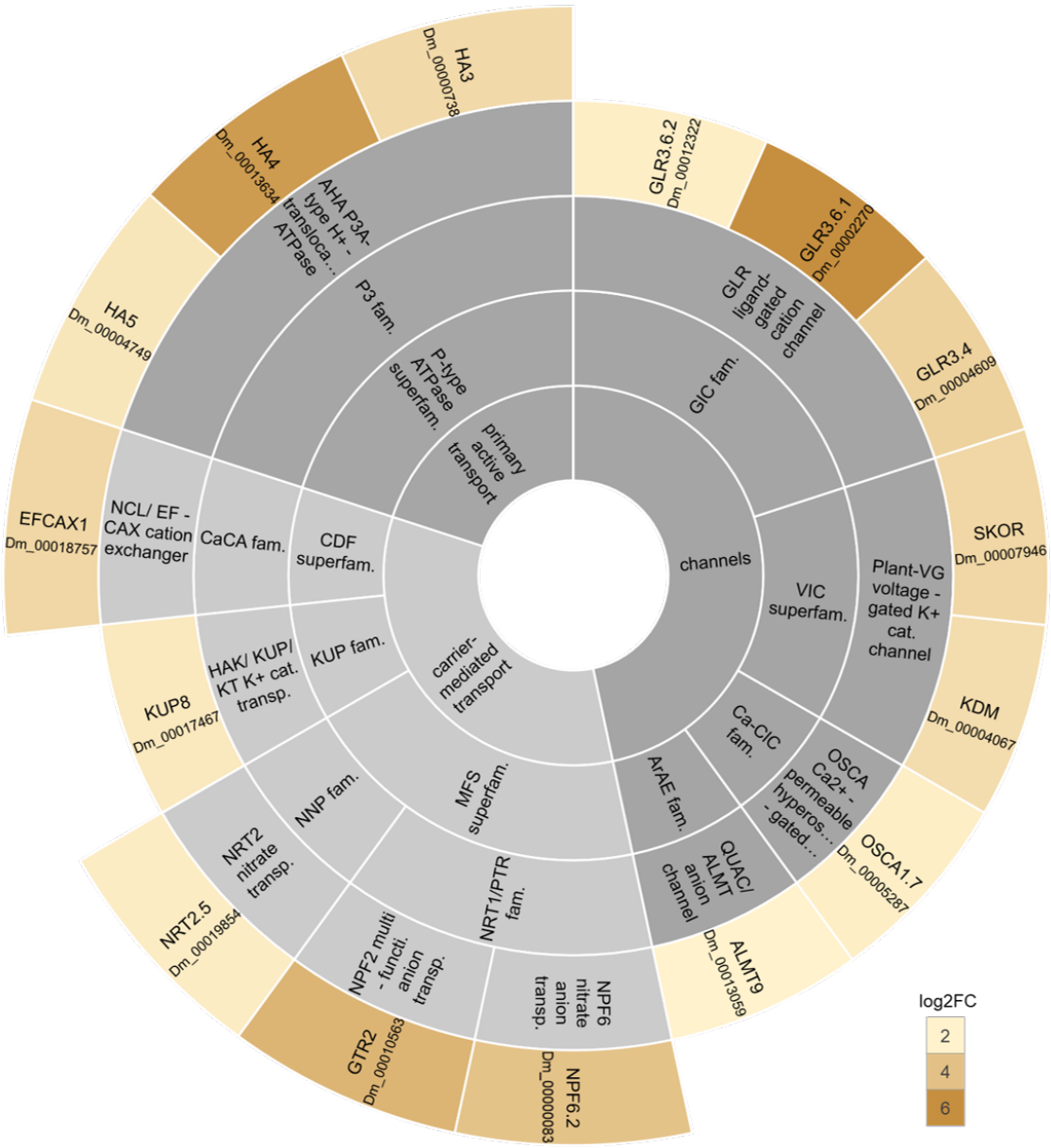

Figure 13: Sunburst chart of upregulated DEGs in adult trap when compared to juvenile trap classified according to Aramemnon Plant Membrane Protein Database. Only electrogenic channels/transporters/pumps are shown. The $\log_2$FC values are respresented as a heatmap. Only DEGs with $\log_2\text{FC} > 2$ are shown. GIC = Glutamate-gated Ion Channel, VIC = Voltage-gated Ion Channel, Ca-ClC = Ca^{2+}-dependent Cl^- Channel, ArAE = The Aromatic Acid Exporter, MFS = Major Facilitator Superfamily, PTR = Proton-dependent Oligopeptide Transporter, CaCA = cation carrier groups, CDF = Cation Diffusion Facilitator.

Next, we wanted to confirm the difference in expression level for the above-mentioned genes via qPCR. Furthermore, since we have previously seen some of these DEGs in the trigger hair-specific list of genes, we wondered how are they expressed in trigger hairs (THs) of juvenile traps. We can see their qPCR expression values in Figure 14. Indeed, they show a lower expression level in juvenile traps and juvenile THs compared to adult traps and adult THs.

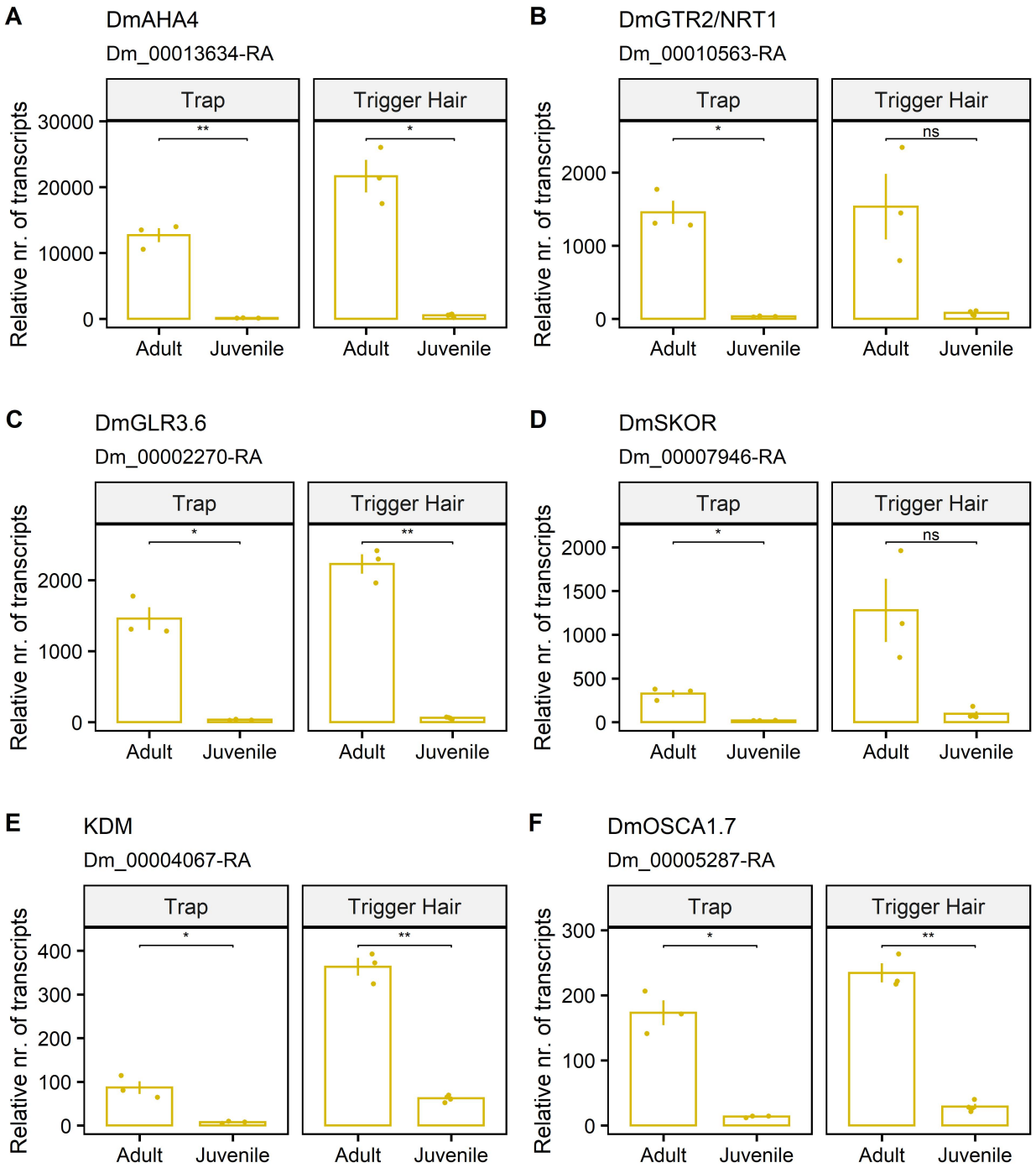

Figure 14: qPCR expression of DmAHA4 proton pump (A), *DmGTR2/NRT1* multi - functional anion transporter (B), *DmGLR3.6* glutamate ligand-gated cation channel (C), *DmSKOR* K^+ outward rectifier channel (D), *KDM1* voltage-gated K^+ inward rectifying channel (E) and *DmOSCA1.7* Ca^{2+} - permeable hyperosmolality - gated channel (F) in whole adult trap and trigger hairs of adult (stage 6) and juvenile (stage 5) stages. The relative number of transcripts is normalised to 10 000 molecules of actin *DmACT1*. The bar chart shows average values +/- SE. T-test p value is represented with stars: * for $p < 0.05$, ** for $p < 0.01$, *** for $p < 0.001$, ns = not significant. p value of Shapiro-Wilk normality test for each group > 0.05, indicating a normal distribution. $n = 3$.

Regarding their function, SKOR makes a good candidate for AP repolarization and AHA4 for hyperpolarization phase of the AP. In order to associate their possible function with their expression, we overlapped the two measurements as it can be seen in Figure 15. We can therefore notice that as the trap enters the mature stage, the AP repolarization duration becomes shorter, while the expression of the possible candidate *SKOR* increases (Figure 15B). Similarly, while there is little hyperpolarization during the juvenile stage, the amplitude increases together with its candidate gene expression *AHA4* as the trap transitions to the adult stage (Figure 15C).

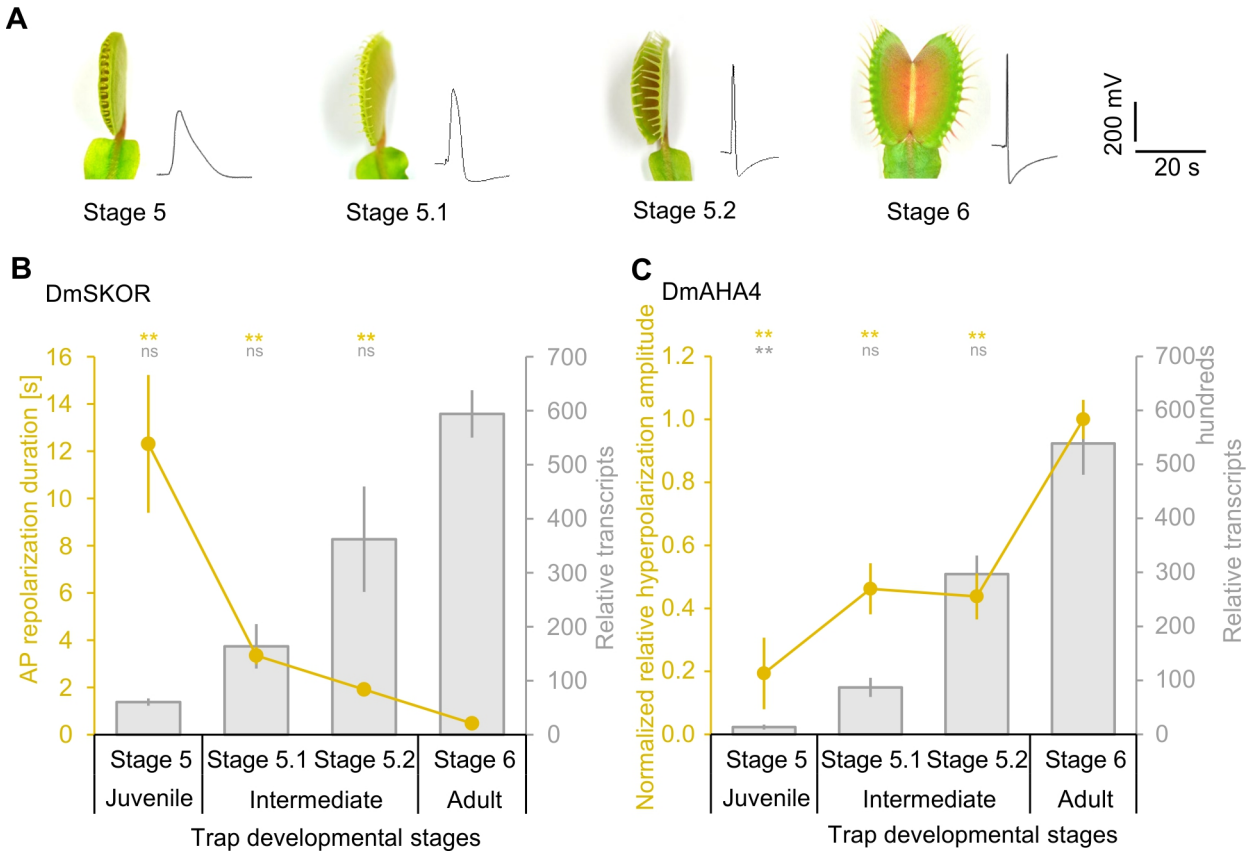

Figure 15: (A) Trap developmental stages of juvenile (5) intermediate stages (5.1 and 5.2) and adult stage (6) together with their representative APs. qPCR expression level of: (B) *DmSKOR* K^+ outward rectifier channel plotted against the AP repolarization duration in different trap developmental stages, and (C) *DmAHA4* proton pump in different trap developmental stages plotted against the AP relative hyperpolarization amplitude of each stage. The hyperpolarization amplitude was normalized to the adult stage (6). The relative number of transcripts is normalised to 10 000 molecules of actin *DmACT1*. The bar chart shows average values +/- SE. Above the chart, the Wilcoxon rank sum test p value between adult stage 6 vs each of the other stages is represented with stars: * for $p < 0.05$, ** for $p < 0.01$, *** for $p < 0.001$, ns = not significant. $n = 6$.

3.1.3.2 The Repolarization Duration Is Prolonged Upon Coronatine

During my experiments, I stumbled across a very curious observation. In later stages of digestion, one can notice that the AP is not as sharp, with its specific short duration (of ~ 1 second), but rather widened with a longer overall duration (Figure 17A).

In order to quantify and to check if there is a statistically significant difference between the AP of an open trap in ready-to-snap configuration and the AP of a sealed trap in full digestion mode, I measured different characteristics of the AP (such as duration, depolarization duration, repolarization duration, hyperpolarization amplitude) during 5 days of digestion process. As it has been shown in our previous research [25, 56, 101], in order to trigger digestion, the molecular mimic of jasmonic acid (JA, or more specifically of the active form: JA-Ile), coronatine (COR), can be sprayed on the open traps and within 24 hours the glands will start secreting, slowly closing their traps and getting filled with digestive fluid. Therefore, I used COR to induce digestion for the first experiment.

The AP measurements show that there is a significant statistical difference before treatment (day 0) and after COR treatment already after 1 day for all measurements (Figure 16). Again, the repolarization duration was affected, becoming as long as 15 seconds, on average, after 5 days (Figure 16C). The hyperpolarization amplitude also decreased slowly during the digestive process, completely vanishing after 5 days (Figure 16D).

In Figure 17B, we see again a possible correlation between the expression level of the candidate genes. As the repolarization duration increases, the expression of *SKOR* decreases during the digestion process (Figure 17B). In the same manner, the hyperpolarization amplitude can be associated with a decrease in the expression of *AHA4* (Figure 17C).

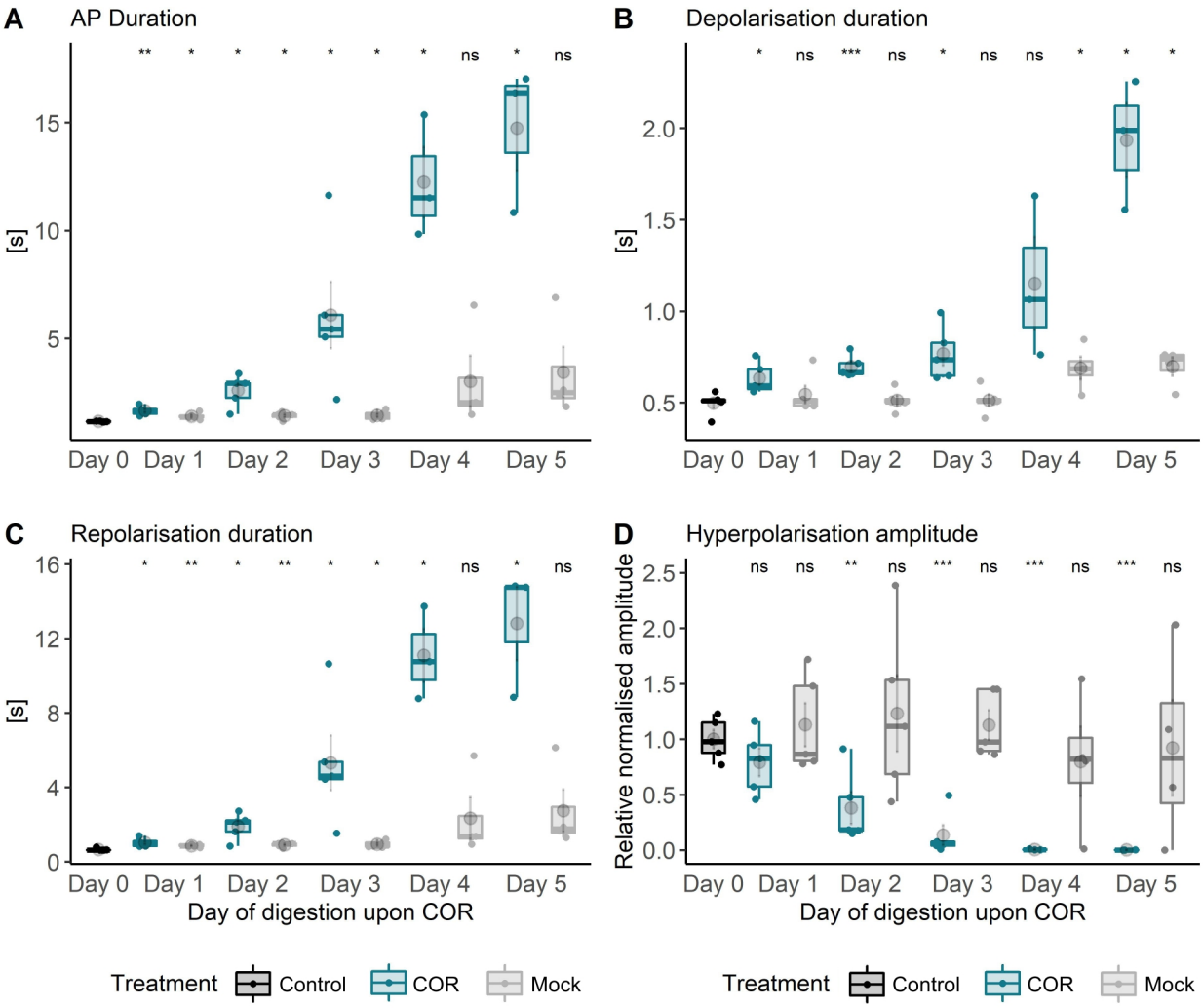

Figure 16: The whole AP duration (A), AP depolarization duration (B), AP repolarization duration (C) and AP hyperpolarization amplitude (D) in COR treated traps. Control group represents completely untreated samples (therefore open traps). As an additional control group, the traps were manipulated and sprayed with water in the same way as COR-treated traps - mock group. The hyperpolarization normalisation was done by dividing each sample to the average value of the reference day 0, for day 0 group, and to their own sample before the treatment started for the rest of the groups. Average value of each group can be seen as grey dot +/- SE. T-test p is represented with stars: * for $p < 0.05$, ** for $p < 0.01$, *** for $p < 0.001$, ns = not significant. p value of Shapiro-Wilk normality test for each group > 0.05, indicating a normal distribution. $n = 3\text{-}6$

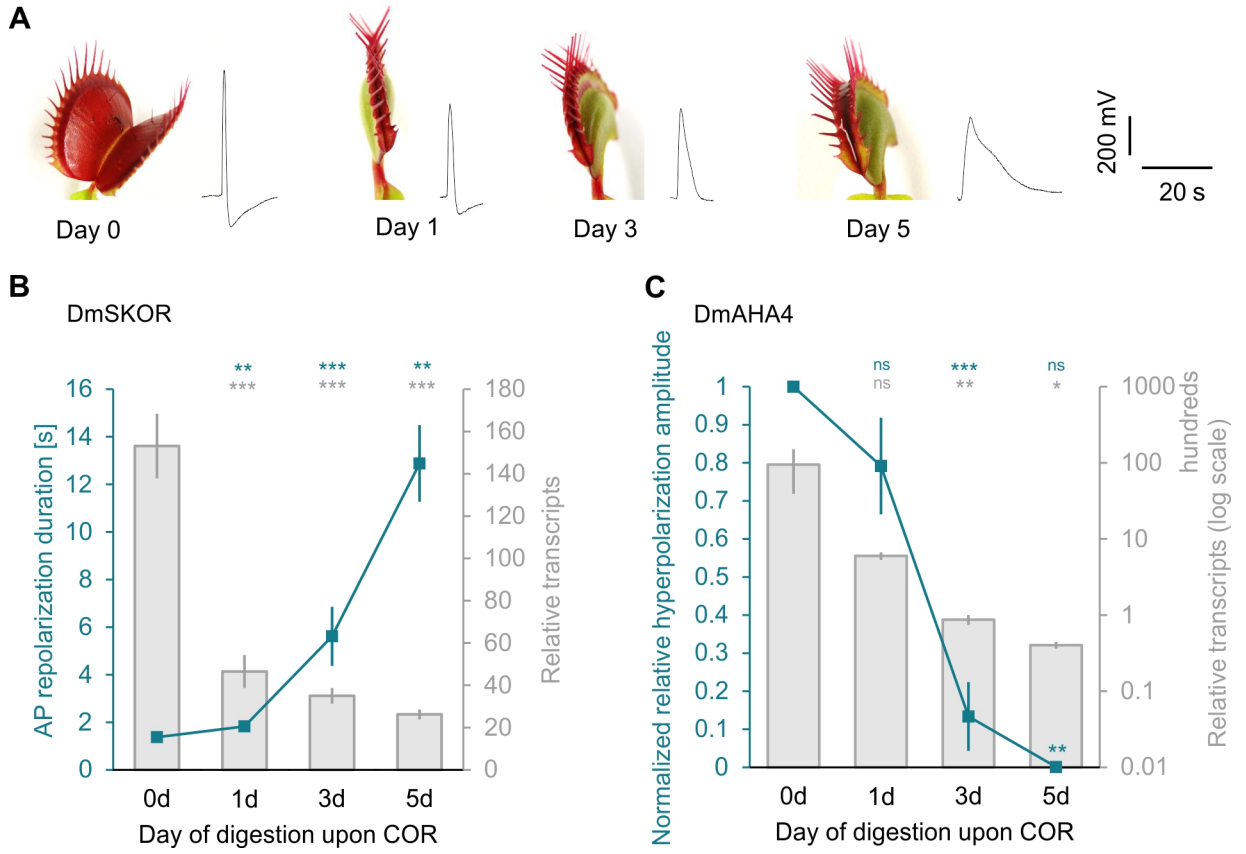

Figure 17: (A) Trap in different digestion states after COR treatment together with representative APs. qPCR expression level upon COR of (B) *DmSKOR* K^+ outward rectifier channel (grey bars) plotted against the AP repolarization duration (turquoise line) and (C) *DmAHA4* proton pump (grey bars) plotted against the AP relative hyperpolarization amplitude (turquoise line) of each day after COR application. The hyperpolarization amplitude was normalized to day 0. The relative number of transcripts is normalised to 10 000 molecules of actin *DmACT1*. The bar chart shows average values +/- SE. Above the chart, the Wilcoxon rank sum test p value between control (day 0) and all the other days after COR treatment is represented with stars: * for $p < 0.05$, ** for $p < 0.01$, *** for $p < 0.001$, ns = not significant. $n = 6$.

3.1.3.3 The Repolarization Duration Is Prolonged During Insect Feeding

The advantage of spraying coronatine (COR) to induce digestion, is that it is more reproducible, as the same amount and concentration can be sprayed on different traps, which should induce a similar response. Moreover, it does not trigger or interfere with other chemo- or mechanosensing processes. However, the disadvantage is, that it is a rather artificial and forced way to induce secretion. This is why, I repeated the experiment using natural prey, such as ants. This time, I was also interested to see if the traps would reopen at the end of digestion and if so, to further investigate if the candidate genes' expression would come back to ground state levels, while the AP regains its original shape.

And indeed, we see that the AP duration is increasing within the first day, continuing to increase until the 9th day when it starts to decrease, coming very close to the original duration on the 13th day. However, regaining the exact original shape would have probably taken a few more days or weeks. Nevertheless, two weeks of digestion gives us a clear idea about the general tendency.

In the case of COR treatment, we have seen a more drastic effect upon the repolarization duration (15 seconds). However, in the case of natural ant-fed traps, the repolarization duration was maximum 10 seconds with an average of 5 seconds in the middle of the digestion process (Figure 18C). The hyperpolarization also changes during digestion, coming back to previous amplitude levels on day 13 (Figure 18D).

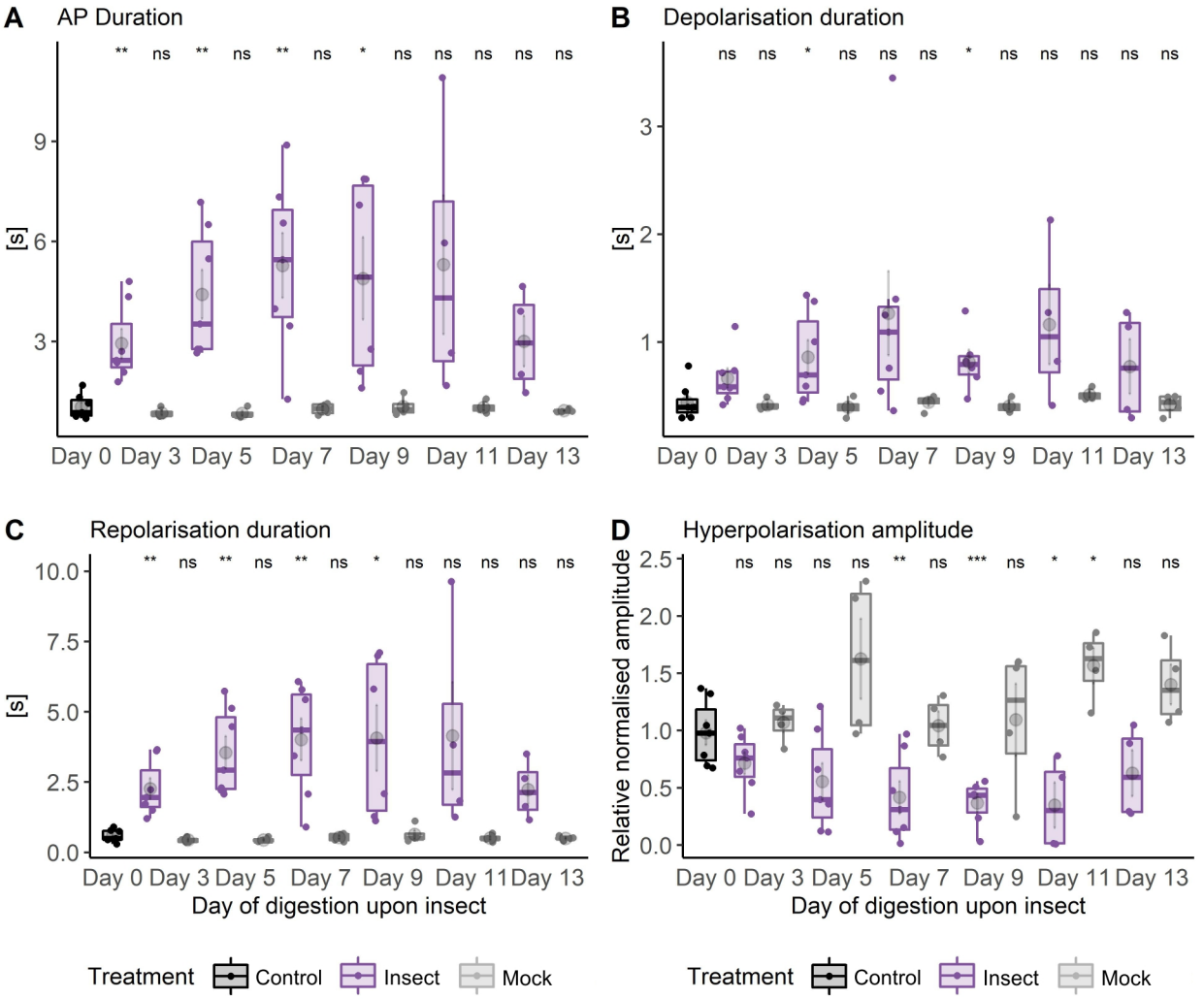

Figure 18: The whole AP duration (A), AP depolarization duration (B), AP repolarization duration (C) and AP hyperpolarization amplitude (D) in insect (ant - *Acromyrmex sp.* fed traps. Control group represents completely untreated samples before the experiment started (therefore open traps). As an additional control group, traps were closed and manipulated in the same way as the insect-fed ones, but no insect was put inside - mock group. The hyperpolarization normalisation was done by dividing each sample to the average value of the reference day 0, for day 0 group, and to their own sample before the treatment started for the rest of the groups. Average value of each group can be seen as grey dot +/- SE. T-test p is represented with stars: * for $p < 0.05$, ** for $p < 0.01$, *** for $p < 0.001$, ns = not significant. p value of Shapiro-Wilk normality test for each group > 0.05, indicating a normal distribution. $n =$ 3-7

Outlined in Figure 19A, are the different shapes of APs during different digestion days in ant-fed traps. We can also observe that *GORK* and *AHA4* start to regain their expression level at the end of digestion (Figure 19B,C). Additionally, we can notice the amount of digestive fluid increasing to the maximum level already after 3 days of digestion when one of the digestive fluid marker enzymes (*SAG12*) is also highly expressed.

While the expression level of *SAG12* starts to decrease, the digestive fluid stays at the same level until day 11. The traps have already reabsorbed the resulting nutrients together with the digestive fluid at the end of digestion (day 13), being completely dry (Figure 19D). We can also see that all the traps within this experiment stayed closed until day 5, while some of them already started to reopen (semi-open) after 7 days, 20% of them being completely open by day 11. On the last day of the experiment, all the traps were completely re-opened (Figure 19E).

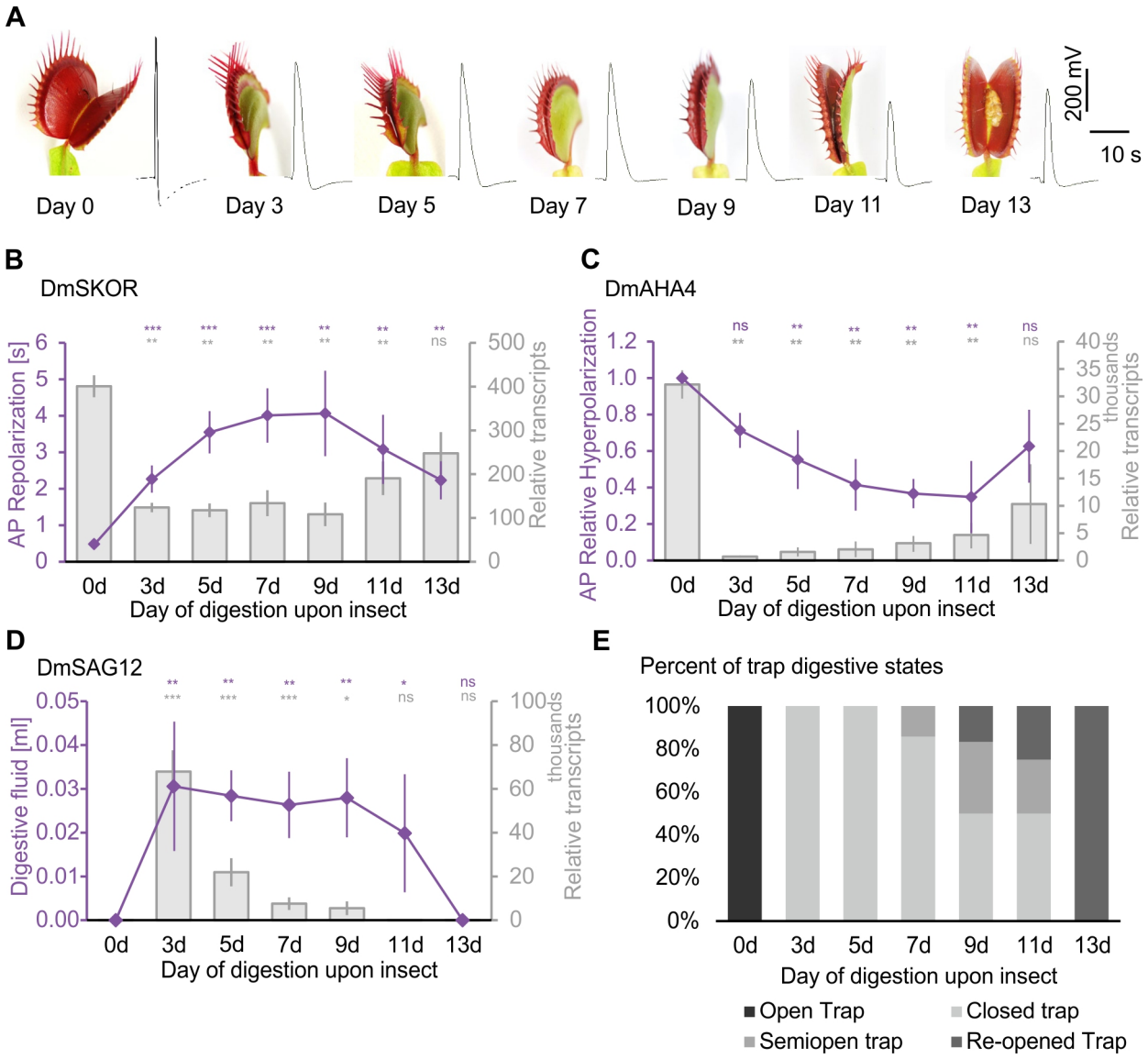

Figure 19: (A) Trap in different digestion states after insect (ant - *Acromyrmex sp.*) feeding together with representative APs. qPCR expression level upon insect feeding of: (B) *DmSKOR* K^+ outward rectifier channel plotted against the AP repolarization duration, (C) *DmAHA4* proton pump after insect digestion plotted against the AP relative hyperpolarization amplitude and (D) *DmSAG12* digestive marker plotted against the amount of digestive fluid secreted during digestion. (E) Percent of each trap digestive states during insect feeding. The hyperpolarization amplitude was normalized to day 0. The relative number of transcripts is normalised to 10 000 molecules of actin *DmACT1*. The bar chart shows average values +/- SE. Above the chart, the Wilcoxon rank sum test p value between control (day 0) and all the other days after insect feeding is represented with stars: * for $p < 0.05$, ** for $p < 0.01$, *** for $p < 0.001$, ns = not significant. $n = 3\text{-}7$.

In conclusion, we have seen that in three distinct cases, the AP shape of *Dionaea muscipula* is different: wider, with a prolonged repolarization phase and absent hyperpolarization. This phenomenon appeared in the juvenile stage of the trap, upon COR treatment and in insect-fed traps. In chapter 3.1.2, we have also seen which genes are enriched in the AP onset site - the trigger hair.

Figure 20 summarises the transcriptomic data of the electrogenic permeome of *Dionaea*, including all the above-mentioned conditions within each pairwise comparison with the adult excitable trap (showing the $\log_2$FC values of each comparison). We can therefore notice that those genes which could be involved in AP elicitation, are highly expressed in adult trap compared to juvenile trap and at the same time are downregulated during digestion induced by COR or insect. Additionally, a high expression in the trigger hair compared to the trap might be an indicator that the gene might be involved in AP initiation. Such genes that fulfil these criteria are: *GTR2, GLR3.6, GLR3.4, KDM1, SKOR* (Figure 20).

	Permeome annotation	Gene Name	DmID	Trap Adult vs Trap Juvenile	Trap COR-24h vs Trap Control	Trap Insect-24h vs Trap Control	Trigger Hair vs Trap Control
carrier-mediated transport	CDF superfamily.CaCA family.NCL/EF-CAX cation exchanger	NCL/EFCAX1	Dm_00018757-RA	3.24	-3.03	-3.50	NA
	KUP family.HAK/KUP/KT potassium cation transporter	KUP8/HAK8	Dm_00017467-RA	2.67	-2.45	-1.95	-1.58
	MFS superfamily.NNP family.NRT2 nitrate transporter	NRT2.5	Dm_00019854-RA	2.31	-2.91	-3.34	NA
	MFS superfamily.NRT1/PTR family.NPF2 multi-functional anion transporter	GTR2/NPF2.11	Dm_00010563-RA	4.72	-1.09	-1.20	1.35
	MFS superfamily.NRT1/PTR family.NPF5-type unspecified transporter	NPF5.5	Dm_00012845-RA	2.65	NA	NA	NA
	MFS superfamily.NRT1/PTR family.NPF6 nitrate anion transporter	NPF6.2/NRT1.4	Dm_00000083-RA	4.10	1.63	1.98	-1.10
channels	ArAE family.QUAC/ALMT anion channel	ALMT9	Dm_00018513-RA	5.26	NA	NA	-1.95
	ArAE family.QUAC/ALMT anion channel	ALMT9	Dm_00013059-RA	2.03	NA	NA	NA
	Ca-ClC family.OSCA Ca2+-permeable hyperosmolality-gated channel	OSCA1.7	Dm_00005287-RA	2.77	-1.21	-1.83	NA
	GIC family.GLR ligand-gated cation channel	GLR3.6	Dm_00002270-RA	6.38	-3.19	-3.13	1.53
	GIC family.GLR ligand-gated cation channel	GLR3.4	Dm_00004609-RA	3.46	-4.43	-2.89	1.21
	GIC family.GLR ligand-gated cation channel	GLR3.6	Dm_00012322-RA	2.24	NA	-1.23	NA
	VIC superfamily.Plant-VG voltage-gated potassium cation channel	SKOR	Dm_00007946-RA	3.23	-1.62	-1.53	2.31
	VIC superfamily.Plant-VG voltage-gated potassium cation channel	KAT1/KDM	Dm_00004067-RA	2.96	-1.63	NA	3.11
primary active transp.	P-type ATPase superfamily.P3 family.AHA P3A-type H^+-translocating ATPase	HA4	Dm_00013634-RA	5.85	-2.79	-3.20	NA
	P-type ATPase superfamily.P3 family.AHA P3A-type H^+-translocating ATPase	HA3	Dm_00000738-RA	3.13	NA	NA	1.01
	P-type ATPase superfamily.P3 family.AHA P3A-type H^+-translocating ATPase	HA5	Dm_00004749-RA	2.58	1.97	1.59	NA

Figure 20: DEGs in adult trap when compared to juvenile trap classified according to Aramemnon Plant Membrane Protein Database and their $\log_2$FC values in other pairwise comparisons. Only electrogenic channels/transporters/pumps are shown. Only DEGs with $\log_2\text{FC} > 2$ in the adult vs juvenile trap comparisons are shown. DEGs were considered genes with $\log_2\text{FC} > 1$ for each pairwise comparison and adjusted p-value < 0.05. NA = not differentially expressed. Transcriptomic data for COR-treated as well as insect-fed traps after 24h was already published in [56].

3.1.4 Discussion

3.1.4.1 Animal vs Plant Action Potential

In animal cells, the ATP-driven Na^+/K^+ pump keeps the membrane potential at around -70 mV together with a strong chemical gradient (of $\sim$ 100 mM K^+ and 10 mM Na^+ inside the cell and 10 mM K^+ and 100 mM Na^+ outside the cell). A predepolarization step of $\sim$ 30 mV activates voltage-dependent Na^+ efflux channels that depolarise the cell up to +40 mV. This is followed by the repolarization, which is a depolarization-activated process mediated by Shaker-type voltage-dependent K^+ channels [32]. In cardiac muscles, voltage-activated inward Ca^{2+} channels also participate in repolarization, giving the AP a specific plateau phase [160]. However, plants lack both animal-type Na^+ channels and voltage-dependent Ca^{2+} channels [90].

3.1.4.2 The Molecular Basis of Plant Action Potential

However incredible it might seem, the exact molecular components involved in depolarization and repolarization phases of the electrical signalling in higher plants remain unrevealed, leaving scientists with an open quest, still under tremendous investigation [167]. Like in a puzzle, more and more pieces are put together, each one bringing candidates to the table. In the following chapter, I will mention possible molecular candidates for each of the action potential phases.

In *Dionaea* cells, the membrane potential is more negative than in animal cells, constantly kept at about -120 mV to -140 mV [32]. While in animal cells the inward-directed Na^+ and outward-directed K^+ gradients build up the main driving force for the animal AP, in *Dionaea*, the extracellular fluid has a low ionic strength ($\sim$ 0.1-1 mM K^+ in the apoplast) and a similar $[K^+]_{cyt}$ to that of the animal cell ($\sim$ 100 mM K^+) [32, 90, 131]. Since plants lack animal-like Na^+ channels, it is hypothesized that plants use outward-directed anion gradient for depolarization, instead [90]. Previous studies of *Dionaea*'s AP [168], are indeed in agreement with the general hypothesis that the depolarization phase is dominated by Cl^- efflux [169, 170, 171] accompanied by an initial depolarization caused by Ca^{2+} influx [121] and finally reversed by K^+ efflux [172, 173] together with H^+ efflux [174]. Apart from its involvement in depolarization, $[Ca^{2+}]_{cyt}$ may activate Ca^{2+}-dependent Cl^- channels [175] and inactivate the H^+-ATPase [160, 176, 177].

In his recent review about advances in plant ion channels, Pantoja summarises the selectivity, activation, direction of ion flux, location at the cell level, as well as the function of major plant channels [178]. Based on this review, candidate channels that could also be involved in action potential are summarised in Table 7.

Table 7: Electrogenic ion channels with a potential link to plant action potential as described in [178]. For details see [178]. C^+ = cations, A^- = anions, Mal^{2-} = malate, ND = not determined, Depol. = depolarization, Hyperpol = hyperpolarization, PM = plasma membrane, T = tonoplast, N = nuclear membrane, GA = Golgi Apparatus, M = mithochondria, C = chloroplast

Channel	Selectivity	Activation	Direction	Location	Function
OSCAs	Ca^{2+}, C^+	Hyperosmolarity	in-out	PM	Osmotic response
GLRs	Ca^{2+}, C^+	Amino acids (Glu)	in	PM	Stomatal closing, Root development, Pollen tube growth
CNGCs	Ca^{2+}, C^+, ND	cNMP, cGMP, Hyperpol.	in/in-out	PM, N, T, GA	Pathogen, Flowering, Stomata opening, Gravitropism, Root nodule symbioses, Pollen tube, Action potential
TPCs	Ca^{2+}, C^+	Depol.	out	T	Osmotic response, Ca^{2+} signalling
MSLs	Cl^-, ND	Tension, ND	out	M, C, PM	ATP synthesis, Pollen tube growth
SLAC/ SLAH	Cl^- ,NO^{3-}	Depol.	out	PM	Stomatal closing, Xylem loading
CLCs	Cl^-, A^-, NO^{3-}/H^+ exchange, ND	ND	ND	T, C	Stomatal functioning, Cl^- phloem recirculation
ALMTs	Cl^-, Mal^{2-}	Hyperpol.-Al^{3+}/ Hyperpol. / Depol.	out	PM, T	Al^{3+} tolerance, Stomatal opening or closing
SKOR/ GORK	K^+	Depol.	out	PM	K^+ xylem loading, Stomatal closing
TPKs	K^+	Ca^{2+}-activated, Hyper- or depol.	in-out	PM, T	K^+ cellular homeostasis, Control of membrane potential
AKTs	K^+	Hyperpol./ Hyper- or depol.	in/in-out	PM	K^+ root absorption, K^+ phloem recirculation
KATs	K^+	Hyperpol.	in	PM	Stomatal opening

Ca^{2+} Influx Channel Candidates That Could Contribute to Predepolarization

Starting with Ca^{2+}-permeable channels that could contribute to predepolarization, are worth mentioning: the hyperosmolality-gated Ca^{2+}-permeable channels OSCA that is activated by membrane tension, making it a good candidate for AP-initiation; the glutamate-like receptors or amino acid-gated Ca^{2+} cation channels GLRs which have been shown to be important for action potential propagation in *Arabidopsis thaliana* [65, 134]; the cyclic nucleotide-gated ion channels CNGCs which are activated by hyperpolarization besides cNMP and cGMP and can facilitate $[Ca^{2+}]_{cyt}$ increase by allowing Ca^{2+} influx from the apoplast (CNGC14) or from the vacuole (CNGC19). Similarly, the tonoplast two-pore channels TPCs also release Ca^{2+} from the vacuole storage, being involved in osmotic responses and Ca^{2+} signalling [178].

Anion Efflux Channel Candidates for Depolarization

Besides Ca^{2+}-permeable influx channels, electrogenic anion efflux channels would represent good candidates for depolarization phase, such as: the mechanosensitive MSL which has been recently shown to allow Cl^- efflux in *Dionaea* upon tension (FLYC1) [133]; the S-type anion channels SLACs which are involved in stomatal closing by allowing Cl^- efflux; the malate anion channels ALMT which can contribute to stomatal closure in the same way as SLAC, by allowing Cl^- efflux (ALMT12) or it can contribute to stomatal opening by allowing Cl^- (ALMT9) or Mal^{2-} (ALMT6) influx into the vacuole; and the voltage-gated Cl^- anion channels CLCs which also play a role in stomatal functioning [178].

K^+ Efflux Channel Candidates for Repolarization

As for repolarization, the following K^+ efflux channels could represent good candidates. The best candidates would be from the voltage-gated K^+ (VGK) channels family. In plants, there are only two Shaker-type voltage-dependent K^+ channels: SKOR (expressed in xylem parenchyma cells) and GORK (expressed in guard cells), that have been shown to operate as outward-rectifying K^+-selective channels [161]. The animal Shaker K^+ channels are activated in the millisecond range, hand in hand with the fast AP duration in mammalian nerve cells [179]. In contrast, the plant Shaker channel orthologs need seconds to fully activate [161], which would correspond with the second-range plant AP. The other plant K^+ channel family comprises the tandem-pore / two-pore channels TPKs which are Ca^{2+}-activated vacuolar channels and can be classified as mechanosensitive, responding to changes in membrane tension or osmotic shock and therefore allowing K^+ flux in and out of the vacuole [178]. TPKs are, therefore, important for maintaining $[K^+]_{cyt}$ homeostasis.

Channel Candidates for Restoring the Resting Potential

For the membrane potential and chemical gradient restoration, facilitating K^+ entry, the hyperpolarization-activated K^+ channel AKT as well as KAT are good candidates. AKT could be modulated in a Ca^{2+}-dependent manner assisted by the interaction with the CBL-CIPK kinases. In *Dionaea*, the KDM1 channel (KAT1 ortholog of *Arabidopsis*) has been electrophysiologically characterised as hyperpolarization - and acid-activated K^+-selective uptake channel [102]. Besides this, the HAK-type H^+/ K^+ symporters might also accompany the above-mentioned channels, in addition, restoring the H^+ gradient. The anions could be taken up by NRT-type H^+/anion symporters [131], while Ca^{2+} could be brought back into the cells by the P-type Ca^{2+} -ATPases and Ca^{2+}/H^+ exchangers (CAXs) [131, 180].

3.1.4.3 The Molecular Basis of *Dionaea muscipula*'s Action Potential

By comparing the transcriptome of excitable *Dionaea muscipula* adult traps with that of not-yet excitable juvenile traps, we could find many of the AP candidates mentioned above as differentially expressed genes (DEGs). Some of them being are expressed in the adult trap vs juvenile trap, while some of them are expressed at a lower degree. Among the ones with high induction ($\log_2$FC value > 2) in the adult trap, we found: *GLRs, AHAs, ALMT9, NRTs, EFCAX1, SKOR, KDM1, OSCA1.7* and *KUP8* (Figure 13, Appendix Figure 64). Still, worth mentioning are also the ones with a lower fold change, such as: *CAX3/2/9, ACA11/10/9, TPK1, CNGC1/14/15, ANO1, HAK5, HKT* (for DmIDs and FPKM expression values see Appendix Figure 64).

Additionally, many of the highly induced genes encoding electrogenic channels/ transporter/ pumps candidates were even higher expressed in the super-specialized mechanosensitive structure of the trap - the trigger hair. The action potential originates in the mechanoreceptor cells found at the trigger hair indentation zone. It would be plausible that channels responsible for the electrical signalling would be found in a higher abundance here. This might be reflected in the high expression of genes encoding those channels in the trigger hair. Among these, highly specific to the trigger hair are: *KDM1, SKOR* and *GLR3.6/3.4*. Also expressed in the trigger hair, but to a similar extent as in the whole trap are: *AHA4, GTR2* and *OSCA1.7* (Figure 14). Moreover, these genes are downregulated when the trap enters digestion mode (Figure 20). Our experiments show that during digestion, the AP shape changes: the depolarization duration becomes longer and the hyperpolarization amplitude decreases (Figure 16, Figure 18). This prolongation of the AP during the digestion phase might indicate a lower activity of the channels involved that could be reflected at the transcriptomic level by the low expression of the respective genes.

This makes *KDM1, SKOR, GLR3.6/3.4* as well as *AHA4, GTR2, OSCA1.7* great candidates for the electrical signalling of *Dionaea muscipula*. In the following paragraphs, I will briefly describe each one of these channels/ transporters/ pumps and summarise the most recent works and findings.

Maybe from the above-mentioned genes, the most surprising is the gene encoding GTR2/ NPF2.11/ NRT1. As part of the Proton-dependent Oligopeptide Transporter (POT/PTR) Family, NPFs can be involved in: low-affinity nitrate transport, peptide transport, glucosinolate and ABA, GA and JA-Ile transport activities [181]. In *Arabidopsis* GTR2/NPF2.11 is part of the glucosinolate transporter group, but besides this, NPF2.11 has been shown to also exhibit low-affinity nitrate transport [182]. Interestingly, its ortholog GTR1/NPF2.10 could be involved in JA/JA-Ile transport from damaged to undamaged leaves during wounding [183]. Glucosinolates are secondary compounds involved in defence mechanisms that are exclusively produced by plants from Brassicales order. However, GTR-homologs or rather GTR-like transporters have

been found in other species that do not contain glucosinolates such as *M. truncatula, G. raimondii, S. lycopersicum, M. esculenta and T. cacao* [184]. It would be interesting to see what affinity does the GTR2 of *Dionaea* have, and if it might be involved in electrical signalling or rather defence mechanisms at all.

Maybe the most special candidate that can play an important role in AP initiation, is the trigger hair-specific MSL10. The fact that it does not appear as a DEG in the adult trap when compared to juvenile trap (and nor does in the insect- or COR-treated trap), is due to its overall low expression at the whole trap tissue level, indicating that this channel is highly specialized for the trigger hair, and maybe highly contributing to its unique mechanosensing ability.

MSL The mechanosensitive channel of small conductance (MscS) superfamily hosts 15 unique subfamilies [185] that are found in bacteria, fungi, algae, and plants are essential for osmotic pressure management [186]. Our finding that *MSL10* is highly expressed and highly specific to the trigger hairs of *Dionaea muscipula*, has been very recently confirmed by a subsequent study. By using *de novo* transcriptome assembly, Procko and colleagues have (independently from our studies) reached the same conclusion, that the *MSL10* is one of the highest enriched genes in the trigger hairs when compared to trap (85 fold higher) [133]. They further characterised the MSL10 channel and renamed it flycatcher FLYC1. They measured the pressure required for half-maximal activation P_{50} as 77.3 ± 4.0 mmHg in cell-attached patch-clamp mode, which is two times lower than that measured in bacterial orthologs (P_{50} = 188 ± 31 mmHg [187]). They argue that due to frequent cell membrane rupture during measurements, they managed to record the full current saturation in very few cells, making the results likely being an underestimation. Finally, they conclude that MSL10/FLYC1 is a chloride-permeable mechanically activated ion channel which can contribute to membrane depolarization in *Dionaea muscipula*'s trigger hairs [133]. This statement is supported by previous studies that show a high electronegativity of the trigger hair's sensory cells [121] (which was been also confirmed in our lab) together with a concentration gradient that can lead to efflux [133]. Furthermore, using RNA in situ hybridization, Procko and colleagues also showed that the mRNA of MSL10/FLYC1 is localised only in the indentation zone, in the mechanosensory cells of the trigger hair (and not in the lever or the lower podium parts). This makes FLYC1 a perfect candidate for the initiation of the AP. Another remarkable aspect that supports this idea, is that the FLYC1 ortholog is also highly expressed in the excitable *Drosera capensis* tentacles up to 40 times higher than in the rest of leaf tissue (without tentacles) [133].

In the newly published *Dionaea* draft genome [25] there are five MSLs, most of which are ubiquitous, making MSL10 the only trigger-hair specific. Similarly, another mechanosensitive channel that is worth mentioning, is the Piezo ion channel, with only one ortholog in *Dionaea*'s draft genome (Dm_00008335-RA) with a low expression in the majority of tissues (< 5 FPKM) and highest in the trigger hair (13.99 FPKM).

New studies on tonoplast-localised *Arabidopsis* Piezo, indicate that it promotes vacuolar fission during tip growth of pollen tube [188].

GLR The glutamate-receptors GLRs can be found in both animals and plants. Animal ionotropic iGLRs are involved in fast excitatory synaptic transmission. Upon agonist binding, the channels allow K^+, Na^+ and/or Ca^{2+} influx (depending on the channel selectivity). The inrush of cations elevates the membrane potential reaching the predepolarization thresholds needed for the activation of voltage-gated channels, resulting in the generation of an animal action potential [189, 190, 191]. In plants, the phloem comprises highly excitable cells with low resistance and a K^+ dominated cytoplasm as an electrolyte, making it suitable to conduct electrical signals, and which therefore represents the closest resemblance to animal neurons [191, 192, 193]. In *Arabidopsis*, GLRs have been shown to be crucial for electrical signal propagation along the phloem in response to wounding or herbivory. The quadruple mutants *glr3.1/3.2/3.3/3.6* presented a reduced duration of the surface potential changed after wounding, with GLR3.3 and GLR3.6 being responsible for signal propagation to neighbouring leaves [65].

The amino-acid glutamate (Glu) is an essential neurotransmitter in animal excitatory systems. Its novel role in plant signalling has just emerged. There is more and more evidence that Glu can be considered a signalling molecule with multiple physiological functions, such as: seed germination, root architecture, pollen tube growth and stress responses upon salt, cold, heat or drought, wound or pathogen attacks [194]. Glu can strengthen the antioxidant activity (of peroxidases, superoxide dismutases, polyphenol oxidase, and phenylalanine ammonia lyases) and lead to proline accumulation, therefore acting as a stress reducer [195]. In addition, it can act as a long-distance signalling transducer via cross-talk between Ca^{2+}, ROS and electrical signalling [65, 134, 194].

In our recent paper, it has been shown that the anaesthetic ether can abolish the touch-induced action potential and Ca^{2+} signalling in *Dionaea*, suggesting that GLRs could be an ether target [196].

MSL-GLR interplay Recently, Moe-Lange and colleagues measured the electrical signalling / SWP (slow-wave potential) in wounded *Arabidopsis* L8 leaves as well as the neighbour L13 leaves, in parallel with the Ca^{2+} signalling in *msl* mutant lines using MatryoshCaMP6 expressing plants. They revealed that the *Arabidopsis* SWP duration is significantly reduced (four times shorter, from $\sim$ 90 seconds to less than 30 seconds) in *msl* quadruple mutant T-DNA insertion lines (*msl4,5,6,9,10*) upon wounding in distant leaf L13 (while wounding leaf L8), with unaffected propagation velocities [197]. Remarkably, single *msl10* and double *msl10glr3.6* mutant lines showed a very similar phenotype as the quadruple mutant. Moreover, the jasmonic acid (JA) wounding marker *JAZ10* had a lower expression in the mutants' distal leaves (L13) compared

to WT (when L8 was wounded). However, the SWP in the wounded leaf L8 of *msl10* mutants, was not statistically significant from WT, indicating that the propagation is affected. Hand in hand with the SWP, the Ca^{2+} signal was indistinguishable from WT in L8 (containing the site of wounding) and significantly reduced (almost half) in distal leaf L13 of *msl10* mutant. Asking the epic question of whether or not the electrical signal precedes the Ca^{2+} wave, the authors argue that an initial hyperpolarization precedes the first detectable Ca^{2+} increase in the distal L13 leaf of WT and *msl10* plants. Based on these observations, they propose the following model: upon wounding, there is: **(i)** a release of Glu into the apoplastic space (mediated by unknown mechanisms) activating GLRs, while in parallel, **(ii)** a turgor change (caused by wounding) activate MSL10 resulting in anion efflux and membrane depolarization - which in turn further participates in the full activation of GLRs and therefore Ca^{2+} efflux [197].

OSCA Besides MSLs, mechanotransduction can occur through the hyperosmolarity-gated channel OSCA. The OSCA/TMEM63 family could be considered one of the largest mechanosensitive channel family that is conserved across both plant and animal kingdoms [198]. In *Arabidopsis thaliana osca1* mutants, Ca^{2+} signalling in guard cells and root cells are impaired, affecting water transpiration regulation and root growth in response to osmotic stress [199]. Stretch-activation of AtOSCA1.1 and AtOSCA1.2 show non-selective cation currents with some Cl^- permeability (OSCA1.1: $P_{Cl}/P_{Na} = 0.21 \pm 0.06$; OSCA1.2: $P_{Cl}/P_{Na} = 0.17 \pm 0.01$). The *Arabidopsis* OSCAs required a half-maximal activation (P_{50}) of $\sim$ -54/-58 mmHg, which is half of that needed for the activation of mouse Piezo1 [166]. In the recently published *Dionaea* genome [25], there are five OSCA orthologs, out of which Dm_00005287-RA has the highest log_2FC value when comparing different trap developmental stages (adult vs juvenile) (Figure 13, Figure 20), with a high expression in the trigger hair as well (Figure 14F). This gene corresponds with the *Arabidopsis* ortholog OSCA1.7 (AT4G02900), based on the best BLAST hit score. Procko and colleagues describe another OSCA ortholog as highly expressed in the *Dionaea* trigger hair, suggesting that OSCA contributes to the FLYC1-mediated depolarization and AP initiation [133].

SKOR As part of the Shaker-like voltage-dependent channel family, there are two outward rectifiers in *Arabidopsis thaliana*: SKOR and GORK. GORK is primarily found in guard cells [161] where it acts as a mediator of intracellular K^+ homeostasis and it is involved in stomatal closure by releasing K^+ and therefore leading to water loss, allowing the guard cells to deflate [162]. *Arabidopsis thaliana gork* mutants show a prolonged repolarization duration. The fact that the whole electrical signal is not abolished in *gork* KO mutants suggests that other tandem players are involved in the signalling, such as the H^+-ATPase [167]. SKOR is found in xylem and it is thought to be responsible for K^+ loading into the xylem network, as *skor* mutants cannot deliver K^+ to the shoot [200]. In *Dionaea*'s genome [25] there is only one ortholog of SKOR/GORK. Based on orthogroup analysis and the phylogeny of the plant Shaker family (see [102]

S2) including *Dionaea*, it is hard to judge whether this ortholog is more similar to SKOR or to GORK. However, by running a simple BLAST, the best hit (with the highest score and lowest E-value) is SKOR. When looking at *SKOR*'s expression levels in isolated guard cells from *Dionaea*'s petiole and trap, there was a much lower expression than other guard cell marker genes (such as *SLAC1*) in guard cell (see [102] S5). SKOR was rather highly expressed in the trap, and as we have already seen, even higher in trigger hair (Figure 62). It then remains an open question of where *SKOR* might be expressed in *Dionaea*'s trap at tissue or cellular level.

AHA The majority of plant proton pumps are localised at the plasma membrane (PM), where, by utilizing ATP as an energy source, it expels H^+ out of the cell, a process that results in pH and electrical potential difference across the PM. This difference builds up the H^+ motive force needed for symporters, antiporters and uniporters to drive their selective ions against the concentration gradient [201, 202]. Recently, by using optogenetic tools, further evidence that AHA H^+-ATPase plays a major role in membrane depolarization has been brought [174]. In *Arabidopsis*, *aha1* mutants the SWP had a longer repolarization duration with reduced amplitude, suggesting AHA as an SWP repolarization phase regulator in response to wounding. Curiously, the JA marker genes *JAZ10* was expressed at a higher extent in distal leaves of the KO mutant than in WT and it was even more resistant to herbivore attack. Furthermore, the SWP duration was shortened in the gain-of-function *AHA1 mutants* [203]. In *Dionaea*, AHA4 is highly expressed in trap and trigger hair (Dm_00013634-RA, 2356.99 and 1306.33 FPKM, respectively) compared to the other eight AHAs expressed in other organs and tissues. This goes hand in hand with the observation that when the AP is prolonged in *Dionaea*, the expression of AHA is also downregulated, indicating its potential participation in AP shaping.

KDM After MSL, KDM1 is the second most specific channel in the trigger hair. Its *Arabidopsis* homologue, the Shaker-type inward rectifier channel KAT, is highly expressed in guard cells where it contributes to stomata opening by allowing K^+ uptake [161]. KDM1 has been electrophysiologically characterised (by members of our lab - Dr. Jennifer Böhm) as a pH-dependent hyperpolarization-activated K^+-selective channel. Moreover, we showed that its expression is predominant in the indentation + podium part of the trigger hair, rather than the lever part [102]. Cs^+, known as a K^+ channel blocker, when applied from outside can jam the pore and therefore halt the K^+ intake [204]. It has been shown to impair the KAT1-mediated stomatal opening [205]. We, therefore, showed that Cs^+ blocks KDM1-mediated steady-state currents (measured in *Xenopus laevis* oocytes expressing KDM1), as well as trigger hair–dependent excitability [102]. This might suggest that KDM1 is involved in K^+ uptake necessary for membrane potential and chemical gradient restoration following the hyperpolarization phase of the AP.

In conclusion, we have identified genes that are highly expressed in ready-to-snap highly-excitable adult traps when compared to unexcitable juvenile traps. Some of these genes encode for suitable candidates that might be involved in Ca^{2+} signalling (such as GLRs, OSCAs, CNGCs), others that might contribute to the AP depolarization phase (such as: ALMTs, ANOs). However, since the AP has a prolonged repolarization phase rather than the depolarization phase (in juvenile traps as well as in adult traps which are in digestion mode), it is more likely that our repolarization candidates (SKOR and AHA4) might have a strong influence in shaping the *Dionaea*-specific sharp AP. Further, we identified upregulated genes encoding for transporters that could be responsible for bringing back the membrane potential by allowing ions to return to their initial concentration in certain cellular spaces (such as KDM, HAKs, HUPs and HKTs for K^+, NRT for anions / nitrate as well as CAX and ACAs for Ca^{2+}).

3.1.5 Conclusion

In short, we discovered that the sharp action potential (AP) of *Dionaea muscipula* is wider, with a prolonged repolarization phase and an absent hyperpolarization under three different circumstances: **(i)** in juvenile traps that are not fully excitable yet, **(ii)** during digestion stage induced by artificial coronatine treatment and **(iii)** during natural digestion of insects. In all cases *GLR3.6, SKOR, AHA4* and *KDM1* had a higher expression in the adult excitable traps than in juvenile traps, being downregulated during digestion (Figure 20). On top of that, all of these candidate genes are trigger hair-specific (to a higher or lower degree). Additionally, we found out that *MSL10* is the most trigger hair-specific gene (Appendix Figure 62).

Therefore, based on the trigger hair-specificity analysis together with transcriptome analysis of excitable (adult traps) vs non-excitable traps (juvenile traps), I would mention the following candidates for each of the AP phases:

- The glutamate-receptor *DmGLR3.6* - highly enriched in the trigger hair, together with the mechanosensitive *DmOSCA1.7* might contribute to Ca^{2+} influx.
- The mechanosensitive *DmMSL10* channel - the most trigger hair-specific gene - might be responsible for the first depolarization that takes place at the trigger hair base upon bending.
- The K^+ outward rectifier *DmSKOR* - also enriched in the trigger hair - might be important for the repolarization phase of the AP by allowing K^+-efflux.
- The H^+-pump *DmAHA4* - might contribute to the repolarization as well as hyperpolarization phase of the AP.
- The K^+ inward rectifier *KDM1* - highly trigger hair-specific - might be needed for re-establishing the membrane potential and recharging the $[K^+]_{cyt}$ battery by allowing K^+-uptake.

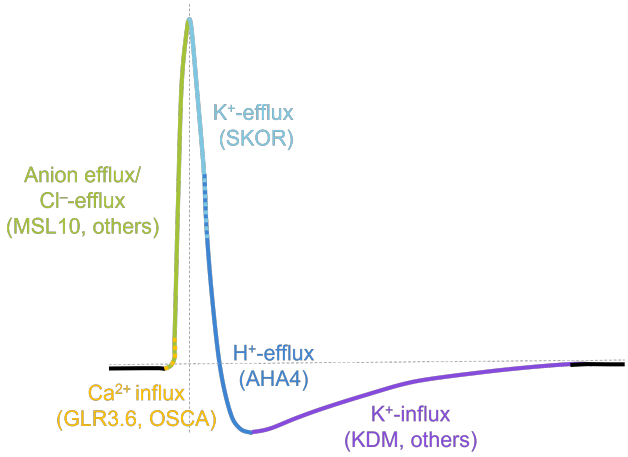

Figure 21: Action potential phases and candidate channels/pumps.

3.1.6 Outlook

Even though the experiments presented in this chapter shed more light onto possible molecular candidates that might generate and shape *Dionaea*'s action potential, in order to prove their proposed function, KO-mutant lines would have to be established in *Dionaea muscipula*.

As a successful *Dionaea*-transformation protocol has already been established by Suda and colleagues [82], it is hopeful that further transformation procedures might also be fortunate.

3.2 The 'ERROR' Mutant - A Snap Trap That Doesn't Snap

3.2.1 The Peculiar Behaviour of The 'ERROR' Mutant

3.2.1.1 Short Introduction

Before diving into the results, a small recap of *Dionaea muscipula*'s key steps necessary for the hunting cycle, is shortly summarised in this chapter. First, a normal and functional wild type (WT) *Dionaea muscipula* would wait for its prey in a literally tensed manner. In the adult stage, the elastic energy is stored within the CWs, arming the trap. When the trigger hairs are touched two times within ∼30 seconds, the elastic energy is suddenly released, snap shutting the trap into a relaxed state [97]. With every touch, an electrical signal (action potential, AP), as well as a Ca^{2+} wave, are generated and spread throughout the trap, alerting the plant of a potential prey [67, 82]. The initial fast signalling triggers two major processes that happen around the same time: the activation of *TCH* genes and the activation of jasmonic acid (JA) pathway-related genes that lead to JA biosynthesis. JA is known as the "wounding" hormone, operating defence mechanisms. However, carnivorous plants have undergone exaptation, in the end using these already at hand molecular pathways for carnivory-related purposes [25, 56]. Consequently, JA activates genes encoding for digestive enzymes, leading to digestive fluid secretion. Within this stage, the trap slowly closes further, sealing the trap and finally forming the green stomach (Figure 22).

In order to understand the trap snapping mechanism as well as the special molecular pathways activated by trigger hair bending (mechanostimulation) that carnivorous plants use in order to activate prey digestion processes, the use of naturally occurring mutants that are unable to react upon mechanostimulation can be of use. Therefore, the functional WT was compared with a non-functional 'ERROR' (ERR) cultivar that cannot snap its trap.

To study the curious behaviour of the 'ERROR' mutant, I performed studies using timelapse photography, for observing the slow trap closure. Additionally, using qPCR, I quantified the expression of marker genes for each of the key steps described above, in various experiments. Since mechanosensing was the main topic of this study, the touch stimulus was used as a reference and compared to other stimuli that trigger similar molecular processes. Thus, the reaction of both WT and ERR traps were monitored upon different stimulations: mechanostimulation (marked in green throughout the thesis), wounding (marked in orange) and coronatine (marked in turquoise) (Figure 22).

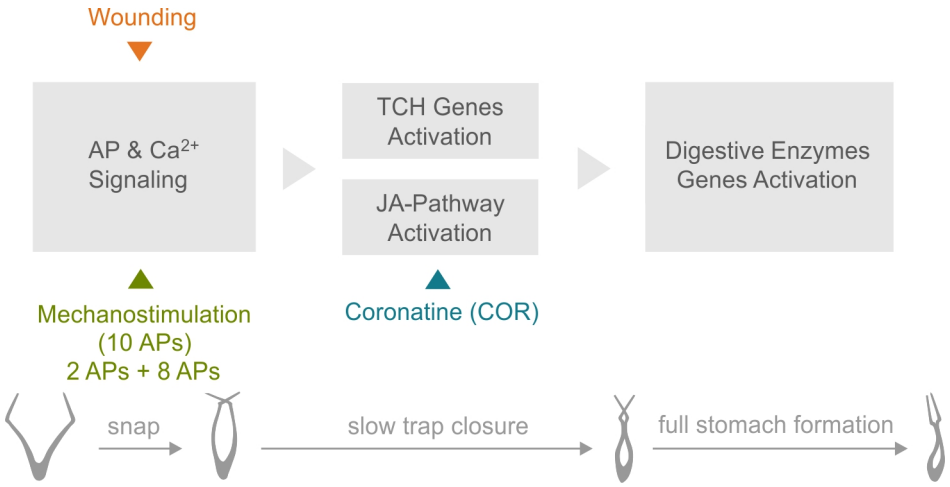

Figure 22: Overview flowchart showing the main molecular milestones activated upon different treatments used in this study. After 2 APs, the WT trap snaps, more than 5 APs will lead to slow trap closure as a preparation step for full stomach formation.

Mechanostimulation was done by bending the trigger hairs (for most of the experiments 10 times, leading to the elicitation of 10 APs). Wounding was done by squeezing the trap lobe once using tweezers without touching the trigger hairs, leading to firing of ~ 5-8 APs. And finally, coronatine (COR) treatment consisted of coronatine (0.1 mM) sprayed on the open trap surface (adaxial side) (see chapter 2.2.3.1, Exp_ERR). COR is the molecular mimic of the active JA active form (JA-Ile), which feeds directly into the JA pathway, bypassing the electrical signalling, and therefore directly activating the digestive enzymes. It has been shown by previous studies, that COR application forces the trap into secretion mode within 24h in the wild type [101]. However, in the 'ERROR' mutant little or nothing is known about the main molecular milestones upon all these different stimuli.

3.2.1.2 The 'ERROR' Mutant Is Able to Fire Action Potentials

As described by the horticulturalist Mathias Maier, the *Dionaea muscipula* 'ERROR' cultivar (or in short, the ERR mutant) is morphologically indistinguishable from the wild type (WT) (Figure 23A,C) and has the same growth habit [4].
When the trigger hair is bent, mechanosensory cells initiate an all-or-nothing electrical response that propagates throughout the whole trap (action potential, AP). The shape of the AP is the same in both phenotypes (Figure 23B,D). As measured by Dr. Sönke Scherzer, the membrane resting potential (∼110 mV), the depolarization amplitude (∼120 mV) and the AP duration (∼1 - 1.5 seconds) are not significantly different in the ERR mutant than in WT.

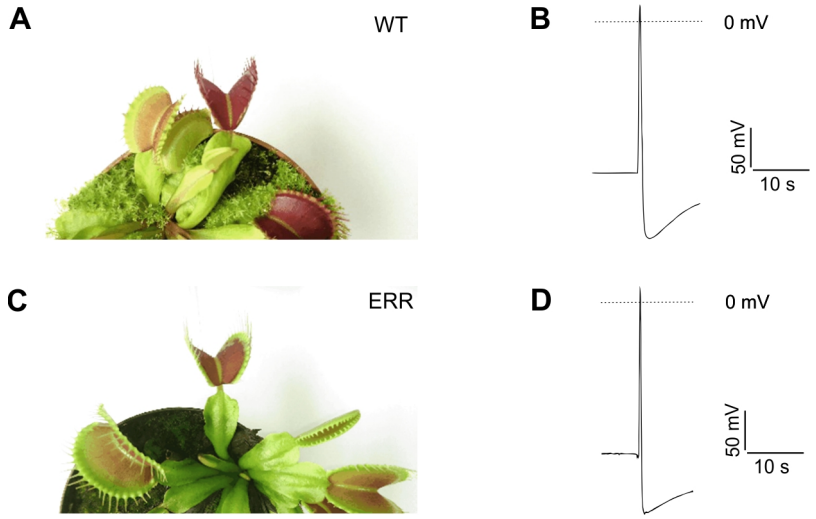

Figure 23: Morphological features as well as electrical excitability are normal (*i.e.* wild type - like) in the 'ERROR' mutant. The two phenotypes look apparently the same: WT (A) and ERR (C). Upon touching the trigger hairs, the AP in ERR (D) looks the same as in WT (B). AP was measured by Dr. Sönke Scherzer.

3.2.1.3 The 'ERROR' Mutant Traps Are Able to Leisurely Close Upon Repeated Mechanostimulation

It has been repeatedly observed by many botanists, that upon elicitation of two action potentials (APs), within a very short time frame, in the majority of cases the WT traps snap shut [7, 64, 67, 108]. In this study, I could confirm it once again. With an interval of 30 seconds, indeed, all of the WT traps snap-shut completely (Figure 24, dark green triangles, lower photo). When applying the same treatment to the ERR, the majority remained open. However, there was one exception. Out of nine traps, one showed a peculiar behaviour: a slow partial closure of the trap (Figure 24, light green triangles, middle photo). During the experiment I made sure that the traps had not seen any previous stimulation in the last 24h. This exception has led to a further investigation of the ERR mutant's response upon repeated mechanostimulation.

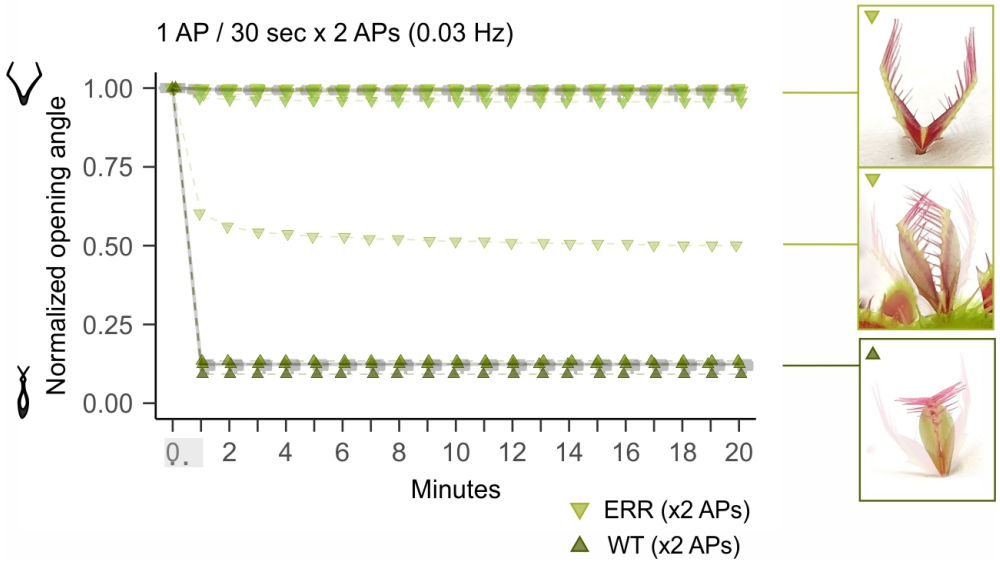

Figure 24: Normalised trap opening angle after the application of two trigger hair touches (inducing 2 APs, with a frequency of 0.03 Hz) in ERR (light green) and WT (dark green). For each sample, the angle values are normalized to the maximum opening angle before the treatment started. 1 = open trap, 0 = sealed trap. The grey highlight on the x-axes represents the duration of the treatment, each point showing when the AP was induced. Representative photos corresponding to ERR traps that did not close (up), half-closed (middle) and WT traps that closed completely (down) are shown. $n = 9$ for ERR and $n = 3$ for WT for each group.

Therefore, I measured the opening angle of the traps after the elicitation of 10 and 20 APs with different frequencies: 0.01 Hz, 0.03 Hz and 0.06 Hz, as seen in Figure 25. We could notice that upon 10 APs, in general, the response was weak for the ERR. However, two to three outliers (out of 12 tested for each group) could be observed, that led to a bimodal distribution. This can be more easily seen in Figure 26A,C,E together with representative pictures of traps at the end of the treatment for each group (Figure 26).

But more interesting was the behaviour upon 20 APs, when most of the traps had a stronger trap closure response no matter the frequency. The strongest signal with 25 - 80% closure, has been observed for the 0.03 Hz frequency (Figure 25D). In my opinion, this indicates that in the case of the 0.01 Hz group, we can see the memory fading, making it harder to reach the threshold after 1 minute. An observation that is valid for all types of treatments, is that

a plateau was reached right after the termination of the treatment. In other words, the traps' response stops together with the mechanostimulation, indicating that the signal is not "stored" for long.

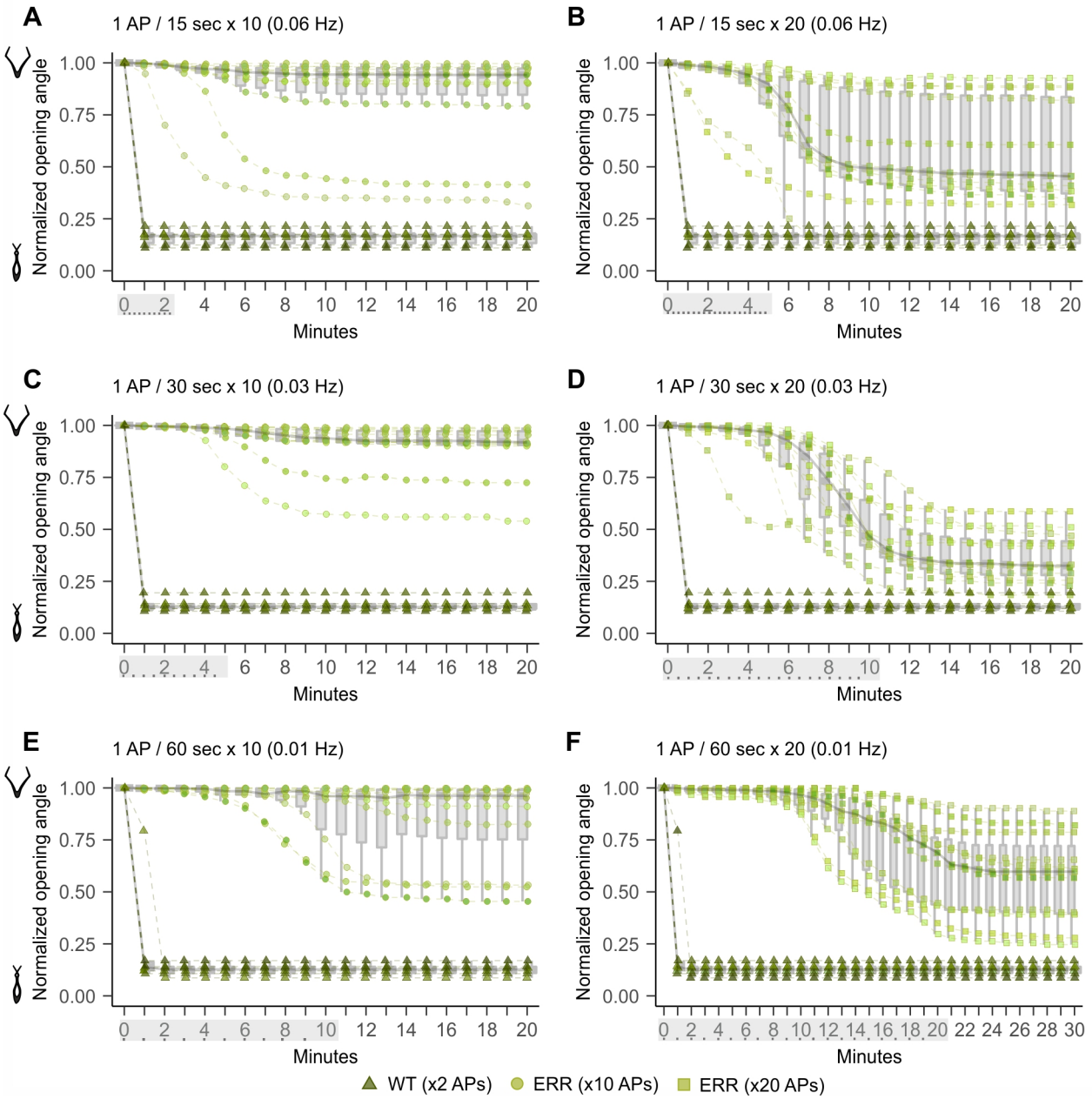

Figure 25: Trap opening angle after the application of 10 and 20 trigger hair touches (inducing 10 and 20 APs, respectively) with different frequencies: 0.01 Hz, 0.03 Hz and 0.06 Hz in ERR (light green) and WT (dark green). In the case of WT, only 2 APs were induced which directly led to trap closure. For each sample, the angle values are normalized to the maximum opening angle before the treatment started. 1=open trap, 0=sealed trap. The grey line connects the median of each boxplot showing the trend across the timeline for each group. The grey highlight on the x-axes represents the duration of the treatment, each point showing when the AP was induced. $n = 12$ for ERR and $n = 6$ for WT for each group.

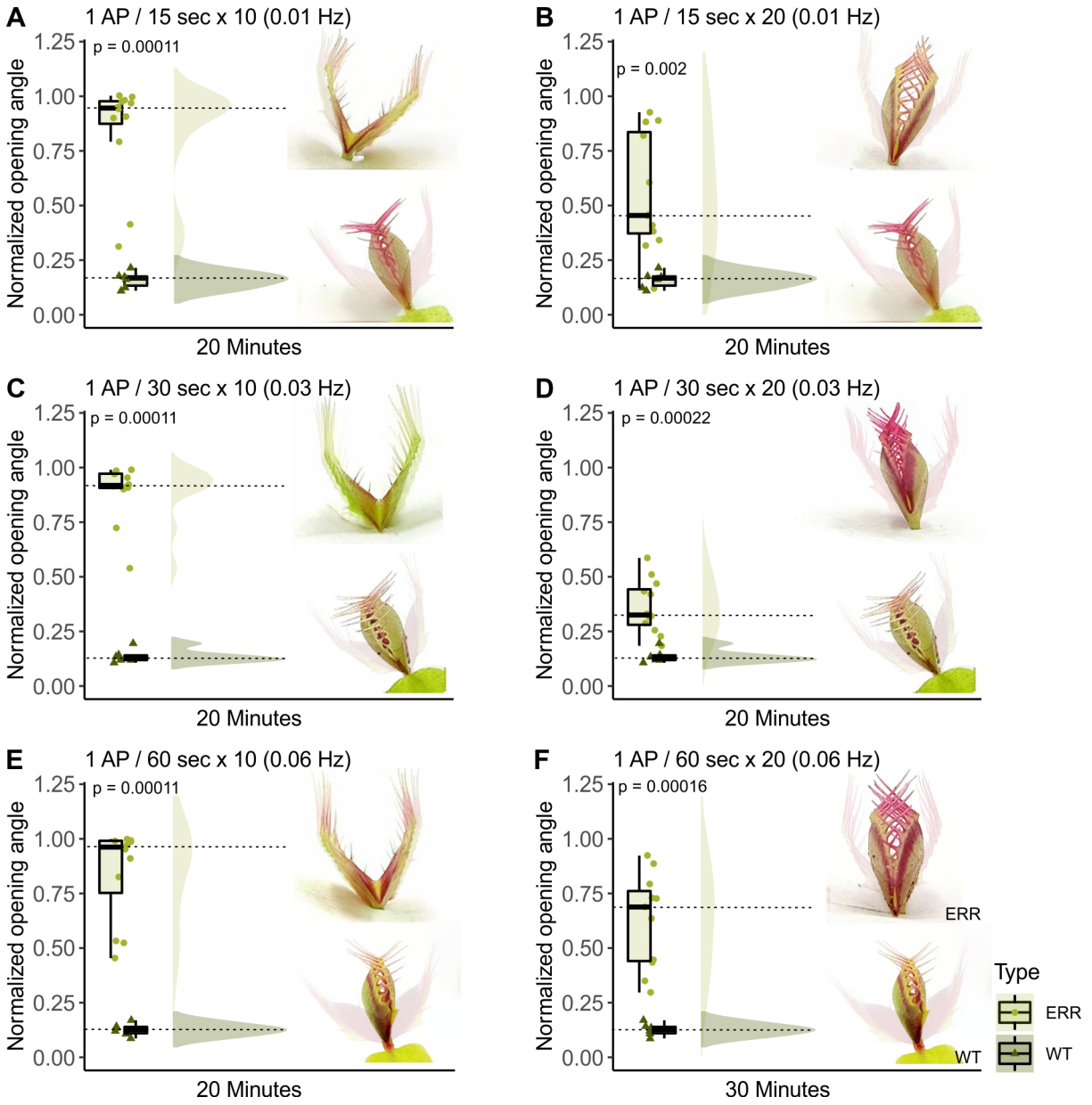

Figure 26: Representative photos showing the trap opening angle before and after the application of 10 and 20 trigger hair touches for each group at the end of the treatment (inducing 10 and 20 APs, respectively) with different frequencies: 0.01 Hz, 0.03 Hz and 0.06 Hz in ERR (light green) and WT (dark green). In case of WT, only 2 APs were induced which directly led to trap closure. For each sample, the angle values are normalized to the maximum opening angle before the treatment started. The boxplot together with the semi-violin plot shows the distribution of the samples in each ERR versus WT group, with a significant difference between the two (Wilcoxon test). $n = 12$ for ERR and $n = 6$ for WT for each group.

3.2.1.4 The 'ERROR' Mutant Traps React Slower Upon Coronatine Treatment

Besides mechanostimulation, as explained in the previous chapter (3.2.1.3), COR (coronatine) can bypass the electrical signalling, turning on the digestive processes right away. Knowing that WT already forms a green stomach 24h after COR application, the next step was to quantify the change in opening angle over a period of 48h. The first interesting observation was that the traps open wider than the starting angle, and then slowly close with a steep curve in the

case of WT as it can be seen in Figure 27A. In my view, this might represent the buckling of the trap, which can be described as a highly accelerated (or very sudden) change in trap geometry from convex to concave [206]. A less steep curve (with many intermediate steps) can be observed in the case of ERR (Figure 27C), suggesting that the buckling system might be defective. In a normal situation upon natural mechanostimulation, after the snapping, the trap continues to close further. This process is accompanied by longitudinal cell elongation (in the midrib to rim direction). The rim is an essential part of the stomach, as it undergoes strong modification so that the trap lobes can strongly press against one another, letting the teeth from each lobe become oriented outwards, parallel to each other. Upon COR application, we might see exactly the process of sealing the trap, but since it precedes the trap snapping, it looks like a trap opening overstretch.

In order to check if there is a significant difference in the curve steepness between the two phenotypes, I measured the closure time (by subtracting the last time point with a value close to the open state of 1 +/-0.05 by the first time point with a value close to the closed state of 0.2 +/-0.5) (Figure 27D) and then calculated the closure speed (Figure 27B). And indeed, there is a statistically significant difference between the two, with a higher closure speed for WT, and implicitly a shorter closure time. Thus, ERR is slower upon COR treatment as well as upon mechanostimulation.

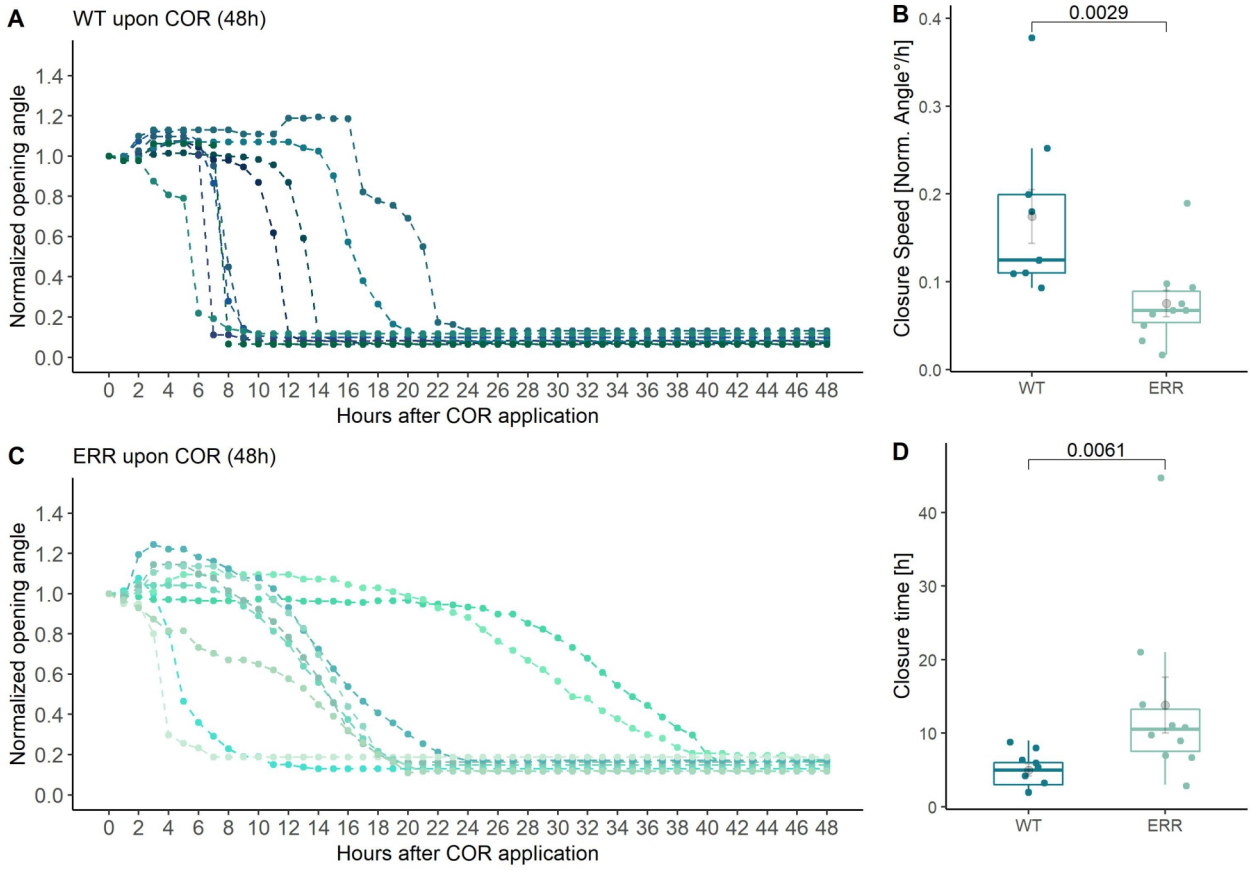

Figure 27: Trap opening angle after the application of coronatine (COR) treatment in WT (A) and ERR (C). The closure speed is shown as normalized opening angle per hour (B). The closure time (D) refers to the time between < 0.9 normalized opening angle value and minimum normalized opening angle value for each sample (representing the slope). Wilcoxon test p-value is shown between the two groups. $n = 10$ for ERR and $n = 10$ for WT for each group.

3.2.1.5 Touch Genes Respond Differently in the 'ERROR' Mutant Traps

We know from *Arabidopsis thaliana*, that the so-called "touch genes" are marker genes that get activated upon mechanostimulation by gently brushing the leaves with a cotton swab, as well as squeezing the leaves or even in the form of light wind or rain touch [207].
During my master thesis [208], I checked the expression of *DmTCH1*, *DmTCH2*, *DmTCH3* and *DmTCH4* in the WT. From all of them, *DmTCH2* and *DmTCH4* turned out to be perfect marker genes upon trigger hair mechanostimulation in *Dionaea muscipula*. Furthermore, I found out that *DmTCH2* is activated by one touch, while *DmTCH4* requires two touches in order to become upregulated (Figure 28). This makes sense in the light of their function. *DmTCH2* encodes for a calmodulin-like protein (CML24), which is already active in the trap's resting state, since the Ca^{2+} wave already occurs after the first stimulation, the DmTCH2 would already be there to bind Ca^{2+} and decode the signal. Further mechanostimulation prepares the trap to respond faster by increasing the expression of *DmTCH2*, guiding the trap into full digestion mode. As for *DmTCH4*, it encodes a cell wall (CW) modifying enzyme (XTH22, a xyloglucan endotransglucosylase). This enzyme might be important for the CW modifications that occur together with cell expansion during the slow trap closure leading to full stomach formation. Therefore, this protein might be needed only after the snapping has taken place.

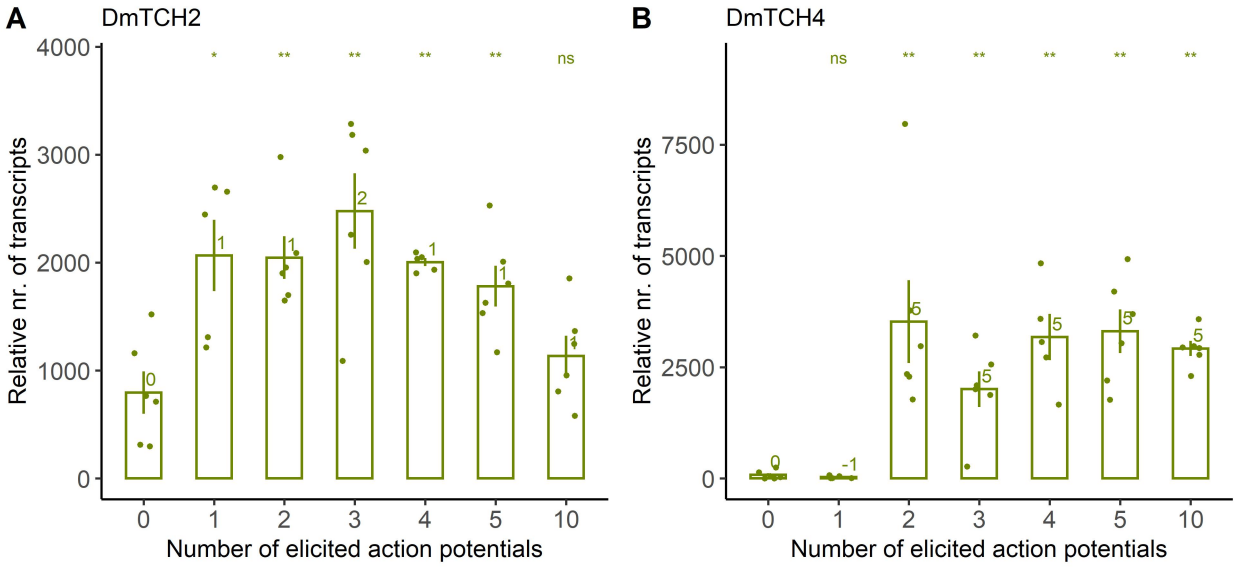

Figure 28: qPCR expression level of *DmTCH2* (A) and *DmTCH4* (B) upon different number of elicited action potentials by mechanostimulation (0.01 Hz) in WT traps after 1h. The relative number of transcripts is normalised to 10 000 molecules of actin *DmACT1*. The bar chart shows average values +/- SE and the dots show the values of each measured sample. The numbers above the bar chart represent $\log_2$FC values relative to the control group. Above the chart, the Wilcoxon rank sum test p-value is represented with stars: * for $p < 0.05$, ** for $p < 0.01$, *** for $p < 0.001$, ns = not significant. $n = 6$.

Having this in mind, the next step was to check how are these genes expressed in the ERR mutant. For this, I applied mechanostimulation treatment (10 APs, 0.01 Hz), and quantified their expression level across the given time frame. What we could see is that for *DmTCH2* the expression was similar in ERR compared to WT, both reaching a peak after around 1h and already fading after 2h (Figure 29A). If we assume that *DmTCH4* is indeed needed for stomach formation, then it is not surprising that *DmTCH4* is not activated in the still open ERR traps,

with a statistically significant difference after 2h ($\log_2$FC = 8 in WT and undefined for the ERR) (Figure 29B).

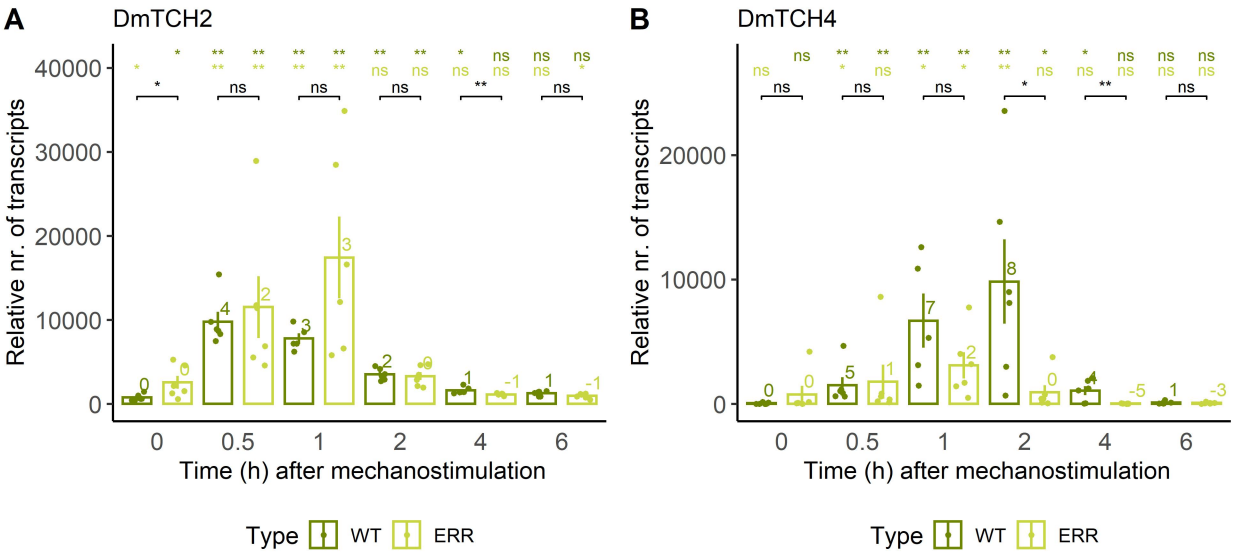

Figure 29: qPCR expression level timeline of *DmTCH2* (A) and *DmTCH4* (B) upon mechanostimulation (10 APs, 0.01Hz) in WT and ERR traps. The relative number of transcripts is normalised to 10 000 molecules of actin *DmACT1*. The bar chart shows average values +/- SE and the dots show the values of each measured sample. The numbers above the bar chart represent $\log_2$FC values relative to the corresponding control of each phenotype. Above the chart, the Wilcoxon rank sum test p-value is represented with stars: * for $p < 0.05$, ** for $p < 0.01$, *** for $p < 0.001$, ns = not significant. The colours of the stars indicate to which control the comparison was made (dark green = WT control, light green = ERR control). $n = 6$.

Further experiments done by other research team members have shown that these two touch genes are activated by other stimuli as well (like cold - experiment done by Katharina Federspiel, and even COR - experiments done by Brigitte Neumann and Kevin Bongers), but not to the same extent as mechanostimulation (Appendix Figure 65). However, upon wounding, the response was also very strong and similar in the expression profile to the touch (Appendix Figure 66).

The next task, was to check whether the activation pathway as well as biosynthesis of the wounding hormone, jasmonic acid (JA), are affected in the ERR.

3.2.1.6 The 'ERROR' Mutant's Jasmonic Acid Level Is Reduced Upon Mechanostimulation and Impaired Upon Wounding

Jasmonic acid (JA) is a plant hormone that is generally involved in stress responses, including defence mechanisms. In carnivorous plants, however, JA plays a pivotal role in the activation of the digestion process, finally leading to the release of hydrolytic enzymes.
First, I checked the expression profile of JA pathway marker genes, such as the JA-Ile (the active form of JA) receptor *DmJAZ1* and its coreceptor *DmCOI* investigated upon mechanostimulation (10 APs, 0.01 Hz). Curiously, there was no statistically significant difference between WT and ERR for both of the genes, with the strongest response after 2h for both (when *DmJAZ1* was upregulated and *DmCOI* downregulated)(Figure 30). However, it seems like there could be a tendency towards lower expression values in the ERR, especially at 1h time point.

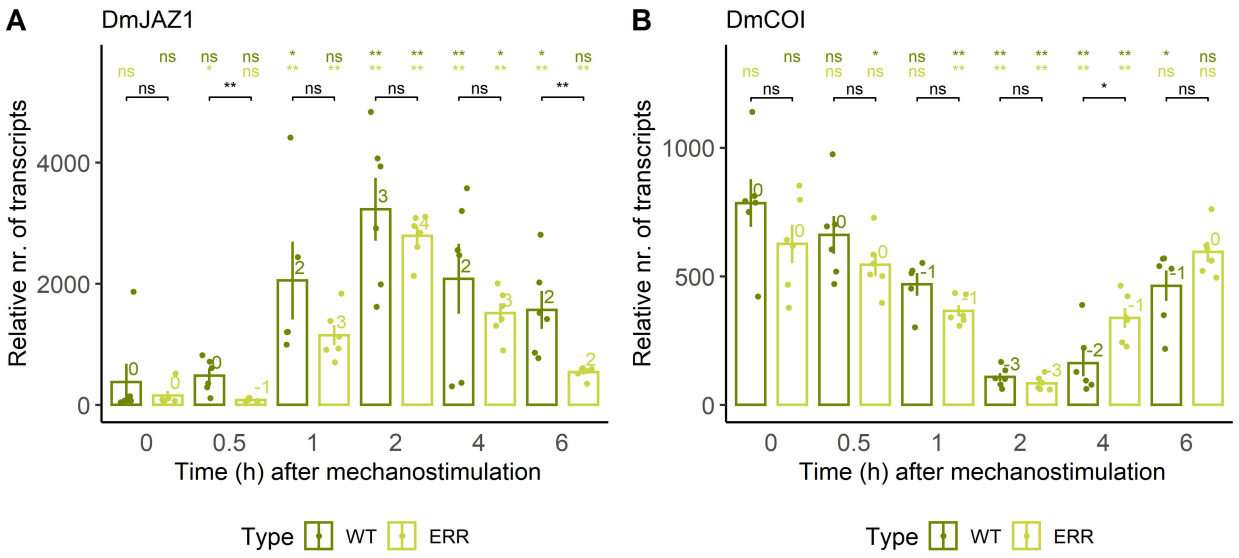

Figure 30: qPCR expression level timeline of *DmJAZ1* (A) and *DmCOI* (B) upon mechanostimulation (10 APs, 0.01Hz) in WT and ERR. The relative number of transcripts is normalised to 10 000 molecules of actin *DmACT1*. The bar chart shows average values +/- SE and the dots show the values of each measured sample. The numbers above the bar chart represent $\log_2$FC values relative to the corresponding control of each phenotype. Above the chart, the Wilcoxon rank sum test p-value is represented with stars: * for $p < 0.05$, ** for $p < 0.01$, *** for $p < 0.001$, ns = not significant. The colours of the stars indicate to which control the comparison was made (dark green = WT control, light green = ERR control). $n = 6$.

On that account, the amount of jasmonates (JA, JA-Ile and OPDA - the precursor of JA) accumulated in the traps after mechanostimulation (10 APs, 0.01 Hz) was further investigated. In WT, all jasmonates had a statistically significant higher level already after 0.25h, returning to resting-state level after 24h (Figure 31A,C,E). In the ERR, the JA and JA-Ile concentrations were around half compared to WT, and faded even faster (after 3h) (Figure 31A,C). The OPDA levels, however, were not statistically different from the WT (Figure 31E).

Since JA is also known as "the wounding hormone" accumulating after inflicting structural leaf injury [209], the next question was: how would the jasmonate levels change after strongly squeezing the trap lobes using sharp tweezers, ensuring cell damage and tissue rupture? As

shown in Figure 31B,D,F, the jasmonates show a high concentration level after 3h in WT, while in the ERR stay at ground state levels throughout the whole experimental time frame. In my judgement, this might indicate that in the functional WT, the mechanostimulation-activated pathway might be different from the wound-induced pathway, even if both may be orchestrated by the stress hormone, JA. This idea is also supported by the fact that in the ERR, the mechanostimulation response is dampened while the wound-induced response seems highly affected.

To look a bit deeper into this issue, we wanted to investigate if the broken response in the ERR is restricted to the trap organ, which has evolved to serve special plant carnivory-related processes such as high sensitivity for prey detection and digestion. So how about the "normal" plant organs, such as the petiole? For this, the petiole (lamina + midrib) was squeezed in the same way as the trap, leading to cell and tissue damage. Interestingly, the JA and JA-Ile levels were as high in the wounded petioles of ERR plants as in WT plants, with a non-significant statistical difference (Figure 32B,D).

That being the case, we can now come back to the mechanostimulation-induced digestion process, and move on to the last step of the digestive cycle: the hydrolase gene induction and digestive fluid secretion.

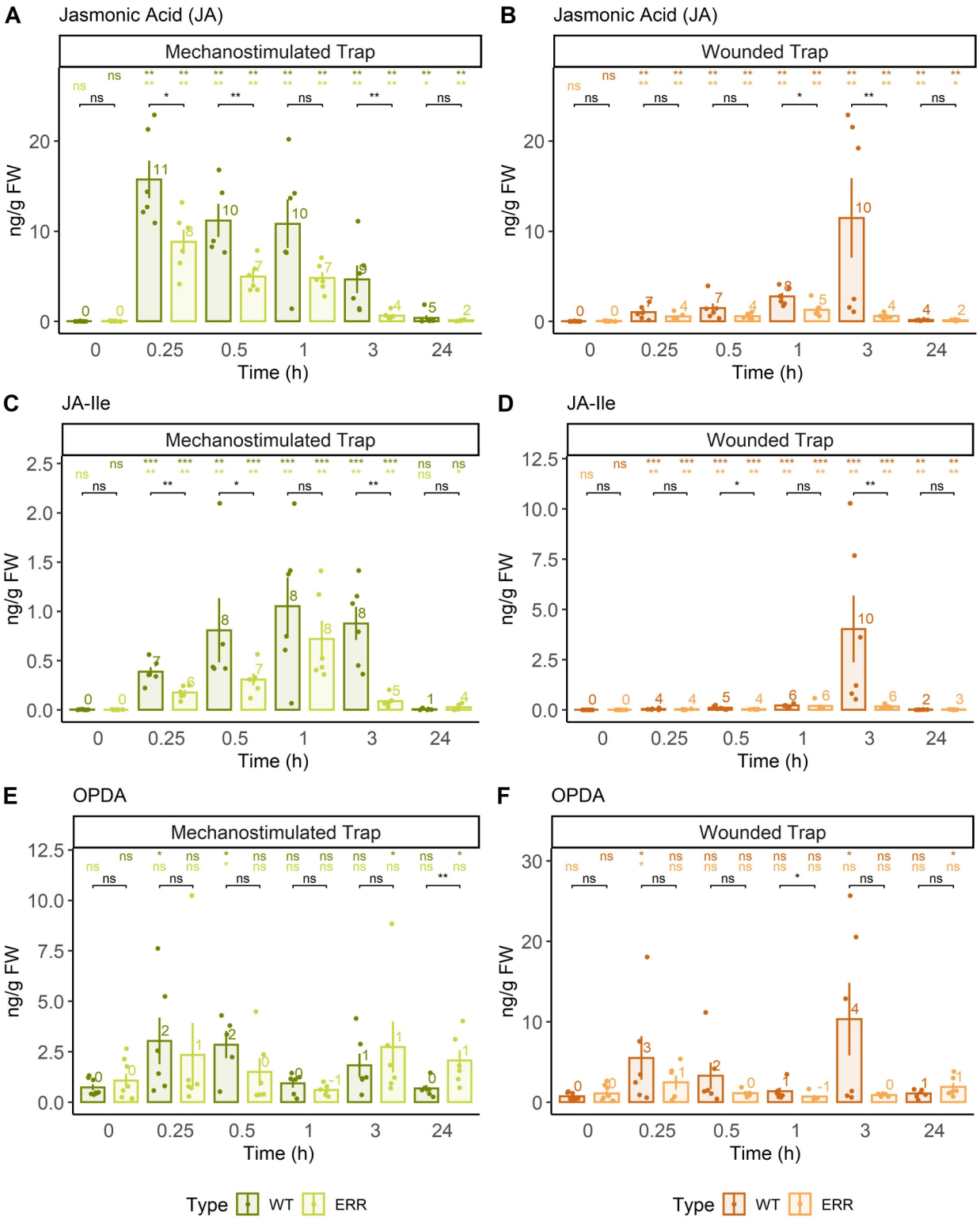

Figure 31: Concentration levels upon mechanostimulation (10 APs, 0.01 Hz) (left) and wounding (right) of JA (A,B), JA-Ile (C,D), OPDA (E,F) in WT and ERR traps. The bar chart shows average values +/- SE and the dots show the values of each measured sample. The numbers above the bar chart represent $\log_2$FC values relative to the corresponding control of each phenotype. Above the chart, the Wilcoxon rank sum test p-value is represented with stars: * for $p < 0.05$, ** for $p < 0.01$, *** for $p < 0.001$, ns = not significant. The colours of the stars indicate to which control the comparison was made (dark colour = WT control, light colour = ERR control). $n = 6$. FW = fresh weight.

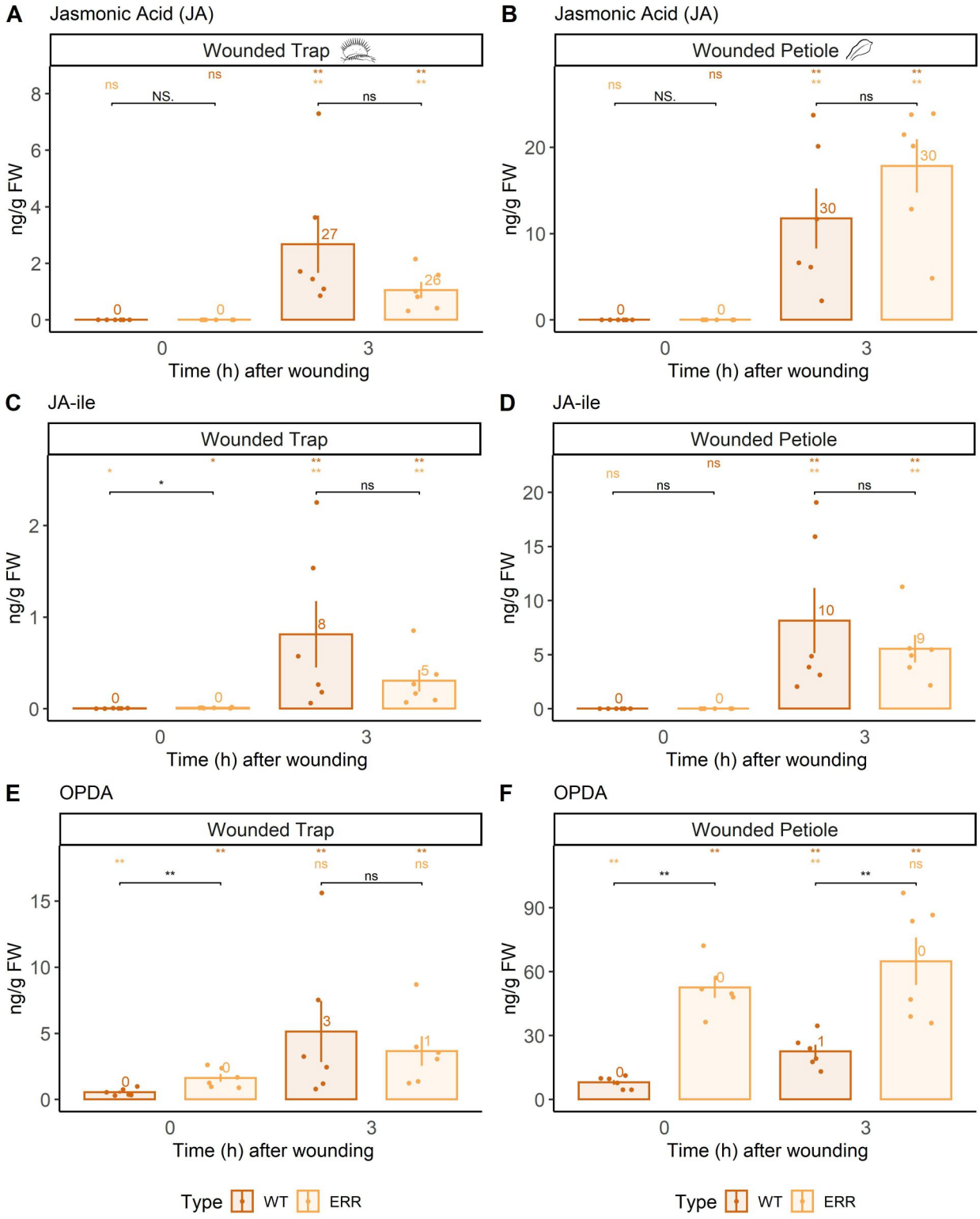

Figure 32: Concentration levels upon wounding traps (left) and petioles (right) of JA (A,B), JA-Ile (C,D), OPDA (E,F) in WT and ERR petioles. The bar chart shows average values +/- SE and the dots show the values of each measured sample. The numbers above the bar chart represent $\log_2$FC values relative to the corresponding control of each phenotype. Above the chart, the Wilcoxon rank sum test p-value is represented with stars: * for $p < 0.05$, ** for $p < 0.01$, *** for $p < 0.001$, ns = not significant. The colours of the stars indicate to which control the comparison was made (dark orange = WT control, light orange = ERR control). $n = 6$.

3.2.1.7 The 'ERROR' Mutant Secretes Digestive Fluid Upon Coronatine Application But Not Upon Mechanostimulation

As already presented in the "Short Introduction" (chapter 3.2.1.1), the last stage investigated throughout the hunting cycle is the activation of digestive enzymes that finally leads to digestive fluid secretion. Therefore, I quantified the expression of the famous marker hydrolases genes: the cysteine protease *DmSAG12* and the chitinase *DmCHIB* [56]. Upon mechanostimulation (10 APs, 0.01Hz), in the case of WT we can see an expression peak reached after 2h for *DmSAG12* (Figure 33A) and after 4h for *DmCHIB* (Figure 33B). Since *Dionaea muscipula* is adapted to the repetitive struggling of a real insect-prey that will hit the trigger hairs more than 10 times, it is not surprising that the expression level vanishes within 6h after only 10 artificially induced APs. When comparing the peak expression of *DmSAG12* between WT and ERR, a lower level, but not statistically significant difference could be observed. But on a small note: the expression level drops much faster in ERR traps (already after 4h) (Figure 33A). Similar results were obtained for *DmSCPL49*, another hydrolase-marker gene. However, *DmCHIB* seems to have a faulty expression profile compared to WT, being already expressed in untreated traps and unchanged after mechanostimulation stimulus was applied.

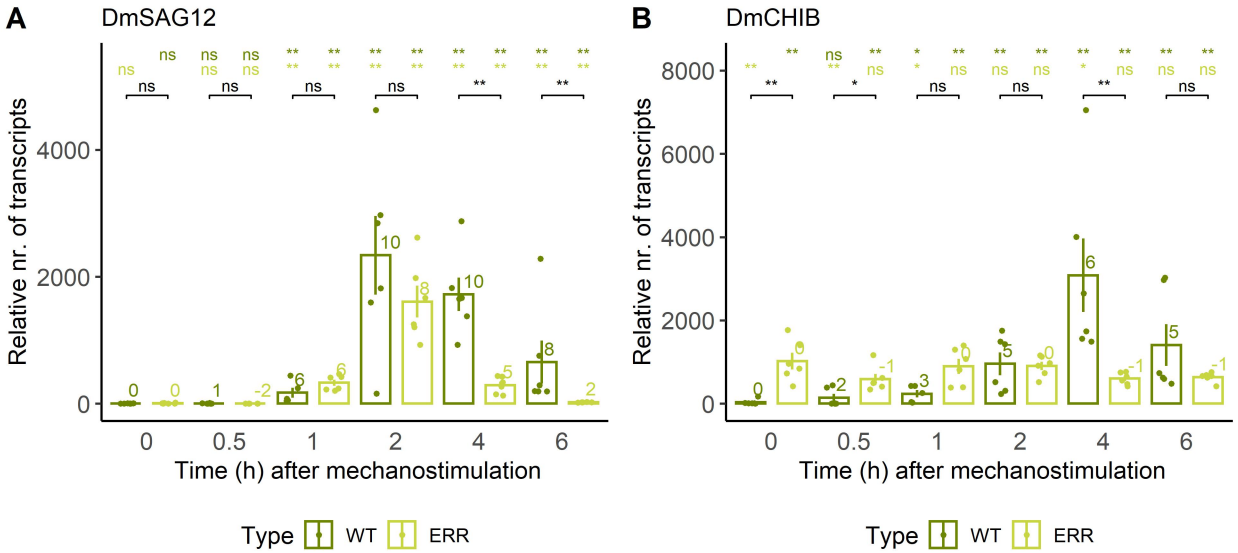

Figure 33: qPCR expression level timeline of *DmSAG12* (A) and *DmCHIB* (B) upon mechanostimulation (10 APs, 0.01Hz) in WT and ERR traps. The relative number of transcripts is normalised to 10 000 molecules of actin *DmACT1*. The bar chart shows average values +/- SE and the dots show the values of each measured sample. The numbers above the bar chart represent $\log_2$FC values relative to the corresponding control of each phenotype. Above the chart, the Wilcoxon rank sum test p-value is represented with stars: * for $p < 0.05$, ** for $p < 0.01$, *** for $p < 0.001$, ns = not significant. The colours of the stars indicate to which control the comparison was made (dark green = WT control, light green = ERR control). $n = 6$.

Since the data indicate that the native (*de novo*) JA biosynthesis is dampened in the ERR (Figure 31), we further wondered if the externally applied jasmonate (in the form of COR) is perceived and therefore leads to the activation of the main digestive-marker enzymes. Similar to mechanostimulation, the expression is lower in ERR traps at the peak (24h), but not statistically significant in the case of *DmSAG12* (Figure 34A), while being statistically significant for *DmCHIB* (Figure 34B).

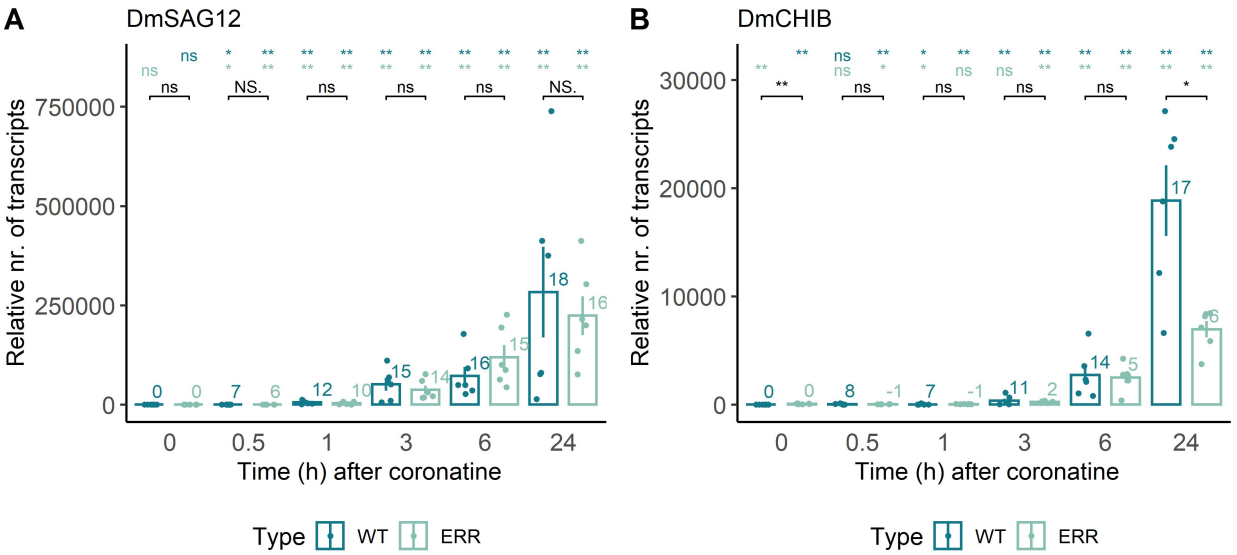

Figure 34: qPCR expression level timeline of *DmSAG12* (A) and *DmCHIB* (B) upon COR (0.1 mM coronatine) in WT and ERR traps. The relative number of transcripts is normalised to 10 000 molecules of actin *DmACT1*. The bar chart shows average values +/- SE and the dots show the values of each measured sample. The numbers above the bar chart represent $\log_2$FC values relative to the corresponding control of each phenotype. Above the chart, the Wilcoxon rank sum test *p*-value is represented with stars: * for $p < 0.05$, ** for $p < 0.01$, *** for $p < 0.001$, ns = not significant. The colours of the stars indicate to which control the comparison was made (dark turquoise = WT control, light turquoise = ERR control). $n = 6$. Experiment done by Brigitte Neumann.

Even though these marker enzymes genes are a good indicator for the digestive processes, I further inspected if the final product, the amount of digestive fluid, is the same or different in the two phenotypes upon mechanostimulation versus COR treatment.

As noted in the previous chapter (3.2.1.3), the strongest response upon mechanostimulation was observed for 20 APs with a frequency of 0.03 Hz, where the trap angle was reduced to roughly 55% in the ERR traps. Therefore, we wanted to know if the amount of secretion is measurable after 24h in this case (upon 20 APs, 0.03 Hz). The results show that in the ERR traps there was almost no secretion, while in the WT traps the digestive fluid was already noticeable (∼8µl, Figure 35A). We know that the digestive process responses fade, if no further stimulation is applied, as already mentioned above. Thus, the next question was: what would happen upon a more intensive mechanostimulation? For this, I applied 120 APs (0.03 Hz) continuously for 1h and 120 APs (0.03 Hz) interrupted (with a block of 20 APs every 1h for 6h). The WT traps secreted the highest amount of digestive fluid for the interrupted type of mechanostimulation (∼30µl, Figure 35C). Interestingly, in the case of ERR, a more intensive stimulation (no matter if it was continuous or interrupted) resulted in a very low amount of liquid, close to detection limits (∼2µl) and statistically significant from WT.

Upon COR treatment, the levels were very high (up to ∼55µl) in both phenotypes (Figure 35D), indicating that external application of jasmonates can redeem the proper function of the trap, at least regarding fluid secretion.

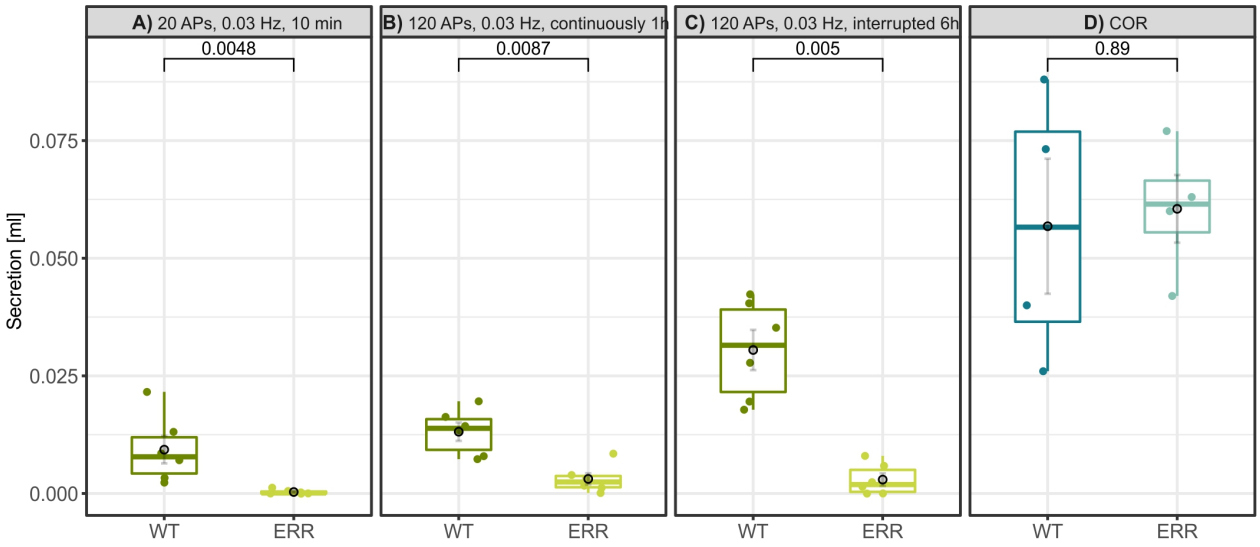

Figure 35: The amount of digestive fluid upon mechanostimulation after 24h with: A) 20 APs (0.03 Hz) elicited within 10 minutes, B) 120 APs (0.03 Hz) elicited continuously for 1h, C) 120 APs (0.03 Hz) elicited in an interrupted manner with a block of 20 APs every 1h for 6h and D) finally COR treatment after 72h by 0.1mM coronatine spraying in WT and ERR traps. Boxplot showing the median (horizontal line), the upper and lower quartiles (vertical lines). Average +/- SE shown as grey dot. The colored dots show the values of each measured sample. Wilcoxon rank sum test p-value is shown for each comparison. $n = 6$ for mechanostimulation, $n = 4$ for COR.

3.2.1.8 Short Summary

In the following summary flowchart, we can see the overall differences in the ERR (when using WT as a reference). The general "take-home message" regarding the expression level of important marker genes as well as the concentration levels of measured compounds for each of the main molecular milestones upon different treatments are sketched in Figure 36.

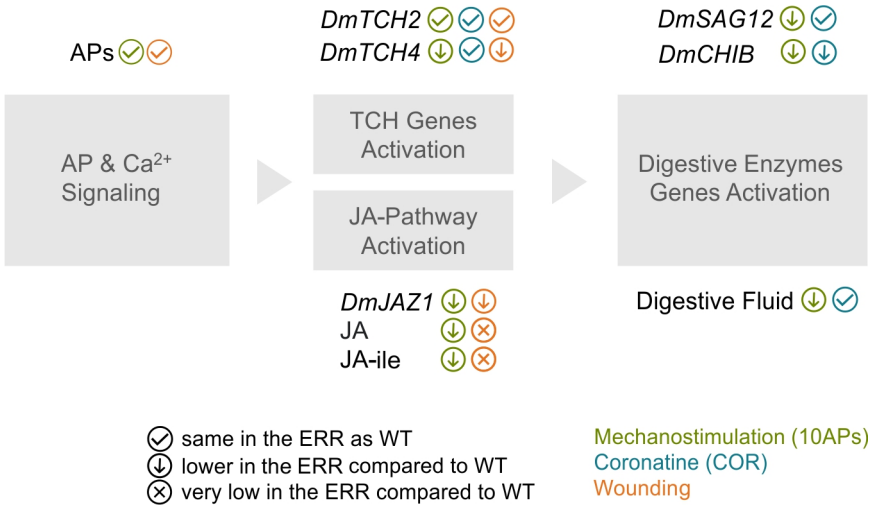

Figure 36: Overview flowchart showing the results summary of the signals/genes/hormones in ERR compared to WT within the main molecular milestones upon different treatments.

In short, it's important to emphasize the following findings:

- The ERR mutant can fire APs (like those of WT).
- Even though not able to snap, the ERR can still move their traps very slowly (within minutes) at various degrees upon repeated mechanostimulation, with the strongest response upon 20 induced APs (with a frequency of 0.03 Hz).
- The ERR mutant traps close slower upon COR treatment compared to WT.
- The touch gene and CW modifier *DmTCH4* is not activated upon touch (or wounding) in ERR to the same extent as in WT, while the calmodulin *DmTCH2* has similar expression levels in both phenotypes.
- Jasmonic acid levels are dampened in touch-treated traps and close to control levels in wounded traps of the ERR compared to WT, while the levels in the wounded petiole are similar in the two phenotypes, indicating that the ERR syndrome might be a trap-restricted phenotype.
- The marker hydrolases genes are slightly lower in the ERR upon mechanostimulation. The digestive fluid amount is lower in the ERR upon mechanostimulation, but similar to WT upon COR treatment.

3.2.2 Decoding The 'ERROR' Mutant's Transcriptome

3.2.2.1 Short Introduction and Overview

To better understand the reasons behind the peculiar behaviour of the 'ERROR' mutant, I delved into its transcriptomic landscape and analysed the transcriptome-wide gene expression upon different stimulations. We were particularly interested in the perception and translation of the touch stimulus.

As described in chapter 3.2.1.5, an important touch gene, *DmTCH4*, already gave us a clue that the ERR mutant presents some transcriptional defects. Besides this, the low jasmonates levels upon touch, also indicate a defect in the biosynthesis pathway (or in the signalling cascade leading to the induction of JA biosynthesis). For this reason, we used the 1h timestamp, when the *TCH* genes, as well as JA-pathway components, are highly active. Furthermore, we asked how the transcriptional profile would look like when external JA was applied. On that account, coronatine (COR), the molecular mimic of the active JA-Ile was sprayed on the open trap surface, which was then harvested at 1h time point as well, in order to have it comparable with the mechanostimulation treatment.

The experimental design overview scheme can be seen in Figure 37. The colours are consistent with previous chapters: green for mechanostimulation, turquoise for COR and additionally yellow for the ground (or resting) state.

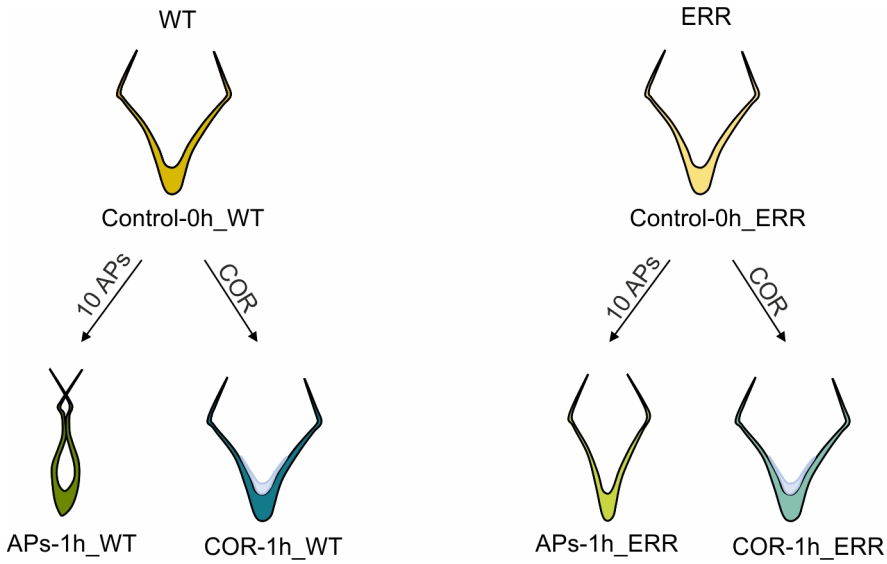

Figure 37: RNA-seq experimental design overview scheme for WT (left, dark shades) and ERR (right, light shades). 10 APs = mechanostimulation of the trigger hairs resulting in elicitation of 10 APs with a frequency of 0.01 Hz (1 AP per minute). COR = 0.1 mM coronatine treatment sprayed on the adaxial surface of the trap. Traps were harvested after 1h for both treatments.

The PCA gives us a great overview of the relation between the control and treatment groups as well as between the two investigated phenotypes. First, we notice that replicates within the same group are in close proximity to each other. This is a good indication that the variance within treatment groups is small. Interestingly, we can see that on the y-axes (which represents 25% of the variance), the WT (triangles) clearly separates from the ERR (circles)(Figure 38), reflecting that the two phenotypes are slightly different at transcriptomic level. The x-axes, which carries a higher variance (55%), separates the control groups from the treatment groups. The furthest away, indicating a strong difference from the rest of the groups, are the mechanostimulated WT replicates.

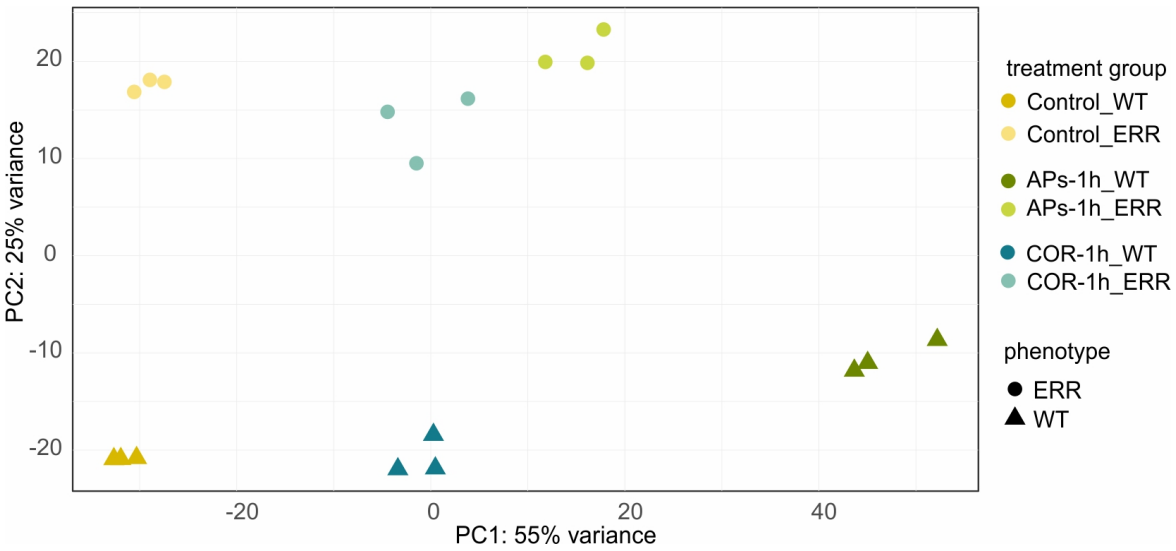

Figure 38: PCA analysis of the replicates. APs-1h = mechanostimulation of the trigger hairs resulting in elicitation of 10 APs with a frequency of 0.01Hz harvested after 1h. COR-1h = 0.1mM coronatine treatment sprayed on the adaxial surface of the trap and harvested after 1h. The treatments were applied for both phenotypes: WT and ERR.

Looking at the clustering of the top 50 most variable genes, based on the $\log_2$-transformed gene expression level (normalised counts) across all treatments, represented as a heatmap in Figure 39, three main branches can be seen. The first one comprises genes that have low expression values in ERR compared to WT across all conditions. Next group contains genes that are activated upon touch as well as COR treatment in both phenotypes, but to a lower extent in ERR. And the last group seems to include genes that are more specific to mechanostimulation (rather than COR), which again show lower expression values in the ERR traps. We will re-encounter and discuss the function of some of these genes in more detail within the analysis of the chapters to follow.

In order to analyse which of these genes are statistically significantly different from the control group, I further performed pairwise differential expression analysis between each treatment group and its own control group, as it is represented in Figure 40A.

The $\log_2$FC values of each pairwise comparison, together with the expression levels (FPKM values) of each condition, are shown in Appendix Table 20 for all the genes that are mentioned in the following chapters and throughout the figures.

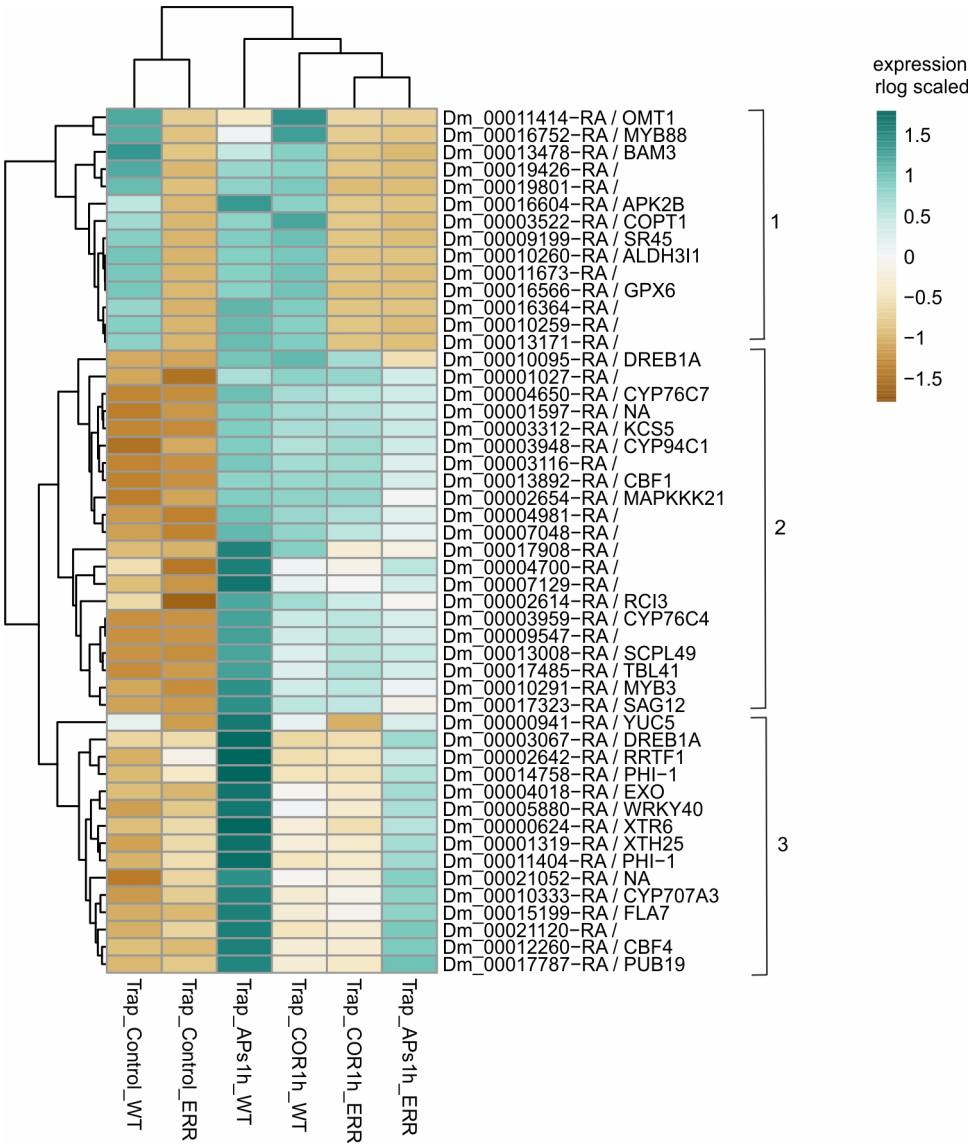

Figure 39: Heatmap showing the expression level of top 50 most variable genes across all conditions for both phenotypes. Euclidian clustering was used for clustering rows as well as the columns. The 3 main branches showing genes with similar expression patterns are marked. The scale shows expression level as regularized logarithm (rlog) calculated by DEseq2 R package. Zero represent average expression values. Genes that are strongly higher or lower than average represent highly variable genes.

Afterwards, I used intersection of differentially expressed genes (DEGs) analysis to distinguish unique genes from shared genes between the two phenotypes upon each of the treatments individually.

In the next chapters, I will present each of these comparisons one by one as follows. First, we will compare the untreated replicates of the two phenotypes in order to understand how different their "background" transcriptomic profile is in the ground state (unstimulated traps) (Figure 40A). Next, we will analyse the differences between the two phenotypes upon mechanostimulation (Figure 40B,D,F). Later we will briefly analyse the effect of COR treatment (Figure 40C,E,G), and last we will shortly outline the transcriptomic landscapes of all conditions (Figure 40H,I).

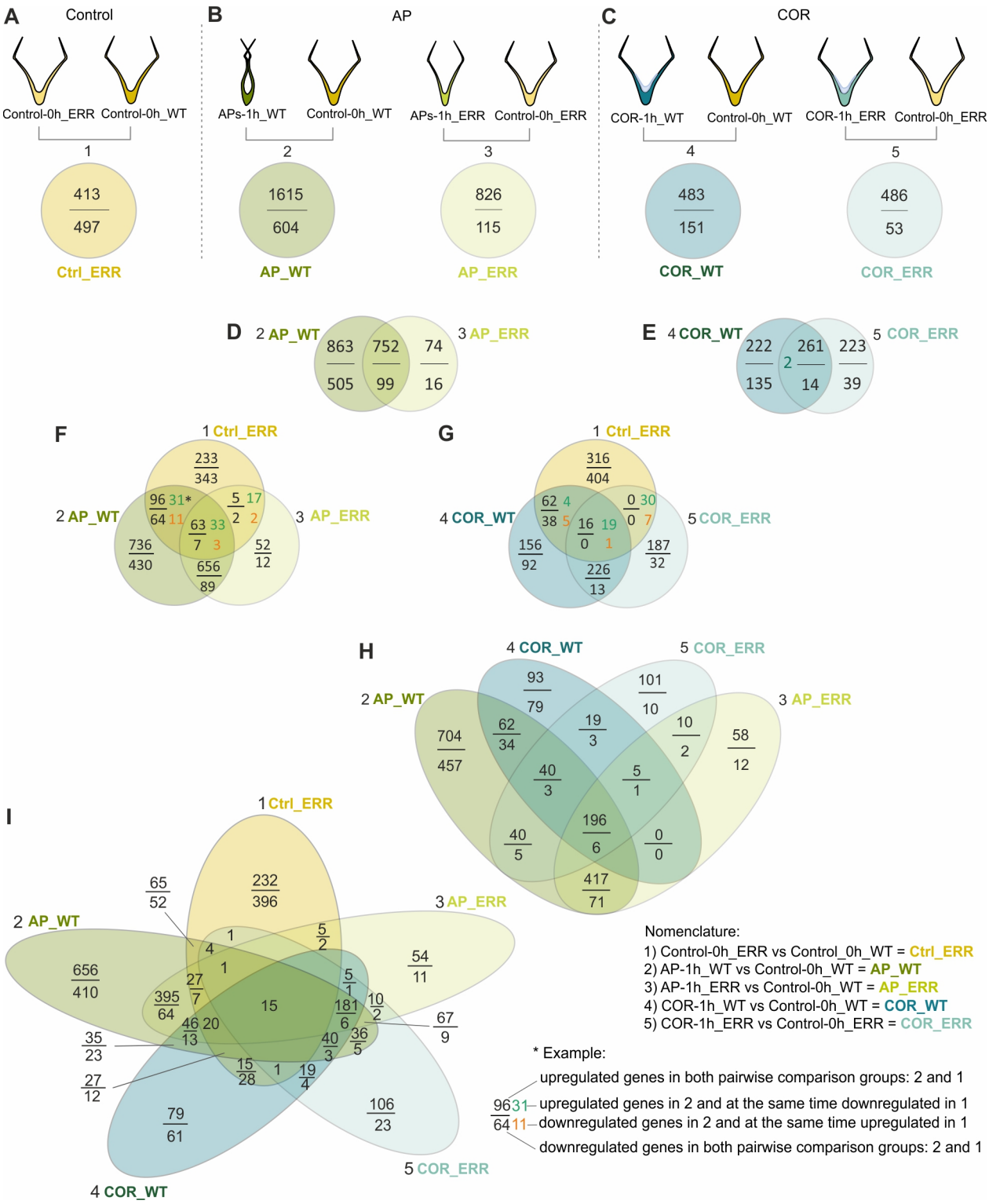

Figure 40: Overview of the five pairwise differential expression analyses (A,B,C). Double Venn showing the intersection of DEGs upon mechanostimulation (D) and coronatine treatment (E) in ERR vs WT. Triple Venns showing the intersection of DEGs upon mechanostimulation (F), and coronatine (G), together with ground-state DEGs in WT and ERR. Quadruple Venn showing the intersection of both treatments on both phenotypes (H) and quintuple Venn showing the intersection of both treatments on both phenotypes together with the ground-state DEGs (G). The numbers on top show the upregulated genes and the numbers on the bottom show the downregulated genes.

3.2.2.2 The 'ERROR' Mutant Transcriptome Slightly Differs in the Ground State From That of Wild Type

From the PCA (Figure 38) we learn that there can be a few differences at transcriptomic level between ERR and WT in the resting state.

When performing differential expression analysis between Control_ERR and Control_WT groups, a similar number of upregulated (431) and downregulated (497) genes could be observed (Figure 41).

The downregulation level seems to be quite extensive, with values down to -10 $\log_2$FC. However, since differential expression analysis is performed by DEseq2 on raw read counts (as suggested by the DEseq2 manual), by looking at the FPKM values, which are expression values normalised by gene length as well as sequencing depth, we end up with very few candidates that are actually highly expressed in Control_WT and close to zero in Control_ERR group. Among these, worth mentioning are the following three genes. *GPX6* (Dm_00016566-RA), a glutathione peroxidase, is important for conferring stress tolerance, especially during drought stress [210]. With a similar function in dehydration and wounding [211], the oxidoreductase *ALDH3I1* (Dm_00010260-RA), is also missing from the ground state of the ERR mutant. Within the same category, the transcription factor *MYB88* (Dm_00016753-RA), has been shown to promote anthocyanin accumulation and hydrogen peroxide detoxification in response to cold [212]. More about their possible role in the big picture will be discussed in the discussion chapter 3.2.3.2.

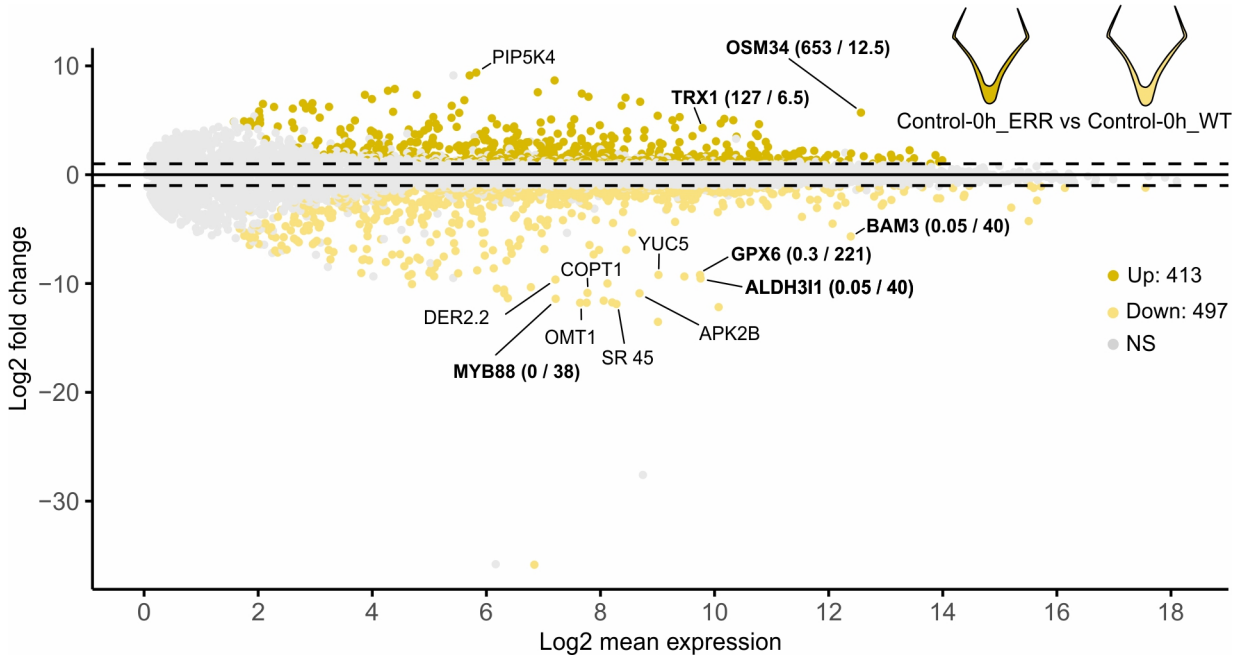

Figure 41: MA plot showing the number upregulated (mustard yellow) and downregulated (yellow) DEGs between Control_ERR vs Control_WT. Top genes with extreme $\log_2$FC values are tagged. Mean expression = DEseq2 normalised counts. In brackets of the bold gene names, the FPKM values for ERR (left) and WT (right) are shown. NS = non-significant genes shown in grey. Unannotated genes are not tagged.

What about the rest of the downregulated genes in Control_ERR group? What is their function? In order to find out, I performed a GO-term enrichment analysis. In Figure 42, the genes annotated with the enriched GO-terms are shown as a network together with their $\log_2$FC values represented as a heatmap. It is easy to spot that all of the genes are under the umbrella of "catalitic activity" GO-term, with two big subgroups showing genes associated with "oxidation-reduction processes". We can see that many genes in this group, accompany the already mentioned *ALDH3I1* and *GPX6*, in their oxidoreductase activity. Besides this, we see genes annotated as part of "structural constituent of cytoskeleton" and "microtubule-based processes" GO-terms that point to cell shape changes.

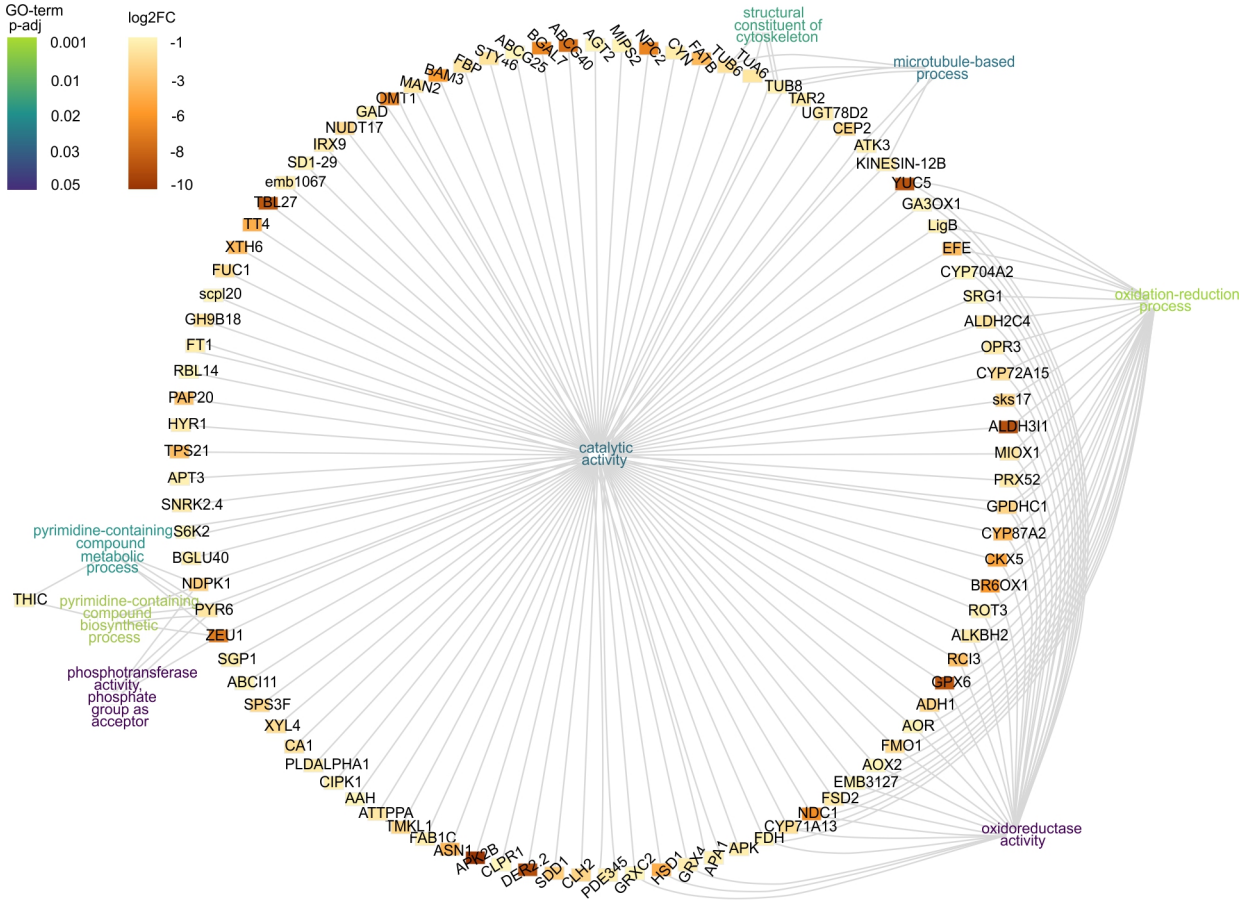

Figure 42: GO-term enrichment gene network of downregulated DEGs between Control_ERR vs Control_WT. Links connect DEGs to their GO-term annotation. The boxes behind gene names represent $\log_2$FC values as a heatmap (see scale). The BH-adj *p* value of enriched GO-terms is represented by the colour of the text (see scale). Only annotated genes are shown.

Since GO-annotation comprises general terms, non-specialised for the plant kingdom, I further investigated the genes' function using the plant-specific MapMan ontologies. Therefore, I performed a MapMan bin enrichment analysis. Similar to what we have previously seen, the bin with the most numerous downregulated DEGs was "enzyme classification.oxidoreductases", followed by "RNA biosynthesis", which validates the GO-term enrichment. However, besides this, we can see the "CW organisation" bin containing the xyloglucan O-acetyltransferase *TBL27* (Dm_00005821-RA) and the leucine-rich repeat/extensin 2 *LRX2* (Dm_00009341-RA) (with overall low FPKM expression values) and expansins *EXPA11* (Dm_00001234-RA), *EXLA2* (Dm_00003377-RA) (with strong contrast between the expression in WT vs ERR).

Figure 43: MapMan bin enrichment of downregulated DEGs between Control_ERR and Control_WT. The number of DEGs belonging to each enriched bin is shown as a bar on the left side of the table. The DEGs with a $\log_2$FC value < -2 are shown as a heatmap. Only annotated genes are shown. Note: read count values were used by DEseq2 for calculating the $\log_2$FC value; when looking at FPKM expression level, many of the genes had overall low values (with the exception of: *PYR6, ZEU1, GPX6, SWN, MYB88, TDF, EXPA11, EXLA2, CYP87A2, CYP71A13, CYP72A15* which were highly expressed in WT and very low in ERR). For full expression profile see Appendix Table 20

.

Next, I did the same analysis for the upregulated genes, and found again signals related to "oxidation-reduction process" confirmed by both methods (Figure 44, Figure 45). We could notice many genes belonging to the cytochrome P450 family (CYP) which are well known for their role in plant stress response (antioxidant biosynthesis, plant defence, hormone regulation) [213]. Out of these, *CYP94B3* (Dm_00001848-RA) is part of JA pathway, being responsible for JA-Ile turnover. Interestingly, as part of OPDA (a JA precursor) biosynthesis, *LOX2* (Dm_00010178-RA), is also highly upregulated in the ERR ground state.

Transcription factor-related GO-terms and MapMan bins were enriched containing multiple WRKYs, which are well known as molecular regulators of stress responses [214]. Out of these, *WRKY50* (Dm_00013547-RA) had the highest FPKM level in Control_ERR compared to Control_WT. Interestingly, studies indicate that it might mediate the salicilic acid- and low oleic acid-dependent repression of JA signalling [215]. The redox responsive transcription factor (*RRTF1*, Dm_00002642-RA) might be a good candidate in charge of orchestrating the entire altered oxidation-reduction processes in the ERR mutant's ground state, but the FPKM values are too low and it could not be confirmed by qPCR (Figure 47).

Enriched by both methods again, we could see "protein modification processes" containing kinases of the TKL superfamily. Besides this, we see "chitin activity"-related GO-terms. Looking back at the qPCR expression of the *CHIB* chitinase, this observation could be confirmed (Figure 33).

Even though not annotated, but part of the top highly expressed genes in Control_ERR group are the osmotin *OSM34* (Dm_00018459-RA) (involved in drought stress and defence against fungi [216]) and the thioredoxin *TRX1* (Dm_00011727-RA) (involved in redox homeostasis [217]) (Figure 41).

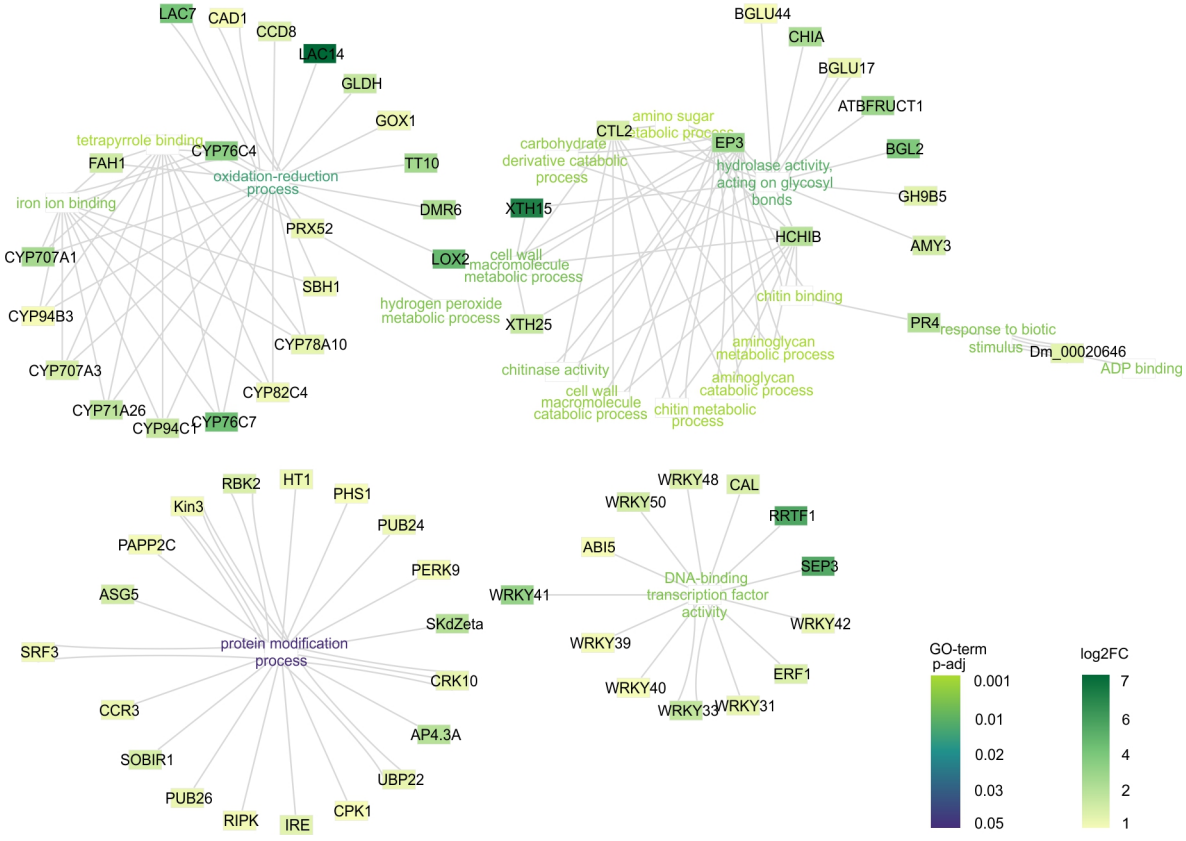

Figure 44: GO-term enrichment network of upregulated DEGs between Control_ERR and Control_WT. Links connect DEGs to their GO-term annotation. The boxes behind gene names represent $\log_2$FC values as a heatmap (see right scale). The BH-adjusted p-value of enriched GO-terms is represented by the colour of the text (see left scale). Only annotated genes are shown.

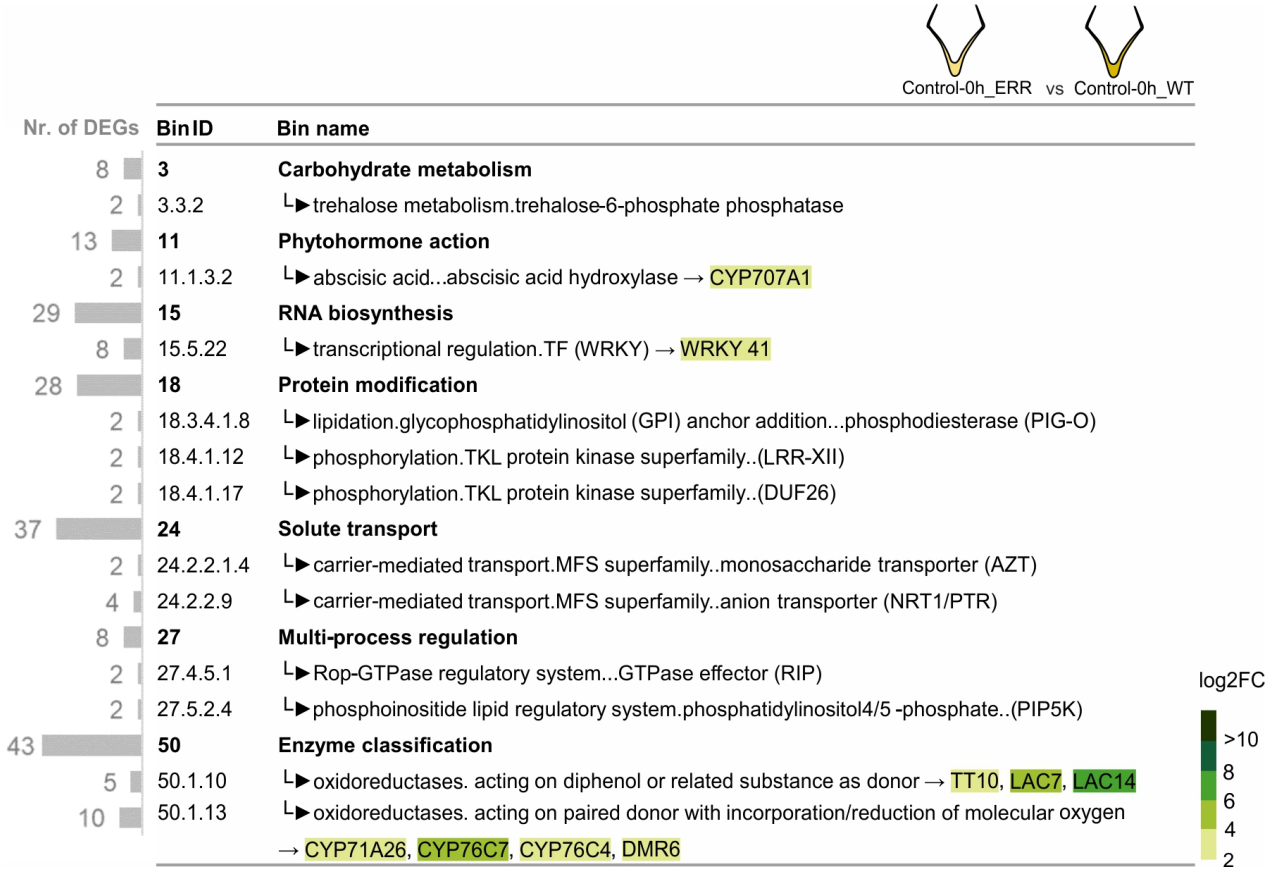

Figure 45: MapMan bin enrichment of upregulated DEGs between Control_ERR vs Control_WT. The number of DEGs belonging to each enriched bin is shown as a bar on the left side of the table. The DEGs with a $\log_2$FC value > 2 are shown as a heatmap.

In short, the most prominent enriched bins of the downregulated DEGs set, in the ground state comparison are the "cell wall organisation" (*EXPA11, EXLA2, FT1, IRX9, RGIL6*) and the "redox homeostasis" (*TRX1*, containing also upregulated DEGs: *GPX1, GLDH*). Additionally, bins that were enriched in both down- and upregulated set of DEGs were the "enzyme classification" (*BBE8, LAC7, CYPs, OMT1, XTH6, HYR1, UGTs, BGLs, FUC1*) and the "RNA biosynthesis" (*BBX21, MYB88, STZ, WRKY50, LBD37*) bins. All the DEGs in ground state comparison as part of enriched MapMan bins and their $\log_2$FC values together with FPKM expression values are shown in Appendix Table 19.

At the extreme end of the spectrum, we find outstanding genes such as strongly upregulated (*OSM34, TRX1*) and strongly downregulated (*BAM3, ALDH3I1, MYB88*) DEGs (Figure 41).

3.2.2.3 The 'ERROR' Mutant Shows Overall Lower Gene Expression Levels Upon Mechanostimulation Compared to Wild Type

Looking at Figure 46, which shows the number of DEGs of mechanostimulation treatment vs control pairwise comparison for each phenotype, we can see a big difference regarding the number of both upregulated and downregulated DEGs. In the case of WT, 2.6 more upregulated (1615) DEGs than downregulated (606) were identified (Figure 46A). Taking WT as a reference, there were 48% less upregulated DEGs (826) and an astonishing 80% less downregulated DEGs (115) in the mechanostimulated ERR traps (Figure 46B).

Top ten outstanding DEGs (with the highest $\log_2$FC or the lowest $\log_2$FC value) are tagged with their gene name. Therefore we can see that some of them are common between the two phenotypes and some are unique. Among the common ones, we can spot the digestive enzymes markers, *SAG12* (Dm_00017323-RA) and *SCPL49* (Dm_00013008-RA), the cytochrome oxidase *CYP76C7* (Dm_00004650-RA) and the transcription factor *DREB1A* (Dm_00010095-RA). These DEGs, that are part of top ten in both phenotypes upon mechanstimulation, might reflect the processes related to these genes' function that are still working in the ERR.

Outstanding genes that are highly expressed in the mechanostimulated WT, but are not part of top ten in the case of ERR, are the CW modifying enzymes *XTH15* (Dm_00002549-RA) and *XTH25* (Dm_00001319-RA) and the transcription factors of Apetala2/Ethylene-responsive element-binding protein (AP2/ERF) family: *CBF1, RRTF1, CBF4* (Dm_00012261-RA, Dm_0000-2642-RA, Dm_00012260-RA). These transcription factors (TFs) might further control other genes that are not differentially expressed in ERR upon mechanostimulation, thus indicating processes that are not working as well as they should (when using the WT as a reference).

In order to get a better perspective on the timescale, I checked the expression of the top two transcription factors (*CBF1* and *RRTF1*) across a wider timeline, using qPCR. The results show a strong difference for 1h time point between ERR and WT, however, at 0.5h time point, we see the peak expression with around half the expression level in ERR compared to WT (Figure 47).

Nevertheless, these easy to remark genes are only the tip of the iceberg. In order to understand the complex processes activated by the touch stimulus, it is necessary to dive into the numerous upregulated DEGs of the WT in order to first understand the "normal" (functional trap) before looking closer at the ERR's response to touch.

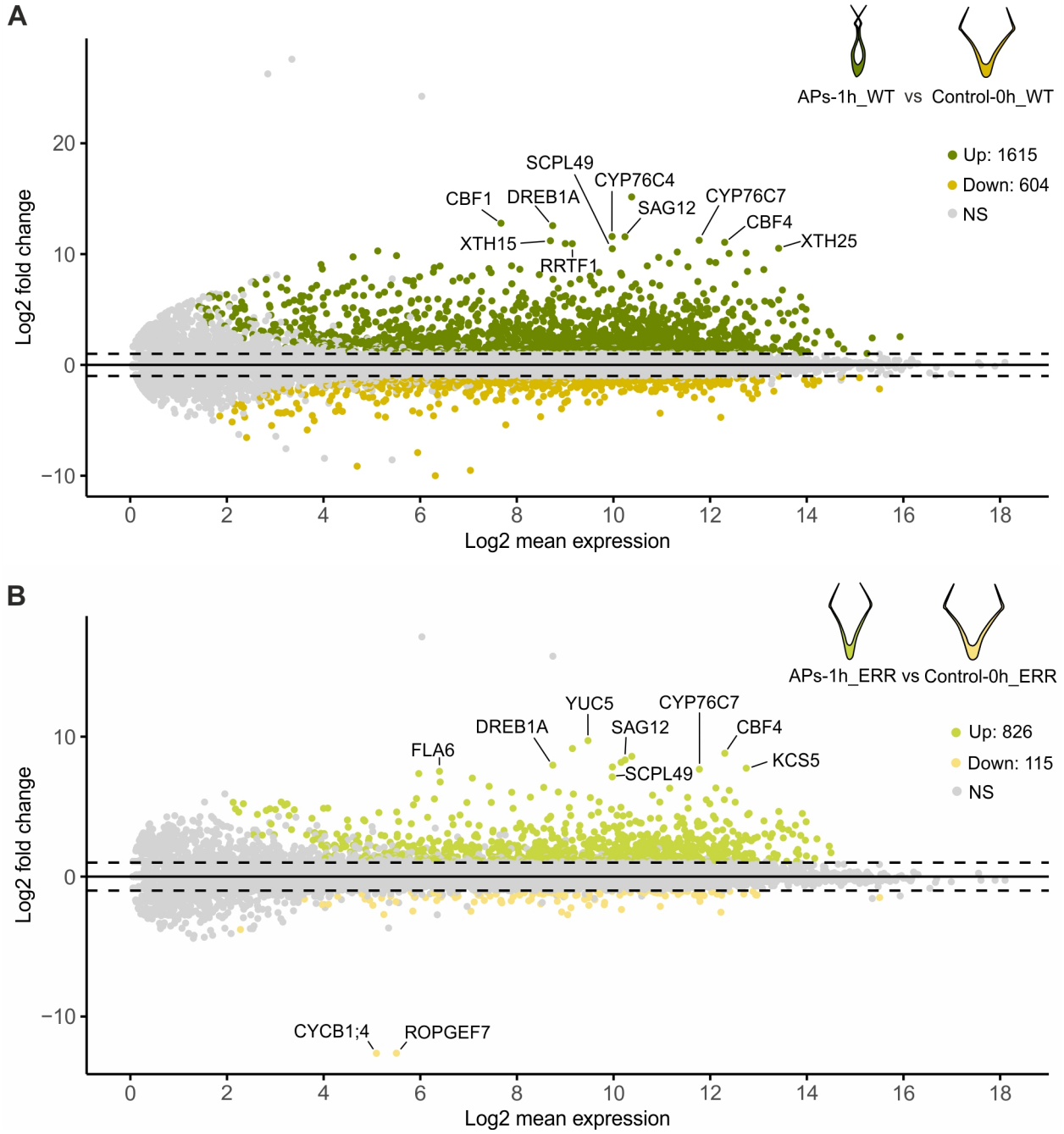

Figure 46: (A) MA plot showing the number upregulated (dark green) and downregulated (mustard yellow) DEGs between mechanostimulated (10 APs, 0.01 Hz) WT trap and its own control group. (B) MA plot showing the number upregulated (light green) and downregulated (yellow) DEGs between mechanostimulated (10 APs, 0.01 Hz) ERR trap and its own control group. Top 10 genes with highest and lowest $\log_2$FC values are tagged. Please note the difference in the y-axes scale between (A) and (B) plots. NS = genes with an adjusted p-value < 0.05. Unannotated genes are not tagged.

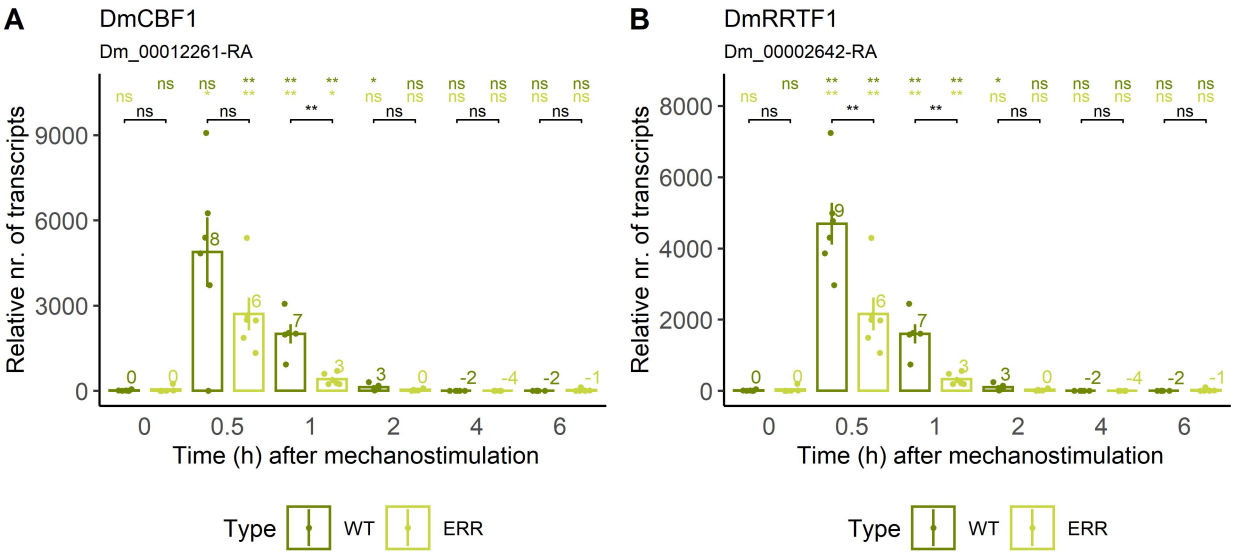

Figure 47: qPCR expression level timeline of *DmCBF1* (A) and *DmRRTF1* (B) upon mechanostimulation (10 APs, 0.01Hz) in WT and ERR traps. The relative number of transcripts is normalised to 10 000 molecules of actin *DmACT1*. The bar chart shows average values +/- SE and the dots show the values of each measured sample. The numbers above the bar chart represent $\log_2$FC values relative to the corresponding control of each phenotype. Above the chart, the Wilcoxon rank sum test p-value is represented with stars: * for $p < 0.05$, ** for $p < 0.01$, *** for $p < 0.001$, ns = not significant. The colours of the stars indicate to which control the comparison was made (dark green = WT control, light green = ERR control). $n = 6$.

Understanding the Norm: AP2/ERF Transcription Factors Might Drive the Mechanostimulation Response in Wild Type

Since wild type (WT) is our reference, we shall first understand how a normal and functional Venus flytrap transcriptomic profile would look like upon touch. I mainly focused on upregulated genes. For this, I used the MapMan bin enrichment analysis in order to get an idea of which are the main plant-specific signalling pathways activated 1h after mechanostimulation (Figure 48).

Starting with the MapMan bin with the highest number of DEGs, the "RNA biosynthesis" (194 DEGs), it shows that many transcription factor (TF) families are highly upregulated, with high $\log_2$FC values. Among the most striking are the ethylene-responsive element-binding factor subfamily (ERF) and the dehydration-responsive element-binding protein subfamily (DREB) with many genes being upregulated more than 16-fold. The DREB subfamily is also categorised as part of the "cold response" (CBF/DREB) MapMan bin. In non-carnivorous plants, these transcription factors are key regulators of a highly interconnected regulatory network in which they respond to hormones, leading to improved plant survival during stress conditions [218].

Next, the numerous “protein modification” enriched bin (with 123 DEGs) contains receptor-like kinases of the CW integrity surveillance system (*THE1, HERK1*). This

is in line with other enriched bins such as “pathogen pattern triggered immunity/ defence mechanisms” (*FLS, PGIP*), “CW organisation” (*CSDL3, FLA6/7/17/11*) as well as “glycosyltransferases” containing genes involved in CW modification (*XTH15, XTR6, XTH25, TCH4*).

Furthermore, the “auxin biosynthesis” bin contains upregulated YUCCA genes (*YUC3/4 /5/7*) known to be involved in cell expansion. This suggests the involvement of these genes in the early stages of trap morphology changes assured by CW modification together with cell elongation, required for digestive stomach formation and trap sealing.

As cytochromes (CYPs) respond strongly upon internal and external stimuli, leading to biosynthesis and regulation of hormones, CW components and defence compounds [213], it is not surprising to see the "oxidoreductase" bin (to which the CYPs belong) enriched as well. Interestingly, many of the above-mentioned bins were not enriched when performing the same enrichment analysis on the few upregulated DEGs in ERR (Figure 48 - bin IDs marked in green).

Briefly summarising the same MapMan bin enrichment procedure for the 604 downregulated DEGs, we can spot processes related to chloroplast function, including regulation of "chloroplast redox homeostasis" and " chloroplast outer envelope protein translocation system" together with "light-" and "gravity-responses" as well a "circadian rhythm regulation" bin. These processes might indicate that the primary metabolism is shut down in the favour of preparation for the digestion processes. Maybe important for the open-state morphology of the trap, the "CW organization expansin activities" (*EXP6, EXPA11*) were also downregulated in WT traps by mechanostimulation (Appendix Figure 67).

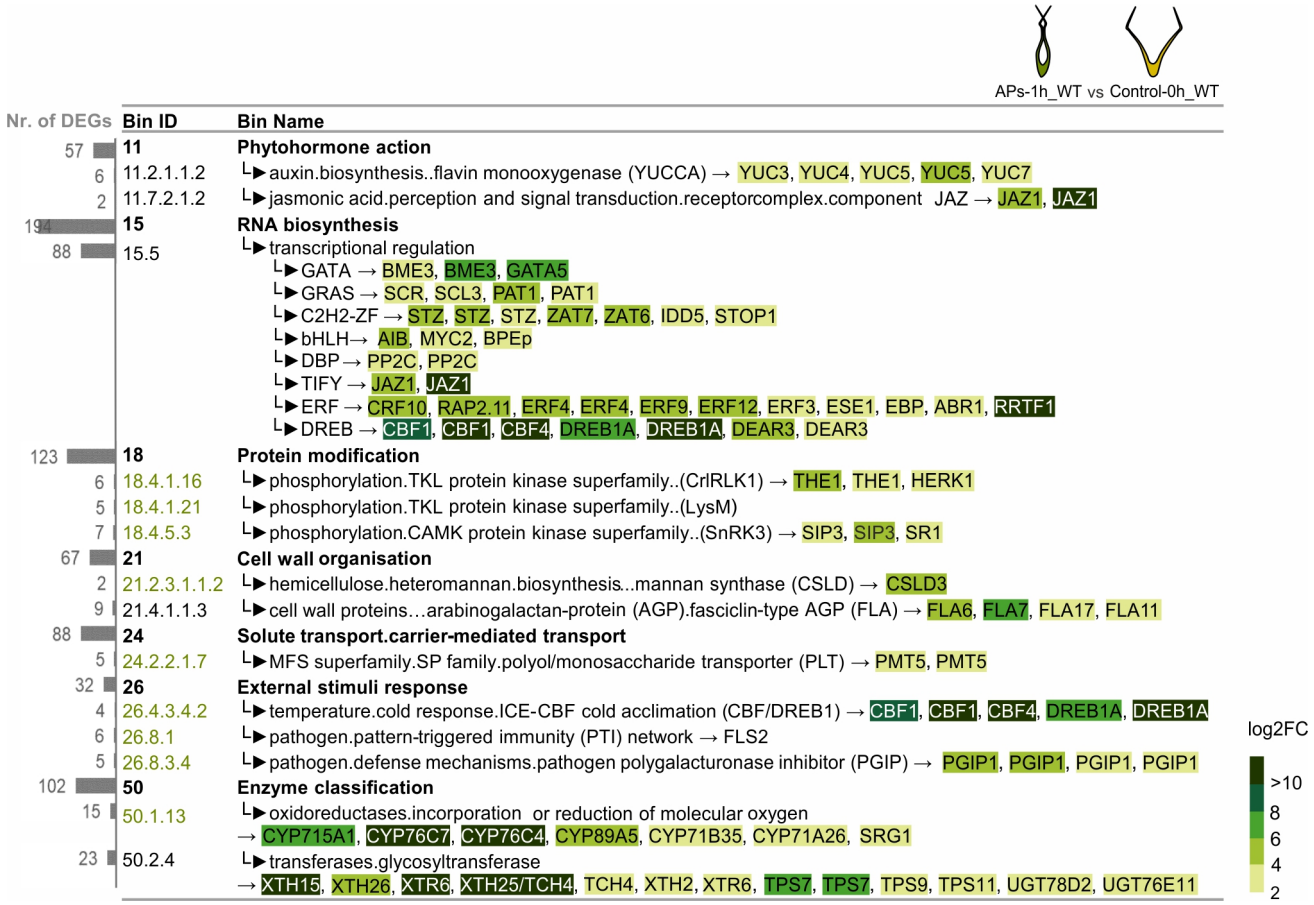

Figure 48: MapMan bin enrichment of upregulated DEGs between mechanostimulated WT and control WT traps. The number of DEGs belonging to each enriched bin is shown as a bar on the left side of the table. The DEGs with a $\log_2$FC value > 2 are shown as a heatmap. Only annotated genes are shown. Bins that are not enriched in ERR upon mechanostimulation are marked in green text.

Stress-Related Processes are Activated in Wild Type But Not in the 'ERROR' Mutant Upon Mechanostimulation

By overlapping the two pairwise comparisons (AP_WT vs Control_WT and AP_ERR vs Control_ERR), in the double Venn diagram, we can see the number of shared DEGs between both phenotypes as well as the number of unique DEGs to each one of them (Figure 49 - Venn diagram). Interestingly, 91% (752 out of 826) of the many upregulated genes and 86% (99 out of 115) of the few downregulated DEGs in ERR were shared with WT. However, the first thing to notice when looking at the heatmap showing the $\log_2$FC values of the shared DEGs in both phenotypes, is the big difference in the expression level between the two, as it is much lower in the ERR.

A closer inspection of the expression levels of shared touch-sensitive DEGs, revealed that half of the upregulated DEGs (436 DEGs) in ERR were between 1 to 2 $\log_2$FC and only a few (55 DEGs) were highly upregulated > 4 $\log_2$FC. In contrast to this, the majority of DEGs in WT were highly upregulated (up to 194 DEGs > 4 $\log_2$FC) (Figure 49 - $\log_2$FC interval bar chart). A similar pattern with an even more drastic tendency was observed

for downregulated genes. In short, upon touch stimulation, the ERR mutant addresses only half of the number of DEGs with half of the expression amplitude compared to WT. In line with the qPCR data (Figure 47) this is reflecting ERR's dampened response to touch stimulation.

Only a small fraction of the genes (74 upregulated DEGs and 16 downregulated DEGs) from the total number of DEGs upon mechanostimulation are specific to the ERR Mutant (Figure 49 - Venn diagram).

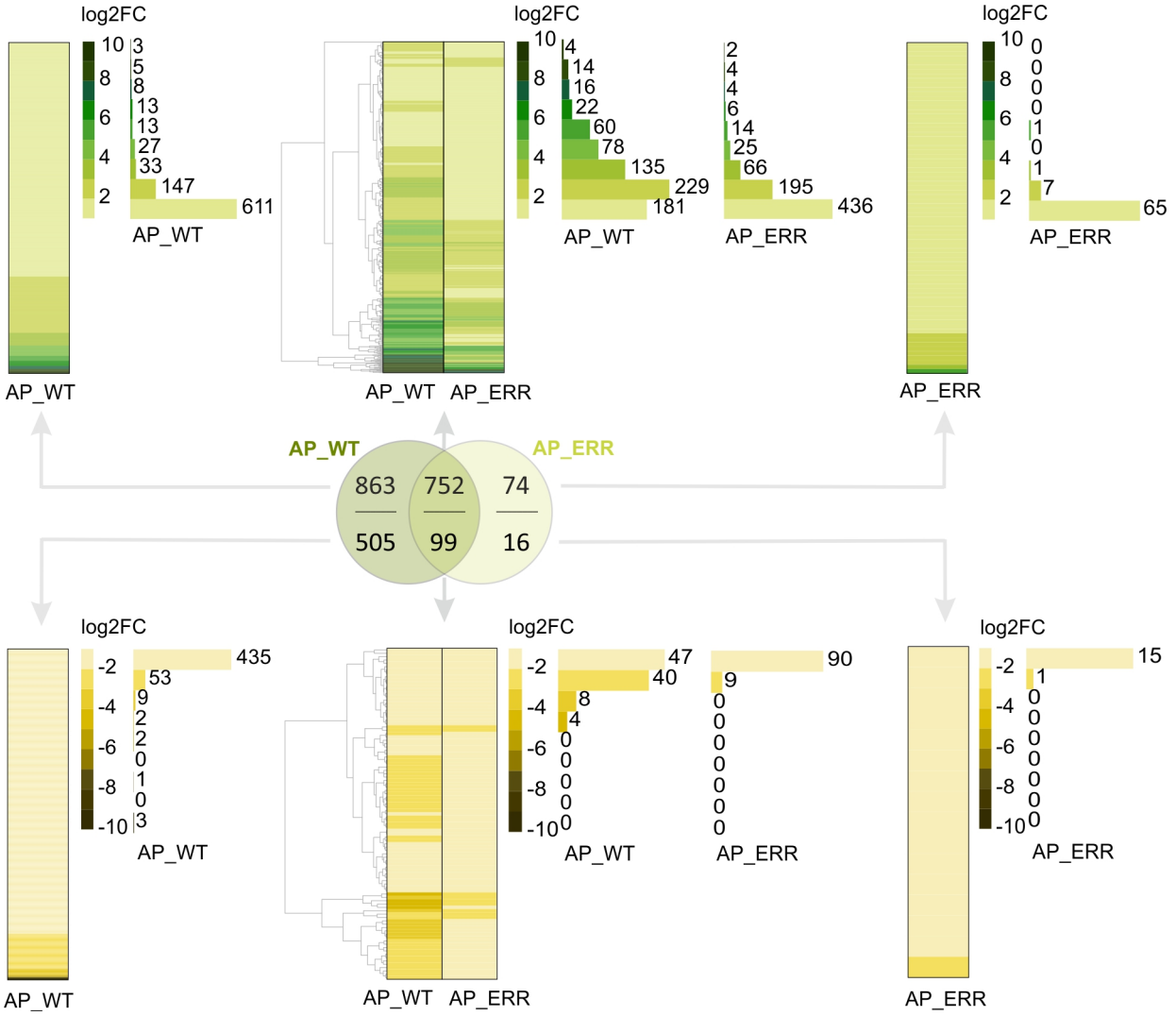

Figure 49: Double Venn diagram showing the intersection of DEGs upon mechano-stimulation (10 APs, 0.01 Hz) in both WT and ERR. Upregulated DEGs are shown above while downregulated DEGs are shown bellow. The log_2FC value of each subset of the Venn diagram is represented as a heatmap with the number of genes in each log_2FC value interval being shown next to the heatmap scale as bar plot (i.e. 181 genes are found between log_2FC value 1 and 2 in the upregulated DEGs of AP-WT shared DEGs subset).

To get a glimpse into the function of the 863 unique genes of the WT, as well as on the 752 DEGs shared between WT and ERR upon mechanostimulation, I performed a GO-term enrichment analysis. From the treemap (Appendix Figure 68), we can notice that many enriched GO-terms are found in both subsets (unique to AP_WT Appendix Figure 68A and shared between the two (Appendix Figure 68B), *e.g.*: "aromatic compound", "nucleobase-containing compound", "RNA metabolic process", "CW macromolecule catabolic process", "phosphorous metabolic process". One exception is the group comprising "response to endogenous stimulus" (marked with a grey rectangle) including "defence response" that seems to be enriched only in the unique to WT subset. Therefore, in order to better comprehend which major metabolic functions and pathways are underrepresented or even missing in the ERR upon mechanostimulation, I performed a more sophisticated analysis.

While GO enrichment is based on the frequency of GO-terms, the MapMan bin enrichment analysis allows us to take into consideration the level of expression (or the $\log_2$FC value) of the genes, besides the number of genes in each bin. Therefore we consider underrepresented functional categories, bins that are enriched (adjusted p-value < 0.05) in the unique subset of WT (863 DEGs), while at the same time, those bins are not enriched (adjusted p-value > 0.05) in the shared subset (752 DEGs) of the ERR upon mechanostimulation (see chapter 2.2.2.6 for details). If the number of DEGs in the underrepresented bins of shared AP_ERR group is zero, we consider those "missing" functional categories in ERR upon AP-treatment. The subsets of the Venn diagram are marked in Figure 50 with a grey rectangle with *continuous* line to emphasize that enriched bins were selected from this Venn subset, while the grey rectangle with dotted line marks the subset from which non-enriched bins were selected.

Accordingly, as part of the underrepresented functional categories in ERR, otherwise highly touch-responsive in WT, we can see: “phytohormone action”, “RNA biosynthesis”, “protein modification”, “protein homeostasis”, “CW organization” and “solute transport” present in both up- and downregulated groups.

Focusing on the upregulated underrepresented bins, we can identify as part of both ”phytohormone action” and “protein modification” bins, the CW integrity sensing hub of the “RALF-peptide receptor” bins comprising the receptor-like kinases (RLKs): *FER, HERK1* and *THE1* and its *LLG1* receptor. Within the same “protein modification” bins we can also see *LYK3/5* associated to chitin responses [219] and *PP2CG* involved in cold and salt tolerance [220]. Within the ”phytohormone action” we can find auxin biosynthesis-related *YUCCA* genes as well as the auxin receptor *AFB4* underrepresented in the mutant. This might indicate that auxin-regulated cell expansion and CW reorganisation processes needed for stomach formation are addressed by the touch stimulation in the WT but not in the ERR. Since the ERR trap remains open after the mechanostimulation treatment, it is not surprising to see this peculiar behaviour

reflected at the transcriptomic level as well.

Further, with a number of DEGs less than expected in the ERR compared to WT (according to the Hypergeometric distribution test, see chapter 2.2.2.7 for details, marked with a yellow triangle in Figure 50) we can see the "protein homeostasis" bin with a large number of RING-H2 type ubiquitin ligases associated to cell death. Among the bins that contain zero DEGs in the shared AP_ERR group, therefore as part of "missing" functional categories in the ERR mutant, we can notice members of the RAV transcription factor family (*TEM1, NGA1* and *RAV1*), previously shown to be touch-sensitive in *Arabidopsis thaliana* [221]. Within the same category, we can see the "S/T protein phosphatase superfamily" bin containing *PP2CG1*, which has been shown to interact with *OST1* kinase regulating plant freezing tolerance [220].

The contrast between ERR and WT helps us understand the necessary molecular equipment needed for stomach formation. Since this is a highly expensive process, it is not surprising to see the "solute transport" bin containing upregulated sugar transporters (SUC2) that might be needed for sugar translocation and consumption within different plant organs.

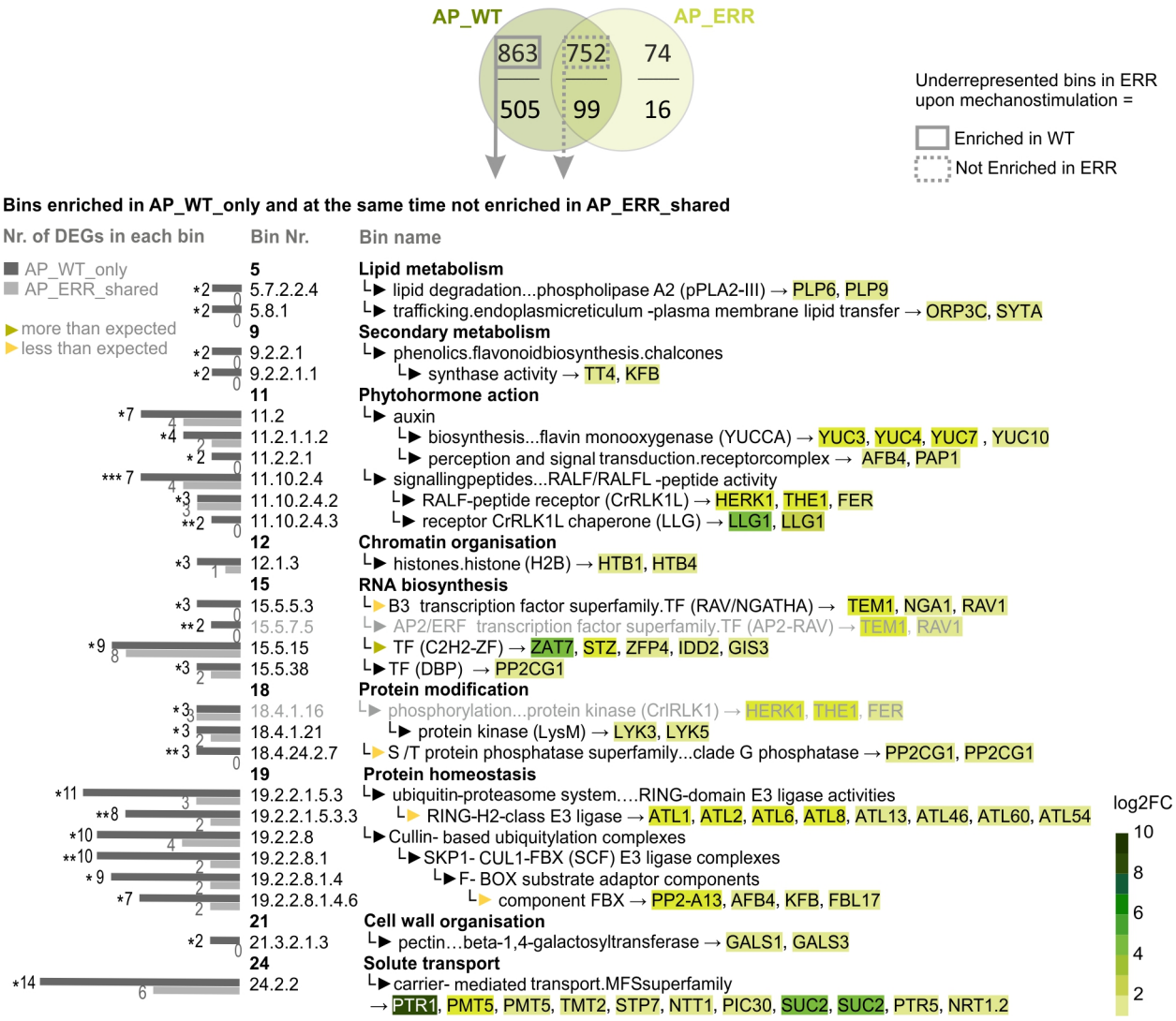

Figure 50: Underrepresented MapMan bins in mechanostimulated ERR as part of the shared DEGs. Underrepresented bins in ERR are bins which are significantly enriched in WT upon mechanostimualtion - in the unique to WT DEGs subset (863 = AP_WT_only), while at the same time these bins are not enriched in the ERR upon mechanostimulation - in the shared DEGs subset (752 = AP_ERR_shared). Enrichment is defined by Wilcoxon Rank Sum Test BH-corrected p-value < 0.05, as shown by stars above the bars on the left (* for $p < 0.05$, ** for $p < 0.01$, *** for $p < 0.001$). Not enriched bins have a BH-corrected p-value > 0.05. Bar chart on the left shows the number of DEGs in each bin of each Venn subset. Marked with colored triangles are bins with a number of DEGs more than expected (green) and less than expected (yellow) in the ERR according to the p-value of the Hypergeometric Distribution Test compared to WT. The upregulated DEGs in mechanostimulated WT traps belonging to each bin are shown with their $\log_2$FC values as a heatmap. See chapters 2.2.2.6 and 2.2.2.7 for more details regarding the method.

The Transcription Factor Network That Is "Missing" in The 'ERROR' Mutant Upon Mechanostimulation

Since we have seen many TFs being highly upregulated in the WT, but with a dimmed expression or not differentially expressed at all (non-DEGs) in the ERR upon touch, I tried to find out which are the DEGs under the control of those TFs. In total I could detect 70 TFs that were specific to AP_WT (see chapter 2.2.2.9 for details). Looking for the TF-binding sites for the identified TFs within the Plant Transcription Factor Database (PlantTFDB), there were 32 TFs with a known motif in *Arabidopsis thaliana* orthologs. I searched for the TF's motif in the upstream region of DEGs specific to AP_WT within the draft genome of the functional WT *Dionaea muscipula*. The resulting TF-network in Figure 51 can be therefore considered the "missing" regulatory network in the ERR as it contains TF and their target genes that are not differentially expressed upon touch in ERR, that could, therefore, be essential for stomach formation.

As we can see, the drought-responsive TF *DREB2C* might act as a master-regulator orchestrating the expression of multiple genes, including other TFs such as: *MYB114* (involved in JA-promoted anthocyanin biosynthesis [222]), the PAMP-triggered immunity regulator *WRKY7* [223] both being also regulated by *GATA1* and the cold-responsive *ICE1* which is also regulated by ethylene-responsive element *ERF3* and *ESE1*. Among regulators with high $\log_2$FC values are the osmotic and drought stress-responsive ABA repressor *ABR1* and the cytokinin responsive factor *CRF10*, both part of ERF TF superfamily. Besides many ABA-induced genes (*PP2CG1, ABR1, ZFP4, DREB2C*), we can also see JA-negative feedback control regulators like *ERF4* and *CYP94C1* as part of the network. Interestingly, *IDD2* seems to be a self-regulator in *Dionaea muscipula*. In rice, it has been found to negatively regulate genes involved in lignin biosynthesis [224]. Showing its role as a CW modification regulator, we can also see among its target genes the xyloglucan transferase *XTH33*. With a similar function, we can spot *OFP1*, which has been shown to negatively regulate cell expansion through direct interaction with the microtubule regulating protein *TON2* [225].
In short, we see many genes involved in responses to pathogen, cold and especially ABA-dependent dehydration, mainly regulated by DREB2C, which might be important for the initiation of green stomach formation.

However, this picture is incomplete. There are many TFs which are strongly upregulated upon mechanostimulation in WT *Dionaea muscipula* and which could have a crucial role in touch-response, but whose binding motifs are not yet known. Moreover, I have used *Arabidopsis thaliana* orthologs, which might not match *Dionaea muscipula*'s genome perfectly, thus being excluded. It is expected that *Dionaea muscipula* could have special binding motifs different from other species, hence a more thorough analysis combining bioinformatics with wet lab, such as TF-binding site prediction analysis together with ChIP-Seq method, would be necessary for getting a more accurate and complete picture of the TF-network.

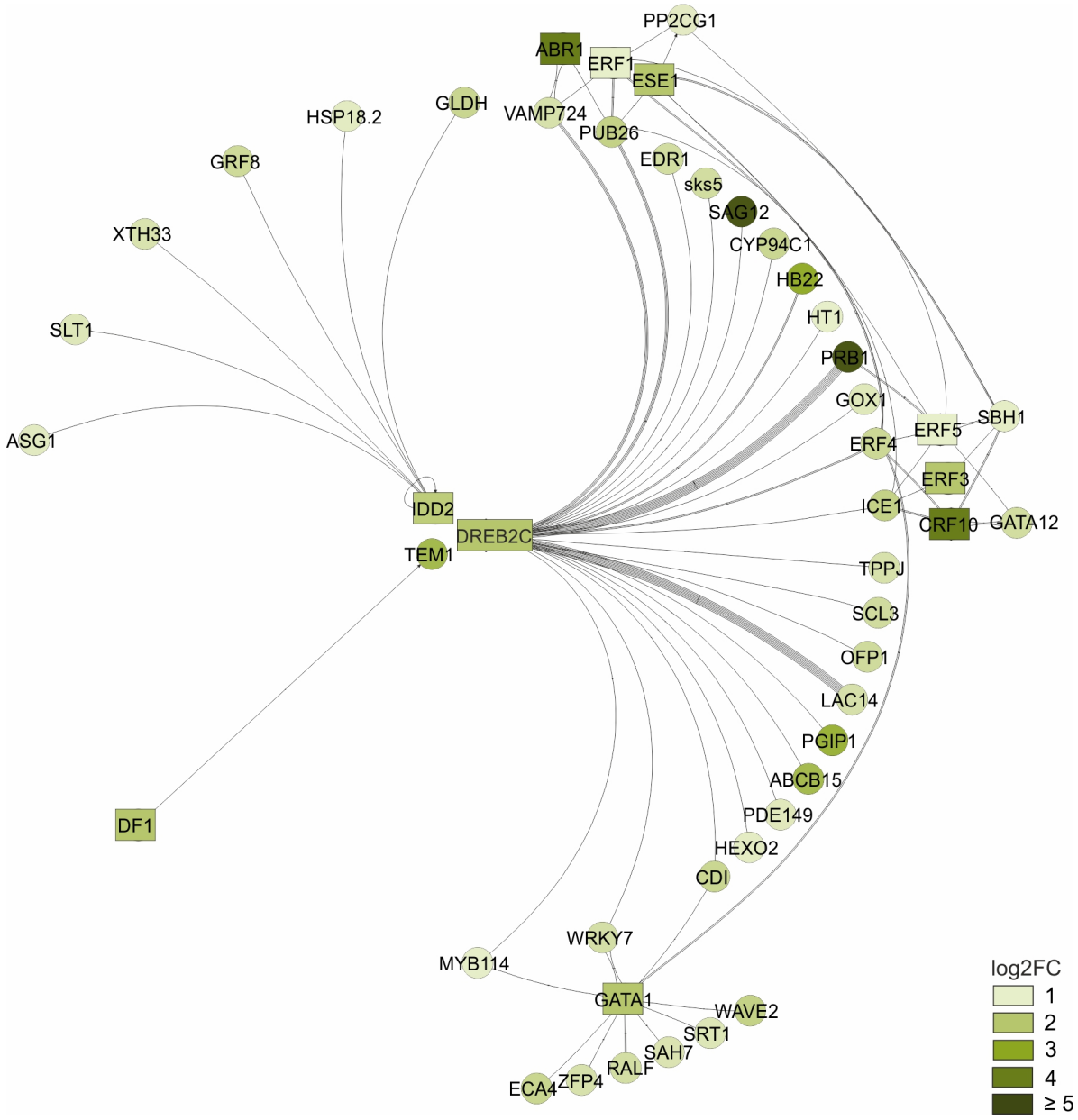

Figure 51: Transcription factors (rectangle) and target genes (circles) network of DEGs in WT and not in ERR upon mechanostimulation. The $\log_2$FC values are represented as heatmap. Target genes are genes that in the upstream region contained the motif of the TF. The number of links between TFs and targets show how many motifs have been found in the promotor region. Motifs from PlantTFDB of *Arabidopsis thaliana* have been used.

Some of the Unresponsive Genes Upon Mechanostimulation Start From a Different Ground Level in The 'ERROR' Mutant

As noticed previously in the PCA plot (Figure 38) there is a clear dissimilarity between control groups of the two phenotypes. Therefore, I wondered if this could be the reason for not having as many DEGs upon mechanostimulation in ERR as in WT (*i.e*: if some genes which should be highly expressed in the ground state are already downregulated in ERR compared to WT, therefore present very low expression level in the Control_ERR group, there is no possibility to become downregulated upon mechanostimulation - meaning the values cannot get more significantly lower). Hence, we added the ground state comparison to the mechanostimulation comparisons.

Surprisingly, only 11% of the upregulated DEGs and 12% of the downregulated DEGs upon mechanostimulation, that were unique to WT, show a different starting point, therefore being also DEGs in the Control_ERR vs Control_WT comparison (Figure 52D). Meanwhile, the majority, 85%, are not differentially expressed in the ground state comparison. This means that the previous analysis from Figure 50 still holds true.

Having a closer look at the "abnormal" minority (11/12%), I identified some genes that have a very strange expression pattern in the ERR. As part of the unique to WT upregulated DEGs upon mechanostimulation and also upregulated DEGs in Control_ERR subgroup (96) (Figure 52A), I would mention the extreme case of the defence responsive osmotin *OSM34* (Dm_00018459-RA) (which was mentioned already in previous chapters), with an astonishing expression in the control state of the ERR (653 FPKM in ERR and 12 FPKM in WT), closely followed by the aquaporin NOD26-like intrinsic protein *NIP1;2* (Dm_00012214-RA). Interestingly, NIP1;2 has been shown to facilitate hydrogen peroxide uptake when expressed in yeast cells [226]. Among the previously mentioned, we rediscover the thioredoxin *TRX* (Dm_00011727-RA) and TF *WRKY50* (Dm_00013547-RA) (Figure 52A).

Worth pointing out is also the subset with DEGs that are downregulated in WT upon mechanostimulation and also downregulated in the ERR's ground state (64) (Figure 52B). Here we can see the expansins *EXPA11* (Dm_00001234-RA) and *EXPA6* (Dm_00003742-RA) (already mentioned before) together with the cell expansion inhibitor *HYR1* (Dm_ 00002224-RA).

Maybe even more "abnormal" is the third subset with DEGs that are uniquely upregulated in WT upon mechanostimulation and at the same time downregulated in Control_ERR when compared to Control_WT (31) (Figure 52C). With a high induction upon touch, was the extensin-like protein *ELP* (Dm_00016399-RA) and with redox-related function the already mentioned glutathione peroxidase *GPX6* (Dm_00016566-RA) and the myo-inositol oxygenase *MIOX1* (Dm_ 00011008-RA).

As a summary, this analysis allowed us to identify touch-specific DEGs in WT (and non-DEGs in ERR), that do not start from a similar expression level in the ground state of ERR when compared to WT. Many of these "abnormal" genes have redox functions as well as CW modification functions.

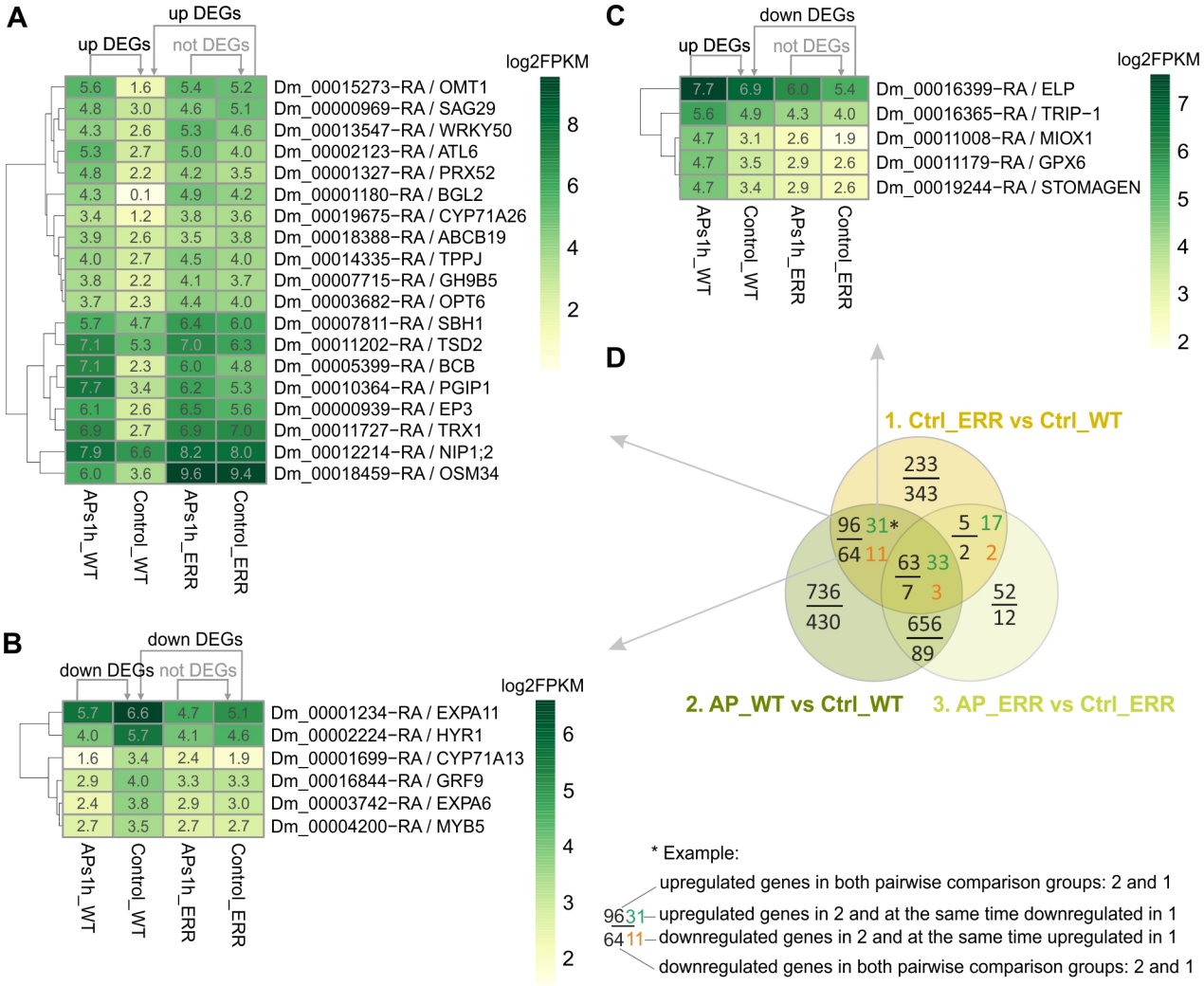

Figure 52: Venn diagram representing the intersection of DEGs in three different pairwise comparisons. The average expression profile (as $\log_2$-transformed mean FPKM values) is shown as a heatmap for DEGs of interest (only annotated genes with FPKM > 10 are shown) which are part of the pinpointed subsets. (A) Expression heatmap of genes that are upregulated DEGs in the AP_WT vs Control_WT comparison as well as in the Control_ERR vs Control_WT comparison and non-DEGs in AP_ERR vs Control_ERR comparison (B) Expression heatmap of genes that are downregulated DEGs in AP_WT vs Control_WT as well as Control_ERR vs Control_WT and non-DEGs in AP_ERR vs Control_ERR comparison (C) Expression heatmap of genes that are upregulated DEGs in the AP_WT vs Control_WT comparison as well as downregulated in the Control_ERR vs Control_WT comparison and non-DEGs in AP_ERR vs Control_ERR comparison. (D) Triple Venn diagram showing the intersection of DEGs in three different pairwise comparisons.

3.2.2.4 The 'ERROR' Mutant's Gene Expression Level Upon Coronatine Treatment Is Similar to Wild Type

Comparing the Coronatine-Treated Traps of Each Phenotype to Their Own Control Shows a Similar Number of DEGs

As presented in the previous chapter 3.2.1.6, the jasmonic acid (JA) levels upon touch are half in ERR compared to WT. Moreover, in chapter (3.2.1.7) we have seen that upon external application of jasmonates trough COR (coronatine) treatment, the proper function of digestive fluid secretion can be redeemed (Figure 35).
In order to investigate if the ERR can respond upon artificial (JA) application at transcriptomic level as well, we wanted to compare the transcriptional response of WT and ERR upon COR spray on the trap surface.

As we have previously seen in the PCA plot (Figure 38), the COR response was not as strong as the one upon AP elicitation. Moreover, a similar response was observed for both phenotypes, shown by the similar distance from each of their own control group. This observation was further confirmed by the differential expression analysis, which revealed a similar number of DEGs in the two phenotypes, at least in the case of upregulated DEGs: 483 upregulated DEGs in WT and 484 DEGs in ERR. Fewer downregulated DEGs (53) were expressed in the ERR compared to WT (149) (Figure 40E).

By having a look at the top 10 upregulated DEGs (based on $\log_2$FC value), we can notice the digestive-marker enzyme *SAG12* in both phenotypes highly expressed upon COR (Figure 53). Yet, out of the four SAG12 paralogs found in *Dionaea muscipula*'s genome, two are DEGs in both phenotypes with a similar FPKM expression level (Dm_00021072-RA, Dm_00017323-RA), and two are DEGs only in WT (Dm_00013767-RA, Dm_00000680-RA) (*e.g.*: Dm_00013767-RA having 85 FPKM in WT, and almost absent - 0.01 FPKM in ERR). This already indicates that untangling the faulty transcriptome of the ERR mutant is not as straightforward as it may seem at first glance.

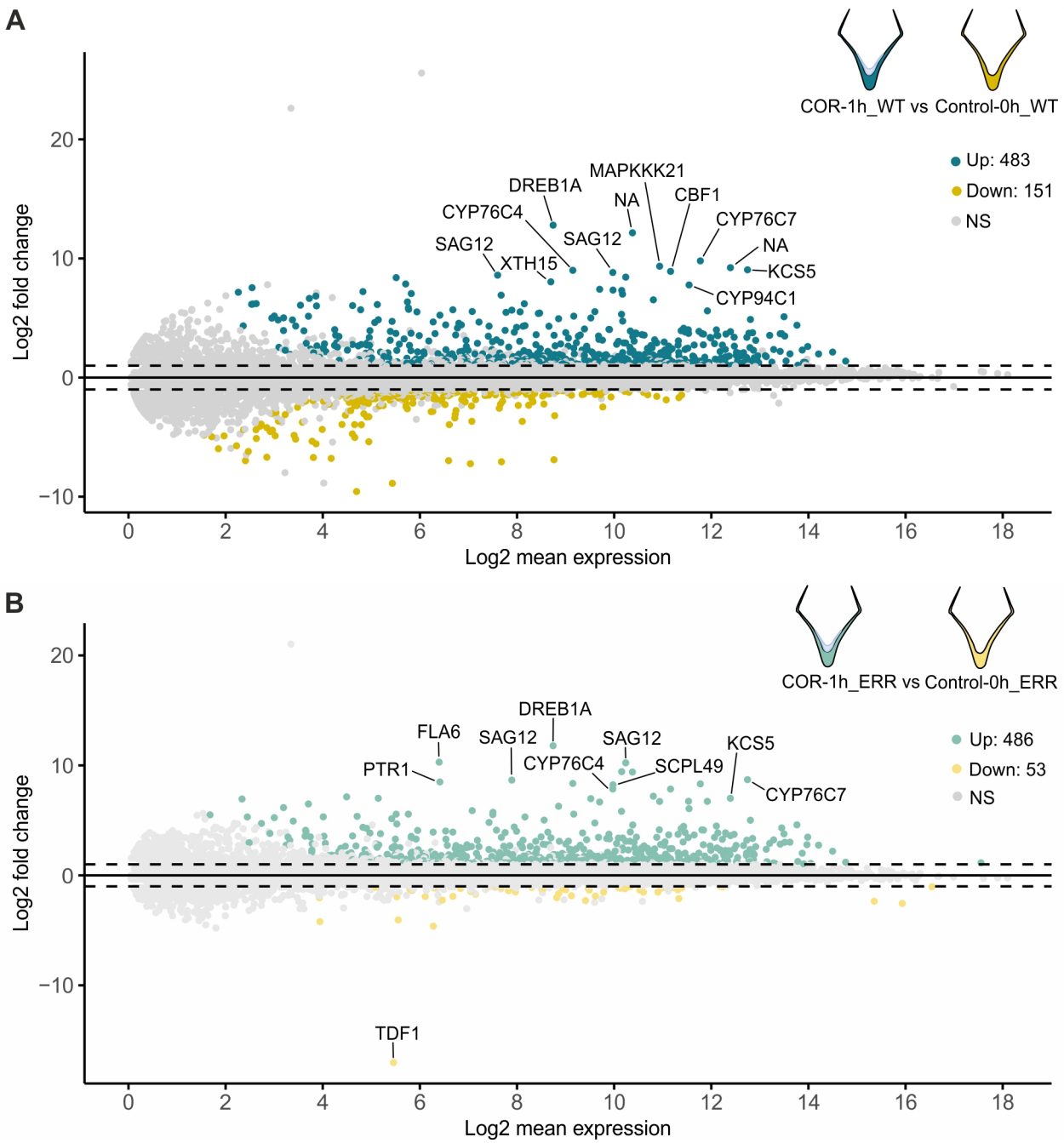

Figure 53: (A) MA plot showing the number upregulated (dark turquoise) and downregulated (mustard yellow) DEGs between COR (0.1 mM COR) WT trap and its own control group. (B) MA plot showing the number upregulated (light turquoise) and downregulated (yellow) DEGs between mechanostimulated (10 APs, 0.01 Hz) ERR trap and its own control group. Top 10 genes with extreme $\log_2$FC values are tagged. NS = non-significant genes. Unannotated genes are not tagged.

The 'ERROR' Mutant Shows More DEGs Involved in Cell Wall Organisation Compared to Wild Type Upon Coronatine

Curiously, even though the number of upregulated DEGs was similar in the two phenotypes, by overlapping the two pairwise comparisons (COR_WT vs Control_WT and COR_ERR vs Control_ERR), only 50% were shared (261)(Figure 54). However, by looking at the induction levels, we can see a similar (if not higher) response in the ERR compared to WT in this group of genes. Still, the induction was rather low in general, many of the upregulated genes being within the 1-2 $\log_2$FC interval, indicating that traps were just beginning to enter the digestion stage.

By simply looking at the number of upregulated DEGs allocated to each of the MapMan bin in each of the double Venn diagram subsets, we can spot bins that have a high number of shared DEGs, and a small number of unique DEGs to each phenotype like the "RNA biosynthesis.transcriptional regulation" bin (containing ERF, MYB, DREB TF superfamilies) and the "protein homeostasis.ubiquitin-proteasome system" bin (Appendix Figure 69).

As in the case of mechanostimulation, we re-encounter "phytohormone action.jasmonic acid" (*CYP94C1, CYP94B3, JAZ1*). These processes might work similarly in the two phenotypes.

One functional category with a higher number of DEGs unique to WT (15) and a lower number of shared (7) or unique to ERR (4) is "enzyme classification.transferases". Interestingly, this group contains many xyloglucan endotransglycosylase (*XTHs*) responsible for CW modifications, which might be impaired in the ERR. Surprisingly, on the other hand, the "cell wall organisation" bin contained 39 DEGs unique to ERR mutant and only 6 DEGs unique to WT DEGs, while 8 DEGs were shared by the two. Out of these, maybe the most interesting group is the "CW organisation.pectin" with 19 unique DEGs to ERR and only 3 shared or unique to WT, followed by "CW proteins.arabinogalactan-protein" with 8 unique to ERR DEGs (Appendix Figure 69).

Observing many CW-related processes activated upon COR is not surprising, since the trap prepares for slow trap closure. However, we know that in ERR the closure speed is much slower as we have seen in Figure 27. This raises the question: does the ERR have such a different CW architecture and components that different molecular mechanisms are addressed upon COR application?

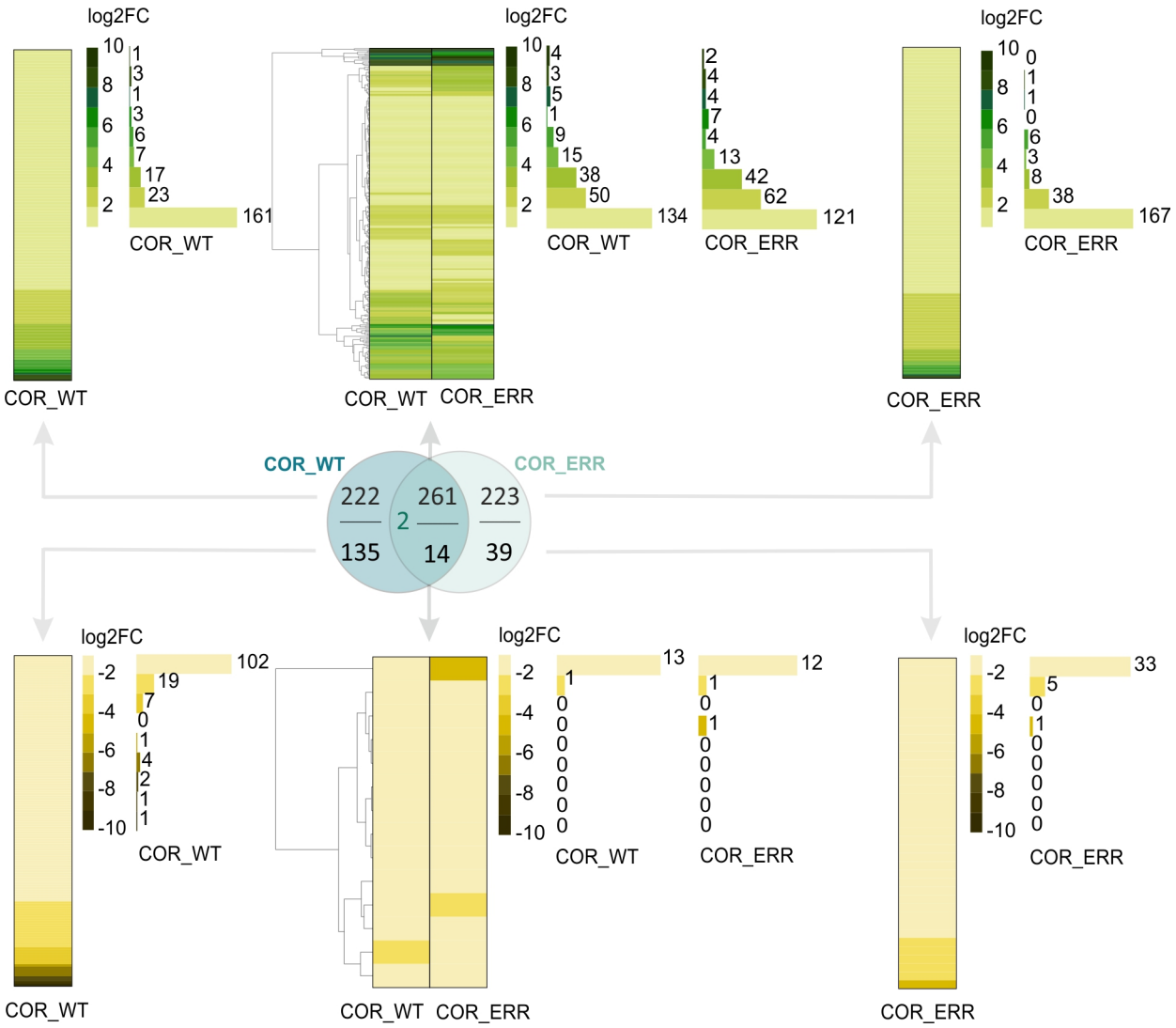

Figure 54: Double Venn diagram showing the intersection of DEGs upon COR (0.1 mM coronatine) in both WT and ERR. Upregulated DEGs are shown above as follows: unique to WT (222), shared between WT and ERR (261) and unique to ERR (223). Downregulated DEGs are shown bellow as follows: unique to WT (135), shared between WT and ERR (14) and unique to ERR (39). 2 DEGs are up COR in ERR but down in WT. The log_2FC value of the shared subset of the Venn diagram is represented as a heatmap with the number of genes in each log_2FC value interval being shown next to the heatmap scale as bar plot (i.e. 134 genes are found between log_2FC value 1 and 2 in the upregulated DEGs of COR-WT shared DEGs subset).

Core Genes Responsive to Both Touch and Coronatine Treatment Highlight the Difference in Expression Pattern Between Wild Type and 'ERROR' Mutant

Overall, the gene set addressed by touch-evoked AP stimulation in both phenotypes was larger than that addressed by COR stimulation. Comparing both treatments between the phenotypes, revealed that the number of DEGs specific to COR treatment in WT was further reduced (93 upregulated DEGs and 79 downregulated DEGs; subset s3 in Figure 55) when compared to mechanostimulation-specific genes (704 upregulated DEGs and 457 downregulated DEGs; subset s1 in Figure 55).

By looking at the expression amplitudes of each subset of the comparison, I could observe that the group exhibiting the highest upregulation level was represented by core DEGs, shared between both treatments and both phenotypes (196 DEGs; subset s8 in Figure 55).
This analysis revealed a fundamental regulatory difference between the two phenotypes and also within the two treatments. Upon mechanostimulation as many as 87 DEGs displayed a $\log_2 FC > 4$ in WT while the same interval in ERR was comprised of only 34 DEGs. Upon COR, within the same expression interval ($\log_2 FC > 4$) a similar number was found in both phenotypes (35 DEGs in WT and 32 DEGs in ERR).

Out of these 196 core DEGs, the majority (181) start from the same ground level, meaning that they are not DEGs within the Control_WT vs Control_ERR comparison (Figure 40I - Venn diagram, Appendix Figure 70A - UpSet plot). Oddly, the number of downregulated DEGs, within the same subset, is only 6 (Appendix Figure 70B - UpSet plot). Which draws our attention back to the ground state comparison. Interestingly, out of the total 497 downregulated DEGs within the ground state pairwise comparison (Figure 40A), 396 were unique to this pairwise comparison (Appendix Figure 70B) when taking all conditions into account, thus not overlapping with any of the treatments. This indicates that many of the faulty downregulated DEGs in the ERR's ground state are not involved in touch or JA-induced responses. Nevertheless, part of the minority are the 52 DEGs that are also downregulated upon touch but only in the WT (Appendix Figure 70B). Among these, at the top of the list, are DEGs that have already been mentioned before such as: *EXPA11/6, HYR1, BAM3*.

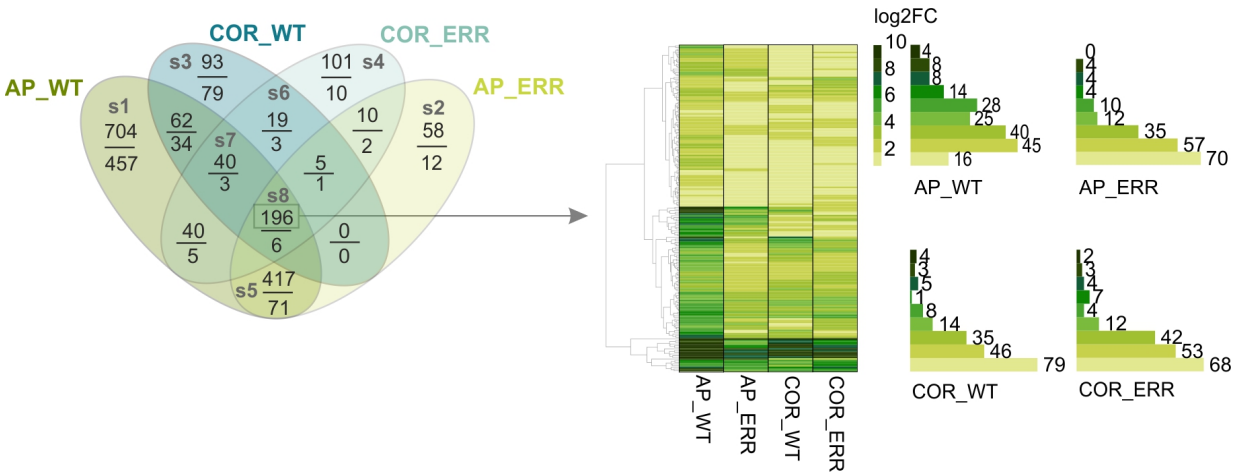

Figure 55: Quadruple Venn diagram showing the intersection of DEGs of each pairwise comparison in both WT and ERR upon mechanostimulation (10 APs, 0.01 Hz) and COR treatment (0.1 mM coronatine). Numbers on top represent upregulated DEGs and on the bottom downregulated DEGs. The $\log_2$FC value of the Venn upregulated DEG subsets is represented as a heatmap with the number of genes in each $\log_2$FC value interval being shown next to the heatmap scale as bar plot.

3.2.2.5 In Search of Unresponsive Ca^{2+}-Signalling Components in the 'ERROR' Mutant

Ca^{2+} signalling accompanies the electrical signalling [131] and it is essential for all plants in order to respond properly to environmental stimuli [227].

Even though we could not spot any Ca^{2+}-related GO-terms (Appendix Figure 68) upon mechanostimulated WT traps, we set to further inspect any genes that could have a Ca^{2+}-related process function.

Since MapMan/Mercator4 annotation does not contain any "calcium signalling" dedicated bin, I selected for any Ca^{2+}-related gene that has been annotated by both Mercator 3.4 and Mercator4 from different bins, ending up with a total of 449 genes. Out of these, 59 were DEGs in at least one of the all analysed conditions for this study, many (40) of them being upregulated after mechanostimulation in WT. Only 11 DEGs were induced in AP treated WT, but not in the AP treated ERR. Among these we can find: calmodulin-like protein *AGD11/CML3* as well as calmodulin-binding protein *IQD2,19*, together with Ca^{2+} channels such as the glutamate activated *GLR2.8* and mechanosensitive *OSCA1.2* channel as well as the pump Ca^{2+}-ATP-ase *ECA4* (Figure 56). Other Ca^{2+}-annotated genes (*CML25,42, CMI1, PBP1, EDA39, CP1, IQD22*) were induced in the ERR upon mechanostimulation but at a lower extent than in WT.

Looking at the FPKM expression level, probably the most outstanding genes (with the highest discrepancy between the FPKM expression level in WT vs ERR upon mechanostimulation) were: *CML42, EDA39, CBL1, IQD19*, making these genes good candidates for Ca^{2+} decoding processes that might be affected in the ERR. The Ca^{2+} decoding elements are essential, since they might influence JA signalling and biosynthesis.

However, if we want to understand the basic differences between the two phenotypes that determine fast responses - therefore have to be present before the mechanostimualtion - we shall rather look at the unstimulated ground state.

Very few of the Ca^{2+}-annotated genes were differentially expressed in the ground state pairwise comparison. Nevertheless, out of these, the majority were upregulated (rather than downregulated, as it would have been expected) in the ERR's ground state compared to WT (such as: *CML42, EDA39, IQD22, GLR2.1*)(Figure 56). While *ACA2* was the only downregulated DEG in unstimulated ERR traps compared to unstimulated WT traps, the range of expression was very low (Dm_00006598-RA, Control_WT = 0.99 FPKM, Control_ERR = 0.15 FPKM).

Ctrl_ERR	AP_WT	AP_ERR	COR_WT	COR_ERR	Gene Name	DmID	AtID	Gene Description	
NA	7.9	4.4	NA	NA	CML25	Dm_00000389-RA	AT1G24620	EF hand calcium-binding protein family	Highly induced in AP_WT Slightly induced in AP_ERR
1.8	6.3	2.8	1.6	NA	CML42	Dm_00001554-RA	AT4G20780	calmodulin like 42	
NA	5.8	2.0	1.1	NA	CMI1	Dm_00018647-RA	AT4G27280	Calcium-binding EF-hand family protein	
NA	5.7	1.4	NA	NA		Dm_00011215-RA	AT3G13600	calmodulin-binding family protein	
NA	5.3	2.2	NA	NA	PBP1	Dm_00009931-RA	AT5G54490	pinoid-binding protein 1	
1.6	5.2	1.8	1.5	1.1		Dm_00011216-RA	AT3G13600	calmodulin-binding family protein	
1.2	5.2	2.7	3.1	2.6		Dm_00015386-RA	AT2G23790	calcium uniporter (DUF607)	
1.3	4.5	1.7	NA	NA	EDA39	Dm_00003855-RA	AT4G33050	calmodulin-binding family protein	
NA	4.1	1.9	4.4	2.4	CP1	Dm_00015718-RA	AT5G49480	Ca2 -binding protein 1	
1.9	3.8	1.4	1.3	NA	IQD22	Dm_00013162-RA	AT4G23060	IQ-domain 22 (CaM binding)	
NA	3.1	1.5	1.0	1.5		Dm_00000418-RA	AT5G54130	Calcium-binding endonuclease/exonuclease/phosphatase family	
1.5	3.1	1.4	NA	NA		Dm_00001189-RA	AT5G04170	Calcium-binding EF-hand family protein	
NA	3.1	3.0	NA	NA		Dm_00001629-RA	AT4G25800	Calmodulin-binding protein	
NA	3.0	2.9	NA	NA	TCH2	Dm_00020642-RA	AT5G37770	EF hand calcium-binding protein family	
NA	2.5	2.3	NA	NA		Dm_00004152-RA	AT3G10300	Calcium-binding EF-hand family protein	
NA	2.5	1.6	NA	NA	CPK16	Dm_00006184-RA	AT2G17890	calcium-dependent protein kinase 16	
NA	2.5	1.3	NA	1.2	CBL1	Dm_00016099-RA	AT4G17615	calcineurin B-like protein 1	
NA	2.2	1.3	1.9	1.0	CBL10	Dm_00011526-RA	AT4G33000	calcineurin B-like protein 10	Similar induction in AP_WT and AP_ERR
1.3	2.2	1.4	NA	NA	GLR2.1	Dm_00000700-RA	AT5G27100	glutamate receptor 2.1	
NA	2.2	1.7	NA	NA	ACA2	Dm_00018589-RA	AT4G37640	calcium ATPase 2	
NA	2.2	1.7	NA	NA	CML25	Dm_00001947-RA	AT1G24620	EF hand calcium-binding protein family	
NA	2.2	1.6	NA	NA	CPK9	Dm_00000864-RA	AT3G20410	calmodulin-domain protein kinase 9	
NA	2.1	1.3	NA	NA	CBP60B	Dm_00003515-RA	AT5G57580	Calmodulin-binding protein	
NA	1.9	1.5	2.2	1.6		Dm_00019071-RA	AT2G38800	Plant calmodulin-binding protein-like protein	
NA	1.9	2.7	NA	NA		Dm_00018051-RA	AT1G18210	Calcium-binding EF-hand family protein	
NA	1.7	1.1	NA	NA		Dm_00004720-RA	AT5G28850	Calcium-binding EF-hand family protein	
NA	1.4	1.3	NA	NA	DCD	Dm_00003259-RA	AT5G61910	DCD (Development and Cell Death) domain protein	
NA	1.3	1.1	NA	NA	IQD2	Dm_00014543-RA	AT5G03040	IQ-domain 2 (CaM binding)	
NA	1.2	1.1	NA	1.6		Dm_00000234-RA	AT3G03000	EF hand calcium-binding protein family	
NA	-1.6	-1.3	NA	NA	GLR3.4	Dm_00004609-RA	AT1G05200	glutamate receptor 3.4	
NA	5.9	NA	NA	NA	AGD11	Dm_00005923-RA	AT3G07490	ARF-GAP domain 11	
NA	3.1	NA	NA	NA	GLR2.8	Dm_00010360-RA	AT2G29110	glutamate receptor 2.8	
NA	2.6	NA	NA	NA		Dm_00000526-RA	AT2G44310	Calcium-binding EF-hand family protein	
NA	2.4	NA	NA	NA	CNGC8	Dm_00004597-RA	AT1G19780	cyclic nucleotide gated channel 8	Induced in AP_WT Absent in AP_ERR
2.2	2.1	NA	NA	NA		Dm_00015225-RA	AT3G29000	Calcium-binding EF-hand family protein	
NA	1.8	NA	NA	NA	IQD2	Dm_00007194-RA	AT5G03040	IQ-domain 2 (CaM binding)	
NA	1.7	NA	NA	NA	ECA4	Dm_00009331-RA	AT1G07670	endomembrane-type CA-ATPase 4	
NA	1.7	NA	NA	NA	OSCA1.2	Dm_00001755-RA	AT4G22120	ERD (early-responsive to dehydration stress) family protein	
NA	1.5	NA	NA	NA	IQD19	Dm_00016508-RA	AT4G14750	IQ-domain 19 (CaM binding)	
-1.4	1.3	NA	NA	1.2		Dm_00001089-RA	AT2G23790	calcium uniporter (DUF607)	
NA	1.0	NA	NA	NA	BAG7	Dm_00012344-RA	AT5G62390	BCL-2-associated athanogene 7	
NA	-1.0	NA	NA	NA	CRK1	Dm_00001271-RA	AT2G41140	CDPK-related kinase 1	
NA	-1.0	NA	NA	NA	SYTC	Dm_00009767-RA	AT5G04220	Calcium-dependent lipid-binding (CaLB domain) family protein	
NA	-1.1	NA	NA	NA	SOS3	Dm_00000455-RA	AT5G24270	Calcium-binding EF-hand family protein	
NA	-1.1	NA	NA	NA	CDPK19	Dm_00009295-RA	AT5G19450	calcium-dependent protein kinase 19	
NA	-1.1	NA	NA	NA	CML25	Dm_00009960-RA	AT1G24620	EF hand calcium-binding protein family	
NA	-1.1	NA	NA	NA	CPK7	Dm_00005101-RA	AT5G12480	calmodulin-domain protein kinase 7	
NA	-1.2	NA	NA	NA	CPK16	Dm_00016911-RA	AT2G17890	calcium-dependent protein kinase 16	
NA	-1.3	NA	NA	NA	NCL	Dm_00018757-RA	AT1G53210	sodium/calcium exchanger family protein / EF hand	
NA	-1.6	NA	NA	NA	CML36	Dm_00012152-RA	AT3G10190	Calcium-binding EF-hand family protein	Downreg . in AP_WT Absent in AP_ERR
NA	NA	1.3	NA	NA	CML14	Dm_00009568-RA	AT1G62820	Calcium-binding EF-hand family protein	
-1.1	NA	1.5	NA	NA		Dm_00001168-RA	AT2G38800	Plant calmodulin-binding protein-like protein	
NA	NA	NA	1.1	1.2	GLR3.4	Dm_00011353-RA	AT1G05200	glutamate receptor 3.4	
1.9	NA	NA	NA	NA	MSL10	Dm_00009130-RA	AT5G12080	mechanosensitive channel of small conductance-like 10	
1.4	NA	NA	NA	NA	NPG1	Dm_00019174-RA	AT2G43040	tetratricopeptide repeat (TPR)-containing protein	
1.0	NA	NA	NA	NA	CPK1	Dm_00012895-RA	AT5G04870	calcium dependent protein kinase 1	
1.0	NA	NA	NA	NA		Dm_00003867-RA	AT2G27480	Calcium-binding EF-hand family protein	
-2.7	NA	NA	NA	NA	ACA2	Dm_00006598-RA	AT4G37640	calcium ATPase 2	DEGs in ground -state only
-1.3	NA	NA	NA	NA		Dm_00001167-RA	AT2G41410	Calcium-binding EF-hand family protein	

Figure 56: Calcium-annotated DEGs in all studied pairwise comparisons according to Mercator 3.5 annotation together with *Arabidopsis thaliana* orthologs and their description. The $\log_2$FC values of DEGs of each pairwise comparison are represented by the heatmap. Ctrl_ERR = Control_ERR vs Control_WT, AP_WT = AP_WT vs Control_WT, AP_ERR = AP_ERR vs Control_ERR, COR_WT = COR_WT vs Control_WT. COR_ERR = COR_ERR vs Control_ERR. NA = not DEG. Genes without name are not properly studied yet, but they contain Ca^{2+}-binding EF-hands.

3.2.2.6 The Deregulated Jasmonic Acid-Pathway Components of The 'ERROR' Mutant

Since the JA, as well as JA-Ile concentrations, were rather low in the ERR upon mechanostimulation (Figure 31), we further wanted to investigate the expression pattern of various JA-associated components upon both treatments.

Starting with genes involved in JA-biosynthesis pathway (Figure 57 left), we see DEGs that are activated upon touch stimulation rather than COR, such as: *LOX3, OPR3* and *JAR*, with lower expression levels in ERR. Not expressed in ERR upon mechanostimulation is *JMT*, that catalyzes the formation of the volatile methyljasmonate involved in interplant communication as well as systemic responses upon stresses [228]. Interestingly, the amidohydrolase *ILL6* contributing to JA-Ile hormone turnover was identified as shared DEG under both experimental conditions in WT (AP- and COR-treated traps). In ERR, however, this gene is not activated by mechanostimulation, but it was activated by COR treatment, indicating that the ERR's defect is upstream of JA recognition. With similar function, jasmonoyl-amino acid hydroxylase *CYP94B3* and *CYP94C1* were induced upon both treatments in both phenotypes even though it was slightly induced in the ERR's ground state from the start (compared to WT's ground state).

Using a high resolution RNA-seq time-series, Hickman and colleagues identified transcription factors (TFs) and their target genes in response to jasmonate application on the *Arabidopsis thaliana*'s leaf surface [229]. Using *Arabidopsis thaliana* orthologs determined in their studies, I wondered how these TFs and their known target genes are expressed in *Dionaea muscipula* upon our conditions. We can see the $\log_2$FC values of JA-responsive transcription factors (TFs) together with their target orthologs of *Arabidopsis thaliana* (Figure 57 right) of all pairwise comparisons. Among JA-responsive TFs, we can spot the JA marker *JAZ1*. Besides this, another TIFY-like TF that shows even higher expression values in WT surprisingly has no *Arabidopsis thaliana* ortholog. We can also spot *MYC2*, a central transcription factor in jasmonate signalling, "acting" normally in the ERR upon both treatments. Even though some JA-induced TFs are upregulated DEGs in the ERR's ground state when compared to WT (besides mechanostimulation and COR treatment) their expression level in Control_ERR group is rather low ($<$ 10 FPKM), therefore they do not represent important regulators that might explain the defects in ERR. In general, many TFs show similar $\log_2$FC values in ERR and WT upon touch and COR (*JAZ1, AIB, DEAR3, WRKY69, MYC2, BT4, MYB73, RD26*) while some seem to be specific to mechanostimulated WT (*MYB78, STZ, TEM1, ABR1, HB22*), therefore unresponsive in ERR. From the target genes, the top branch of the heatmap (Figure 57 right, up) outlines strongly responsive genes in both phenotypes upon both treatments (*SAG12, CYP76C/94C, TBL41*). Unlike the TFs, the target genes of the ERR seem to be differentially expressed most of the time as well but at a lower extent upon touch.

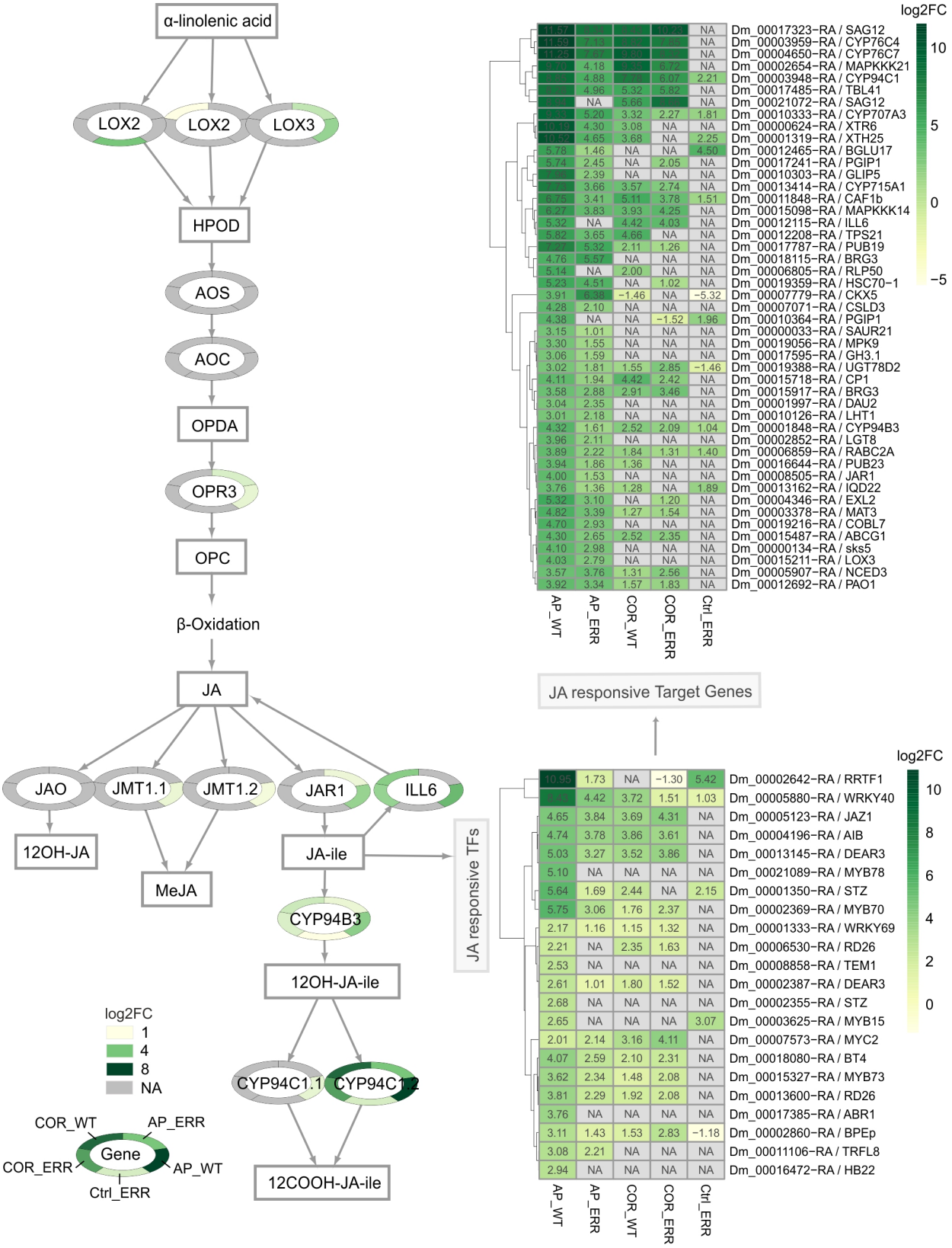

Figure 57: JA biosynthesis pathway (left) together with $\log_2$FC values of DEGs in each of the pairwise comparisons indicated by the circular heatmap. The JA pathway was built according to different literature sources [156, 157, 158]. The $\log_2$FC values are also shown as a heatmap (right) for the JA responsive TFs (down) together with their target genes (up) as described in Arabidopsis orthologs [229]. For space reasons, only target genes with a $\log_2$FC > 3 in AP_WT are shown. Only annotated genes are shown. Ctrl_ERR = Control_ERR vs Control_WT, AP_WT = AP_WT vs Control_WT, AP_ERR = AP_ERR vs Control_ERR, COR_WT = COR_WT vs Control_WT. COR_ERR = COR_ERR vs Control_ERR. NA = not DEG.

In the end, it is difficult to explain the low JA content upon touch stimulation of ERR traps. It could be the low expression of JAR1 responsible for JA-Ile synthesis, it could be one of the TFs that are not activated upon mechanostimulation in order to amplify the signal. Or maybe MeJA has a very important role in signal spreading and positive feedback for more JA biosynthesis, that is highly dependent on *JMT1* activation, which does not occur in the ERR. Taken together, many altered processes point to a compromised, malfunctioning immune system in the ERR traps that is affecting the carnivory syndrome as well.

3.2.2.7 Short Summary

The most striking DEGs, throughout the transcriptomic analysis, together with their relevant function are depicted in Figure 58. In conclusion, I would like to emphasize the following main findings:

- Even without stimulation, in the ground state, ERR traps seem to have a defect in oxidation-reduction processes (shown by the GO-enrichment) that are reflected in the upregulated as well as downregulated DEGs when compared to WT. Moreover, genes involved in cell wall (CW) modification are downregulated (Figure 58A).
- We learn that in the functional WT trap, upon mechanostimulation, defence signalling pathways are activated as well as cell elongation processes regulated by the growth hormone auxin together with CW-modifications by the respective enzymes (XTHs), which might be needed for digestion and stomach formation (Figure 58B).
- Functions such as CW modification, CW integrity system and auxin biosynthesis that might be linked to cell growth together with defence-related processes that might be necessary for stomach formation are are strongly underrepresented in the mechanostimulated ERR trap. These results go hand in hand with the previous observations that the ERR traps do not undergo full stomach formation upon elicitation of 10 APs (Figure 58C).
- We re-encounter a few defence, redox and CW modification-related processes that are altered in the ERR ground state and fail to provide a touch-induced response upon mechanostimulation in the ERR traps (Figure 58E).
- Activation of digestive hydrolases, JA-signalling pathway as well as stress and defence-related functions are triggered by COR application in both WT and ERR. These processes can, therefore, be rescued (at least partially) upon external jasmonate application in the ERR. Nevertheless, CW-related processes seem to differ within the two phenotypes many being uniquely expressed in the ERR, suggesting again that the ERR CW structure and architecture might be different from the normal WT (Figure 58D).

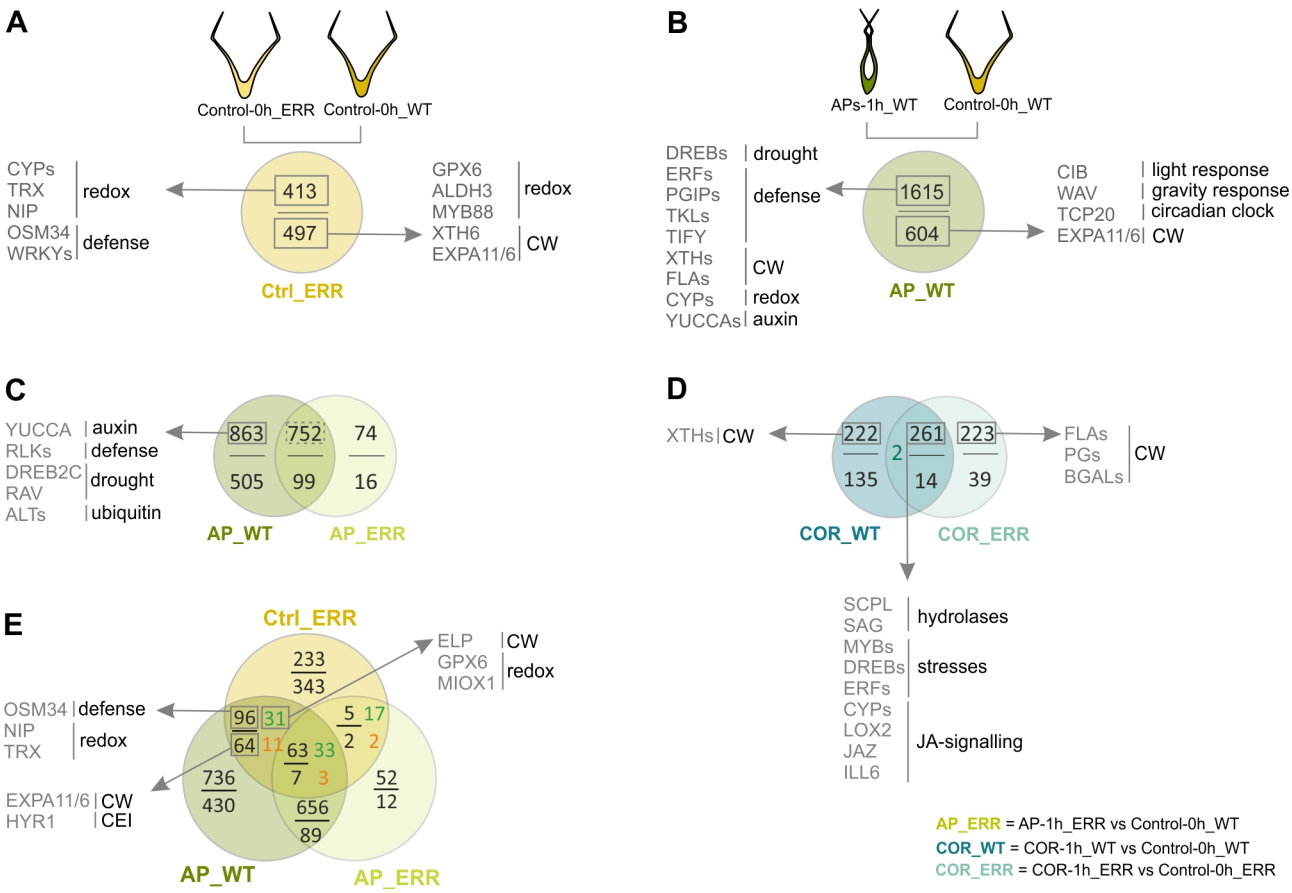

Figure 58: Short summary of the main findings, emphasizing genes and their general function in subsets of: (A) Ground state comparison of upregulated (left) and downregulated (right) DEGs. (B) Mechanostimulated WT trap of the upregulated (left) and downregulated (right) DEGs, (C) DEGs as part of enriched MapMan bins in the unique subset of WT and at the same time not enriched in the ERR shared subset. (D) DEGs as part of COR-treated traps unique to WT subset (left), shared subset (down) and unique to ERR (right) subset. (E) DEGs that are: (left, up) upregulated after mechanostimulation only in WT traps (and not in ERR) and are at the same time upregulated already in the ERR ground state (compared to WT ground state); (left, down) downregulated after mechanostimulation only in WT traps (not in ERR) and are at the same time downregulated in the ERR ground state (compared to WT ground state); (right, up) upregulated after mechanostimulation only in WT traps (not in ERR) and are at the same time already downregulated in the ERR ground (compared to WT ground state).

3.2.3 Discussion

In order to understand the molecular mechanosensing mechanisms of the carnivorous plant *Dionaea muscipula*, starting from trigger hair bending to fast trap snapping movement and underlying molecular pathways activated for further stomach formation, we used a contrasting phenotype: the 'ERROR' mutant (ERR). This naturally occurring cultivar is unable to snap upon trigger hair bending.

In search of answers to the simple question of why the snapping mechanism is hindered, I investigated the ERR mutant's physiological responses as well as its whole-transcriptome gene expression profile in the resting state or after mechanical stimulation in comparison to WT. In non-carnivorous plants, mechanical stimulation and wounding induces defence responses that are triggered by a trio of regulators: electrical signals, cytosolic Ca^{2+} concentration changes and reactive oxygen species (ROS), each with special signatures [230]. This results in the accumulation of phytohormones such as JA, ET, ABA, auxin and SA that are important for adaptive stress responses [231, 232].

3.2.3.1 Ca^{2+} Signalling Components Might Be Malfunctioning in the 'ERROR' Mutant

We know that in *Arabidopsis thaliana* [134] as well as in *Dionaea muscipula* [82] upon touch or wounding, together with the electrical signalling, a Ca^{2+} wave is generated and propagated.

Starting with the first and fastest physiological reaction - the electrical signal - we found out that the ERR mutant can fire normal, WT-like APs, when the trigger hairs are touched (Figure 23D). If the signalling pathway is faulty, then it must be downstream of AP signalling. Interestingly, upon repeated mechanostimulation, depending on the frequency of the stimulus application, some traps close slowly. When 10 action potentials are induced by bending the trigger hairs, at least two out of 12 plants closed their traps no matter the frequency. When the number of APs was doubled to 20, more plants responded by slowly closing their trap. All 12 plants had their traps at least half closed when one AP was applied every 30 seconds. However, when decreasing the frequency (one AP every minute), the response was weaker, indicating that the Ca^{2+}-mediated "memory" was fading (Figure 25). In order to check if the Ca^{2+} memory might be affected in the ERR mutant, we further investigated the expression of Ca^{2+}-related genes, wondering whether the Ca^{2+} signalling, transport or decoding mechanism could be malfunctioning in the ERR (Figure 56).

The Ca^{2+} sensor calmodulin-like 24 (*TCH2*), a perfect touch gene in *Dionaea muscipula*, was upregulated to similar extent in ERR as in WT after mechanostimulation or wounding (Appendix Figure 66A,B).

Looking at the whole-transcriptome level, no Ca^{2+}-related GO-terms emerged from the functional enrichment analysis of WT specific DEGs upon mechanostimulation. Nevertheless, having a closer look into the raw DEG list, we found a few upregulated DEGs in the ERR's ground state compared to WT (such as: *CML42, EDA39, IQD22, GLR2.1*). Among the annotated genes which were strongly induced upon mechanostimulation in WT (with $>$ 30 FPKM), but not differentially expressed in the mechanostimulated ERR mutant, we can see: *AGD11/CML3, IQD22,19, GLR2.8 and ECA4* (Figure 56).

As many studies have pointed out, the activation of glutamate-like receptors GLR3.3 and GLR3.6 are necessary for the cytosolic Ca^{2+} changes to occur upon wounding [65, 134, 233] and are also essential for spreading the signal from damaged to undamaged leaves [192]. However, after bending the trigger hairs of *Dionaea muscipula*, at transcriptomic level, there were no changes in the expression level of *GLR3.6* or *GLR3.3* in neither WT nor ERR mutant (at the 1h time point). As for other GLR paralogues we can see: one *GLR3.4* (Dm_00004609-RA) downregulated upon mechanostimulation in both WT and ERR, while another GLR3.4 (Dm_00011353-RA) is upregulated upon coronatine in both phenotypes and GLR2.8 (Dm_00010360-RA) which was uniquely upregulated in AP-treated WT traps. *GLR2.1* (Dm_00000700-RA) was the only glutamate receptor differentially expressed in the ERR mutant ground state compared to WT ground state ($\log_2$FC $= 1.28$). However, it was upregulated in both phenotypes upon touch (Figure 56).

Calmodulins (CaM) and calmodulin-like proteins are important Ca^{2+} sensors that perceive and transduce Ca^{2+} signals into cellular responses by regulation of target proteins. AGD11/CML3 has been shown to be involved in peroxisome metabolism by mediating dimerisation of peroxisomal DEG15 protease [234]. IQD-proteins are CaM targets with a role in microtubule cytoskeleton organisation and dynamics with potential impact on cell shape and organ morphology, some of them being regulated by auxin [235, 236]. Hand in hand with this goes the observation that after touch stimulation, the "auxin biosynthesis" MapMan bin, containing *YUCCA* genes that are uniquely upregulated in WT but not in ERR (Figure 50), suggesting that trap morphological changes are already initiated for the green stomach formation and are also restricted to WT only.

As already mentioned, the Ca^{2+} signalling is one of the fastest responses in *Dionaea* [82]. It would be, therefore, expected that genes encoding Ca^{2+} decoders to be active in the resting state, in order to produce enough proteins that assure the quick response. For that reason, it would be important to look at DEGs in the Control_ERR vs Control_WT comparison, in order to understand if there are any preliminary differences between the two phenotypes in the ground state.

Out of all Ca^{2+}-related genes, *CML42* and *EDA39* have the highest expression upon mechanostimulation in WT ($>$ 200 FPKM), while in ERR they respond with half the

amplitude (< 100 FPKM). Besides this, they are upregulated DEGs in the ERR mutant ground state, suggesting an altered early Ca^{2+}-signalling response.

Curiously, it has been proposed that the calmodulin-like CML42 may play a role as a negative regulator in the JA-signalling pathway, as *cml42 Arabidopsis* mutants show a higher expression level of JA-responsive *VSP2* and *THI2.1* genes and a higher $[Ca^{2+}]_{cyt}$ four minutes after external JA application. However, the JA levels upon herbivorous insect feeding were not different in the KO mutant compared to WT *Arabidopsis thaliana* [237]. Other studies suggest that CML42 might be important for trichome branching, as in early developmental stages, KO mutants show an increased number of branches [238].

With a direct role in JA biosynthesis, EDA39 (Embryo Sac Development Arrest), also called IQM1 (IQ-motif containing protein), has been shown to increase the defence against necrotrophic pathogens in a Ca^{2+}-independent manner, as *iqm1* mutants had three times lower JA levels after the infection with *Botrytis cinerea* than the WT. In the ERR mutant, the JA levels are also lower compared to WT after touch stimulation (Figure 31). Could, therefore, *DmIQM1* be involved in JA biosynthesis in *Dionaea* as well? Furthermore, the authors of this recent study show that IQM1 directly interacts with the peroxisomal proteins CAT1/3 which have H_20_2 scavenging and defense response functions [239]. Previous studies show that IQM1 is predominantly expressed in stomata and might be involved in stomatal movement by modulating ROS-related genes. T-DNA insertion lines showed a higher level of ROS in the guard cells and smaller stomatal aperture and no response upon light, dark, ABA or chitin. Even more, microarray analysis revealed upregulated chitin-responsive genes in *iqm1* mutants, suggesting a defect in chitin signalling [240]. In older studies, IQM1 was indeed listed as a chitin-inducible TF [241]. In *Dionaea*, *EDA39/IQM1* is slightly upregulated in ERR ground state (Dm_00003855-RA, Control_WT = 9.93, AP_WT = 217.83, Control_ERR = 23.97, AP_ERR = 79.41 FPKM). Could this partly explain the presence of many enriched redox- and chitin-related GO-terms in the upregulated DEGs in the ERR within the ground state comparison? Also, it is very curious that the chitinase *CHIB* had an increased transcription level in resting state and did not further increase upon mechanostimulation as expected (Figure 33), suggesting that the ERR mutant might be compromised in chitin signalling as well.

3.2.3.2 Redox-Related Genes Are Deregulated in the 'ERROR' Mutant

Besides calcium, as the most important and universal second messenger that triggers signalling cascades in response to a wide variety of stresses in plants, ROS has been more recently acknowledged as another important signalling molecule [242, 243]. An autopropagating ROS wave can be triggered by different abiotic stresses such as high light, heat, salinity, cold, or mechanical injury, mediating cell-to-cell communication to activate counteracting mechanisms in plants [227]. In *Arabidopsis thaliana*, ROS

wave propagation is sustained by the ROS-producing enzyme Respiratory Burst Oxidase Homolog D (AtRBOHD) [244]. In *Dionaea muscipula*, *RBOHB* is upregulated upon touch in both WT ($\log_2$FC = 3.1) and ERR ($\log_2$FC = 1.7), with a small tendency of a higher expression values in Control_ERR, indicating that the ROS production still occurs in the mutant (Dm_00000603-RA, Control_WT = 5.23, AP_WT = 47.00, Control_ERR = 9.88, AP_ERR = 33.19 FPKM).

High quantity of ROS is toxic, thus plant cells have evolved a high capacity to scavenge ROS via antioxidants such as ascorbates, glutathione, catalases and superoxide dismutases [245]. However, recent studies suggest that antioxidants should rather be called "ROS-processing enzymes", since their role is not only to keep ROS levels low but also to allow the plant cells to sense and signal the altered ROS availability and redox perturbations [246]. Interestingly, many redox-related DEGs (as part of enriched GO-terms) appear in the ground state comparison (Control_ERR vs Control_WT, as part of downregulated DEGs: Figure 42, and upregulated DEGs: Figure 44), some of them being also induced by mechanostimulation in WT but not in ERR (*TRX1, NIP1;2, PRXs, CYPs, GPX6, MIOX1*, Figure 52).

TRX1 The most outstanding gene is the thioredoxin *TRX1* that is highly induced in WT after mechanostimulation. Additionally, in the ERR mutant control group (Control_ERR), this gene is highly upregulated to the same extent as in mechanostimulated WT (when compared to Control_WT) and the expression does not increase further when mechanostimulation is applied on ERR (Dm_00011727-RA, Control_WT = 6.50, AP_WT = 115.85, Control_ERR = 127.75, AP_ERR = 121.06 FPKM). Thioredoxins are redox regulators found across all life kingdoms. Even though many plant TRXs are found in chloroplast, TRX1 is a thioredoxin H-type 1, found in mitochondria, cytoplasm [217] and apoplast [247]. Relevant for this study is their role of mediating redox signalling in plant immunity by reversing diverse oxidative protein modifications. Even more, there are studies suggesting that TRXs are able to prevent antioxidant enzymes from becoming inactivated by thiol oxidation, therefore protecting them from harmful oxidative damage in a ROS rich environment [248]. In *O. sativa* , TRXh1 over-expression lines showed a lower H_20_2 accumulation in the control group as well as during salt stress compared to WT, leading to a salt-sensitive phenotype [247]. This raises the question: could this be the case in the ERR mutant as well?

NIP1;2 Another outstanding gene with similar expression pattern, is the aquaporin homolog NOD26-like intrinsic protein *NIP1;2* (Dm_00012214-RA, Control_WT = 97.85, AP_WT = 239.62, Control_ERR = 257.17, AP_ERR = 300.78 FPKM). NOD26-like intrinsic proteins are unique to plants and have first been discovered in leguminous soybean where they are presumed to be involved in exchange of metabolites between the host and the symbiont [249]. Besides this, they are involved in glycerol transport as well as aluminium [250] and arsenite [251] tolerance. However, relevant

for the redox-topic is the fact that NIP;2 facilitates H_20_2 transport as well [226]. Conceivably, in *Dionaea muscipula*, with each touch, the amount of H_20_2 produced by the RBOHD would increase in the CW, making its transport into the cytoplasm suitable in order to spread the signal on one hand and to get more efficiently detoxified when needed on the other hand. Could the high expression of the H_20_2 permeable NIP1;2 in ERR mutant's resting state be another hint to a low ROS concentration in the CW? Since aquaporins are important turgor regulators, their potential role in trap closure is not excluded. However, at transcriptomic level, we could not find any other aquaporin gene expression change upon touch in either of the phenotypes (with the exception of *NIP1;1* Dm_00009360-RA paralogue which is induced in AP_WT but at a very low extent).

CYPs Besides the prominent mentioned DEGs, many CYPs (*CYP82C4, CYP76C4, CYP71A26, CYP94B3, CYP707A1*) were upregulated in Control_ERR when compared to Control_WT (Figure 44). CYPs are part of the cytochrome P450 family, the largest enzyme family found across all the domains of life, being responsible for NADPH- and/or O_2-dependent hydroxylation reactions. In higher plants, they act as versatile catalysts and are important for secondary metabolites, antioxidants, and phytohormones biosynthesis [211].

PRXs Involved in catalysing redox reaction, six slightly upregulated peroxidases were found in the ERR ground state (such as: *PER39, PRX47, PRX52*, Dm_00009093-RA, Dm_00018980-RA, Dm_00001327-RA). Besides their role in ROS metabolism, peroxidases have a multitude of functions including: signalling regulation, root and shoot elongation, auxin catabolism, defence responses, wound healing, lignification and suberisation as well as CW metabolism [252].

Peroxidases can cross-link extensins, using pectins as an anchor, creating a dense, solid network that brings CW stiffness. This makes the CW harder to penetrate by the pathogen invaders, thus ensuring defence through CW structure modifications [253, 254]. On the other hand, the resulting increase of mechanical strength can also protect the plant against abiotic factors such as drought, frost or high salinity, cases in which the plant needs to endure tough changes in turgor. The increased mechanical strength also prevents cell expansion [253].

Different studies show different responses to the same abiotic factors (drought, salinity), in some cases CW becoming looser in other cases more rigid [255]. What influences the balance between stiffness and loosening is the peroxide activity, their substrates' availability and types of ROS produced during stress. For example, if peroxidase activity is decreased (or substrate levels are low), the production of hydroxyl radicals will take over [253]. It has been shown that highly reactive hydroxyl radical can cleave polysaccharide glycosidic bonds without enzymatic activity, leading to CW loosening [256, 257]. Therefore, a high level of peroxidase-encoding gene expression might be

linked to an improper ROS-signalling and possibly stiffer CW architecture in the ERR mutant.

All these deregulated redox-responsive genes in the untreated ERR traps, might indicate that the complex redox-system might be malfunctioning in the ERR mutant, and it might be linked to the CW plasticity.

3.2.3.3 Cell Wall Architecture Might Be Off the Wall in the 'ERROR' Mutant

In land plants, cell walls (CW) are mainly composed of three types of polysaccharides: cellulose, hemicelluloses (non-cellulosic polysaccharides, such as xyloglucan) and pectins. Besides this, polyphenols (such as lignin) and proteins (such as enzymes, receptors and structural components) can have a high influence on CW properties. CW loosening enzymes such as expansins and XET/XTH, target the so-called "hot-spots", the sites where xyloglucan makes contact with cellulose microfibrils, enabling cell expansion. Pectins are responsible for CW porosity maintenance by constituting a hydrated gel phase in which the cellulose and hemicelluloses are embedded [253, 258, 259].

Besides its nutrient and messenger role, Ca^{2+} is an important structural component of the CW. Ca^{2+} determines the CW rigidity by cross-linking negatively charged carboxyl groups of de-esterified pectins [260, 261]. Having an important role in signalling, ROS are also influencing CW architecture. Their presence in the apoplast initiates pH changes, protein phosphorylation, changes in protein structure through disulfide bond formation, as well as polysaccharide cross-linking or chain rupture [230, 253, 262]. The "ROS machine" RBOH can be activated by directly binding Ca^{2+} via EF-hand domains after the Ca^{2+} influx into the cell, as well as by phosphorylation events mediated by Ca^{2+}-dependent kinases, such as: Calcineurin B-like (CBL)-Interacting Protein Kinases (CIPKs) and the SnRK2 protein kinase Open Stomata1 OST1. Apoplastic superoxide further activates Ca^{2+} influx into neighbouring cells, leading to a positive feedback loop that amplifies the signal [246]. H_20_2 accumulation in the CW during stress can lead to CW stiffening and therefore reduced cellular elongation also due to the fact that it attracts peroxidases in the apoplast [263]. Finally, RBOH could be inhibited post-translationally by nitric oxide [264].

Interestingly, many cell-wall modifying enzymes-encoding genes are downregulated in the ERR ground state, which are part of the enriched "CW organisation" MapMan bin, such as: expansins (*EXPA11,6,EXLA2)*, hydroxyproline-rich glycoprotein arabinogalactan-protein (AGP) (*FT1*), hemicellulose (xylan) biosynthesis *IRX9*, hemicellulose (xyloglucan) modification and degradation *XYL1*, pectin modification and degradation (pectin lyase-like superfamily protein, Dm_00008368-RA) (Appendix Table19).

Expansins Might Help to Build Up the Ready-To-Snap Trap Configuration

Expansins are characterised by their unique ability to rapidly induce creep and stress relaxation of CWs without lytic activity, in a pH-dependent manner. In order for cell enlargement to occur, the CWs that enclose and provide the shape of the cells have to be loosened, finally allowing water uptake and cell expansion. Even though it is thought that expansins disrupt the hemicellulose–cellulose hydrogen bonds, allowing them to slide among each other, the exact mechanism is still unknown [265].

There are two major families: α-expansins (EXPA) and β-expansins (EXPB). While the first ones are involved in CW loosening, the second ones include grass pollen allergens about which very little is known. Additionally, there are two smaller families: expansin-like A and B (EXLA, EXLB). In Angiosperms, the expansins families range between 18 members (in *Medicago truncatula*) up to 88 members in maize. They are also found in non-flowering plants (such as *Selaginella moellendorffii* and *Physcomitrella patens*), algae (*Micrasterias denticulata*) and other CW-bearing organisms such as bacteria and fungi [265].

Marowa and colleagues provide a very informative summary of many expansins OE and KO mutant line phenotypes. In short, KO mutants presented firmer fruits (*LeEXPA1, SlEXPA1*), reduced root and leaf sizes (*OsEXPB2*), delayed germination (*AtEXPA2*), reduced sensitivity of stomata to stimuli (*AtEXPA1*) and even resistance to necrotrophic pathogens (*AtEXPLA2*). On the other hand, the OE line show softer fruits, increased cells, larger leaves, longer stems, increased root mass (in short, enhanced growth), faster germination and increased rate of light-induced stomatal opening [266].

In *Dionaea muscipula*'s genome [25], there are 16 expansin homologs: *EXPA1,4,6,7,8,9, 10,11,23* and *EXPB3* as well as two paralogs of expansin-like *EXLA2* genes. Despite the high redundancy, *EXPA11* seems to be the only DEG with an exuberant expression level in the unstimulated open-trap state of the WT (771.27 FPKM), followed by EXLA2 (464.10 FPKM), and EXPA6 (44.64 FPKM), while the rest have a low expression level throughout all conditions (Table 8). They were also downregulated after mechanostimulation in WT (DEGp2 column of Table 8). This might indicate that they might have an important function in the resting state rather than stomach formation. Furthermore, all expansins that are highly expressed in WT's ground state, have much lower expression values in the ERR mutant's ground state, being downregulated DEGs when compared to WT (DEGp1 column of Table 8).

Table 8: Expansins expression: log_2FC values of DEGp1 = Control_ERR vs Control_WT, DEGp2 = AP_WT vs Control_WT and DEGp3 = AP_ERR vs Control_ERR, followed by FPKM expression values in each condition.

DmID	Gene	DEGp1	DEGp2	DEGp3	Ctrl_WT	AP_WT	Ctrl_ERR	AP_ERR
Dm_00001234-RA	EXPA11	-2.17	-1.34	NA	771.27	303.92	170.88	108.08
Dm_00003377-RA	EXLA2	-2.84	NA	1.03	464.11	717.01	64.99	133.05
Dm_00003742-RA	EXPA6	-1.09	-2.04	NA	44.64	10.99	21.04	17.80
Dm_00000118-RA	EXPA11	NA	-2.02	-1.77	70.25	17.34	82.45	24.13
Dm_00001989-RA	EXPA10	NA	-1.46	NA	70.13	25.57	98.59	62.53
Dm_00017798-RA	EXPA8	NA	NA	-2.01	33.07	33.92	74.56	18.48
Dm_00003161-RA	EXPB3	NA	NA	NA	12.19	14.34	5.21	5.62
Dm_00019243-RA	EXPA8	NA	NA	NA	5.85	5.49	7.78	3.41
Dm_00010386-RA	EXPA1	NA	NA	NA	3.48	2.27	2.45	2.65
Dm_00015175-RA	EXLA2	NA	1.03	NA	2.54	5.20	2.16	3.86
Dm_00007426-RA	EXPA4	NA	NA	NA	1.70	1.27	1.47	1.97
Dm_00006854-RA	EXPA9	NA	NA	NA	0.48	1.84	1.49	1.88
Dm_00020115-RA	EXPA11	NA	NA	NA	0.30	0.14	0.28	0.16
Dm_00005372-RA	EXPA1	NA	NA	NA	0.15	1.10	0.03	0.13
Dm_00011103-RA	EXPA23	NA	NA	NA	0.03	0.10	0.05	0.06
Dm_00015801-RA	EXPA7	NA	NA	NA	0.02	0.01	0.14	0.14

Could the low expression levels of expansin genes contribute to ERR's inability to snap? The snapping mechanism of the Venus flytrap has long been studied, and still, it is not clearly understood [95, 96, 97, 120, 267].
The most accepted and plausible explanation thus far is "the hydraulic model", which implies osmotically driven fast water flow between layers of cells [268]. For details about the closure mechanism see chapter 1.4. In this case, expansins might be responsible for trap "arming"/"loading" by allowing full expansion of the trap's upper (also called inner) layer of cells, which is necessary for a curved convex geometry. Could the convex-shaped lobes of the trap be essential for the snapping mechanism?

R. Sasche and colleagues very recently studied in detail the snapping mechanisms using 3D digital image correlation for the outer and inner trap surfaces. They conclude that full trap turgescence is a prerequisite for successful buckled snapping and that the movement is driven by differential tissues changes (such as swelling or shrinking, or no change at all) [91].

The accumulation of internal hydrostatic pressure, which creates wall stress, may contribute to the strong trap-lobe curving into a convex shape, creating the buckling instability. Therefore, the accumulated elastic energy is quickly released by the hydraulically driven lobe deformation [90, 91, 105]. From a physics point of view, buckling arises when the equilibrium state of an elastic medium becomes unstable, rapidly changing from one state to another even upon a smooth change in a key parameter [206].

In their models, R. Sachse and colleagues included 3-layers: the outer epidermis, the mesophyll cells and the inner epidermis. This 3-layered model suggests that *Dionaea muscipula*'s fast trap closure is driven by simultaneous expansion of the outer epidermis

and shrinkage of the inner epidermis, while the mesophyll has no contribution in the motion but rather act as a lever. The higher the contribution of the inner layer (by shrinking), the less prestress strain is required for fast snapping. Their models which didn't include prestress, even though were able to close, never exhibited buckling [91].

This kind of unhurried trap closure can be observed in juvenile traps that open for the first time and did not reach full maturity and maximum trap "arming" (or full turgescence). Similar lazy closure behaviour can be seen in dehydrated plants as well (only 3 out of 9 dehydrated traps reacted in Sachse and colleagues studies [91]). Counter-intuitively, the dehydrated trap had a larger opening angle in the resting state (before dehydration mean = 69°, after dehydration mean = 83° [91]). Interestingly, the ERR phenotype presents a smaller opening angle (mean = 65°) than WT (mean = 73°) in the resting state (Figure 59A,C). This might indicate that there is an optimum (*goldilocks*) opening angle at which the maximum instability can be reached.

Furthermore, the trap lobe curvature is significantly different between the two phenotypes. While WT traps show a pronounced convex surface of the adaxial side, the ERR curvature is hardly observable with a rather plane surface (Figure 59B,C). Hence, this might suggest that the ERR mutant traps lack the perfect ready-to-snap configuration (given by the trap geometry), for a successful fast closure. Expansins, in this regard, might facilitate trap "arming" or "loading" the trap by allowing strong cell expansion of the upper layer of cells, which increases the upper trap surface, resulting in trap curvature into a convex shape. Therefore, the convex geometry of the trap in the open ready-to-snap configuration might be crucial for a successful buckling-dependent and accelerated trap closure. Supporting this idea is the fact that in a transverse trap section, one can observe that the upper layers of cells are much bigger in volume, while the lower layers (a few of them) contain numerous small cells [122].

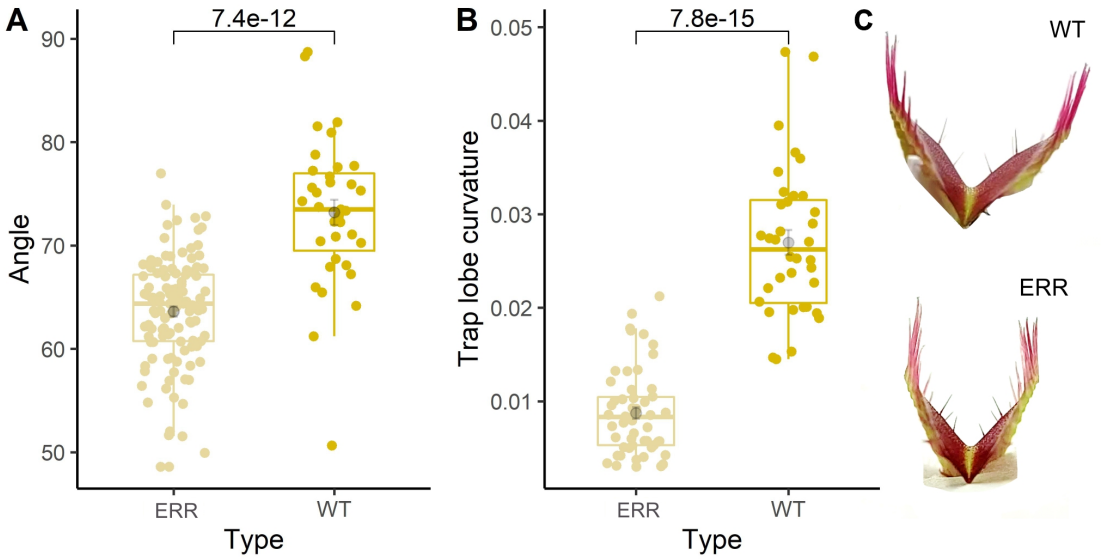

Figure 59: (A) Trap opening angle in the resting state of WT and ERR traps. n=35-70. p-value of Wilcoxon rank sum test between the two groups is shown. (B) Trap lobe curvature during open resting state in both WT and ERR mutant measured with Kappa ImageJ plugin. The trap lobe curvature is represented by the Average Curvature (mm^{-1}). Both lobes of each trap were measured. n=36-54. (C) Representative images of WT and ERR traps in resting state.

Another observation that adds to this idea is that *EXPA11*, is specifically expressed in the unstimulated trap, and it is not expressed in other growing tissues of *Dionaea muscipula* such as petiole, roots or flower (and at a very low extent in sub-components of the trap such as rim and trigger hairs). Even more, *EXPA11* has a low expression in the juvenile trap, where growth processes are highly active (Appendix Figure 63). This might point again to *EXPA11* as having a highly specialized function that might serve carnivory-related purposes (such as trap closure), rather than normal growth processes.

Still, the next question is: how does the water flow from the fully turgid upper layer of cells to the others? As mentioned in the introduction chapter 1.4, Forterre and colleagues doubt that the process is a hydraulically driven lobe deformation. They calculated the water diffusion across a leaf thickness as given by the poroelastic time to be 20-150 seconds [125]. If aquaporins are involved in the water transport process, the question remains: how do they get activated upon mechanostimulation? Aquaporins (AQPs) can be regulated in many ways: through phosphorylation and dephosphorylation, by tetramerization, by hormones (gibberellins, ABA, cytokinins and auxins) and even by pH and ROS. However, in *Dionaea muscipula* the AQPs activation mechanism still remains unsolved.

Interestingly, another outstanding DEG in the ERR's ground state when compared to WT, which is upregulated to a high degree and that might influence the cell turgidity, is the osmotin 34 (*OSM34*) (Dm_00018459-RA, Control_WT=12.51, AP_WT=63.18, Control_ERR=653.23, AP_ERR=775.68). Osmotin has first been described based on its induction by osmotic stress due to low water potential during salt desiccation [269].

Overexpressing lines in many crops (potato, tobacco, strawberry, tomatoes, chilli peper, soybean) have been linked to proline accumulation and a high salt tolerance [216]. The opposite effects have been very recently observed in *Arabidopsis thaliana osm34* KO mutants: decreased proline accumulation as well as reduced expression of ABA responsive-genes upon ABA treatment [270]. Proline is a multifunctional amino acid working as both osmolyte and antioxidant, by increasing the relative water content and also by preventing the accumulation of ROS [216, 271]. Interestingly, proline is an important source of the CW matrix, contributing to the CW architecture. CW matrix is enriched with proline residues which are integrated in the form of hydroxyproline-rich O-glycoproteins (HRGPs). Among these, classified as moderately glycosylated, are the extensins (EXTs) and as hyperglycosylated are the arabinogalactan proteins (AGPs). These HRGPs glycoproteins act as collagen in animals, assuring tensile strength [272].

Besides a possible influence upon CW structure, osmotin's function as an osmolyte suggest that water efflux might be prevented. Consequently, one might ask if the high expression of osmotin *OSM34* during ERR's resting state might result in impaired turgor-changes needed for fast trap closure, due to high osmolality levels. Furthermore, a high osmolality level means high turgidity. Could this explain a lower opening angle of the ERR mutant traps when compared to WT? While a certain turgidity level might be necessary for fast trap buckling as explained by R. Sasche and colleagues, what if the optimum/goldilocks could also be exceeded? A too high turgor pressure combined with increased CW stiffness and a lack of expansins that do not allow strong curvature, might contribute to the ERR mutant's inability of fast-snap closure.

In conclusion, what we learn from this data is that a functional buckling system might rather possess a flexible CW of the upper layer of cells in order to have a big contribution, when shrinking / "deflating", to the collapse of the metastable system. On the other hand, in the case of the unfunctional ERR mutant, a very rigid CW would not allow such a drastic change in cell volume to occur upon water loss. Additionally it would also prevent curvature into a convex shape, in order to bring the open-trap into a ready-to-snap configuration that is a prerequisite for the speed booster buckling system. Adding to this mechanical hindrance, the high expression of the osmotin *OSM34* might also contribute to the ERR's inability to snap by preventing water loss (if proline accumulation occurs).

Downregulated Cell Wall Modifying Enzymes Bring More Evidence Toward a Different Cell Wall in the 'ERROR' Mutant

Besides expansins, other CW-modifying enzymes are downregulated in the ERR ground state compared to WT (*FUC1, FT1, PRP4, RGIL6, XTH6*) that could maybe help us understand better what could be different in the CW anatomy of the ERR (Table 9).

Table 9: CW-related DEGs: $\log_2$FC values of DEGp1 = Control_ERR vs Control_WT, DEGp2 = AP_WT vs Control_WT and DEGp3 = AP_ERR vs Control_ERR, followed by FPKM expression values in each condition.

DmID	Gene	DEGp1	DEGp2	DEGp3	Ctrl_WT	AP_WT	Ctrl_ERR	AP_ERR
Dm_00017887-RA	FUC1	-2.31	NA	NA	103.76	68.11	20.96	18.64
Dm_00011567-RA	FT1	-1.54	NA	-1.62	24.41	13.91	8.37	2.72
Dm_00005762-RA	IRX9	-1.60	NA	NA	120.31	131.28	39.63	48.80
Dm_00007519-RA	RGIL	-1.75	NA	NA	32.09	26.14	9.55	12.62
Dm_00013957-RA	XTH6	-4.26	-2.17	-1.50	3949.82	875.83	205.95	72.94

As part of the CW, glycopolymers are composed of different types of monosaccharide that act as a building block: glucose (Glc), galactose (Gal), arabinose (Ara), galacturonic acid (GalA), xylose (Xyl), rhamnose (Rha), and fucose (Fuc) [273]. The hemicellulose, xyloglucan, is the load-bearing component of the plant CWs, due to the 'hot-spots' created through cross-linking of the cellulose microfibers. The backbone formed by xylosylated glucan can be substituted with a diverse array of glycosyl and nonglycosyl residues, depending on species, tissue and developmental stage. In order to describe the side chains, a one-letter based nomenclature has been given: G represents the unsubstituted glucosyl residue, X stands for a backbone glucosyl residue that harbours a xylosyl residue. And further on, the glucosyl and the xylosyl backbones can be substituted with d- and l-galactosyl (L), l-fucosyl (F) etc. [274].

Xyloglucan metabolism in the CW is thought to play a significant role in turgor-driven cell expansion. The xyloglucan backbone is susceptible to hydrolysis by numerous enzymes such as: xyloglucan β-1,4-endoglucanase, α-D-xylosidase, β-D-galactosidase, α-L-fucosidase and β-D-glucosidase [275]. Terminal α-l-substituents of xyloglucan (such as L-fucose) seem to be involved in the binding of xyloglucan to cellulose [276].

FUC α-L-fucosidases are important for their role of releasing the L-fucose residues from the xyloglucan branches. In the unstimulated state of *Dionaea muscipula* WT, alpha-L-fucosidase 1 (*FUC1*) is highly expressed (103.76 FPKM). In contrast, it has a low expression in the ERR (20.96 FPKM). Another fucosidase (*FUC95A*), seems to be involved in trap CW-modification after the prey capture, since it has low expression values in ground state and high after mechanostimulation (Control_WT = 14.67, AP_WT = 128.95, Control_ERR= 13.93, AP_ERR =37.41).

It has been shown that in *axy8* mutants with a lack of fucosidase activity (*FUC95A*), leads to an increase in fucosylation (the process of adding fucose) on the xyloglucan

backbone compared with WT levels [277]. Fucosylated xyloglucan oligosaccharides are thought to act as signalling molecules, inhibiting auxin-dependent cell elongation [277, 278]. AtAXY8 converts the xyloglucan fragment XXFG (containing fucose residues) to XXLG (without fucose residues) [279]. The amount of XXLG in *axy8* mutant is reduced by 80%. XXLG is unique as it represents the substrate for the fucosyltransferase (FT1)[277]. Fucosyltransferase 1 *FT1* is also downregulated in the ERR mutant ground state as well. In general, this hints to the possibility that the hemicellulose biosynthesis might not work appropriately in the ERR mutant.

IRX Also involved in secondary CW xylan backbone biosynthesis, is the xylosyltransferase transmembrane protein IRX9, named after the KO mutant phenotype IRregular Xylem. At cellular level, xylan biosynthesis and packaging into secretory vesicles occur in the centre of the Golgi cisternae. In *Arabidopsis thaliana irx9* mutant, the Golgi apparatus is modified, with increased cisternal fenestration and tubulation, the xylan product being arranged in successive concentric rings of the Golgi cisternae [280]. Other studies show that loss of function in IRX9, IRX10 and IRX14 results in reduced xylan chain length. Homologs IRX9L, IRX10L and IRX14L can produce a small quantity of defective xylan, therefore decreasing the mutant's phenotype severity. Plants which have reduced xylan synthase activity have a secondary CW weakness sufficient to result in xylem vessel collapse, even without major changes in CW composition [281, 282, 283].

In *Dionaea muscipula* there are 13 IRX paralogues, out of which only one of the IRX9 paralogues seems to be strongly expressed in the WT's ground state (*IRX9*), while it is downregulated (low expression) in the ERR's ground state comapred to WT (Table 10). This might indicate that IRX9 is the most important gene involved in xylan backbone biosynthesis in WT. If so, by showing a downregulated IRX9 activity in the ground state, the ERR mutant might present a CW structure with reduced amounts of xylan or with reduced xylan chain length. Since xyloglucan is the load-bearing component of the plant CWs, this might indicate that a certain xyloglucan composition might be crucial for the whole CW architecture in *Dionaea muscipula*, that would enable the trap to form the tensile strength necessary for fast snapping and buckling (which might be missing in the ERR).

Table 10: *IRX* genes: $\log_2$FC values of DEGp1 = Control_ERR vs Control_WT, DEGp2 = AP_WT vs Control_WT and DEGp3 = AP_ERR vs Control_ERR, followed by FPKM expression values in each condition.

DmID	Gene	DEGp1	DEGp2	DEGp3	Ctrl_WT	AP_WT	Ctrl_ERR	AP_ERR
Dm_00005762-RA	IRX9	-1.60	NA	NA	120.31	131.28	39.63	48.80
Dm_00005329-RA	IRX14-L	NA	NA	NA	28.01	23.78	29.78	30.33
Dm_00002492-RA	IRX9-L	NA	NA	NA	23.57	31.94	19.80	21.90
Dm_00000667-RA	IRX1	NA	-1.03	NA	9.57	4.67	4.92	4.31
Dm_00006196-RA	IRX12	NA	NA	NA	6.21	3.12	5.61	3.30
Dm_00002410-RA	IRX14	NA	NA	NA	4.22	4.54	2.47	3.52
Dm_00012595-RA	IRX9-L	NA	NA	NA	3.98	6.66	6.19	9.65
Dm_00012744-RA	IRX12	NA	NA	NA	3.24	2.68	2.81	2.67
Dm_00000653-RA	IRX9-L	NA	NA	NA	1.44	2.29	1.46	1.68
Dm_00020340-RA	IRX9	NA	NA	NA	1.41	2.35	2.28	4.72
Dm_00001012-RA	IRX3	NA	NA	NA	0.96	1.41	1.02	1.05
Dm_00017894-RA	IRX6	NA	3.47	2.45	0.75	8.41	0.51	2.78
Dm_00002408-RA	IRX15-L	NA	NA	NA	0.26	0.22	0.23	0.73

RGIL6 As part of the "pectin lyase-like superfamily protein", *RGIL6*, a rhamnogalacturonan-I-lyase, showed the highest expression (197.52 FPKM) in unstimulated WT among all the other genes within this family, while being downregulated in the ERR ground state. Transgenic poplar lines expressing *Arabidopsis thaliana AtRGIL6* showed enhanced cell–cell separation suggesting a decreased cell–cell adhesion which might help CW enzymes to access the target microfibrils easier [284]. A similar function was suggested for strawberry FaRGLyase1. Silenced lines showed highly packed parenchymatic cells with less intercellular space and dense CWs [285]. Since *RGIL6* is highly expressed in Control_WT and downregulated upon mechanostimulation, this emphasizes their possible role during ground state in maintaining a loose CW architecture facilitating expansins to act effortlessly. In ERR, however, this is not the case, as the low *EXP*'s expression might indicate a low level of EXPs and a low expression of *RGIL6* might indicate a crammed/compact CW structure.

XTH6 The xyloglucan endotransglucosylase/hydrolase 6 *XTH6* is by far the CW-modifying enzyme encoding gene with the highest expression level in the WT's ground state (3949.82 FPKM) (Table 11). Its role in the trap open-state is indicated by its downregulation after touch-stimulus. Interestingly, it is also strongly downregulated in the ERR mutant's ground state, pointing to a role similar to that of expansins in the snapping mechanism. The XTH proteins have two different catalytic activities: xyloglucan endo-transglucosylase (XET activity) and xyloglucan endo-hydrolase (XEH activity), with two antagonistic effects. While XET activity results in the elongation of xyloglucan (by cleaving and rejoining xyloglucan chains), the XEH activity leads to xyloglucan chain shortening (by rejoining the xyloglucan reducing end to a water molecule). Despite their antagonistic modes of action, they both lead to an increased CW extensibility necessary for root and hypocotyl elongation, vein differentiation, flower opening, petal abscission and fruit softening [286, 287].

Former *Arabidopsis thaliana* microarray studies show that some XTHs (including *XTH6, and others: XTH7, XTH8, XTH15, XTH16 and XTH28*), are slightly downregulated upon touch stimulus, while others are highly induced after the stimulation [288]. Similar, in *Dionaea muscipula*, after mechanostimulation many *XTHs* are strongly upregulated, such as *XTH25* (with the highest upregulation: 2300.55 FPKM) followed by *XTR6* (1646.67 FPKM) and *TCH4* (149.15 FPKM) and other with a lower expression (*XTH26,6,33,15,8*).
The majority of *XTHs* have a very low expression in Control_ERR, pointing again to a different CW architecture which might be less extensible.

Table 11: *XTH* genes: $\log_2$FC values of DEGp1 = Control_ERR vs Control_WT, DEGp2 = AP_WT vs Control_WT and DEGp3 = AP_ERR vs Control_ERR, followed by FPKM expression values in each condition.

DmID	Gene	DEGp1	DEGp2	DEGp3	**Ctrl_WT**	AP_WT	Ctrl_ERR	AP_ERR
Dm_00013957-RA	XTH6	-4.26	-2.17	-1.50	3949.82	875.83	205.95	72.94
Dm_00011868-RA	XTH5	NA	NA	NA	202.28	172.13	245.03	208.63
Dm_00007070-RA	XTH30	NA	NA	NA	131.73	135.06	68.43	76.76
Dm_00004862-RA	XTR6	NA	3.99	2.60	103.93	1646.67	131.72	797.20
Dm_00016904-RA	XTH30	NA	NA	NA	103.88	85.43	76.38	71.80
Dm_00007066-RA	XTH30	NA	NA	NA	81.04	73.80	45.78	51.91
Dm_00008428-RA	XTH28	NA	NA	NA	49.75	52.35	52.88	61.24
Dm_00009369-RA	XTH33	NA	1.32	NA	17.78	44.31	18.93	21.75
Dm_00009037-RA	XTH9	NA	NA	NA	17.36	16.75	27.29	18.87
Dm_00005513-RA	XTH8	NA	1.80	1.04	14.50	50.58	11.82	24.37
Dm_00018539-RA	XTH2	NA	3.22	1.68	9.94	92.91	19.47	62.19
Dm_00000758-RA	XTR6	NA	1.64	NA	8.68	27.14	15.33	13.48
Dm_00001319-RA	XTH25	2.25	10.52	4.65	1.56	2300.55	7.43	187.11
Dm_00010438-RA	XTH2	NA	NA	NA	0.53	0.43	0.11	0.20
Dm_00000624-RA	XTR6	NA	10.19	4.30	0.45	518.59	1.50	29.33
Dm_00005775-RA	XTH26	NA	4.06	NA	0.25	4.23	0.15	0.20
Dm_00010241-RA	XTH32	NA	NA	NA	0.20	0.48	0.06	0.27
Dm_00010949-RA	XTH9	NA	NA	NA	0.12	1.24	0.22	0.78
Dm_00004558-RA	XTH32	NA	NA	NA	0.07	0.07	0.17	0.26
Dm_00006815-RA	XTH1	NA	NA	NA	0.05	0.00	0.02	0.00
Dm_00002549-RA	XTH15	6.70	11.21	3.38	0.02	46.91	2.07	21.50
Dm_00011577-RA	XTH15	NA	NA	NA	0.02	1.50	0.03	0.59
Dm_00016754-RA	XTH10	NA	NA	NA	0.01	0.01	0.00	0.07
Dm_00010437-RA	XTH2	NA	NA	NA	0.00	0.05	0.01	0.09
Dm_00013125-RA	XTH2	NA	NA	NA	0.00	0.00	0.00	0.00
Dm_00013126-RA	XTH7	NA	NA	NA	0.00	0.00	0.00	0.00
Dm_00016993-RA	XTH8	NA	NA	NA	0.00	0.09	0.00	0.00
Dm_00002331-RA	TCH4	NA	2.47	1.73	26.83	149.15	27.56	91.72
Dm_00002317-RA	TCH4	NA	NA	NA	0.08	0.02	0.04	0.22

In the following table, critical DEGs in the ERR mutant ground state that have been discussed so far are summarised together with their known mutant phenotypes from literature (Table 12).

Table 12: Mutant phenotypes selected from literature in other plant species for the CW-related DEGs discussed above. KO = knockout mutant, OE = overexpression line.

Gene	M	Mutant phenotype	Species	Bib
exla2	KO	reduced susceptibility to necrotrphic *B. cinerea*, *A. brassicicola* and more susceptible to *P. syringae* hypersensitivity towards increased salt and cold	arabidopsis	[281, 282] [283]
irx9	KO	IRregular Xylem, reduced xylan chain length, CW weakness sufficient to result in xylem vessel collapse	arabidopsis	[282]
prp	KO	increase in free cellular proline	tomato	[289, 290]
RGIL6	OE	enhanced cell–cell separation	poplar	[284]
RGLyase1	KO	packed cells with less intercellular space and dense CW	strawberry	[285]
XTH9, XTH6	OE	faster fruit ripening (with decreased firmness)	strawberry	[291]

In short, downregulation of all these CW-related genes in ERR's ground state when compared to WT's ground state might indicate a defect in xyloglucan metabolism such as different side-chain decoration of the xyloglucan backbone (see *FUC1, FT1*) or even shorter xylan chain length (see *IRX9*) and low CW elasticity (see *EXTs*) and extensibility (see *XTHs*) with little intercellular space (see *RGIL6*) and possibly thinner and weaker CWs (see *IRX9*).

However, the transcriptomic data can only point to certain directions in which more investigations have to be done. In this case, a thorough analysis of the CW composition, structure, thickness and network would have to be analysed for the ERR mutant, in order to validate these assumptions.

3.2.3.4 Cell Wall Integrity Surveillance System Is Not Activated Upon Touch in the 'ERROR' Mutant

From the convex-shaped open state of the trap to concave-shaped closed trap, one might assume that besides entire trap morphological modifications, major deformations might also occur at CW level. CW integrity (CWI) sensors are responsible for detection of any changes in the mechanical properties of the CW [253]. Besides detection, CWI system sensors activate signal transduction pathways resulting in signalling cascades (that involve ROS, JA, SA, ACC and ABA), leading to downstream adaptation of CW metabolism [292]. We know that in *Dionaea muscipula*, after fast trap closure, further morphological changes are needed for slow stomach formation (state in which the two trap lobes are tightly sealed at the rim, making the teeth from one lobe parallel to the other), which implies further CW-modifications that enable cell expansion.

After mechanostimualtion-induced trap closure, the WT trap expresses many *YUCCA* genes as part of the enriched MapMan bin "auxin.biosynthesis" needed for cell expansion, as well as CWI surveillance system *HERK1, THE1, FER* as part of "RALF-peptide receptor (CrRLKs)" together with receptor CrRLK1L chaperone *LLG* (Figure 50). Remarkably, none of these MapMan bins are enriched in the ERR mutant

after touch stimulation, indicating a reduced activation of the CWI surveillance system in the ERR.

Catharanthus roseus receptor-like kinases (CrRLKs) like Theseus1 (THE1) and Feronia (FER) are key elements in CWI maintenance, hence well characterised. Both THE1 and FER are localised in the plasma membrane, with extracellular malectin domains and cytoplasmic kinase domains.

THE1 THE1 was first identified from a suppressor screen in the short hypocotyl phenotype of the Cellulose Synthase 6–deficient mutant *procuste1-1* (*prc1-1*) [293]. In short, THE1 might negatively regulate cell growth after CW perturbation [294]. *the1-4* as well as *herk1-1* and *fer* show a semi-dwarf phenotype further suggesting their role in cell growth regulation [294].

FER FER works as a signalling hub in a wide range of processes such as male and female fertility, ROS signalling, mechanosensation, growth regulation, hormone signalling and defence [295, 296]. For example, in roots of *fer*, ROS levels were significantly lower than in WT. The authors suggest that FER regulates ROS-mediated root hair growth in a RAC/ROP-signaled NADPH oxidase-dependent fashion [297]. Similarly, in *fer* gametophytes, ROS do not accumulate at the filiform apparatus/synergid cell region of the female gametophyte (as it does in WT), in order to induce pollen tube rupture and sperm release during the fertilisation process in *Arabidopsis thaliana* [298]. Curiously, FER is suggested to be involved in regulating leaf-morphology by influencing lobe formation, due to *fer* leaves showing box-shaped epidermal cells [298]. Furthermore, *fer* roots have limited mechanosensitivity, showing pronounced spatiotemporal fluctuations in root expansion profile assays when compared to WT. In concert with this, upon hypoosmotic stress the touch gene *TCH4* was highly induced in the WT but not in the *fer* loss-of-function mutant [299].

As for hormone signalling and defence, FER seems to be a promising candidate for mediating CWI and pathogen triggered immunity (PTI) [300]. Plant pathogens as well as herbivores, degrade plant CW during their invasion. Chemical signals such as pathogen-associated molecular patterns (PAMPs such as chitin from fungi, flagellin from bacteria and other microbial metabolites) as well as damage-associated molecular patterns (DAMPs, such as cellobiose, xyloglucan, extracellular ATP and endogenous peptides) are released and afterwards perceived by sensors that activate PTI [253, 301]. FER can interact with the central PTI-component BRI1-Associated Kinase1 (BAK1), activating PTI. However, in *Dionaea muscipula*, *BAK1* is not differentially expressed upon touch in neither WT nor ERR (at least at the 1h time point). In *Arabidopsis thaliana* FER also interacts with apoplastic peptide RALF23 which leads to the inhibition of MYC2, a master TF in activating JA-responsive genes and inhibiting SA signalling. In *Dionaea muscipula*, *RALF33* is upregulated upon touch in both WT and ERR (but to a lower extent in ERR).

On the other hand, FER inhibits ABA responses by controlling the activity of ABI2. FER might also influence the apoplastic pH by inhibiting the AHA2 H^+-ATP-ase, in a RALF-dependent manner. A higher pH level also facilitates RALF34-THE1 interaction which inhibits growth. Additionally, THE1 activates general stress responses by inducing JA signalling and lignin deposition under extreme conditions [300]. Also part of the CWI system, LLG1 (together with LRE), can act as both chaperones and co-receptors of FER. LLG1 associates with FLS2 for flg22-induced BIK1 phosphorylation and ROS production [294]. Nevertheless, it seems that in *Dionaea muscipula* the CWI surveillance system *HERK1, THE1, FER, LLG1* becomes activated upon mechanostimulation leading to further hormone-signalling pathways modulation. Therefore, in the untreated ground state, these genes have a low expression level, which makes them harder to detect as downregulated in ERR mutant's ground state when compared to WT. Accordingly, none of them were DEGs in the ground state comparison.

The following table summarises the discussed mutant phenotype of CWI-related DEGs (Table 13).

Table 13: Mutant phenotypes selected from literature in other plant species for the CWI-system DEGs discussed above. KO = knockout mutant, OE = overexpression line.

Gene	M	Mutant phenotype	Species	Bib
the1-4	KO	semi-dwarf phenotype	arabidopsis	[294]
herk1-1	KO	semi-dwarf phenotype	arabidopsis	[294]
fer	KO	semi-dwarf phenotype lower ROS accumulation in roots and female gametophyte leaves with box-shaped epidermal cells roots with limited mechanosensitivity	arabidopsis	[294, 297] [298, 299]

In short, CWI-related *THEs, HERKs and FER* are all involved in growth-related processes, possibly mediating growth-defence trade-offs (*e.g: THE1* is a negative growth regulator activated by CW perturbations while *FER* regulates leaf morphology and might indirectly activate JA pathway, probably through a potential link to the touch-marker gene *TCH4* and ROS signalling).

3.2.3.5 Transcription Factors That Are Essential for Stress Regulation Are Not Expressed in the 'ERROR' Mutant Upon Mechanostimulation

MYB88 Transcription Factor Is Not Expressed in the 'ERROR' Mutant's Transcriptome

Interestingly, the *Arabidopsis thaliana mur3-1* and *mur3-2* phenotype phenotypically resemble a normal WT, and they show detectable amounts of MUR3 protein [302], even thought it lacks the F side-chain (XXFG and XLFG subunits) xyloglucan [303, 304]. However, *mur3-3* (also showing no detectable amount of F-side chain) has a dwarf cabbage-like growth phenotype with short etiolated hypocotyls, endomembrane aggregation, hypersensitive to salt stress but constitutively resistant to *Hyaloperonospora parasitica* oomycete infection [305]. In their study, Xu and

colleagues, selected 11 downregulated DEGs in *mur3-3* compared to *Arabidopsis thaliana* WT and overexpressed them for a complementation test. The *mur3-3* phenotype was partially rescued by the overexpression of: four CW-related genes (*XTH4, XTH30, PME3 and EXPA11*), a TF (*MYB88*), a hormone-related gene (*ROT3*), two protein kinase genes (AT5G37790 and *WAG2*) and an aquaporin gene (*TIP2;3*) [306]. Out of these, *EXPA11* and *ROT3* are also downregulated in the ERR mutant, while *MYB88* is completely missing in all of the ERR conditions (0 FPKM). It would be interesting to see if the ERR mutant phenotype could be rescued by overexpressing *EXPA11* and possibly *MYB88* as well.

MYB88 together with its paralogue FLP(/MYB124) are well known for their role in stomata development, ensuring that stomata have only two guard cells (*flp1-myb88* mutants harbour abnormal clustered stomata) [307]. In *Dionaea muscipula FLP1* has a very low expression value across all tissues (with the highest expression in roots and ERR trap: Control_ERR = 2.7 FPKM). Despite this, the ERR mutant presents normal-looking stomata (personal observation). This pair of paralogues seem to work together in other physiological processes as well: regulation of female reproductive development [308], brassinosteroids biosynthesis [309], regulation of auxin transporters *PIN3* and *PIN7* for gravity sensing and lateral root formation [310], regulation of cold-responsive genes [212] and most interestingly regulate root xylem development in apple tree (*Malus x domestica* Borkh) [311]. In the latter study, the authors showed that MdMYB88 and MdMYB124 directly modulate the expression of MdMYB46 leading to root xylem vessel development in response to drought conditions. Indeed MYB46 together with MYB83 are known master switches for secondary CW biosynthesis [312]. In *Dionaea muscipula*, both show high expression in WT juvenile traps, indicating their involvement in xylem vessel development. This observation goes hand in hand with the other signs that ERR mutant's CW architecture might be different from WT (as explained in previous chapters).

Moreover, *flp1-myb88* mutants show little or no expression of stress-marker genes such as *WRKY40, ERF6, ZAT10, ZAT12* and *DREB2A* after high-salt treatment [313]. In *Dionaea muscipula*, *WRKY40* is highly expressed upon touch in WT and dimly expressed in ERR (Dm_00005880-RA, Control_WT=3.90, AP_WT=1351.51, Control_ERR=7.97, AP_ERR=170.48). As it will be thoroughly explained later, ERFs, ZATs and DREBs have a very low expression or not at all in ERR upon touch while being strongly upregulated in the WT. Since these are important transcription factors that initiate stress responses, their absence or dim expression might explain the overall weak response upon mechanostimulation in the ERR, with half the number of DEGs and half the expression level of existing DEGs compared to WT (Figure 49).

C2H2-ZF and RAV Transcription Factor Families Genes Are Underrepresented in Mechanostimulated 'ERROR' Trap

The MapMan bin enrichment analysis showing underrepresented functional categories in ERR after mechanostimulation, comprises the "C2H2-ZF" TF family containing *ZAT7* (with the highest expression in the WT and lowest in the ERR), *STZ, ZFP4, IDD2, GIS3*.

ZAT7 and STZ/ZAT10 are Cys2His2 (C2H2)-type zinc-finger protein (ZFP) family of TFs (C1-2i subclass) generally involved in development and stress responses. ZAT7 has first been identified due to its responsiveness to oxidative stress. Overexpression lines of ZAT7 showed a decreased growth but increased salt stress tolerance. ZAT10 is also induced by ROS, and besides this, it is responsive to other stresses such as: ABA, salt, drought, cold, osmotic stress treatments [314]. Transgenic plants which constitutively express ZAT10 show enhanced adaptation to these treatments. Inducer of CBF Expression (ICE1), as its name suggests, induces the expression of CBF, which in turn has been shown to induce ZAT10 [314]. In *Dionaea muscipula ICE1* is induced upon touch treatment in WT but not in the ERR traps. Hand in hand with this, CBF1 (Dm_00012261-RA) is highly upregulated in mechanostimulated WT traps while it is not in the ERR. However, other CBF1 (Dm_00013892-RA) paralogue and CBF4 (Dm_00012260-RA) show a very small expression in mechanostimulated ERR. Furthermore, studies show that ZAT10 is activated through phosphorylation by MPK3/6, which is indispensable for osmotic stress response [315]. In *Dionaea muscipula MPK3* is upregulated in both WT and ERR upon mechanostimulation, but to a lower extent in the ERR.

As part of *Dionaea muscipula*'s TF-network upon mechanostimulation that is "missing" (not differentially expressed) in ERR, IDD2 targets the xyloglucan:xyloglucosyl transferase XTH33 with function in CW-modification, SLT1 involved in salt-stress tolerance and GLDH involved in ascorbic acid biosynthesis among others (Figure 51).

Besides this, the "RAV/NGATHA-TF" superfamily MapMan bin was also highly enriched in mechanostimulated WT and not enriched in mechanostimulated ERR, with none of the following three genes being DEGs in the ERR: *TEM1, NGA1, RAV1*. Furthermore, the hypergeometric-distribution analysis shows that this bin has less than expected DEGs (0) compared to WT (3) (Figure 50).

In *Arabidopsis thaliana*, RAV1 is induced upon a multitude of biotic and abiotic factors: spray, wind, touch [316], pathogen attack, wounding, H_20_2, SA, ABA, Me-JA, ET, salt, cold [316] and downregulated by BR (epiBL) [317]. RAV transgenic lines showed enhanced resistance against infection by *Pseudomonas syringae*, salt and dehydration [316]. Besides this, RAV members play major roles in the regulation of flowering time (especially TEM1 and TEM2), light responses, senescence induction and growth inhibition [318]. Indeed, it has been proposed that RAV1 together with other TFs (such as ZAT6/10/12, KAN1, ZF2/3) regulates growth–defence tradeoffs under JA signalling [319].

DREB2C Gene Is at the Centre of the Transcription Factor Network That Is Not Expressed in the Mechanostimulated 'ERROR' Traps

In WT *Dionaea muscipula*, ERF and DREB TF subfamilies seem to play an important role in touch-response initiation, containing the highest number of DEGs with high expression values (Figure 48). The four major subfamilies: AP2 (APetala 2), RAV (Related To Abscisic Acid Insensitive/Viviparous), DREBs (Dehydration-Responsive Element Binding) and ERFs (Ethylene-Responsive Factors) are part of the larger group of APetala2/Ethylene Responsive Factor (AP2/ERFs) family [320]. They are characterised by their APetala2 (AP2)/Ethylene Responsive Element Binding Factor (EREB) domain involved in DNA binding. DREBs are major regulators of cold, drought, heat and salt stress responses while inhibiting growth. And ERF, AP2 and RAV subfamilies are involved in freezing, hypoxia/flooding and salt stress tolerance [218].

The TF-network analysis of *Dionaea muscipula* including genes that are upregulated upon mechnostimulation in WT, but not in ERR, shows that DREB2C has the highest number of target genes, including other TFs such as the ABA repressor (ABR1), the cold response inducer of CBF (ICE1), as well as ethylene-responsive TF (ERF4). Besides this, DREB2C induces the following genes: laccase LAC14 (involved in wound healing and lignification), ovate family protein 1 OFP1 (which regulates cell elongation), polygalacturonase inhibiting protein 1 PGIP1 (which inhibits CW pectin degrading enzymes), SKU5 similar 5 sks5 (with oxidoreductase activity), cytochrome P450 CYP94C1 (which regulates the negative feedback control of JA-Ile), enhanced disease resistance 1 EDR1 (a negative regulator of ethylene-induced senescence), pathogenesis-related protein (PRB1). However, in this analysis TF motifs from PlantTFDB were used. Since not all upregulated DEGs TFs have a known motif, therefore are missing from the database, the TF-network is incomplete. Moreover, special studies must be conducted for *Dionaea muscipula* promoter sequences for discovering new motifs specific for this special carnivorous species.

Even though not present in the network, the Redox Responsive Transcription Factor1 RRTF1 (/ERF109) seems to be an important TF for stress regulation. It has been proposed that in *Arabidopsis thaliana* "*elevated levels of the highly conserved RRTF1 induce ROS accumulation in response to ROS and ROS-producing abiotic and biotic stress signals*" [321]. Moreover, besides H_20_2, WRKY18/40/60 are necessary for RRTF1 upregulation [321], as well as JA [322]. In *Dionaea muscipula*, *WRKY40* seems to be a good candidate for this job since it's highly upregulated upon touch (Dm_00005880-RA, Contro_WT=3.90, AP_WT=1351.51, Control_ERR=7.97, AP_ERR=170.48). In the ERR mutant, after touch stimulation, the expression of RRTF1 is not as high ($log_2FC=1.73$) as in WT ($log_2FC=10.95$) (Dm_00002642-RA, Contro_WT=0.06, AP_WT=116.60, Control_ERR =2.52, AP_ERR=8.38). Therefore, could this unresponsiveness of RRTF in the ERR mutant be linked to the altered redox-activity in the ground state and maybe lack of ROS accumulation after

mechanostimulation?

Although the JA pathway has a major role in plant defence, ET is highly important for fine-tuning these responses [323]. In their review, C. Broekgaarden and colleagues describe the JA-signalling pathway as having two separate branches: the "ERF TF branch" and the "MYC TF branch". While the ET-driven ERF-branch is responsible for defence against necrotrophic pathogen attack, MYC-branch synergises the ABA-signalling resulting in defence against herbivore insect attack [323]. Even though the crucial JA marker JAZ1/TIFY is highly upregulated upon mechanostimulation and MYC2 is also upregulated (but to a very low extent), among all the TF families upregulated in the WT upon touch, the Apetala2/Ethylene Responsive Factor (AP2/ERFs) family seems to be the most outstanding, with a high number of DEGs (44% in WT and 23% in ERR). On that account, could this indicate that carnivorous syndrome has evolved from necrotrophic pathogen defence pathways, rather than wounding or herbivore insect attack pathways? In any case, this observation reminds us of the differences between mechanostimulation and wounding in *Dionaea muscipula*.

3.2.3.6 Jasmonic Acid Signalling Is Dampened in Response to Touch in the 'ERROR' Mutant

Jasmonic acid (JA) together with its derivatives (MeJA, JA-Ile) are a class of fatty acids, collectively known as jasmonates (JAs). Even though they were first identified as stress-related hormones, JAs are also important for growth and developmental processes, nutrient uptake and glucose transport. As signalling molecules, JAs mediate responses against environmental stresses such as mechanical, herbivore, insect attack and pathogen infection by inducing the expression of JA-responsive genes which promote plant defence mechanisms, secondary metabolites synthesis and resistance [156, 222, 324, 325].

Interestingly, the JAs accumulation over time was very different between mechanostimulation and wounding in *Dionaea muscipula* WT. While JA-Ile accumulated slowly, reaching a peak within 1h ($\log_2$FC of 8), JA levels sprung to a $\log_2$FC of 11 only after 15 minutes. Upon wounding, however, the levels were quite low until 3h, when the peak was suddenly reached ($\log_2$FC of 10) for both JA and JA-Ile (Figure 31).

In contrast, A. Pavlovič and colleagues concluded that *Dionaea muscipula* cannot discriminate between wounding and mechanical trigger hair stimulation. They found no difference in JA and JA-Ile upon wounding and mechanostimulaton after 2h [68]. The reason for such an opposite result might be the type of treatment they used. A constant stimulation (trigger hair bending or wounding by piercing the trap with a needle) every 3 min, for 2h continuously, resulted in a total of 40 stimulations. They were looking at the jasmonates accumulation after only one time point: 2h after the initiation of stimulation (and therefore right after termination of stimulation).

Even so, around the 2h time point in our data, we can see similar levels of JA in mechanostimulated as well as wounded traps due to the refractory period that was allowed after stimuli application in our case. We see from Figure 31 how important the refractory period is, in order to understand the differences between the two stimuli.

The ERR mutant responds differently upon the two stimuli as well. While mechanostimulation induces only half of the JA and JA-Ile levels, the response upon wounding seems to be completely absent. Which hints again, to at least two different JA-signalling pathways highly dependent on the type of stimuli.

The reasons for such a low level of jasmonates in the ERR mutant upon touch stimulation, could be many factors such as: lower expression of genes involved in JA biosynthesis (*LOX3*) or JA-Ile biosynthesis (*JAR1*) as well as MeJA biosynthesis (*JMT* is not a DEG in ERR) (Figure 57) which is also an important volatile signalling molecule that spreads easier to other tissues and that has been shown to regulate many TFs, including ZAT10 [326]. This might contribute to the positive feedback loop which results in more JA biosynthesis. Another reason could be the JA inhibition in the first place. For example, WRKY50 which is already upregulated in the ERR ground state has been shown to negatively regulate JA signalling [215].

Two different pathways for JA biosynthesis are not excluded, since there are studies showing OPR3-independent pathway in which dnOPDA enters the β-oxidation pathway to produce 4,5-ddh-JA as a direct precursor of JA [327].

3.2.3.7 Short Summary

The most prominent differences at transcriptomic level between the WT and the ERR mutant in the ground state were: **(i)** an expression pattern of genes involved in CW architecture (which might point to altered hemicellulose and low level of expansins in the ERR mutant traps), **(ii)** a different expression pattern of genes involved in redox system that might suggest an impairment in proper ROS signalling needed for signal amplification and suitable immune response. By comparing the mechanostimulated state of the two phenotypes, we can see a lack of expression of genes encoding for Ca^{2+} decoding and signalling, stress-related TFs and CWI surveillance system.

These differences are depicted in Figure 60, in the context of the hunting cycle, showing their influence on the trap snapping mechanism and further on the molecular pathways that lead to stomach formation.

Based on these findings I propose the following hypothesis:
The ready-to-snap configuration bearing the pre-stress seems to be of high importance for the buckle-mediated snapping of the trap. For the first time, these data suggest that the CW architecture might play a crucial role in conferring the perfect mechanical properties of the trap. In the ready-for-capture state, the WT traps are "armed", with a high turgidity and expanded upper layer of cells, which keeps the trap opening at an optimum angle and confer the convex shape of the trap lobes. This process might be mediated by expansins (*EXPA11*). When trigger hairs are touched by a potential prey, APs are elicited together with Ca^{2+} signals, disturbing the electrochemical gradient. The water exits the upper-layer cells, leading to a lower turgor pressure and therefore shrinkage of the upper cell layer, which corresponds with the trap snapping. This points again to the necessity of a flexible CW of the upper layer, in order to allow the "collapse" to occur. Further AP elicitation and Ca^{2+} waves induced by a struggling prey (which might act together with ROS signalling) would further ring the "stress alarm". However, Ca^{2+} signature needs to be decoded (*CaMs, CaMLs, CDPKs, CBLs/CIPKs*), which is an essential step for further JA biosynthesis and activation of stress-related TFs (*RRTF, DREBs, CBF, ZAT, JAZ*). This will result in the activation of defence mechanisms and finally biosynthesis of hydrolases needed for digestive fluid (*SAG12, SCPL, CHIB*). At the same time, due to the modifications that have occurred in the CW during the transition from convex to concave state and whole trap configuration changes, the CWI-system (*FER, THE1, HERK, LLG1*) also rings the alarm for activation of stomach formation, switching off general plant growth processes and switching on defence mechanisms. Besides this, upregulated TFs further activate auxin biosynthesis (*YUCCA*) and other CW modifying enzymes (*XTHs*) for further cell elongation and expansion of the lower layer, slowly morphing the trap into a green stomach.

Nevertheless, so far, there has been too little research on touch-induced ROS-signalling in carnivorous plants, and no studies (to my knowledge) about the cell wall architecture

and microfibrils orientation as well as composition and structure of different cell types of different layers in *Dionaea muscipula* before and after closure of the trap. The data in this study draws attention for the first time to the importance of the CW for a functional buckling-dependent snap-closure.

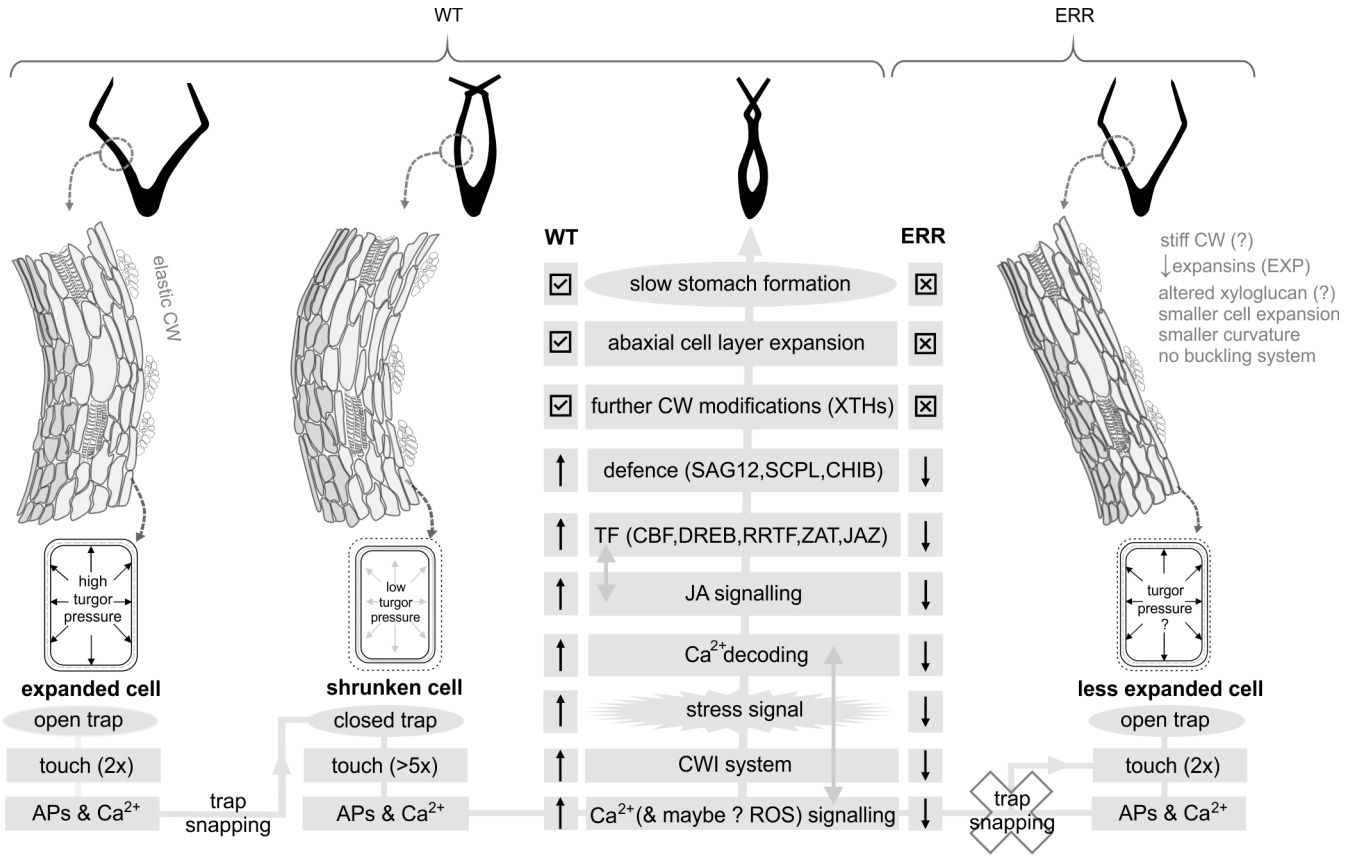

Figure 60: Schematic representation of key steps involved in trap closure and later green stomach formation, in the context of the hunting cycle, emphasizing dampened and missing elements in the ERR mutant. In the open, resting state, the adaxial cell layer of the WT trap presents highly turgid cells that exhibit stress against the CW and contributes to the covex ready-to-snap configuration. The CW stress is released once APs and Ca^{2+} waves are elicited, resulting in turgor drop, cell shrinkage and therefore trap snapping. Redox signalling might be activated, while possible CW alterations might be perceived by the CWI system. In the WT, this stress signal activates JA signalling and stress-induced TFs (CBFs, DREBs, RRTFs, ZATs, JAZ) which in turn might lead to the activation of hydrolases needed for digestive fluid secretion (SAG12, SCPL, CHIB) and other defence mechanisms. Meanwhile, general plant growth is inhibited. However, cell expansion might still occur via auxin-signalling pathway which together with further CW modifications accompanied by XTHs lead to abaxial cell layer expansion and finally green stomach formation. The ERR mutant has a less curved trap morphology, with possibly altered CW architecture (possibly rich in peroxidases and altered xyloglucan composition which might increase stiffness and decrease elasticity needed for buckling). Furthermore, maybe the most crucial, expansins' expression is very low, impairing the CW flexibility, while redox-signalling might be altered and CWI-system might be unresponsive, which affects further downstream elements leading to a dampened JA signalling as well as stress-TFs activation and no further CW modifications needed for green stomach formation.

3.2.4 Conclusion

By its inability to snap and further turn into a green stomach, the *Dionaea muscipula* 'ERROR' mutant traps can help us to elucidate the key milestones necessary for a successful carnivorous lifestyle. By comparing its transcriptome in the resting state as well as after mechanostimulation to that of a functional wild type, the data points to an altered cell wall architecture in the 'ERROR' mutant. This emphasises the necessity of a special cell wall composition equipped with the right cell wall modifying proteins (such as expansins) which confer high flexibility for a functional trap buckling system. Furthermore, the data suggest that some Ca^{2+}-signalling components as well as some redox-related ones might also contribute to the malfunctioning of the 'ERROR' mutant, leading to an improper immune response upon stresses, which is also reflected in the low JA levels post stimulation. We know that plant carnivory has evolved by repurposing old defence molecular pathways to serve for prey perception and digestion [25, 56]. Therefore, this study highlights the importance of a functional immune system suitable for plant carnivory as well as a special cell wall architecture that ensures trap morphing through different digestive stages during its hunting cycle.

3.2.5 Outlook

The work in this thesis only scratches the surface of the vast molecular network mechanisms that arise as a response to mechanostimulation. The transcriptomic data of only one time point is not enough to give us a clear understanding of the molecular processes. On that account, in the best case, a high-resolution time series (including at least 24 hours post-stimulation time point) might give us a better overview of the complexity of gene expression patterns. Especially in the case of external JA application (or COR), a 24 hour time point in both WT and ERR would give us more information about the peak expression upon this treatment and would clarify the similarities and differences upon this treatment in ERR vs WT.

Nevertheless, by analysing the transcriptomic data one hour after the mechanical stimulation, it shows us where to look next. Experiments regarding Ca^{2+}-, pH- and ROS signalling in the ERR mutant would help us verify or reject the proposed hypothesis. For this, transformed plants bearing Ca^{2+} or pH fluorescent sensors in the WT as well as ERR background would give us information regarding the time-scale in which these changes, waves and oscillations might occur in *Dionaea*. ROS assays have never been reported in the Venus flytrap (according to my knowledge, so far), therefore new protocols would have to be established.

The comparison of unstimulated ground state of ERR vs WT, gave us new experimental ideas and it urges us to study the CW of the ERR mutant in comparison to WT. For this, AFM (atomic force microscopy) as well as NMR (nuclear magnetic resonance) analysis of the matrix-cellulose interactions and network would have to be carried out. CW composition as well as CW mechanical properties of both WT and ERR mutant cell types would have to be assessed, such as: creep, extensibility, elastic modulus, isotropy, poroelasticity, stiffness, strain rate or turgor pressure. Immunogold labelling of CW using antibodies against expansins would give us information regarding the position, density and abundance of expansins in ERR compared to WT in different cell types.

Furthermore, regarding the high discrepancy of certain TFs' expression level after mechanostimulation between the WT and ERR, ChIP-seq technique for genome-wide profiling of DNA-binding proteins would be appropriate in order to better understand the "real" TF-network of *Dionaea* upon touch-induced traps.

Last but not least, since we had a look only at transcriptomic level, the next step would be to have a look at the whole genome of the ERR mutant. In this way we would gain information regarding SNPs, indels and possible insertion of retrotransposons into the promoter region of certain genes, that might contribute to the ERR mutant phenotype.

References

[1] Barry E Flanary and Gunther Kletetschka. Analysis of telomere length and telomerase activity in tree species of various life-spans, and with age in the bristlecone pine pinus longaeva. *Biogerontology*, 6(2):101–111, 2005.

[2] George W Koch, Stephen C Sillett, Gregory M Jennings, and Stephen D Davis. The limits to tree height. *Nature*, 428(6985):851–854, 2004.

[3] Aaron M Ellison and Lubomír Adamec. *Carnivorous plants: physiology, ecology, and evolution*. Oxford University Press, 2018.

[4] Tim Bailey and Stewart McPherson. *Dionaea: The Venus's Flytrap*. Redfern Natural History Productions, 2012.

[5] Patrick D Moldowan, M Alex Smith, Teskey Baldwin, Timothy Bartley, Njal Rollinson, and Hannah Wynen. Nature's pitfall trap: salamanders as rich prey for carnivorous plants in a nutrient-poor northern bog ecosystem. *Ecology*, 100(10):e02770, 2019.

[6] Charles Darwin and Francis Darwin. *Insectivorous plants*. J. Murray, 1888.

[7] Francis Ernest Lloyd. *The carnivorous plants*. Read Books Ltd, 2011.

[8] BE Juniper, RJ Robins, and DM Joel. *The carnivorous plants Academic Press*. 1989.

[9] Marianne Peroutka, Wolfram Adlassnig, Michael Volgger, Thomas Lendl, Walter G Url, and Irene K Lichtscheidl. Utricularia: a vegetarian carnivorous plant? *Plant Ecology*, 199(2):153–162, 2008.

[10] Marianne Koller-Peroutka, Thomas Lendl, Margarete Watzka, and Wolfram Adlassnig. Capture of algae promotes growth and propagation in aquatic utricularia. *Annals of Botany*, 115(2):227–236, 2015.

[11] Laurent Legendre. The genus pinguicula l.(lentibulariaceae): an overview. *Acta Botanica Gallica*, 147(1):77–95, 2000.

[12] Matt Candeias. *In Defense of Plants: An Exploration Into the Wonder of Plants*. Mango Media Inc., 2021.

[13] Jonathan A Moran, Charles M Clarke, and Barbara J Hawkins. From carnivore to detritivore? isotopic evidence for leaf litter utilization by the tropical pitcher plant nepenthes ampullaria. *International Journal of Plant Sciences*, 164(4):635–639, 2003.

[14] Daniel Cosgrove Cosgrove et al. Comparative structure and biomechanics of plant primary and secondary cell walls. *Frontiers in plant science*, 3:204, 2012.

[15] Ayufu Yilamujiang, Anting Zhu, Rodrigo Ligabue-Braun, Stefan Bartram, Claus-Peter Witte, Rainer Hedrich, Mitsuyasu Hasabe, Caroline R Schöner, Michael G Schöner, Gerald Kerth, et al. Coprophagous features in carnivorous nepenthes plants: a task for ureases. *Scientific reports*, 7(1):1–9, 2017.

[16] Vincent Bazile, Jonathan A Moran, Gilles Le Moguedec, David J Marshall, and Laurence Gaume. A carnivorous plant fed by its ant symbiont: a unique multi-faceted nutritional mutualism. *PLoS One*, 7(5):e36179, 2012.

[17] Francis J Nge and Hans Lambers. Reassessing protocarnivory–how hungry are triggerplants? *Australian Journal of Botany*, 66(4):325–330, 2018.

[18] DW Darnowski, David M Carroll, B Płachno, E Kabanoff, and E Cinnamon. Evidence of protocarnivory in triggerplants (stylidium spp.; stylidiaceae). *Plant Biology*, 8(06):805–812, 2006.

[19] Douglas W Darnowski, Deborah Carroll, and JM Stielper. Are triggerplants (stylidium; stylidiaceae) carnivorous. In *Proceedings of the 4th International Carnivorous Plant Conference, Tokyo, Japan*, volume 2002, pages 209–213, 2002.

[20] George G Spomer. Evidence of protocarnivorous capabilities in geranium viscosissimum and potentilla arguta and other sticky plants. *International Journal of Plant Sciences*, 160(1):98–101, 1999.

[21] Ashish Malik. Purification and properties of plant chitinases: A review. *Journal of Food Biochemistry*, 43(3):e12762, 2019.

[22] Aaron M Ellison and Nicholas J Gotelli. Energetics and the evolution of carnivorous plants—darwin's 'most wonderful plants in the world'. *Journal of Experimental Botany*, 60(1):19–42, 2009.

[23] Qianshi Lin, Cécile Ané, Thomas J Givnish, and Sean W Graham. A new carnivorous plant lineage (triantha) with a unique sticky-inflorescence trap. *Proceedings of the National Academy of Sciences*, 118(33), 2021.

[24] Simon Poppinga, Siegfried Richard Heinrich Hartmeyer, Robin Seidel, Tom Masselter, Irmgard Hartmeyer, and Thomas Speck. Catapulting tentacles in a sticky carnivorous plant. 2012.

[25] Gergo Palfalvi, Thomas Hackl, Niklas Terhoeven, Tomoko F Shibata, Tomoaki Nishiyama, Markus Ankenbrand, Dirk Becker, Frank Förster, Matthias Freund, Anda Iosip, et al. Genomes of the venus flytrap and close relatives unveil the roots of plant carnivory. *Current Biology*, 30(12):2312–2320, 2020.

[26] Andreas Fleischmann, Jan Schlauer, Stephen A Smith, Thomas J Givnish, AM Ellison, and L Adamec. Evolution of carnivory in angiosperms. *Carnivorous plants: physiology, ecology, and evolution*, pages 22–42, 2018.

[27] John D Degreef. Fossil aldrovanda. *Carnivorous Plant Newsletter*, 26:93–97, 1997.

[28] Zuzana Heřmanová and Jiří Kvaček. Late cretaceous palaeoaldrovanda, not seeds of a carnivorous plant, but eggs of an insect. *Journal of the National Museum (Prague), Natural History Series*, (179), 2010.

[29] Dallas C Mildenhall. New zealand late cretaceous and cenozoic plant biogeography: a contribution. *Palaeogeography, palaeoclimatology, palaeoecology*, 31:197–233, 1980.

[30] Wilfried Krutzsch. Zur kenntnis fossiler disperser tetradenpollen. *Paläontol. Abh. B*, 3(3/4):399–426, 1970.

[31] Eva-Maria Sadowski, Leyla J Seyfullah, Friederike Sadowski, Andreas Fleischmann, Hermann Behling, and Alexander R Schmidt. Carnivorous leaves from baltic amber. *Proceedings of the National Academy of Sciences*, 112(1):190–195, 2015.

[32] Rainer Hedrich and Kenji Fukushima. On the origin of carnivory: Molecular physiology and evolution of plants on an animal diet. *Annual Review of Plant Biology*, 72:133–153, 2021.

[33] Enrique Ibarra-Laclette, Eric Lyons, Gustavo Hernández-Guzmán, Claudia Anahí Pérez-Torres, Lorenzo Carretero-Paulet, Tien-Hao Chang, Tianying Lan, Andreanna J Welch, María Jazmín Abraham Juárez, June Simpson, et al. Architecture and evolution of a minute plant genome. *Nature*, 498(7452):94–98, 2013.

[34] Tianying Lan, Tanya Renner, Enrique Ibarra-Laclette, Kimberly M Farr, Tien-Hao Chang, Sergio Alan Cervantes-Pérez, Chunfang Zheng, David Sankoff, Haibao Tang, Rikky W Purbojati, et al. Long-read sequencing uncovers the adaptive topography of a carnivorous plant genome. *Proceedings of the National Academy of Sciences*, 114(22):E4435–E4441, 2017.

[35] Evgeny V Leushkin, Roman A Sutormin, Elena R Nabieva, Aleksey A Penin, Alexey S Kondrashov, and Maria D Logacheva. The miniature genome of a carnivorous plant genlisea aurea contains a low number of genes and short non-coding sequences. *BMC genomics*, 14(1):1–11, 2013.

[36] Yoshikazu Hoshi, Masako Azumatani, Chika Suyama, and Lubomír Adamec. Determination of ploidy level and nuclear dna content in the droseraceae by flow cytometry. *Cytologia*, 82(3):321–327, 2017.

[37] Kenneth M Cameron, Kenneth J Wurdack, and Richard W Jobson. Molecular evidence for the common origin of snap-traps among carnivorous plants. *American Journal of Botany*, 89(9):1503–1509, 2002.

[38] Tanya Renner and Chelsea D Specht. A sticky situation: assessing adaptations for plant carnivory in the caryophyllales by means of stochastic character mapping. *International Journal of Plant Sciences*, 172(7):889–901, 2011.

[39] Fernando Rivadavia, Katsuhiko Kondo, Masahiro Kato, and Mitsuyasu Hasebe. Phylogeny of the sundews,

drosera (droseraceae), based on chloroplast rbcl and nuclear 18s ribosomal dna sequences. *American Journal of Botany*, 90(1):123–130, 2003.

[40] Thomas C Gibson and Donald M Waller. Evolving darwin's 'most wonderful'plant: ecological steps to a snap-trap. *New Phytologist*, 183(3):575–587, 2009.

[41] JD Degreef. The evolution of aldrovanda and dionaea traps. *Carnivorous Plant Newsletter*, 17:119–125, 1988.

[42] Simon Poppinga, Tim Kampowski, Amélie Metzger, Olga Speck, and Thomas Speck. Comparative kinematical analyses of venus flytrap (dionaea muscipula) snap traps. *Beilstein journal of nanotechnology*, 7(1):664–674, 2016.

[43] David H Benzinq. The origin and rarity of botanical carnivory. *Trends in Ecology & Evolution*, 2(12):364–369, 1987.

[44] Simon Poppinga, Siegfried RH Hartmeyer, Tom Masselter, Irmgard Hartmeyer, and Thomas Speck. Trap diversity and evolution in the family droseraceae. *Plant signaling & behavior*, 8(7):e24685, 2013.

[45] Devendra Kumar Biswal, Sureni Yanthan, Ruchishree Konhar, Manish Debnath, Suman Kumaria, and Pramod Tandon. Phylogeny and biogeography of the carnivorous plant family droseraceae with representative drosera species from northeast india. *F1000Research*, 6(1454):1454, 2017.

[46] Florent Delplace, Carine Huard-Chauveau, Richard Berthomé, and Dominique Roby. Network organization of the plant immune system: from pathogen perception to robust defense induction. *The Plant Journal*, 2021.

[47] Thomas Sebastian Nuhse. Cell wall integrity signaling and innate immunity in plants. *Frontiers in plant science*, 3:280, 2012.

[48] Sarah Johns, Takuma Hagihara, Masatsugu Toyota, and Simon Gilroy. The fast and the furious: rapid long-range signaling in plants, 2021.

[49] Matthew J Marcec, Simon Gilroy, BW Poovaiah, and Kiwamu Tanaka. Mutual interplay of ca2+ and ros signaling in plant immune response. *Plant Science*, 283:343–354, 2019.

[50] Eunyoung Seo and Doil Choi. Functional studies of transcription factors involved in plant defenses in the genomics era. *Briefings in functional genomics*, 14(4):260–267, 2015.

[51] Madiha Zaynab, Mahpara Fatima, Safdar Abbas, Yasir Sharif, Muhammad Umair, Muhammad Hammad Zafar, and Khalida Bahadar. Role of secondary metabolites in plant defense against pathogens. *Microbial pathogenesis*, 124:198–202, 2018.

[52] K Prasannath. Plant defense-related enzymes against pathogens: a review. 2017.

[53] Amrita Pradhan, Srayan Ghosh, Debashis Sahoo, and Gopaljee Jha. Fungal effectors, the double edge sword of phytopathogens. *Current Genetics*, 67(1):27–40, 2021.

[54] Daniel Couto and Cyril Zipfel. Regulation of pattern recognition receptor signalling in plants. *Nature Reviews Immunology*, 16(9):537–552, 2016.

[55] Paulina Paszota, Maria Escalante-Perez, Line R Thomsen, Michael W Risør, Alicja Dembski, Laura Sanglas, Tania A Nielsen, Henrik Karring, Ida B Thøgersen, Rainer Hedrich, et al. Secreted major venus flytrap chitinase enables digestion of arthropod prey. *Biochimica et Biophysica Acta (BBA)-Proteins and Proteomics*, 1844(2):374–383, 2014.

[56] Felix Bemm, Dirk Becker, Christina Larisch, Ines Kreuzer, Maria Escalante-Perez, Waltraud X Schulze, Markus Ankenbrand, Anna-Lena Van de Weyer, Elzbieta Krol, Khaled A Al-Rasheid, et al. Venus flytrap carnivorous lifestyle builds on herbivore defense strategies. *Genome Research*, 26(6):812–825, 2016.

[57] Eric Davies. Electrical signals in plants: facts and hypotheses. In *Plant electrophysiology*, pages 407–422. Springer, 2006.

[58] Pierre Bertholon. *De l'electricite du corps humain dans l'état de santé et de maladie...* chez Didot le jeune,

1786.

[59] John Scott Burdon-Sanderson. I. note on the electrical phenomena which accompany irritation of the leaf of dionæa muscipula. *Proceedings of the Royal Society of London*, 21(139-147):495–496, 1873.

[60] Rainer Stahlberg. Historical overview on plant neurobiology. *Plant Signaling & Behavior*, 1(1):6–8, 2006.

[61] Barbara G Pickard. Action potentials in higher plants. *The Botanical Review*, 39(2):172–201, 1973.

[62] František Baluška, Stefano Mancuso, and Elizabeth Van Volkenburgh. Barbara g. pickard-queen of plant electrophysiology. *Plant Signaling & Behavior*, 16(6):1911400, 2021.

[63] Edward E Farmer, Yong-Qiang Gao, Gioia Lenzoni, Jean-Luc Wolfender, and Qian Wu. Wound-and mechanostimulated electrical signals control hormone responses. *New Phytologist*, 227(4):1037–1050, 2020.

[64] Takao Sibaoka. Rapid plant movements triggered by action potentials. *The botanical magazine= Shokubutsu-gaku-zasshi*, 104(1):73–95, 1991.

[65] Seyed AR Mousavi, Adeline Chauvin, François Pascaud, Stephan Kellenberger, and Edward E Farmer. Glutamate receptor-like genes mediate leaf-to-leaf wound signalling. *Nature*, 500(7463):422–426, 2013.

[66] Peter Marhavỳ, Andrzej Kurenda, Shahid Siddique, Valerie Dénervaud Tendon, Feng Zhou, Julia Holbein, M Shamim Hasan, Florian MW Grundler, Edward E Farmer, and Niko Geldner. Single-cell damage elicits regional, nematode-restricting ethylene responses in roots. *The EMBO journal*, 38(10):e100972, 2019.

[67] Jennifer Böhm, Sönke Scherzer, Elzbieta Krol, Ines Kreuzer, Katharina von Meyer, Christian Lorey, Thomas D Mueller, Lana Shabala, Isabel Monte, Roberto Solano, et al. The venus flytrap dionaea muscipula counts prey-induced action potentials to induce sodium uptake. *Current Biology*, 26(3):286–295, 2016.

[68] Andrej Pavlovič, Jana Jakšová, and Ondřej Novák. Triggering a false alarm: wounding mimics prey capture in the carnivorous venus flytrap (dionaea muscipula). *New Phytologist*, 216(3):927–938, 2017.

[69] Yoko Nakamura, Michael Reichelt, Veronika E Mayer, and Axel Mithöfer. Jasmonates trigger prey-induced formation of 'outer stomach'in carnivorous sundew plants. *Proceedings of the Royal Society B: Biological Sciences*, 280(1759):20130228, 2013.

[70] Miroslav Krausko, Zdeněk Perutka, Marek Šebela, Olga Šamajová, Jozef Šamaj, Ondřej Novák, and Andrej Pavlovič. The role of electrical and jasmonate signalling in the recognition of captured prey in the carnivorous sundew plant drosera capensis. *New Phytologist*, 213(4):1818–1835, 2017.

[71] Axel Mithöfer, Michael Reichelt, and Yoko Nakamura. Wound and insect-induced jasmonate accumulation in carnivorous d rosera capensis: two sides of the same coin. *Plant Biology*, 16(5):982–987, 2014.

[72] Stephen E Williams and Roger M Spanswick. Propagation of the neuroid action potential of the carnivorous plant drosera. *Journal of comparative physiology*, 108(2):211–223, 1976.

[73] Toshio Iijima and Takao Sibaoka. Action potential in the trap-lobes of aldrovanda vesiculosa. *Plant and cell physiology*, 22(8):1595–1601, 1981.

[74] Jana Jakšová, Lubomír Adamec, Ivan Petřík, Ondřej Novák, Marek Šebela, and Andrej Pavlovič. Contrasting effect of prey capture on jasmonate accumulation in two genera of aquatic carnivorous plants (aldrovanda, utricularia). *Plant Physiology and Biochemistry*, 2021.

[75] Ayufu Yilamujiang, Michael Reichelt, and Axel Mithöfer. Slow food: insect prey and chitin induce phytohormone accumulation and gene expression in carnivorous nepenthes plants. *Annals of Botany*, 118(2):369–375, 2016.

[76] Michaela Saganová, Boris Bokor, Tibor Stolárik, and Andrej Pavlovič. Regulation of enzyme activities in carnivorous pitcher plants of the genus nepenthes. *Planta*, 248(2):451–464, 2018.

[77] Elisa Masi, Marzena Ciszak, Ilaria Colzi, Lubomir Adamec, and Stefano Mancuso. Resting electrical network activity in traps of the aquatic carnivorous plants of the genera aldrovanda and utricularia. *Scientific reports*, 6(1):1–11, 2016.

[78] Ondřej Kocáb, Jana Jakšová, Ondřej Novák, Ivan Petřík, René Lenobel, Ivo Chamrád, and Andrej Pavlovič. Jasmonate-independent regulation of digestive enzyme activity in the carnivorous butterwort pinguicula× tina. *Journal of experimental botany*, 71(12):3749–3758, 2020.

[79] Daniel R Gallie and Su-Chih Chang. Signal transduction in the carnivorous plant sarracenia purpurea (regulation of secretory hydrolase expression during development and in response to resources). *Plant Physiology*, 115(4):1461–1471, 1997.

[80] Andrej Pavlovič and Axel Mithöfer. Jasmonate signalling in carnivorous plants: copycat of plant defence mechanisms. *Journal of experimental botany*, 70(13):3379–3389, 2019.

[81] Christopher R Hatcher, David B Ryves, and Jonathan Millett. The function of secondary metabolites in plant carnivory. *Annals of botany*, 125(3):399–411, 2020.

[82] Hiraku Suda, Hiroaki Mano, Masatsugu Toyota, Kenji Fukushima, Tetsuro Mimura, Izuo Tsutsui, Rainer Hedrich, Yosuke Tamada, and Mitsuyasu Hasebe. Calcium dynamics during trap closure visualized in transgenic venus flytrap. *Nature Plants*, 6(10):1219–1224, 2020.

[83] Tim S Bailey. *Miraculum Naturae Venus's Flytrap: The Natural History and Culture of the Most Wonderful Plant in the World; to which is Added the Early Botanical History of the Tipitiwichet Sensitive (1759-1800) with Selected Biographical Memoirs; Bartram, John, Bartram, William. Collinson, Peter. Dobbs, Arthur. Ellis, John. Garden, Dr. Alexander. Gordon, James. Linnaeus, Carl. Solander, Daniel. Young, William*. Trafford Publishing, 2008.

[84] Arthur Dobbs. *A. Dobbs to P. Collinson (Brunswick, 2 April 1759)*. Linnean Society of London, 1759.

[85] E Charles Nelson. *Dionaea D. Solander ex J. Ellis (Droseraceae): notes on the nomenclature and typification of Venus's Fly-trap*, volume 99. Oxford University Press, 1989.

[86] John Ellis. *ELLIS, J., 1768. [Letter about Venus's fly-trap]. Thursday September 1 to Saturday September 3 1768, No. 1172: p.4*. The St James's Chronicle; or The British Evening-Post, 1768.

[87] John Ellis. *J. Ellis to Dr D. Skene (Grays Inn 24 September 1768)*. The Library, University of Aberdeen (AVL MS 38/109), 1768.

[88] John Ellis. *Directions for Bringing Over Seeds and Plants from the East-Indies and Other Distant Countries in a State of Vegetation... to which is Added the Figure and Botanical Description of a New Sensitive Plant, Called Dionaea Muscipula, Or Venus's Fly-trap, by John Ellis...* L. Davis, 1770.

[89] Adam T Cross, Thilo A Krueger, Paulo M Gonella, Alastair S Robinson, and Andreas S Fleischmann. Conservation of carnivorous plants in the age of extinction. *Global Ecology and Conservation*, page e01272, 2020.

[90] Rainer Hedrich and Erwin Neher. Venus flytrap: how an excitable, carnivorous plant works. *Trends in Plant Science*, 23(3):220–234, 2018.

[91] Renate Sachse, Anna Westermeier, Max Mylo, Joey Nadasdi, Manfred Bischoff, Thomas Speck, and Simon Poppinga. Snapping mechanics of the venus flytrap (dionaea muscipula). *Proceedings of the National Academy of Sciences*, 117(27):16035–16042, 2020.

[92] Jürgen Kreuzwieser, Ursel Scheerer, Jörg Kruse, Tim Burzlaff, Anne Honsel, Saleh Alfarraj, Plamen Georgiev, Jörg-Peter Schnitzler, Andrea Ghirardo, Ines Kreuzer, et al. The venus flytrap attracts insects by the release of volatile organic compounds. *Journal of experimental botany*, 65(2):755–766, 2014.

[93] Simon Poppinga and Marc Joyeux. Different mechanics of snap-trapping in the two closely related carnivorous plants dionaea muscipula and aldrovanda vesiculosa. *Physical review E*, 84(4):041928, 2011.

[94] Anna S Westermeier, Renate Sachse, Simon Poppinga, Philipp Vögele, Lubomir Adamec, Thomas Speck, and Manfred Bischoff. How the carnivorous waterwheel plant (aldrovanda vesiculosa) snaps. *Proceedings of the Royal Society B: Biological Sciences*, 285(1878):20180012, 2018.

[95] Ruoting Yang, Scott C Lenaghan, Mingjun Zhang, and Lijin Xia. A mathematical model on the closing and opening mechanism for venus flytrap. *Plant signaling & behavior*, 5(8):968–978, 2010.

[96] Yongfeng Li, Scott C Lenaghan, and Mingjun Zhang. Nonlinear dynamics of the movement of the venus flytrap. *Bulletin of mathematical biology*, 74(10):2446–2473, 2012.

[97] Yoël Forterre, Jan M Skotheim, Jacques Dumais, and Lakshminarayanan Mahadevan. How the venus flytrap snaps. *Nature*, 433(7024):421–425, 2005.

[98] Andreas Jürgens, Ashraf M El-Sayed, and D Max Suckling. Do carnivorous plants use volatiles for attracting prey insects? *Functional Ecology*, 23(5):875–887, 2009.

[99] Elsa Youngsteadt, Rebecca E Irwin, Alison Fowler, Matthew A Bertone, Sara June Giacomini, Michael Kunz, Dale Suiter, and Clyde E Sorenson. Venus flytrap rarely traps its pollinators. *The American Naturalist*, 191(4):539–546, 2018.

[100] Sönke Scherzer, Lana Shabala, Benjamin Hedrich, Jörg Fromm, Hubert Bauer, Eberhard Munz, Peter Jakob, Khaled AS Al-Rascheid, Ines Kreuzer, Dirk Becker, et al. Insect haptoelectrical stimulation of venus flytrap triggers exocytosis in gland cells. *Proceedings of the National Academy of Sciences*, 114(18):4822–4827, 2017.

[101] María Escalante-Pérez, Elzbieta Krol, Annette Stange, Dietmar Geiger, Khaled AS Al-Rasheid, Bettina Hause, Erwin Neher, and Rainer Hedrich. A special pair of phytohormones controls excitability, slow closure, and external stomach formation in the venus flytrap. *Proceedings of the National Academy of Sciences*, 108(37):15492–15497, 2011.

[102] Anda L Iosip, Jennifer Böhm, Sönke Scherzer, Khaled AS Al-Rasheid, Ingo Dreyer, Jörg Schultz, Dirk Becker, Ines Kreuzer, and Rainer Hedrich. The venus flytrap trigger hair–specific potassium channel kdm1 can reestablish the k+ gradient required for hapto-electric signaling. *PLoS Biology*, 18(12):e3000964, 2020.

[103] Mary E Williams and Hugh N Mozingo. The fine structure of the trigger hair in venus's flytrap. *American Journal of Botany*, 58(6):532–539, 1971.

[104] Brigitte Buchen, Dorothea Hensel, and Andreas Sievers. Polarity in mechanoreceptor cells of trigger hairs of dionaea muscipula ellis. *Planta*, 158(5):458–468, 1983.

[105] S Scherzer, W Federle, KAS Al-Rasheid, and R Hedrich. Venus flytrap trigger hairs are micronewton mechano-sensors that can detect small insect prey. *Nature plants*, 5(7):670–675, 2019.

[106] M Casser, D Hodick, B Buchen, and A Sievers. Correlation of excitability and bipolar arrangement of endoplasmic reticulum during the development of sensory cells in trigger hairs of dionaea muscipula ellis. *Eur J Cell Biol*, 36, 1985.

[107] Waltraud X Schulze, Kristian W Sanggaard, Ines Kreuzer, Anders D Knudsen, Felix Bemm, Ida B Thøgersen, Andrea Bräutigam, Line R Thomsen, Simon Schliesky, Thomas F Dyrlund, et al. The protein composition of the digestive fluid from the venus flytrap sheds light on prey digestion mechanisms. *Molecular & Cellular Proteomics*, 11(11):1306–1319, 2012.

[108] Joseph R Di Palma, Robert Mohl, and William Best. Action potential and contraction of dionaea muscipula (venus flytrap). *Science*, 133(3456):878–879, 1961.

[109] Jan T Burri, Eashan Saikia, Nino F Läubli, Hannes Vogler, Falk K Wittel, Markus Rüggeberg, Hans J Herrmann, Ingo Burgert, Bradley J Nelson, and Ueli Grossniklaus. A single touch can provide sufficient mechanical stimulation to trigger venus flytrap closure. *PLoS biology*, 18(7):e3000740, 2020.

[110] Joseph R DiPalma, Robert McMichael, and Maria DiPalma. Touch receptor of venus flytrap, dionaea muscipula. *Science*, 152(3721):539–540, 1966.

[111] Alexander G Volkov, Shawn L Harris II, Chrystelle L Vilfranc, Veronica A Murphy, Joseph D Wooten, Henoc Paulicin, Maia I Volkova, and Vladislav S Markin. Venus flytrap biomechanics: forces in the dionaea muscipula trap. *Journal of plant physiology*, 170(1):25–32, 2013.

[112] Sönke Scherzer, Elzbieta Krol, Ines Kreuzer, Jörg Kruse, Franziska Karl, Martin von Rüden, Maria Escalante-Perez, Thomas Müller, Heinz Rennenberg, Khaled AS Al-Rasheid, et al. The dionaea muscipula ammonium channel dmamt1 provides nh4+ uptake associated with venus flytrap's prey digestion. *Current Biology*, 23(17):1649–1657, 2013.

[113] Sönke Scherzer, Jennifer Böhm, Elzbieta Krol, Lana Shabala, Ines Kreuzer, Christina Larisch, Felix Bemm, Khaled AS Al-Rasheid, Sergey Shabala, Heinz Rennenberg, et al. Calcium sensor kinase activates potassium uptake systems in gland cells of venus flytraps. *Proceedings of the National Academy of Sciences*, 112(23):7309–7314, 2015.

[114] Wolfram Adlassnig, Marianne Koller-Peroutka, Sonja Bauer, Edith Koshkin, Thomas Lendl, and Irene K Lichtscheidl. Endocytotic uptake of nutrients in carnivorous plants. *The Plant Journal*, 71(2):303–313, 2012.

[115] Andrej Pavlovič and Michaela Saganová. A novel insight into the cost–benefit model for the evolution of botanical carnivory. *Annals of botany*, 115(7):1075–1092, 2015.

[116] Tet Fatt Chia, Hnin Hnin Aung, Anatoly N Osipov, Ngoh Khang Goh, and Lian Sai Chia. Carnivorous pitcher plant uses free radicals in the digestion of prey. *Redox Report*, 9(5):255–261, 2004.

[117] Enrique Ibarra-Laclette, Victor A Albert, Claudia A Pérez-Torres, Flor Zamudio-Hernández, María de J Ortega-Estrada, Alfredo Herrera-Estrella, and Luis Herrera-Estrella. Transcriptomics and molecular evolutionary rate analysis of the bladderwort (utricularia), a carnivorous plant with a minimal genome. *BMC Plant Biology*, 11(1):1–16, 2011.

[118] William H Brown. The mechanism of movement and the duration of the effect of stimulation in the leaves of dionaea. *American Journal of Botany*, pages 68–90, 1916.

[119] Casimir de Candolle. *Sur la structure et les mouvements des feuilles du'Dionaea muscipula'*. éditeur non identifié, 1876.

[120] Stephen E Williams and Alan B Bennett. Leaf closure in the venus flytrap: an acid growth response. *Science*, 218(4577):1120–1122, 1982.

[121] Dieter Hodick and Andreas Sievers. On the mechanism of trap closure of venus flytrap (dionaea muscipula ellis). *Planta*, 179(1):32–42, 1989.

[122] Wayne R Fagerberg and Douglas G Howe. A quantitative study of tissue dynamics in venus's flytrap dionaea muscipula (droseraceae). ii. trap reopening. *American journal of botany*, 83(7):836–842, 1996.

[123] Qiaohang Guo, Eric Dai, Xiaomin Han, Stephen Xie, Eric Chao, and Zi Chen. Fast nastic motion of plants and bioinspired structures. *Journal of the Royal Society Interface*, 12(110):20150598, 2015.

[124] Yoël Forterre. Slow, fast and furious: understanding the physics of plant movements. *Journal of experimental botany*, 64(15):4745–4760, 2013.

[125] Mathieu Colombani and Yoel Forterre. Biomechanics of rapid movements in plants: poroelastic measurements at the cell scale. *Computer Methods in Biomechanics and Biomedical Engineering*, 14(sup1):115–117, 2011.

[126] Vladislav S Markin, Alexander G Volkov, and Emil Jovanov. Active movements in plants: mechanism of trap closure by dionaea muscipula ellis. *Plant signaling & behavior*, 3(10):778–783, 2008.

[127] Marc Joyeux. Elastic models of the fast traps of carnivorous dionaea and aldrovanda. *Physical Review E*, 88(3):034701, 2013.

[128] Minoru Ueda, Takashi Tokunaga, Masahiro Okada, Yoko Nakamura, Noboru Takada, Rie Suzuki, and Katsuhiko Kondo. Trap-closing chemical factors of the venus flytrap (dionaea muscipulla ellis). *ChemBioChem*, 11(17):2378–2383, 2010.

[129] Camilla Pandolfi, Elisa Masi, Boris Voigt, Sergio Mugnai, Dieter Volkmann, and Stefano Mancuso. Gravity affects the closure of the traps in dionaea muscipula. *BioMed research international*, 2014, 2014.

[130] Markus Goldermann and Wolfgang Hanke. Ion channel are sensitive to gravity changes. *Microgravity science and technology*, 13(1):35–38, 2001.

[131] Jennifer Böhm and Sönke Scherzer. Signaling and transport processes related to the carnivorous lifestyle of plants living on nutrient-poor soil. *Plant Physiology*, 187(4):2017–2031, 2021.

[132] Jörg Fromm and Silke Lautner. Electrical signals and their physiological significance in plants. *Plant, cell & environment*, 30(3):249–257, 2007.

[133] Carl Procko, Swetha Murthy, William T Keenan, Seyed Ali Reza Mousavi, Tsegaye Dabi, Adam Coombs, Erik Procko, Lisa Baird, Ardem Patapoutian, and Joanne Chory. Stretch-activated ion channels identified in the touch-sensitive structures of carnivorous droseraceae plants. *Elife*, 10:e64250, 2021.

[134] Masatsugu Toyota, Dirk Spencer, Satoe Sawai-Toyota, Wang Jiaqi, Tong Zhang, Abraham J Koo, Gregg A Howe, and Simon Gilroy. Glutamate triggers long-distance, calcium-based plant defense signaling. *Science*, 361(6407):1112–1115, 2018.

[135] Yajun Pan, Xuyang Chai, Qifei Gao, Liming Zhou, Sisi Zhang, Legong Li, and Sheng Luan. Dynamic interactions of plant cngc subunits and calmodulins drive oscillatory ca2+ channel activities. *Developmental cell*, 48(5):710–725, 2019.

[136] Maria Duszyn, Brygida Świeżawska, Adriana Szmidt-Jaworska, and Krzysztof Jaworski. Cyclic nucleotide gated channels (cngcs) in plant signalling—current knowledge and perspectives. *Journal of plant physiology*, 241:153035, 2019.

[137] Yuanjun Zhai, Zhaohong Wen, Yang Han, Wenqing Zhuo, Fang Wang, Chao Xi, Jin Liu, Ping Gao, Heping Zhao, Yingdian Wang, et al. Heterogeneous expression of plasma-membrane-localised ososca1. 4 complements osmotic sensing based on hyperosmolality and salt stress in arabidopsis osca1 mutant. *Cell Calcium*, 91:102261, 2020.

[138] Seyed AR Mousavi, Adrienne E Dubin, Wei-Zheng Zeng, Adam M Coombs, Khai Do, Darian A Ghadiri, William T Keenan, Chennan Ge, Yunde Zhao, and Ardem Patapoutian. Piezo ion channel is required for root mechanotransduction in arabidopsis thaliana. *Proceedings of the National Academy of Sciences*, 118(20), 2021.

[139] Maria Casser. *Cytologische Untersuchungen zur Entwicklung der Sinnesborste von Dionaea muscipula Ellis*. PhD thesis, Rheinischen Friedrich-Wilhelms-Universität Bonn, 1985.

[140] Fastqc - a quality control tool for high throughput sequence data. `https://www.bioinformatics.babraham.ac.uk/projects/fastqc/`.

[141] Philip Ewels, Måns Magnusson, Sverker Lundin, and Max Käller. Multiqc: summarize analysis results for multiple tools and samples in a single report. *Bioinformatics*, 32(19):3047–3048, 2016.

[142] Alexander Dobin, Carrie A Davis, Felix Schlesinger, Jorg Drenkow, Chris Zaleski, Sonali Jha, Philippe Batut, Mark Chaisson, and Thomas R Gingeras. Star: ultrafast universal rna-seq aligner. *Bioinformatics*, 29(1):15–21, 2013.

[143] Simon Anders, Paul Theodor Pyl, and Wolfgang Huber. Htseq—a python framework to work with high-throughput sequencing data. *bioinformatics*, 31(2):166–169, 2015.

[144] Simon Anders and Wolfgang Huber. Differential expression analysis for sequence count data. *Nature Precedings*, pages 1–1, 2010.

[145] Michael I Love, Wolfgang Huber, and Simon Anders. Moderated estimation of fold change and dispersion for rna-seq data with deseq2. *Genome biology*, 15(12):1–21, 2014.

[146] Sebastian Bauer, Steffen Grossmann, Martin Vingron, and Peter N Robinson. Ontologizer 2.0—a multifunctional tool for go term enrichment analysis and data exploration. *Bioinformatics*, 24(14):1650–1651, 2008.

[147] Marc Lohse, Axel Nagel, Thomas Herter, Patrick May, Michael Schroda, Rita Zrenner, Takayuki Tohge, Alisdair R Fernie, Mark Stitt, and Björn Usadel. Mercator: a fast and simple web server for genome scale functional annotation of plant sequence data. Technical report, Wiley Online Library, 2014.

[148] Rainer Schwacke, Gabriel Y Ponce-Soto, Kirsten Krause, Anthony M Bolger, Borjana Arsova, Asis Hallab, Kristina Gruden, Mark Stitt, Marie E Bolger, and Björn Usadel. Mapman4: a refined protein classification and annotation framework applicable to multi-omics data analysis. *Molecular plant*, 12(6):879–892, 2019.

[149] Timothy L Bailey, James Johnson, Charles E Grant, and William S Noble. The meme suite. *Nucleic acids research*, 43(W1):W39–W49, 2015.

[150] Paul Shannon, Andrew Markiel, Owen Ozier, Nitin S Baliga, Jonathan T Wang, Daniel Ramage, Nada Amin, Benno Schwikowski, and Trey Ideker. Cytoscape: a software environment for integrated models of biomolecular interaction networks. *Genome research*, 13(11):2498–2504, 2003.

[151] Annapaula Giulietti, Lut Overbergh, Dirk Valckx, Brigitte Decallonne, Roger Bouillon, and Chantal Mathieu. An overview of real-time quantitative pcr: applications to quantify cytokine gene expression. *Methods*, 25(4):386–401, 2001.

[152] Jonathan Schug, Winfried-Paul Schuller, Claudia Kappen, J Michael Salbaum, Maja Bucan, and Christian J Stoeckert. Promoter features related to tissue specificity as measured by shannon entropy. *Genome biology*, 6(4):1–24, 2005.

[153] Niklas Terhoeven. *Genomics of carnivorous Droseraceae and Transcriptomics of Tobacco pollination as case studies for neofunctionalisation of plant defence mechanisms*. PhD thesis, University of Würzburg, 2019.

[154] Fran Supek, Matko Bošnjak, Nives Škunca, and Tomislav Šmuc. Revigo summarizes and visualizes long lists of gene ontology terms. *PloS one*, 6(7):e21800, 2011.

[155] Matthias Freund. Comparative genomics of carnivorous droseraceae. Master's thesis, University of Würzburg, 2019.

[156] Jingjun Ruan, Yuexia Zhou, Meiliang Zhou, Jun Yan, Muhammad Khurshid, Wenfeng Weng, Jianping Cheng, and Kaixuan Zhang. Jasmonic acid signaling pathway in plants. *International journal of molecular sciences*, 20(10):2479, 2019.

[157] Alfonso Méndez-Bravo, Carlos Calderón-Vázquez, Enrique Ibarra-Laclette, Javier Raya-González, Enrique Ramírez-Chávez, Jorge Molina-Torres, Angel A Guevara-García, José López-Bucio, and Luis Herrera-Estrella. Alkamides activate jasmonic acid biosynthesis and signaling pathways and confer resistance to botrytis cinerea in arabidopsis thaliana. *PloS one*, 6(11):e27251, 2011.

[158] Valentin Marquis, Ekaterina Smirnova, Laure Poirier, Julie Zumsteg, Fabian Schweizer, Philippe Reymond, and Thierry Heitz. Stress-and pathway-specific impacts of impaired jasmonoyl-isoleucine (ja-ile) catabolism on defense signalling and biotic stress resistance. *Plant, cell & environment*, 43(6):1558–1570, 2020.

[159] Marc Legeay, Nadezhda T Doncheva, John H Morris, and Lars Juhl Jensen. Visualize omics data on networks with omics visualizer, a cytoscape app. *F1000Research*, 9, 2020.

[160] Elżbieta Król, H Dziubinska, and K Trebacz. What do plants need action potentials for. *Action Potential: Biophysical and Cellular Context, Initiation, Phases and Propagation. DuBois ML.(ed)*, pages 1–26, 2010.

[161] Rainer Hedrich. Ion channels in plants. *Physiological reviews*, 92(4):1777–1811, 2012.

[162] Eric Hosy, Alain Vavasseur, Karine Mouline, Ingo Dreyer, Frédéric Gaymard, Fabien Porée, Jossia Boucherez, Anne Lebaudy, David Bouchez, Anne-Aliénor Véry, et al. The arabidopsis outward k+ channel gork is involved in regulation of stomatal movements and plant transpiration. *Proceedings of the National Academy of Sciences*, 100(9):5549–5554, 2003.

[163] Rainer Schwacke, Anja Schneider, Eric van der Graaff, Karsten Fischer, Elisabetta Catoni, Marcelo Desimone, Wolf B Frommer, Ulf-Ingo Flugge, and Reinhard Kunze. Aramemnon, a novel database for arabidopsis integral membrane proteins. *Plant physiology*, 131(1):16–26, 2003.

[164] Stéphane Pien, Joanna Wyrzykowska, Simon McQueen-Mason, Cheryl Smart, and Andrew Fleming. Local expression of expansin induces the entire process of leaf development and modifies leaf shape. *Proceedings of the National Academy of Sciences*, 98(20):11812–11817, 2001.

[165] Yong Liu, Dongcheng Liu, Haiying Zhang, Hongbo Gao, Xiaoli Guo, Daowen Wang, Xiangqi Zhang, and Aimin Zhang. The α-and β-expansin and xyloglucan endotransglucosylase/hydrolase gene families of wheat: Molecular cloning, gene expression, and est data mining. *Genomics*, 90(4):516–529, 2007.

[166] Swetha E Murthy, Adrienne E Dubin, Tess Whitwam, Sebastian Jojoa-Cruz, Stuart M Cahalan, Seyed Ali Reza Mousavi, Andrew B Ward, and Ardem Patapoutian. Osca/tmem63 are an evolutionarily conserved family of mechanically activated ion channels. *Elife*, 7:e41844, 2018.

[167] Tracey Ann Cuin, Ingo Dreyer, and Erwan Michard. The role of potassium channels in arabidopsis thaliana long distance electrical signalling: Akt2 modulates tissue excitability while gork shapes action potentials. *International Journal of Molecular Sciences*, 19(4):926, 2018.

[168] E Krol, H Dziubinska, M Stolarz, and K Trebacz. Effects of ion channel inhibitors on cold-and electrically-induced action potentials in dionaea muscipula. *Biologia Plantarum*, 50(3):411–416, 2006.

[169] Mary Jane Beilby. Action potential in charophytes. *International review of cytology*, 257:43–82, 2007.

[170] LJ Mullins. Efflux of chloride ions during the action potential of nitella. *Nature*, 196(4858):986–987, 1962.

[171] Rainer Hedrich and Dirk Becker. Green circuits—the potential of plant specific ion channels. *Signals and Signal Transduction Pathways in Plants*, pages 401–414, 1994.

[172] Joseph I Kourie. Transient cl-and k+ currents during the action potential in chara inflata (effects of external sorbitol, cations, and ion channel blockers). *Plant physiology*, 106(2):651–660, 1994.

[173] Kenji Oda. Recording of the potassium efflux during a single action potential in chara corallina. *Plant and Cell Physiology*, 16(3):525–528, 1975.

[174] Antonella Reyer, Melanie Häßler, Sönke Scherzer, Shouguang Huang, Jesper Torbøl Pedersen, Khaled AS Al-Rascheid, Ernst Bamberg, Michael Palmgren, Ingo Dreyer, Georg Nagel, et al. Channelrhodopsin-mediated optogenetics highlights a central role of depolarization-dependent plant proton pumps. *Proceedings of the National Academy of Sciences*, 117(34):20920–20925, 2020.

[175] Tetsuro Mimura and Teruo Shimmen. Characterization of the ca2+-dependent cl- efflux in perfused chara cells. *Plant and cell physiology*, 35(5):793–800, 1994.

[176] Vladimir Sukhov and Vladimir Vodeneev. A mathematical model of action potential in cells of vascular plants. *Journal of Membrane Biology*, 232(1):59–67, 2009.

[177] VA Vodeneev, VA Opritov, and SS Pyatygin. Reversible changes of extracellular ph during action potential generation in a higher plant cucurbita pepo. *Russian Journal of Plant Physiology*, 53(4):481–487, 2006.

[178] Omar Pantoja. Recent advances in the physiology of ion channels in plants. *Annual Review of Plant Biology*, 72, 2021.

[179] Carlos Gonzalez, Eduardo Rosenman, Francisco Bezanilla, Osvaldo Alvarez, and Ramon Latorre. Modulation of the shaker k+ channel gating kinetics by the s3–s4 linker. *The Journal of general physiology*, 115(2):193–208, 2000.

[180] Vadim Demidchik, Sergey Shabala, Stanislav Isayenkov, Tracey A Cuin, and Igor Pottosin. Calcium transport across plant membranes: mechanisms and functions. *New Phytologist*, 220(1):49–69, 2018.

[181] Ya-Yun Wang, Yu-Hsuan Cheng, Kuo-En Chen, and Yi-Fang Tsay. Nitrate transport, signaling, and use efficiency. *Annual Review of Plant Biology*, 69:85–122, 2018.

[182] Hussam Hassan Nour-Eldin, Tonni Grube Andersen, Meike Burow, Svend Roesen Madsen, Morten Egevang Jørgensen, Carl Erik Olsen, Ingo Dreyer, Rainer Hedrich, Dietmar Geiger, and Barbara Ann Halkier. Nrt/ptr transporters are essential for translocation of glucosinolate defence compounds to seeds. *Nature*, 488(7412):531–534, 2012.

[183] Yasuhiro Ishimaru, Takaya Oikawa, Takeshi Suzuki, Syohei Takeishi, Hideyuki Matsuura, Kosaku Takahashi, Shin Hamamoto, Nobuyuki Uozumi, Takafumi Shimizu, Mitsunori Seo, et al. Gtr1 is a jasmonic acid and jasmonoyl-l-isoleucine transporter in arabidopsis thaliana. *Bioscience, biotechnology, and biochemistry*, 81(2):249–255, 2017.

[184] Morten Egevang Jørgensen, Deyang Xu, Christoph Crocoll, Heidi Asschenfeldt Ernst, David Ramírez, Mohammed Saddik Motawia, Carl Erik Olsen, Osman Mirza, Hussam Hassan Nour-Eldin, and Barbara Ann

Halkier. Origin and evolution of transporter substrate specificity within the npf family. *Elife*, 6:e19466, 2017.

[185] Hannah R Malcolm and Joshua A Maurer. The mechanosensitive channel of small conductance (mscs) superfamily: not just mechanosensitive channels anymore. *Chembiochem*, 13(14):2037–2043, 2012.

[186] Eric S Hamilton, Angela M Schlegel, and Elizabeth S Haswell. United in diversity: mechanosensitive ion channels in plants. *Annual review of plant biology*, 66:113–137, 2015.

[187] Bradley Akitake, Andriy Anishkin, and Sergei Sukharev. The "dashpot" mechanism of stretch-dependent gating in mscs. *The Journal of general physiology*, 125(2):143–154, 2005.

[188] Ivan Radin, Ryan A Richardson, Joshua H Coomey, Ethan R Weiner, Carlisle S Bascom, Ting Li, Magdalena Bezanilla, and Elizabeth S Haswell. Plant piezo homologs modulate vacuole morphology during tip growth. *Science*, 373(6554):586–590, 2021.

[189] Stacey S Willard and Shahriar Koochekpour. Glutamate, glutamate receptors, and downstream signaling pathways. *International journal of biological sciences*, 9(9):948, 2013.

[190] Stephen F Traynelis, Lonnie P Wollmuth, Chris J McBain, Frank S Menniti, Katie M Vance, Kevin K Ogden, Kasper B Hansen, Hongjie Yuan, Scott J Myers, and Ray Dingledine. Glutamate receptor ion channels: structure, regulation, and function. *Pharmacological reviews*, 62(3):405–496, 2010.

[191] Michael M Wudick, Erwan Michard, Custódio Oliveira Nunes, and José A Feijó. Comparing plant and animal glutamate receptors: common traits but different fates? *Journal of Experimental Botany*, 69(17):4151–4163, 2018.

[192] Rainer Hedrich, Vicenta Salvador-Recatalà, and Ingo Dreyer. Electrical wiring and long-distance plant communication. *Trends in Plant Science*, 21(5):376–387, 2016.

[193] Alexander Gallé, Silke Lautner, Jaume Flexas, and Jörg Fromm. Environmental stimuli and physiological responses: the current view on electrical signalling. *Environmental and Experimental Botany*, 114:15–21, 2015.

[194] Xue-Mei Qiu, Yu-Ying Sun, Xin-Yu Ye, and Zhong-Guang Li. Signaling role of glutamate in plants. *Frontiers in plant science*, 10:1743, 2020.

[195] Walquíria Fernanda Teixeira, Luís Henrique Soares, Evandro Binotto Fagan, Simone da Costa Mello, Klaus Reichardt, and Durval Dourado-Neto. Amino acids as stress reducers in soybean plant growth under different water-deficit conditions. *Journal of Plant Growth Regulation*, 39(2):905–919, 2020.

[196] Sönke Scherzer, Shouguang Huang, Anda Iosip, Ines Kreuzer, Ken Yokawa, Khaled AS AL-Rasheid, Manfred Heckmann, and Rainer Hedrich. Ether anesthetics prevents touch-induced trigger hair calcium-electrical signals excite the venus flytrap. *Scientific Reports*, 12(1):1–10, 2022.

[197] Jacob Moe-Lange, Nicoline M Gappel, Mackenzie Machado, Michael M Wudick, Cosima SA Sies, Stephan N Schott-Verdugo, Michele Bonus, Swastik Mishra, Thomas Hartwig, Margaret Bezrutczyk, et al. Interdependence of a mechanosensitive anion channel and glutamate receptors in distal wound signaling. *Science advances*, 7(37):eabg4298, 2021.

[198] JM Kefauver, AB Ward, and A Patapoutian. Discoveries in structure and physiology of mechanically activated ion channels. *Nature*, 587(7835):567–576, 2020.

[199] Fang Yuan, Huimin Yang, Yan Xue, Dongdong Kong, Rui Ye, Chijun Li, Jingyuan Zhang, Lynn Theprungsirikul, Tayler Shrift, Bryan Krichilsky, et al. Osca1 mediates osmotic-stress-evoked ca 2+ increases vital for osmosensing in arabidopsis. *Nature*, 514(7522):367–371, 2014.

[200] Frédéric Gaymard, Guillaume Pilot, Benoît Lacombe, David Bouchez, Dominique Bruneau, Jossia Boucherez, Nicole Michaux-Ferriere, Jean-Baptiste Thibaud, and Hervé Sentenac. Identification and disruption of a plant shaker-like outward channel involved in k+ release into the xylem sap. *Cell*, 94(5):647–655, 1998.

[201] Miguel Arango, Frédéric Gévaudant, Mohammed Oufattole, and Marc Boutry. The plasma membrane

proton pump atpase: the significance of gene subfamilies. *Planta*, 216(3):355–365, 2003.

[202] Michael G Palmgren. Plant plasma membrane h+-atpases: powerhouses for nutrient uptake. *Annual review of plant biology*, 52(1):817–845, 2001.

[203] Archana Kumari, Aurore Chételat, Chi Tam Nguyen, and Edward E Farmer. Arabidopsis h+-atpase aha1 controls slow wave potential duration and wound-response jasmonate pathway activation. *Proceedings of the National Academy of Sciences*, 116(40):20226–20231, 2019.

[204] John R Clay and Michael F Shlesinger. Analysis of the effects of cesium ions on potassium channel currents in biological membranes. *Journal of theoretical biology*, 107(2):189–201, 1984.

[205] Audrey M Ichida, Zhen-Ming Pei, Victor M Baizabal-Aguirre, Kelly J Turner, and Julian I Schroeder. Expression of a cs+-resistant guard cell k+ channel confers cs+-resistant, light-induced stomatal opening in transgenic arabidopsis. *The Plant Cell*, 9(10):1843–1857, 1997.

[206] Richard J Morris and Mark Blyth. How water flow, geometry, and material properties drive plant movements. *Journal of experimental botany*, 70(14):3549–3560, 2019.

[207] Janet Braam and Ronald W Davis. Rain-, wind-, and touch-induced expression of calmodulin and calmodulin-related genes in arabidopsis. *Cell*, 60(3):357–364, 1990.

[208] Anda-Larisa Iosip. Understanding the molecular mechanosensing mechanisms of the carnivorous plant *Dionaea muscipula* by *TCH* genes expression analysis. Master's thesis, Babeș-Bolyai University, Faculty of Biology and Geology, M. Sc. Molecular Biotechnology, Cluj-Napoca, Romania, 2016.

[209] Abraham JK Koo and Gregg A Howe. The wound hormone jasmonate. *Phytochemistry*, 70(13-14):1571–1580, 2009.

[210] M Aydın Akbudak, Ertugrul Filiz, Recep Vatansever, and Kubra Kontbay. Genome-wide identification and expression profiling of ascorbate peroxidase (apx) and glutathione peroxidase (gpx) genes under drought stress in sorghum (sorghum bicolor l.). *Journal of Plant Growth Regulation*, 37(3):925–936, 2018.

[211] Junyi Zhao, Tagnon D Missihoun, and Dorothea Bartels. The role of arabidopsis aldehyde dehydrogenase genes in response to high temperature and stress combinations. *Journal of experimental botany*, 68(15):4295–4308, 2017.

[212] Yinpeng Xie, Pengxiang Chen, Yan Yan, Chana Bao, Xuewei Li, Liping Wang, Xiaoxia Shen, Haiyan Li, Xiaofang Liu, Chundong Niu, et al. An atypical r2r3 myb transcription factor increases cold hardiness by cbf-dependent and cbf-independent pathways in apple. *New Phytologist*, 218(1):201–218, 2018.

[213] BA Pandian, R Sathishraj, M Djanaguiraman, PVV Prasad, and M Jugulam. Role of cytochrome p450 enzymes in plant stress response. antioxidants, 9 (5), 454, 2020.

[214] Ujjal J Phukan, Gajendra S Jeena, and Rakesh K Shukla. Wrky transcription factors: molecular regulation and stress responses in plants. *Frontiers in plant science*, 7:760, 2016.

[215] Qing-Ming Gao, Srivathsa Venugopal, Duroy Navarre, and Aardra Kachroo. Low oleic acid-derived repression of jasmonic acid-inducible defense responses requires the wrky50 and wrky51 proteins. *Plant physiology*, 155(1):464–476, 2011.

[216] S Anil Kumar, P Hima Kumari, G Shravan Kumar, C Mohanalatha, and PB Kavi Kishor. Osmotin: a plant sentinel and a possible agonist of mammalian adiponectin. *Frontiers in plant science*, 6:163, 2015.

[217] Peter Geigenberger, Ina Thormählen, Danilo M Daloso, and Alisdair R Fernie. The unprecedented versatility of the plant thioredoxin system. *Trends in plant science*, 22(3):249–262, 2017.

[218] Zhouli Xie, Trevor M Nolan, Hao Jiang, and Yanhai Yin. Ap2/erf transcription factor regulatory networks in hormone and abiotic stress responses in arabidopsis. *Frontiers in plant science*, 10:228, 2019.

[219] Jinrong Wan, Kiwamu Tanaka, Xue-Cheng Zhang, Geon Hui Son, Laurent Brechenmacher, Tran Hong Nha Nguyen, and Gary Stacey. Lyk4, a lysin motif receptor-like kinase, is important for chitin signaling and plant innate immunity in arabidopsis. *Plant physiology*, 160(1):396–406, 2012.

[220] Jian Lv, Jingyan Liu, Yuhang Ming, Yiting Shi, Chunpeng Song, Zhizhong Gong, Shuhua Yang, and Yanglin Ding. Reciprocal regulation between the negative regulator pp2cg1 phosphatase and the positive regulator ost1 kinase confers cold response in arabidopsis. *Journal of Integrative Plant Biology*, 2021.

[221] Yasuaki Kagaya and Tsukaho Hattori. Arabidopsis transcription factors, rav1 and rav2, are regulated by touch-related stimuli in a dose-dependent and biphasic manner. *Genes & genetic systems*, 84(1):95–99, 2009.

[222] Ting Li, Kun-Peng Jia, Hong-Li Lian, Xu Yang, Ling Li, and Hong-Quan Yang. Jasmonic acid enhancement of anthocyanin accumulation is dependent on phytochrome a signaling pathway under far-red light in arabidopsis. *Biochemical and biophysical research communications*, 454(1):78–83, 2014.

[223] Paulina Arraño-Salinas, José Domínguez-Figueroa, Ariel Herrera-Vásquez, Diego Zavala, Joaquin Medina, Jesús Vicente-Carbajosa, Claudio Meneses, Paulo Canessa, Adrián A Moreno, and Francisca Blanco-Herrera. Wrky7,-11 and-17 transcription factors are modulators of the bzip28 branch of the unfolded protein response during pamp-triggered immunity in arabidopsis thaliana. *Plant Science*, 277:242–250, 2018.

[224] Peng Huang, Hideki Yoshida, Kenji Yano, Shunsuke Kinoshita, Kyosuke Kawai, Eriko Koketsu, Masako Hattori, Sayaka Takehara, Ji Huang, Ko Hirano, et al. Osidd2, a zinc finger and indeterminate domain protein, regulates secondary cell wall formation. *Journal of integrative plant biology*, 60(2):130–143, 2018.

[225] Xiaowei Zhang, Jiali Wu, Qin Yu, Ruiyan Liu, Zhi-Yong Wang, and Yu Sun. Atofps regulate cell elongation by modulating microtubule orientation via direct interaction with tonneau2. *Plant Science*, 292:110405, 2020.

[226] Marek Dynowski, Gabriel Schaaf, Dominique Loque, Oscar Moran, and Uwe Ludewig. Plant plasma membrane water channels conduct the signalling molecule h2o2. *Biochemical Journal*, 414(1):53–61, 2008.

[227] Simon Gilroy, Nobuhiro Suzuki, Gad Miller, Won-Gyu Choi, Masatsugu Toyota, Amith R Devireddy, and Ron Mittler. A tidal wave of signals: calcium and ros at the forefront of rapid systemic signaling. *Trends in plant science*, 19(10):623–630, 2014.

[228] Guepil Jang, Jae Sung Shim, Choonkyun Jung, Jong Tae Song, Han Yong Lee, Pil Joong Chung, Ju-Kon Kim, and Yang Do Choi. Volatile methyl jasmonate is a transmissible form of jasmonate and its biosynthesis is involved in systemic jasmonate response in wounding. *Plant biotechnology reports*, 8(6):409–419, 2014.

[229] Richard Hickman, Marcel C Van Verk, Anja JH Van Dijken, Marciel Pereira Mendes, Irene A Vroegop-Vos, Lotte Caarls, Merel Steenbergen, Ivo Van der Nagel, Gert Jan Wesselink, Aleksey Jironkin, et al. Architecture and dynamics of the jasmonic acid gene regulatory network. *The Plant Cell*, 29(9):2086–2105, 2017.

[230] Won-Gyu Choi, Gad Miller, Ian Wallace, Jeffrey Harper, Ron Mittler, and Simon Gilroy. Orchestrating rapid long-distance signaling in plants with ca2+, ros and electrical signals, 2017.

[231] Corné MJ Pieterse, Dieuwertje Van der Does, Christos Zamioudis, Antonio Leon-Reyes, and Saskia CM Van Wees. Hormonal modulation of plant immunity. *Annual review of cell and developmental biology*, 28:489–521, 2012.

[232] Steven H Spoel and Xinnian Dong. Making sense of hormone crosstalk during plant immune responses. *Cell host & microbe*, 3(6):348–351, 2008.

[233] Chi Tam Nguyen, Andrzej Kurenda, Stéphanie Stolz, Aurore Chételat, and Edward E Farmer. Identification of cell populations necessary for leaf-to-leaf electrical signaling in a wounded plant. *Proceedings of the National Academy of Sciences*, 115(40):10178–10183, 2018.

[234] Esther Dolze, Fatima Chigri, Timo Höwing, Georg Hierl, Erika Isono, Ute C Vothknecht, and Christine Gietl. Calmodulin-like protein atcml3 mediates dimerization of peroxisomal processing protease atdeg15 and contributes to normal peroxisome metabolism. *Plant molecular biology*, 83(6):607–624, 2013.

[235] Katharina Bürstenbinder, Dipannita Mitra, and Jakob Quegwer. Functions of iqd proteins as hubs in cellular

calcium and auxin signaling: a toolbox for shape formation and tissue-specification in plants? *Plant signaling & behavior*, 12(6):1692–1708, 2017.

[236] Katharina Bürstenbinder, Birgit Möller, Romina Plötner, Gina Stamm, Gerd Hause, Dipannita Mitra, and Steffen Abel. The iqd family of calmodulin-binding proteins links calcium signaling to microtubules, membrane subdomains, and the nucleus. *Plant physiology*, 173(3):1692–1708, 2017.

[237] Jyothilakshmi Vadassery, Michael Reichelt, Bettina Hause, Jonathan Gershenzon, Wilhelm Boland, and Axel Mithöfer. Cml42-mediated calcium signaling coordinates responses to spodoptera herbivory and abiotic stresses in arabidopsis. *Plant physiology*, 159(3):1159–1175, 2012.

[238] Stephanie Dobney, David Chiasson, Polly Lam, Steven P Smith, and Wayne A Snedden. The calmodulin-related calcium sensor cml42 plays a role in trichome branching. *Journal of Biological Chemistry*, 284(46):31647–31657, 2009.

[239] Tianxiao Lv, Xiaoming Li, Tian Fan, Huiting Luo, Chuping Xie, Yuping Zhou, and Chang-en Tian. The calmodulin-binding protein iqm1 interacts with catalase2 to affect pathogen defense. *Plant physiology*, 181(3):1314–1327, 2019.

[240] Yu-Ping Zhou, Jun Duan, Takahiro Fujibe, Kotaro T Yamamoto, and Chang-En Tian. Atiqm1, a novel calmodulin-binding protein, is involved in stomatal movement in arabidopsis. *Plant molecular biology*, 79(4-5):333–346, 2012.

[241] Marc Libault, Jinrong Wan, Tomasz Czechowski, Michael Udvardi, and Gary Stacey. Identification of 118 arabidopsis transcription factor and 30 ubiquitin-ligase genes responding to chitin, a plant-defense elicitor. *Molecular plant-microbe interactions*, 20(8):900–911, 2007.

[242] Ron Mittler, Sandy Vanderauwera, Nobuhiro Suzuki, GAD Miller, Vanesa B Tognetti, Klaas Vandepoele, Marty Gollery, Vladimir Shulaev, and Frank Van Breusegem. Ros signaling: the new wave? *Trends in plant science*, 16(6):300–309, 2011.

[243] Tedrick Thomas Salim Lew, Volodymyr B Koman, Kevin S Silmore, Jun Sung Seo, Pavlo Gordiichuk, Seon-Yeong Kwak, Minkyung Park, Mervin Chun-Yi Ang, Duc Thinh Khong, Michael A Lee, et al. Real-time detection of wound-induced h 2 o 2 signalling waves in plants with optical nanosensors. *Nature plants*, 6(4):404–415, 2020.

[244] Gad Miller, Karen Schlauch, Rachel Tam, Diego Cortes, Miguel A Torres, Vladimir Shulaev, Jeffery L Dangl, and Ron Mittler. The plant nadph oxidase rbohd mediates rapid systemic signaling in response to diverse stimuli. *Science signaling*, 2(84):ra45–ra45, 2009.

[245] Sarvajeet Singh Gill and Narendra Tuteja. Reactive oxygen species and antioxidant machinery in abiotic stress tolerance in crop plants. *Plant physiology and biochemistry*, 48(12):909–930, 2010.

[246] Graham Noctor, Jean-Philippe Reichheld, and Christine H Foyer. Ros-related redox regulation and signaling in plants. In *Seminars in Cell & Developmental Biology*, volume 80, pages 3–12. Elsevier, 2018.

[247] Cui-Jun Zhang, Bing-Chun Zhao, Wei-Na Ge, Ya-Fang Zhang, Yun Song, Da-Ye Sun, and Yi Guo. An apoplastic h-type thioredoxin is involved in the stress response through regulation of the apoplastic reactive oxygen species in rice. *Plant Physiology*, 157(4):1884–1899, 2011.

[248] Capilla Mata-Pérez and Steven H Spoel. Thioredoxin-mediated redox signalling in plant immunity. *Plant science*, 279:27–33, 2019.

[249] Marc G Fortin, Nigel A Morrison, and Desh Pal S Verma. Nodulin-26, a peribacteroid membrane nodulin is expressed independently of the development of the peribacteroid compartment. *Nucleic acids research*, 15(2):813–824, 1987.

[250] Yuqi Wang, Ruihong Li, Demou Li, Xiaomin Jia, Dangwei Zhou, Jianyong Li, Sangbom M Lyi, Siyu Hou, Yulan Huang, Leon V Kochian, et al. Nip1; 2 is a plasma membrane-localized transporter mediating aluminum uptake, translocation, and tolerance in arabidopsis. *Proceedings of the National Academy of Sciences*, 114(19):5047–5052, 2017.

[251] Wenzhong Xu, Wentao Dai, Huili Yan, Sheng Li, Hongling Shen, Yanshan Chen, Hua Xu, Yangyang Sun,

Zhenyan He, and Mi Ma. Arabidopsis nip3; 1 plays an important role in arsenic uptake and root-to-shoot translocation under arsenite stress conditions. *Molecular plant*, 8(5):722–733, 2015.

[252] Krisztina Bela, Riyazuddin Riyazuddin, Edit Horváth, Ágnes Hurton, Ágnes Gallé, Zoltán Takács, Laura Zsigmond, László Szabados, Irma Tari, and Jolán Csiszár. Comprehensive analysis of antioxidant mechanisms in arabidopsis glutathione peroxidase-like mutants under salt-and osmotic stress reveals organ-specific significance of the atgpxl's activities. *Environmental and Experimental Botany*, 150:127–140, 2018.

[253] Lazar Novaković, Tingting Guo, Antony Bacic, Arun Sampathkumar, and Kim L Johnson. Hitting the wall—sensing and signaling pathways involved in plant cell wall remodeling in response to abiotic stress. *Plants*, 7(4):89, 2018.

[254] Filippo Passardi, Claude Penel, and Christophe Dunand. Performing the paradoxical: how plant peroxidases modify the cell wall. *Trends in plant science*, 9(11):534–540, 2004.

[255] Raimund Tenhaken. Cell wall remodeling under abiotic stress. *Frontiers in plant science*, 5:771, 2015.

[256] Stephen C Fry. Oxidative scission of plant cell wall polysaccharides by ascorbate-induced hydroxyl radicals. *Biochemical Journal*, 332(2):507–515, 1998.

[257] Peter Schopfer. Hydroxyl radical-induced cell-wall loosening in vitro and in vivo: implications for the control of elongation growth. *The Plant Journal*, 28(6):679–688, 2001.

[258] Kim L Johnson, Michael J Gidley, Antony Bacic, and Monika S Doblin. Cell wall biomechanics: a tractable challenge in manipulating plant cell walls 'fit for purpose'! *Current opinion in biotechnology*, 49:163–171, 2018.

[259] Monika S Doblin, Filomena Pettolino, and Antony Bacic. Plant cell walls: the skeleton of the plant world. *Functional Plant Biology*, 37(5):357–381, 2010.

[260] Kathrin Thor. Calcium—nutrient and messenger. *Frontiers in Plant Science*, 10:440, 2019.

[261] Carlisle S Bascom Jr, Peter K Hepler, and Magdalena Bezanilla. Interplay between ions, the cytoskeleton, and cell wall properties during tip growth. *Plant physiology*, 176(1):28–40, 2018.

[262] Aaron Baxter, Ron Mittler, and Nobuhiro Suzuki. Ros as key players in plant stress signalling. *Journal of experimental botany*, 65(5):1229–1240, 2014.

[263] Filippo Passardi, Claudia Cosio, Claude Penel, and Christophe Dunand. Peroxidases have more functions than a swiss army knife. *Plant cell reports*, 24(5):255–265, 2005.

[264] Byung-Wook Yun, Angela Feechan, Minghui Yin, Noor BB Saidi, Thierry Le Bihan, Manda Yu, John W Moore, Jeong-Gu Kang, Eunjung Kwon, Steven H Spoel, et al. S-nitrosylation of nadph oxidase regulates cell death in plant immunity. *Nature*, 478(7368):264–268, 2011.

[265] Daniel J Cosgrove. Plant expansins: diversity and interactions with plant cell walls. *Current opinion in plant biology*, 25:162–172, 2015.

[266] Prince Marowa, Anming Ding, and Yingzhen Kong. Expansins: roles in plant growth and potential applications in crop improvement. *Plant cell reports*, 35(5):949–965, 2016.

[267] Otto Stuhlman. A physical analysis of the opening and closing movements of the lobes of venus' fly-trap. *Bulletin of the Torrey Botanical Club*, pages 22–44, 1948.

[268] Bruria S Hill and Geoffrey P Findlay. The power of movement in plants: the role of osmotic machines. *Quarterly reviews of biophysics*, 14(2):173–222, 1981.

[269] Narendra K Singh, Charles A Bracker, Paul M Hasegawa, Avtar K Handa, Scott Buckel, Mark A Hermodson, ED Pfankoch, Fred E Regnier, and Ray A Bressan. Characterization of osmotin: a thaumatin-like protein associated with osmotic adaptation in plant cells. *Plant physiology*, 85(2):529–536, 1987.

[270] Eun-Joo Park and Tae-Houn Kim. Arabidopsis osmotin 34 functions in the aba signaling pathway and is regulated by proteolysis. *International journal of molecular sciences*, 22(15):7915, 2021.

[271] László Szabados and Arnould Savouré. Proline: a multifunctional amino acid. *Trends in plant science*, 15(2):89–97, 2010.

[272] Polavarapu B Kavi Kishor, P Hima Kumari, MSL Sunita, and Nese Sreenivasulu. Role of proline in cell wall synthesis and plant development and its implications in plant ontogeny. *Frontiers in Plant Science*, 6:544, 2015.

[273] Maria J Soto, Pradeep Kumar Prabhakar, Hsin-Tzu Wang, Jason Backe, Digantkumar Chapla, Max Bartetzko, Ian M Black, Parastoo Azadi, Maria J Peña, Fabian Pfrengle, et al. Atfut4 and atfut6 are arabinofuranose-specific fucosyltransferases. *Frontiers in plant science*, 12:132, 2021.

[274] Markus Pauly and Kenneth Keegstra. Biosynthesis of the plant cell wall matrix polysaccharide xyloglucan. *Annual review of plant biology*, 67:235–259, 2016.

[275] Joana Cardoso, Luís Fonseca, and Isabel Abrantes. α-l-fucosidases from bursaphelenchus xylophilus secretome—molecular characterization and their possible role in breaking down plant cell walls. *Forests*, 11(3):265, 2020.

[276] Samuel Levy, William S York, Rainer Stuike-Prill, Bernd Meyer, and L Andrew Staehelin. Simulations of the static and dynamic molecular conformations of xyloglucan. the role of the fucosylated sidechain in surface-specific sidechain folding. *The Plant Journal*, 1(2):195–215, 1991.

[277] Markus Günl, Lutz Neumetzler, Florian Kraemer, Amancio de Souza, Alex Schultink, Maria Pena, William S York, and Markus Pauly. Axy8 encodes an α-fucosidase, underscoring the importance of apoplastic metabolism on the fine structure of arabidopsis cell wall polysaccharides. *The Plant Cell*, 23(11):4025–4040, 2011.

[278] William S York, Alan G Darvill, and Peter Albersheim. Inhibition of 2, 4-dichlorophenoxyacetic acid-stimulated elongation of pea stem segments by a xyloglucan oligosaccharide. *Plant Physiology*, 75(2):295–297, 1984.

[279] Renaud Léonard, Martin Pabst, Jayakumar Singh Bondili, Gérard Chambat, Christiane Veit, Richard Strasser, and Friedrich Altmann. Identification of an arabidopsis gene encoding a gh95 alpha1, 2-fucosidase active on xyloglucan oligo-and polysaccharides. *Phytochemistry*, 69(10):1983–1988, 2008.

[280] Miranda J Meents, Sanya Motani, Shawn D Mansfield, and A Lacey Samuels. Organization of xylan production in the golgi during secondary cell wall biosynthesis. *Plant physiology*, 181(2):527–546, 2019.

[281] Nuno Faria-Blanc, Jenny C Mortimer, and Paul Dupree. A transcriptomic analysis of xylan mutants does not support the existence of a secondary cell wall integrity system in arabidopsis. *Frontiers in plant science*, 9:384, 2018.

[282] Maria J Peña, Ruiqin Zhong, Gong-Ke Zhou, Elizabeth A Richardson, Malcolm A O'Neill, Alan G Darvill, William S York, and Zheng-Hua Ye. Arabidopsis irregular xylem8 and irregular xylem9: implications for the complexity of glucuronoxylan biosynthesis. *The Plant Cell*, 19(2):549–563, 2007.

[283] Ai-Min Wu, Christophe Rihouey, Martial Seveno, Emma Hörnblad, Sunil Kumar Singh, Toshiro Matsunaga, Tadashi Ishii, Patrice Lerouge, and Alan Marchant. The arabidopsis irx10 and irx10-like glycosyltransferases are critical for glucuronoxylan biosynthesis during secondary cell wall formation. *The Plant Journal*, 57(4):718–731, 2009.

[284] Haibing Yang, Matheus R Benatti, Rucha A Karve, Arizona Fox, Richard Meilan, Nicholas C Carpita, and Maureen C McCann. Rhamnogalacturonan-i is a determinant of cell–cell adhesion in poplar wood. *Plant biotechnology journal*, 18(4):1027–1040, 2020.

[285] Francisco J Molina-Hidalgo, Antonio R Franco, Carmen Villatoro, Laura Medina-Puche, José A Mercado, Miguel A Hidalgo, Amparo Monfort, José Luis Caballero, Juan Muñoz-Blanco, and Rosario Blanco-Portales. The strawberry (fragaria× ananassa) fruit-specific rhamnogalacturonate lyase 1 (farglyase1) gene encodes an enzyme involved in the degradation of cell-wall middle lamellae. *Journal of Experimental Botany*, 64(6):1471–1483, 2013.

[286] Meng Wang, Zongchang Xu, Anming Ding, and Yingzhen Kong. Genome-wide identification and expression

profiling analysis of the xyloglucan endotransglucosylase/hydrolase gene family in tobacco (nicotiana tabacum l.). *Genes*, 9(6):273, 2018.

[287] Jocelyn KC Rose, Janet Braam, Stephen C Fry, and Kazuhiko Nishitani. The xth family of enzymes involved in xyloglucan endotransglucosylation and endohydrolysis: current perspectives and a new unifying nomenclature. *Plant and cell physiology*, 43(12):1421–1435, 2002.

[288] Dennis Lee, Diana H Polisensky, and Janet Braam. Genome-wide identification of touch-and darkness-regulated arabidopsis genes: a focus on calmodulin-like and xth genes. *New Phytologist*, 165(2):429–444, 2005.

[289] Ranjit Singh Gujjar, Suhas G Karkute, Ashutosh Rai, Major Singh, and Bijendra Singh. Proline-rich proteins may regulate free cellular proline levels during drought stress in tomato. 2018.

[290] Banashree Saikia, Sanjay Singh, Johni Debbarma, Natarajan Velmurugan, Hariprasanna Dekaboruah, Kallare P Arunkumar, and Channakeshavaiah Chikkaputtaiah. Multigene crispr/cas9 genome editing of hybrid proline rich proteins (hyprps) for sustainable multi-stress tolerance in crops: the review of a promising approach. *Physiology and Molecular Biology of Plants*, 26(5):857–869, 2020.

[291] Lucia D Witasari, Fong-Chin Huang, Thomas Hoffmann, Wilfried Rozhon, Stephen C Fry, and Wilfried Schwab. Higher expression of the strawberry xyloglucan endotransglucosylase/hydrolase genes fv xth 9 and fv xth 6 accelerates fruit ripening. *The Plant Journal*, 100(6):1237–1253, 2019.

[292] Thorsten Hamann. The plant cell wall integrity maintenance mechanism—concepts for organization and mode of action. *Plant and Cell Physiology*, 56(2):215–223, 2015.

[293] Kian Hématy, Pierre-Etienne Sado, Ageeth Van Tuinen, Soizic Rochange, Thierry Desnos, Sandrine Balzergue, Sandra Pelletier, Jean-Pierre Renou, and Herman Höfte. A receptor-like kinase mediates the response of arabidopsis cells to the inhibition of cellulose synthesis. *Current Biology*, 17(11):922–931, 2007.

[294] Christina Maria Franck, Jens Westermann, and Aurélien Boisson-Dernier. Plant malectin-like receptor kinases: from cell wall integrity to immunity and beyond. *Annual Review of Plant Biology*, 69:301–328, 2018.

[295] Chao Li, H-M Wu, and Alice Y Cheung. Feronia and her pals: functions and mechanisms. *Plant physiology*, 171(4):2379–2392, 2016.

[296] Yue Rui and José R Dinneny. A wall with integrity: surveillance and maintenance of the plant cell wall under stress. *New Phytologist*, 225(4):1428–1439, 2020.

[297] Qiaohong Duan, Daniel Kita, Chao Li, Alice Y Cheung, and Hen-Ming Wu. Feronia receptor-like kinase regulates rho gtpase signaling of root hair development. *Proceedings of the National Academy of Sciences*, 107(41):17821–17826, 2010.

[298] Qiaohong Duan, Daniel Kita, Eric A Johnson, Mini Aggarwal, Laura Gates, Hen-Ming Wu, and Alice Y Cheung. Reactive oxygen species mediate pollen tube rupture to release sperm for fertilization in arabidopsis. *Nature communications*, 5(1):1–10, 2014.

[299] Han-Wei Shih, Nathan D Miller, Cheng Dai, Edgar P Spalding, and Gabriele B Monshausen. The receptor-like kinase feronia is required for mechanical signal transduction in arabidopsis seedlings. *Current Biology*, 24(16):1887–1892, 2014.

[300] Lauri Vaahtera, Julia Schulz, and Thorsten Hamann. Cell wall integrity maintenance during plant development and interaction with the environment. *Nature plants*, 5(9):924–932, 2019.

[301] Laura Bacete, Hugo Mélida, Eva Miedes, and Antonio Molina. Plant cell wall-mediated immunity: cell wall changes trigger disease resistance responses. *The Plant Journal*, 93(4):614–636, 2018.

[302] Kentaro Tamura, Tomoo Shimada, Maki Kondo, Mikio Nishimura, and Ikuko Hara-Nishimura. Katamari1/murus3 is a novel golgi membrane protein that is required for endomembrane organization in arabidopsis. *The Plant Cell*, 17(6):1764–1776, 2005.

[303] María J Peña, Peter Ryden, Michael Madson, Andrew C Smith, and Nicholas C Carpita. The galactose residues of xyloglucan are essential to maintain mechanical strength of the primary cell walls in arabidopsis during growth. *Plant physiology*, 134(1):443–451, 2004.

[304] Michael Madson, Christophe Dunand, Xuemei Li, Rajeev Verma, Gary F Vanzin, Jeffrey Caplan, Douglas A Shoue, Nicholas C Carpita, and Wolf-Dieter Reiter. The mur3 gene of arabidopsis encodes a xyloglucan galactosyltransferase that is evolutionarily related to animal exostosins. *The Plant Cell*, 15(7):1662–1670, 2003.

[305] Yingzhen Kong, Maria J Peña, Luciana Renna, Utku Avci, Sivakumar Pattathil, Sami T Tuomivaara, Xuemei Li, Wolf-Dieter Reiter, Federica Brandizzi, Michael G Hahn, et al. Galactose-depleted xyloglucan is dysfunctional and leads to dwarfism in arabidopsis. *Plant physiology*, 167(4):1296–1306, 2015.

[306] Zongchang Xu, Meng Wang, Dachuan Shi, Gongke Zhou, Tiantian Niu, Michael G Hahn, Malcolm A O'Neill, and Yingzhen Kong. Dge-seq analysis of mur3-related arabidopsis mutants provides insight into how dysfunctional xyloglucan affects cell elongation. *Plant Science*, 258:156–169, 2017.

[307] Lien B Lai, Jeanette A Nadeau, Jessica Lucas, Eun-Kyoung Lee, Tsuyoshi Nakagawa, Liming Zhao, Matt Geisler, and Fred D Sack. The arabidopsis r2r3 myb proteins four lips and myb88 restrict divisions late in the stomatal cell lineage. *The Plant Cell*, 17(10):2754–2767, 2005.

[308] Srilakshmi Makkena, Eunkyoung Lee, Fred D Sack, and Rebecca S Lamb. The r2r3 myb transcription factors four lips and myb88 regulate female reproductive development. *Journal of experimental botany*, 63(15):5545–5558, 2012.

[309] Xiaofang Liu, Caide Zhao, Yuqi Gao, Yao Xu, Shujin Wang, Chaoshuo Li, Yinpeng Xie, Pengxiang Chen, Peizhi Yang, Li Yuan, et al. A multifaceted module of bri1 ethylmethane sulfonate supressor1 (bes1)-myb88 in growth and stress tolerance of apple. *Plant Physiology*, 185(4):1903–1923, 2021.

[310] Hong-Zhe Wang, Ke-Zhen Yang, Jun-Jie Zou, Ling-Ling Zhu, Zi Dian Xie, Miyo Terao Morita, Masao Tasaka, Jiří Friml, Erich Grotewold, Tom Beeckman, et al. Transcriptional regulation of pin genes by four lips and myb88 during arabidopsis root gravitropism. *Nature Communications*, 6(1):1–9, 2015.

[311] Dali Geng, Pengxiang Chen, Xiaoxia Shen, Yi Zhang, Xuewei Li, Lijuan Jiang, Yinpeng Xie, Chundong Niu, Jing Zhang, Xiaohua Huang, et al. Mdmyb88 and mdmyb124 enhance drought tolerance by modulating root vessels and cell walls in apple. *Plant physiology*, 178(3):1296–1309, 2018.

[312] J-H Ko, H-W Jeon, W-C Kim, J-Y Kim, and K-H Han. The myb46/myb83-mediated transcriptional regulatory programme is a gatekeeper of secondary wall biosynthesis. *Annals of botany*, 114(6):1099–1107, 2014.

[313] Zidian Xie, Dongmei Li, Lijun Wang, Fred D Sack, and Erich Grotewold. Role of the stomatal development regulators flp/myb88 in abiotic stress responses. *The Plant Journal*, 64(5):731–739, 2010.

[314] Minmin Xie, Jinhao Sun, Daping Gong, and Yingzhen Kong. The roles of arabidopsis c1-2i subclass of c2h2-type zinc-finger transcription factors. *Genes*, 10(9):653, 2019.

[315] Xuan Canh Nguyen, Sun Ho Kim, Kyunghee Lee, Kyung Eun Kim, Xiao-Min Liu, Hay Ju Han, My Hanh Thi Hoang, Shin-Woo Lee, Jong Chan Hong, Yong-Hwan Moon, et al. Identification of a c 2 h 2-type zinc finger transcription factor (zat10) from arabidopsis as a substrate of map kinase. *Plant cell reports*, 31(4):737–745, 2012.

[316] Kee Hoon Sohn, Sung Chul Lee, Ho Won Jung, Jeum Kyu Hong, and Byung Kook Hwang. Expression and functional roles of the pepper pathogen-induced transcription factor rav1 in bacterial disease resistance, and drought and salt stress tolerance. *Plant molecular biology*, 61(6):897–915, 2006.

[317] Yu Xin Hu, Yong Hong Wang, Xin Fang Liu, and Jia Yang Li. Arabidopsis rav1 is down-regulated by brassinosteroid and may act as a negative regulator during plant development. *Cell research*, 14(1):8–15, 2004.

[318] Luis Matías-Hernández, Andrea E Aguilar-Jaramillo, Esther Marín-González, Paula Suárez-López, and Soraya Pelaz. Rav genes: regulation of floral induction and beyond. *Annals of botany*, 114(7):1459–1470, 2014.

[319] Nailou Zhang, Bin Zhao, Zhijin Fan, Dongyan Yang, Xiaofeng Guo, Qifan Wu, Bin Yu, Shuang Zhou, and Haiying Wang. Systematic identification of genes associated with plant growth–defense tradeoffs under ja signaling in arabidopsis. *Planta*, 251(2):1–14, 2020.

[320] Yoh Sakuma, Qiang Liu, Joseph G Dubouzet, Hiroshi Abe, Kazuo Shinozaki, and Kazuko Yamaguchi-Shinozaki. Dna-binding specificity of the erf/ap2 domain of arabidopsis drebs, transcription factors involved in dehydration-and cold-inducible gene expression. *Biochemical and biophysical research communications*, 290(3):998–1009, 2002.

[321] Mitsuhiro Matsuo, Joy Michal Johnson, Ayaka Hieno, Mutsutomo Tokizawa, Mika Nomoto, Yasuomi Tada, Rinesh Godfrey, Junichi Obokata, Irena Sherameti, Yoshiharu Y Yamamoto, et al. High redox responsive transcription factor1 levels result in accumulation of reactive oxygen species in arabidopsis thaliana shoots and roots. *Molecular Plant*, 8(8):1253–1273, 2015.

[322] Wenkun Zhou, Jose L Lozano-Torres, Ikram Blilou, Xiaoyue Zhang, Qingzhe Zhai, Geert Smant, Chuanyou Li, and Ben Scheres. A jasmonate signaling network activates root stem cells and promotes regeneration. *Cell*, 177(4):942–956, 2019.

[323] Colette Broekgaarden, Lotte Caarls, Irene A Vos, Corné MJ Pieterse, and Saskia CM Van Wees. Ethylene: traffic controller on hormonal crossroads to defense. *Plant physiology*, 169(4):2371–2379, 2015.

[324] Aarti Gupta, Hiroshi Hisano, Yuko Hojo, Takakazu Matsuura, Yoko Ikeda, Izumi C Mori, and Muthappa Senthil-Kumar. Global profiling of phytohormone dynamics during combined drought and pathogen stress in arabidopsis thaliana reveals aba and ja as major regulators. *Scientific reports*, 7(1):1–13, 2017.

[325] Marcelo L Campos, Jin-Ho Kang, and Gregg A Howe. Jasmonate-triggered plant immunity. *Journal of chemical ecology*, 40(7):657–675, 2014.

[326] Kuo Yang, Jian-Ping An, Chong-Yang Li, Xue-Na Shen, Ya-Jing Liu, Da-Ru Wang, Xing-Long Ji, Yu-Jin Hao, and Chun-Xiang You. The apple c2h2-type zinc finger transcription factor mdzat10 positively regulates ja-induced leaf senescence by interacting with mdbt2. *Horticulture research*, 8(1):1–14, 2021.

[327] Andrea Chini, Isabel Monte, Angel M Zamarreno, Mats Hamberg, Steve Lassueur, Philippe Reymond, Sally Weiss, Annick Stintzi, Andreas Schaller, Andrea Porzel, et al. An opr3-independent pathway uses 4, 5-didehydrojasmonate for jasmonate synthesis. *Nature chemical biology*, 14(2):171–178, 2018.

Appendix

Table 14: All the primer pairs used for qPCR experiments. Dir = primer direction (fw = forward, rev = reverse), Temp = Primer annealing temperature, Size = PCR product size.

Gene Name	Dir	Sequence (5' to 3')	Temp [°C]	Size [bp]
DmACT	fw	TCT TTG ATT GGG ATG GAA GC	50-60	137
	rev	GCA ATG CCA GGG AAC ATA GT		
DmSCPL49	fw	AGG TCC ATA GGT ATT CA	53-57	400
	rev	ACT TAA TCC GGG TAT CA		
DmCHIB/VfChitinase I	fw	CTT TAC CAC ACT CAA CG	50-57	295
	rev	GAA AGT TAT TAC GGT CG		
DmSAG12	fw	CAA CAT TCC TTT GCA TC	53-62	386
	rev	CGC ATT CGA GTA TAT GA		
DmTCH2	fw	AGGATAAGAATGGACTG	48-60	275
	rev	CTGTTGCTTCCTTCAAT		
DmTCH4	fw	CAGAGGAATTACATGGT	55-60	185
	rev	ATTCGCTATGCTATAAATC		
DmJAZ1	fw	GTG TTC AAC GAC TTC C	50-60	307
	rev	TTG TTA AGG TGT ATG GC		
DmCOI1	fw	TTA CGT CGG ACT GTA T	48-62	449
	rev	AAC TCT AAG CTA AGA CAT		
DmRRTF1	fw	AGTCAGAGGAATTCTAACC	51 - 59	252
	rev	CTTCTTCTTCTTCTTGTTTG		
DmCBF1	fw	TGCTGATTCTGCATCAATTA	51 - 59	201
	rev	GTACTCTGTTTCGTCTGTG		
DmOSCA1.7	fw	TGGACGCCATTGACTACTAT	50-60	163
	rev	GATTGCTGAGTTTGAGCACA		
DmGLR3.6	fw	CCTCTTTCAAGACGTTTATC	60	198
	rev	AATTCTTAAGCATGGTAGTT		
DmGTR2/NRT1	fw	GGGAGTGATCAAGGAAAT	50-60	158
	rev	ACATATCCTTTACAAGAACG		
DmSKOR/GORK	fw	GAC TTA AAT CAG CTA AGG	55	237
	rev	CTG CTG TGT AGA TCC ATA		
DmAHA4	fw	TAAGAAGAGCTTCTCAGGA	47-62	211
	rev	TGGTCGGCAATGGTTAATA		
KDM1	fw	GAT ACG CAC CCT GAT CCA AAG	53 - 59	246
	rev	CCC ATG AAC GAC AAG ATT CGT C		

Table 15: FastQC of the trigger hair in comparison to other tissues of the RNA-seq experiment (Exp_TH). Data for flower, glands, petiole, rim, root and trap tissues was published under the Project ID PRJNA203407 [56] and the trigger hair tissue data was published under the Project ID PRJEB38423 [102]. Dups = duplications, GC = GC content, Length = read length, M Seq = million sequences/reads.

SRA ID	Sample Name	% Dups	% GC	Length	M Seqs
SRR2807648	R01_Flower_Control_WT_P1	46.7	46	92 bp	68.2
SRR2807648	R01_Flower_Control_WT_P2	44	46	91 bp	68.2
SRR2807650	R02_Flower_Control_WT_P1	52.4	46	94 bp	81.8
SRR2807650	R02_Flower_Control_WT_P2	48.5	46	93 bp	81.8
SRR2807649	R03_Flower_Control_WT_P1	49.1	46	94 bp	69.2
SRR2807649	R03_Flower_Control_WT_P2	46.1	46	92 bp	69.2
SRR2807635	R01_Glands_Control_WT_P1	50.1	46	92 bp	50
SRR2807635	R01_Glands_Control_WT_P2	46.8	46	90 bp	50
SRR2807636	R02_Glands_Control_WT_P1	50.4	46	94 bp	39.1
SRR2807636	R02_Glands_Control_WT_P2	46.3	46	92 bp	39.1
SRR2807637	R03_Glands_Control_WT_P1	51.6	46	93 bp	56.4
SRR2807637	R03_Glands_Control_WT_P2	48.7	46	92 bp	56.4
SRR2807633	R01_Petiole_Control_WT_P1	45.2	46	94 bp	41.3
SRR2807633	R01_Petiole_Control_WT_P2	48.2	46	95 bp	41.3
SRR2807634	R02_Petiole_Control_WT_P1	44.1	46	94 bp	37.4
SRR2807634	R02_Petiole_Control_WT_P2	46.4	46	94 bp	37.4
SRR2807644	R03_Petiole_Control_WT_P1	55	46	94 bp	92.9
SRR2807644	R03_Petiole_Control_WT_P2	57.6	46	95 bp	92.9
SRR2807654	R01_Rim_Control_WT_P1	46.2	46	93 bp	49.2
SRR2807654	R01_Rim_Control_WT_P2	44	46	92 bp	49.2
SRR2807655	R02_Rim_Control_WT_P1	54.2	46	95 bp	69.4
SRR2807655	R02_Rim_Control_WT_P2	55.4	46	95 bp	69.4
SRR2807656	R03_Rim_Control_WT_P1	51.8	46	93 bp	78.2
SRR2807656	R03_Rim_Control_WT_P2	48.3	46	91 bp	78.2
SRR2807642	R01_Root_Control_WT_P1	51.2	47	91 bp	48.2
SRR2807642	R01_Root_Control_WT_P2	48.1	46	90 bp	48.2
SRR2807641	R02_Root_Control_WT_P1	49.9	46	93 bp	35.8
SRR2807641	R02_Root_Control_WT_P2	46.4	46	92 bp	35.8
SRR2807643	R03_Root_Control_WT_P1	60.6	47	94 bp	59
SRR2807643	R03_Root_Control_WT_P2	57.2	47	87 bp	59
SRR2807638	R01_Trap_Control_WT_P1	48.6	47	93 bp	52.5
SRR2807638	R01_Trap_Control_WT_P2	46.3	46	92 bp	52.5
SRR2807639	R02_Trap_Control_WT_P1	55.3	46	95 bp	73.5
SRR2807639	R02_Trap_Control_WT_P2	56.3	46	95 bp	73.5
SRR2807640	R03_Trap_Control_WT_P1	46.1	46	93 bp	39.9
SRR2807640	R03_Trap_Control_WT_P2	43.4	46	91 bp	39.9
ERR4508085	R01_Hair_Control_WT_P1	80.2	46	97 bp	52.6
ERR4508085	R01_Hair_Control_WT_P2	81.2	46	97 bp	52.6
ERR4508086	R02_Hair_Control_WT_P1	67.5	45	98 bp	56.8
ERR4508086	R02_Hair_Control_WT_P2	69.7	45	97 bp	56.8
ERR4508087	R03_Hair_Control_WT_P1	73.9	46	98 bp	67
ERR4508087	R03_Hair_Control_WT_P2	75.7	46	96 bp	67

Table 16: FastQC of the juvenile and adult traps in the RNA-seq experiment (Exp_Juv).

Library ID	Sample Name	% Dups	% GC	Length	M Seqs
lib229052_5684_6_1	R01_Trap_Juvenile_WT_P1	67.9	46	151 bp	37.5
lib229052_5684_6_2	R01_Trap_Juvenile_WT_P2	66.4	47	151 bp	37.5
lib227895_5673_8_1	R02_Trap_Juvenile_WT_P1	65.4	46	151 bp	46
lib227895_5673_8_2	R02_Trap_Juvenile_WT_P2	61.2	47	151 bp	46
lib227896_5673_8_1	R03_Trap_Juvenile_WT_P1	65	46	151 bp	48.7
lib227896_5673_8_2	R03_Trap_Juvenile_WT_P2	60.1	47	151 bp	48.7
lib227897_5673_8_1	R01_Trap_Control_WT_P1	64.5	46	151 bp	41.6
lib227897_5673_8_2	R01_Trap_Control_WT_P2	58.4	47	151 bp	41.6
lib227898_5673_8_1	R02_Trap_Control_WT_P1	65.8	46	151 bp	38.7
lib227898_5673_8_2	R02_Trap_Control_WT_P2	61.4	47	151 bp	38.7
lib227899_5673_5_1	R03_Trap_Control_WT_P1	63.9	46	151 bp	30
lib227899_5673_5_2	R03_Trap_Control_WT_P2	64.5	47	151 bp	30

Table 17: FastQC of the ERR mutant RNA-seq experiment (Exp_ERR).

Library ID	Sample Name	% Dups	% GC	Length	M Seqs
lib242191_6012_1_1	R01_Trap_Control_WT_P1	69.1	47	151 bp	50.8
lib242191_6012_1_2	R01_Trap_Control_WT_P2	68.2	47	151 bp	50.8
lib242192_6012_1_1	R02_Trap_Control_WT_P1	73.7	46	151 bp	62.4
lib242192_6012_1_2	R02_Trap_Control_WT_P2	72.2	47	151 bp	62.4
lib242193_6012_1_1	R03_Trap_Control_WT_P1	75.9	46	151 bp	56.1
lib242193_6012_1_2	R03_Trap_Control_WT_P2	73.2	47	151 bp	56.1
lib242194_6027_8_1	R01_Trap_APs-1h_WT_P1	66.2	47	151 bp	24.2
lib242194_6027_8_2	R01_Trap_APs-1h_WT_P2	62.2	48	151 bp	24.2
lib242195_6012_1_1	R02_Trap_APs-1h_WT_P1	72.8	48	151 bp	43.1
lib242195_6012_1_2	R02_Trap_APs-1h_WT_P2	70.2	48	151 bp	43.1
lib242196_6012_1_1	R03_Trap_APs-1h_WT_P1	73.6	46	151 bp	61.7
lib242196_6012_1_2	R03_Trap_APs-1h_WT_P2	71.3	47	151 bp	61.7
lib242197_6027_8_1	R01_Trap_COR-1h_WT_P1	76.1	47	151 bp	57.5
lib242197_6027_8_2	R01_Trap_COR-1h_WT_P2	71.2	47	151 bp	57.5
lib242198_6012_1_1	R02_Trap_COR-1h_WT_P1	79.6	46	151 bp	73.2
lib242198_6012_1_2	R02_Trap_COR-1h_WT_P2	77.2	47	151 bp	73.2
lib242199_6027_8_1	R03_Trap_COR-1h_WT_P1	62.7	47	151 bp	22.6
lib242199_6027_8_2	R03_Trap_COR-1h_WT_P2	59.4	47	151 bp	22.6
lib242200_6012_2_1	R01_Trap_Control_ERR_P1	73.4	46	151 bp	57.8
lib242200_6012_2_2	R01_Trap_Control_ERR_P2	71.9	47	151 bp	57.8
lib242201_6012_2_1	R02_Trap_Control_ERR_P1	74.2	47	151 bp	60.6
lib242201_6012_2_2	R02_Trap_Control_ERR_P2	73.1	47	151 bp	60.6
lib242202_6012_2_1	R03_Trap_Control_ERR_P1	70.6	46	151 bp	51.9
lib242202_6012_2_2	R03_Trap_Control_ERR_P2	69.4	47	151 bp	51.9
lib242203_6012_2_1	R01_Trap_APs-1h_ERR_P1	67.8	46	151 bp	51.6
lib242203_6012_2_2	R01_Trap_APs-1h_ERR_P2	66.8	47	151 bp	51.6
lib242204_6012_2_1	R02_Trap_APs-1h_ERR_P1	69.6	46	151 bp	46.9
lib242204_6012_2_2	R02_Trap_APs-1h_ERR_P2	68.2	47	151 bp	46.9
lib242205_6012_2_1	R03_Trap_APs-1h_ERR_P1	73.7	46	151 bp	57.2
lib242205_6012_2_2	R03_Trap_APs-1h_ERR_P2	69.9	47	151 bp	57.2
lib242206_6027_8_1	R01_Trap_COR-1h_ERR_P1	61.6	46	151 bp	26
lib242206_6027_8_2	R01_Trap_COR-1h_ERR_P2	55.8	47	151 bp	26
lib242207_6012_8_1	R02_Trap_COR-1h_ERR_P1	79.2	47	151 bp	60.1
lib242207_6012_8_2	R02_Trap_COR-1h_ERR_P2	71.6	47	151 bp	60.1
lib242208_6012_8_1	R03_Trap_COR-1h_ERR_P1	64.4	46	151 bp	28.7
lib242208_6012_8_2	R03_Trap_COR-1h_ERR_P2	56.9	47	151 bp	28.7

Table 18: Mapping rate for all RNA-seq experiments. For the already published sequences the SRA ID is given, and for unpublished data, the library number is given.

SRA ID / lib	Sample Name	Uniquely mapped reads %	% of reads mapped to multiple loci
SRR2807648	R01_Flower_Control_WT	91.23%	2.87%
SRR2807650	R02_Flower_Control_WT	91.57%	2.82%
SRR2807649	R03_Flower_Control_WT	90.58%	2.96%
SRR2807635	R01_Glands_Control_WT	87.2%	3.15%
SRR2807636	R02_Glands_Control_WT	86.55%	3.19%
SRR2807637	R03_Glands_Control_WT	86.99%	3.19%
SRR2807633	R01_Petiole_Control_WT	91.15%	2.81%
SRR2807634	R02_Petiole_Control_WT	91.86%	2.63%
SRR2807644	R03_Petiole_Control_WT	92.27%	2.63%
SRR2807654	R01_Rim_Control_WT	91%	2.89%
SRR2807655	R02_Rim_Control_WT	90.92%	2.83%
SRR2807656	R03_Rim_Control_WT	91.63%	2.78%
SRR2807642	R01_Root_Control_WT	87.39%	3.18%
SRR2807641	R02_Root_Control_WT	89.29%	3.08%
SRR2807643	R03_Root_Control_WT	88.11%	3.13%
SRR2807638	R01_Trap_Control_WT	88.28%	3.39%
SRR2807639	R02_Trap_Control_WT	89.22%	3.31%
SRR2807640	R03_Trap_Control_WT	87.87%	3.51%
ERR4508085	R01_Hair_Control_WT	82.06%	3.44%
ERR4508086	R02_Hair_Control_WT	86.62%	3.04%
ERR4508087	R03_Hair_Control_WT	80.85%	3.42%
lib229052_5684_6	R01_Trap_Juvenile_WT	85.41%	2.4%
lib227895_5673_8	R02_Trap_Juvenile_WT	84.27%	2.48%
lib227896_5673_8	R03_Trap_Juvenile_WT	83.87%	2.46%
lib227897_5673_8	R01_Trap_Control_WT	83.28%	2.68%
lib227898_5673_8	R02_Trap_Control_WT	84.58%	2.59%
lib227899_5673_5	R03_Trap_Control_WT	84.64%	2.58%
lib242191_6012_1	R01_Trap_Control_WT	82.38%	2.45%
lib242192_6012_1	R02_Trap_Control_WT	84.56%	2.4%
lib242193_6012_1	R03_Trap_Control_WT	84.99%	2.36%
lib242194_6027_8	R01_Trap_APs-1h_WT	82.05%	2.81%
lib242195_6012_1	R02_Trap_APs-1h_WT	80.59%	3.14%
lib242196_6012_1	R03_Trap_APs-1h_WT	87.92%	2.75%
lib242197_6027_8	R01_Trap_COR-1h_WT	87.77%	2.34%
lib242198_6012_1	R02_Trap_COR-1h_WT	85.44%	2.45%
lib242199_6027_8	R03_Trap_COR-1h_WT	86.39%	2.51%
lib242200_6012_2	R01_Trap_Control_ERR	87.29%	2.45%
lib242201_6012_2	R02_Trap_Control_ERR	84.84%	2.53%
lib242202_6012_2	R03_Trap_Control_ERR	86.88%	2.49%
lib242203_6012_2	R01_Trap_APs-1h_ERR	88.06%	2.48%
lib242204_6012_2	R02_Trap_APs-1h_ERR	87.56%	2.45%
lib242205_6012_2	R03_Trap_APs-1h_ERR	87.54%	2.44%
lib242206_6027_8	R01_Trap_COR-1h_ERR	88.3%	2.45%
lib242207_6012_8	R02_Trap_COR-1h_ERR	85.3%	2.46%
lib242208_6012_8	R03_Trap_COR-1h_ERR	87.97%	2.5%

Figure 61: Rolling *Dionaea* trap around a piece of wet meat (beef) that did not touch the trigger hairs. After 1 day of digestion (left) and after 4 days of digestion (right).

Superfamily/Family	Family/Group	Gene Name	DmID	Hair FPKM	$Q_{gene\|hair}$
ABC superfamily	ABC-B group	ABCB11	Dm_00009382-RA	111.71	2.79
ABC superfamily	ABC-B group	ABCB11	Dm_00012144-RA	44.49	3.78
ABC superfamily	ABC-D group	ABCD1	Dm_00008485-RA	123.76	3.74
ABC superfamily	ABC-G group	PEN3	Dm_00003460-RA	533.64	2.95
ABC superfamily	ABC-G group	ABCG40	Dm_00005053-RA	79.76	3.30
ABC superfamily	ABC-G group	ABCG12	Dm_00007763-RA	203.91	3.62
ABC superfamily	ABC-G group	ABCG40	Dm_00013401-RA	299.75	2.19
ABC superfamily	ABC-G group	ABCG32	Dm_00016540-RA	211.71	3.05
P-type ATPase superfamily	P2 family	ACA2	Dm_00018589-RA	188.18	3.21
P-type ATPase superfamily	P3 family	HA4	Dm_00013634-RA	1306.34	3.19
P-type ATPase superfamily	P4 family	ALA1	Dm_00010528-RA	28.53	3.39
P-type ATPase superfamily	P4 family	ALA9	Dm_00011429-RA	27.89	3.57
CDF superfamily	CaCA family	CAX9	Dm_00008759-RA	42.49	3.74
CDF superfamily	CaCA family	MHX	Dm_00012610-RA	46.54	3.68
CDF superfamily	CaCA family	NCL	Dm_00018757-RA	372.54	2.68
GIC family	**GLR ligand-gated cation channel**	**GLR3.6.1**	**Dm_00002270-RA**	**395.78**	**1.92**
GIC family	GLR ligand-gated cation channel	GLR3.6.2	Dm_00012322-RA	53.96	3.72
GIC family	GLR ligand-gated cation channel	GLR3.4	Dm_00004609-RA	310.11	2.67
VIC superfamily	**Plant-VG voltage-gated potassium cation channel**	**KAT1**	**Dm_00004067-RA**	**122.12**	**1.70**
VIC superfamily	**Plant-VG voltage-gated potassium cation channel**	**SKOR**	**Dm_00007946-RA**	**190.18**	**2.15**
KUP family	HAK/KUP/KT potassium cation transporter	KUP8	Dm_00010980-RA	172.31	3.64
MscS family	**MSL4+-like mechanosensitive ion channel**	**MSL4/10**	**Dm_00009130-RA**	**26.70**	**1.13**

Figure 62: Trigger hair permeome classified according to Aramemnon – Plant Protein Database. Genes are considered highly expressed trigger hair-specific if Shannon entropy $Qgene|hair$ value < 3.9 and hair expression FPKM > 20. The "Hair FPKM" column represents the average expression level of 3 replicates in the hair tissue. The "$Qgene|hair$" column represents the specificity level according to the Shannon entropy method for tissues specificity where low values represent high specificity.

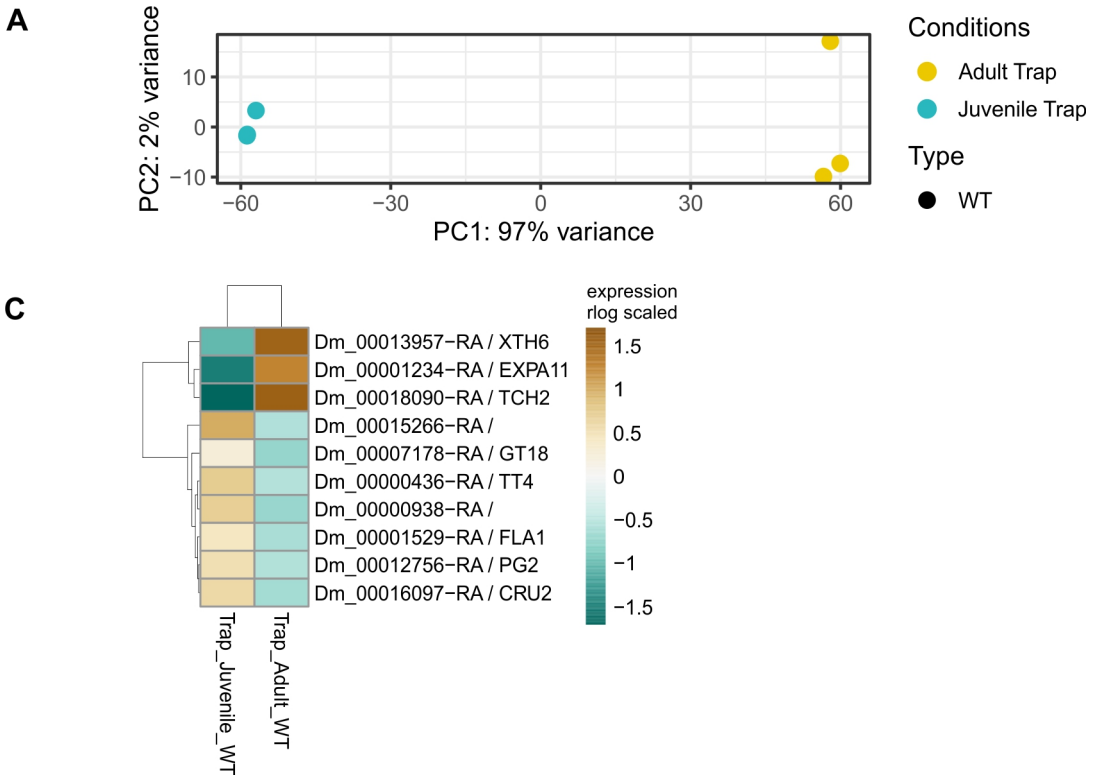

Figure 63: (A) PCA with replicates in each group: juvenile (stage5) and adult (stage 6) traps. Note: There are three replicates for each group and in case of the juvenile group two replicates are overlapping. (B) Top 10 most variable genes in adult traps vs juvenile traps shown by RNA-seq expression comparison.

	Permeome_annotation	Gene Name	DmID	log2FC	Expression (FPKM) Adult Trap	Juv. Trap
carrier-mediated transport	CDF superfamily.CaCA family.CAX cation antiporter	CAX3	Dm_00008275-RA	1.77	67.33	19.71
	CDF superfamily.CaCA family.CAX cation antiporter	CAX2	Dm_00013438-RA	0.58	72.68	48.51
	CDF superfamily.CaCA family.CCX cation:calcium cation exchanger	CAX9	Dm_00008759-RA	1.23	20.44	8.71
	CDF superfamily.CaCA family.NCL/EF-CAX cation exchanger	NCL/EFCAX1	Dm_00018757-RA	3.24	302.26	32.04
	KUP family.HAK/KUP/KT potassium cation transporter	KUP8/HAK8/KT8	Dm_00017467-RA	2.67	147.54	23.19
	KUP family.HAK/KUP/KT potassium cation transporter	HAK5	Dm_00018445-RA	1.77	58.17	17.01
	KUP family.HAK/KUP/KT potassium cation transporter	HAK5	Dm_00006186-RA	1.66	11.86	3.76
	KUP family.HAK/KUP/KT potassium cation transporter	HAK8	Dm_00010980-RA	1.23	114.09	48.46
	MFS superfamily.NNP family.NRT2 nitrate transporter.	NRT2.5	Dm_00019854-RA	2.31	37.46	7.58
	MFS superfamily.NRT1/PTR family.NPF2 multi-functional anion transporter (GTR)	GTR2/NPF2.11	Dm_00010563-RA	4.72	189.53	7.18
	MFS superfamily.NRT1/PTR family.NPF5-type unspecified transporter	NPF5.5	Dm_00012845-RA	2.65	76.56	12.22
	MFS superfamily.NRT1/PTR family.NPF6 nitrate anion transporter (CHL1)	NPF6.2/NRT1.4	Dm_00000083-RA	4.10	107.66	6.26
	MFS superfamily.NRT1/PTR family.NPF6 nitrate anion transporter (CHL1)	NPF6.3/NRT1.1	Dm_00013432-RA	1.81	109.38	31.22
	TRK family.HKT potassium/sodium cation transporter	HKT1	Dm_00018208-RA	0.74	19.91	11.96
channels	ArAE family.QUAC/ALMT anion channel	ALMT9	Dm_00018513-RA	5.26	32.08	0.85
	ArAE family.QUAC/ALMT anion channel	ALMT9	Dm_00013059-RA	2.03	9.43	2.31
	ArAE family.QUAC/ALMT anion channel	ALMT4	Dm_00000208-RA	0.51	56.89	40.00
	Ca-ClC family.Ca-ClC unspecified channel	ANO1	Dm_00008043-RA	1.51	79.87	27.97
	Ca-ClC family.OSCA Ca2+-permeable hyperosmolality-gated channel (OSCA1/2/3)	OSCA1.7	Dm_00005287-RA	2.77	99.34	14.55
	Ca-ClC family.OSCA Ca2+-permeable hyperosmolality-gated channel (OSCA1/2/3)	OSCA4.1	Dm_00013412-RA	0.20	20.38	17.73
	GIC family.GLR ligand-gated cation channel	GLR3.6	Dm_00002270-RA	6.38	145.25	1.74
	GIC family.GLR ligand-gated cation channel	GLR3.4	Dm_00004609-RA	3.46	135.70	12.37
	GIC family.GLR ligand-gated cation channel	GLR3.6	Dm_00012322-RA	2.24	71.10	15.01
	GIC family.GLR ligand-gated cation channel	GLR2.1	Dm_00000700-RA	1.71	12.78	3.93
	GIC family.GLR ligand-gated cation channel	GLR2.8	Dm_00018929-RA	1.41	19.57	7.35
	MCU family.MCU calcium uniporter complex.channel component MCU	MICU	Dm_00001147-RA	1.57	4.96	1.66
	MCU family.MCU calcium uniporter complex.channel component MCU	MICU	Dm_00015386-RA	1.48	19.08	6.82
	MCU family.MCU calcium uniporter complex.channel component MCU	MICU	Dm_00006505-RA	0.43	94.27	69.69
	MCU family.MCU calcium uniporter complex.regulator component MICU	MICU	Dm_00011939-RA	1.89	64.63	17.39
	VIC superfamily.Plant-CNGC cyclic nucleotide-gated cation channel	CNGC15	Dm_00004216-RA	0.79	23.81	13.78
	VIC superfamily.Plant-CNGC cyclic nucleotide-gated cation channel	CNGC14	Dm_00011087-RA	0.64	61.99	39.87
	VIC superfamily.Plant-CNGC cyclic nucleotide-gated cation channel	CNGC1	Dm_00000462-RA	0.36	61.02	47.61
	VIC superfamily.Plant-VG voltage-gated potassium cation channel	SKOR	Dm_00007946-RA	3.23	39.93	4.25
	VIC superfamily.Plant-VG voltage-gated potassium cation channel	KAT1 / KDM	Dm_00004067-RA	2.96	15.23	1.97
	VIC superfamily.TPK/KCO voltage-gated potassium cation channel	KCO1 / TPK1	Dm_00002682-RA	0.87	23.95	13.06
primary active transport	P-type ATPase superfamily.P2 family.ACA P2B-type calcium cation-transporting ATPase	ACA11	Dm_00014685-RA	1.16	61.02	27.30
	P-type ATPase superfamily.P2 family.ACA P2B-type calcium cation-transporting ATPase	ACA10	Dm_00009018-RA	0.70	91.89	56.61
	P-type ATPase superfamily.P2 family.ACA P2B-type calcium cation-transporting ATPase	ACA9	Dm_00005472-RA	0.43	7.10	5.29
	P-type ATPase superfamily.P3 family.AHA P3A-type proton-translocating ATPase	HA4	Dm_00013634-RA	5.85	2856.90	49.61
	P-type ATPase superfamily.P3 family.AHA P3A-type proton-translocating ATPase	HA3	Dm_00000738-RA	3.13	176.82	20.19
	P-type ATPase superfamily.P3 family.AHA P3A-type proton-translocating ATPase	HA5	Dm_00004749-RA	2.58	442.65	73.86

Figure 64: Permeome annotated using Aramamnon - plant membrane protein database. All electrogenic genes with $\log_2$FC value > 0 in adult trap compared to juvenile trap are shown together with their FPKM expression values. GIC = Glutamate-gated Ion Channel, VIC = Voltage-gated Ion Channel, Ca-ClC = Ca^{2+}-dependent Cl^- Channel, ArAE = The Aromatic Acid Exporter, MFS = Major Facilitator Superfamily, CDF = Cation Diffusion Facilitator.

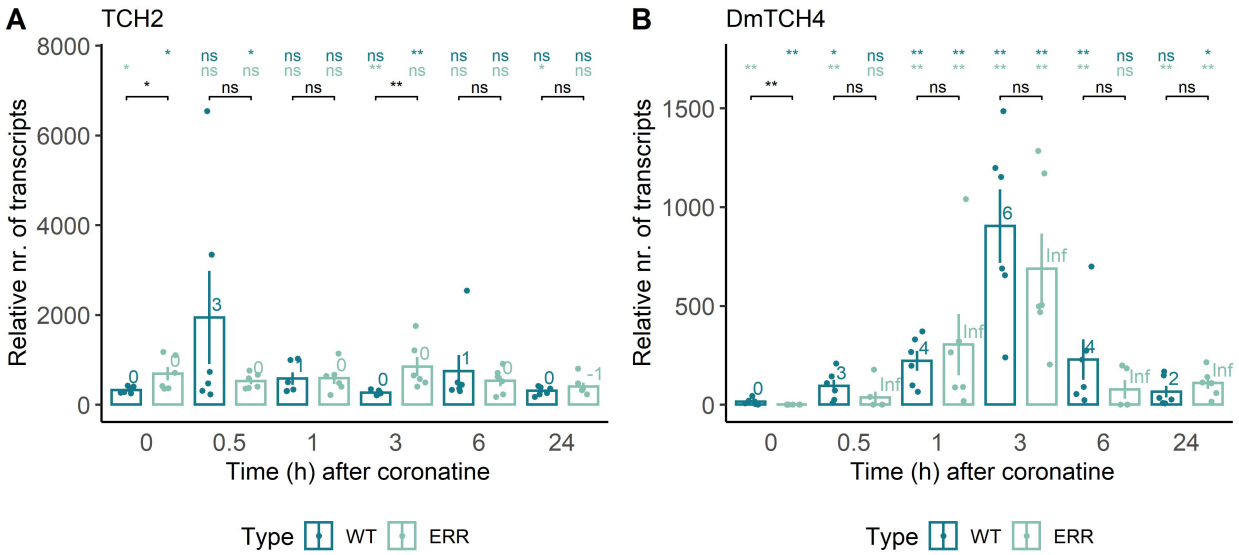

Figure 65: qPCR expression level timeline of *DmTCH2* (A) and *DmTCH4* (B) upon COR (0.1 mM coronatine) in WT and ERR traps. The relative number of transcripts is normalised to 10 000 molecules of actin *DmACT1*. The bar chart shows average values +/- SE and the dots show the values of each measured sample. The numbers above the bar chart represent $\log_2$FC values relative to the corresponding control of each phenotype. Above the chart, the Wilcoxon rank sum test p-value is represented with stars: * for $p < 0.05$, ** for $p < 0.01$, *** for $p < 0.001$, ns = not significant. The colours of the stars indicate to which control the comparison was made (dark turquoise = WT control, light turquoise = ERR control). $n = 6$. Experiment done by Brigitte Neumann with the help of Kevin Bongers.

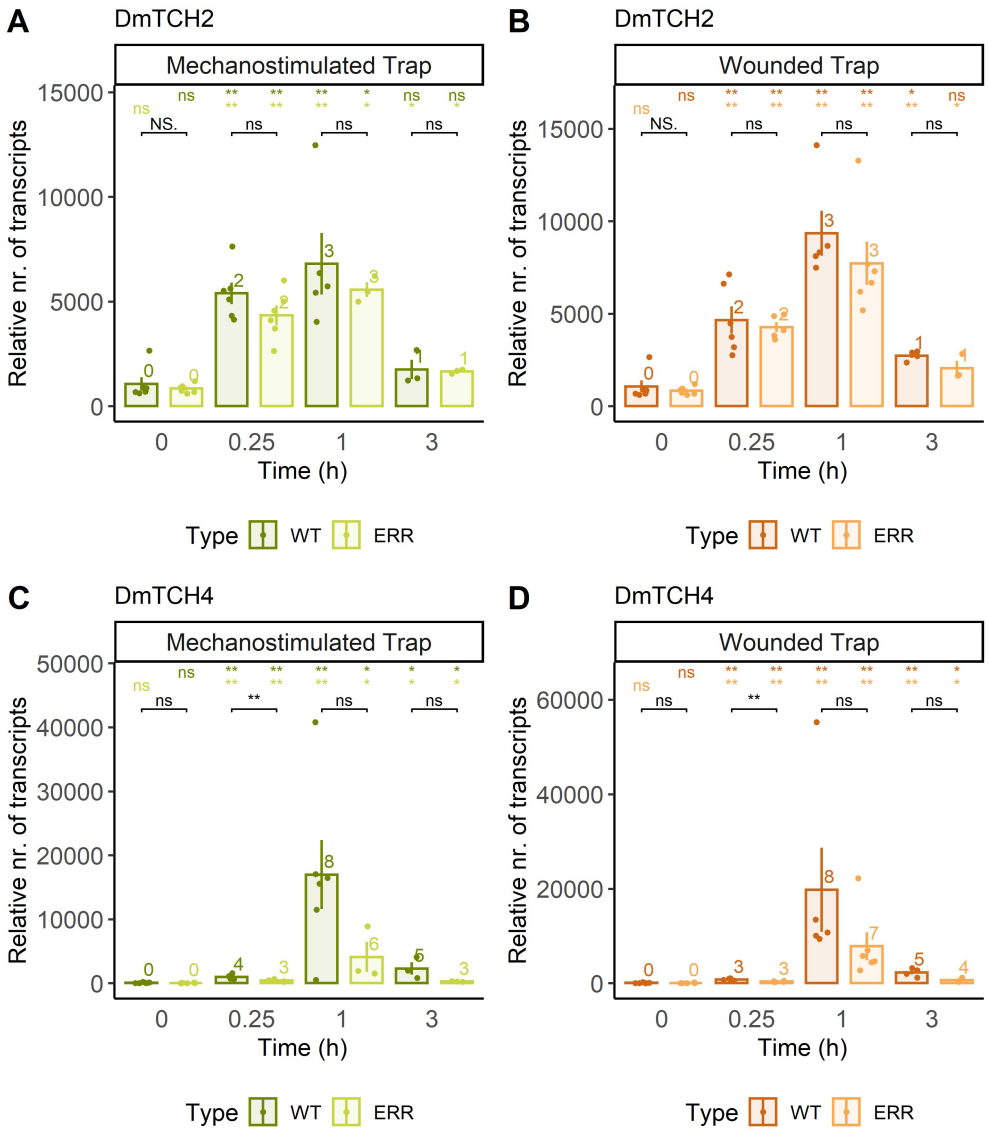

Figure 66: qPCR expression levels upon mechanostimulation (10 APs, 0.01 Hz) (left) and wounding (right) of *DmTCH2* (A,B) and *DmTCH4* (C,D) in WT and ERR traps. The relative number of transcripts is normalised to 10 000 molecules of actin *DmACT1*. The bar chart shows average values +/- SE and the dots show the values of each measured sample. The numbers above the bar chart represent $\log_2$FC values relative to the corresponding control of each phenotype. Above the chart, the Wilcoxon rank sum test *p*-value is represented with stars: * for $p < 0.05$, ** for $p < 0.01$, *** for $p < 0.001$, ns = not significant. The colours of the stars indicate to which control the comparison was made (dark colour = WT control, light colour = ERR control). $n = 6$. FW = fresh weight.

Table 19: DEGs in ground state comparison as part of enriched MapMan bins. Log_2FC values and expression values are shown as follows: column 1 = log_2FC values of Control_ERR vs Control_WT comparison, column 2 = Control_WT_FPKM , column 3 = Control_ERR_FPKM. the DmIDs, gene names and MapMan bins in which they belong are also shown. Only upregulated DEGs with $log_2FC > 1.5$ and FPKM expression values > 10 in Control_ERR, as well as downregulated DEGs with $log_2FC < -1.5$ and FPKM expression values > 10 in Control_WT were selected.

1	2	3	DmID	Gene Name	Bin	Bin Name
-1.88	123.74	33.53	Dm_00001034-RA	ALDH2C4	21.5.1	Cell wall organisation
-2.17	771.27	170.88	Dm_00001234-RA	EXPA11	21.4.2.1	Cell wall organisation
-2.84	464.11	64.99	Dm_00003377-RA	EXLA2	21.4.2.2	Cell wall organisation
-1.54	24.41	8.37	Dm_00011567-RA	FT1	21.4.1.1.5.2	Cell wall organisation
-1.68	16.70	5.23	Dm_00018171-RA	CYP86A8	21.9.1.1	Cell wall organisation
-1.60	120.31	39.63	Dm_00005762-RA	IRX9	21.2.2.1.3.1	Cell wall organisation
-1.54	24.41	8.37	Dm_00011567-RA	FT1	21.2.1.1.4	Cell wall organisation
-2.31	197.52	39.92	Dm_00008368-RA	RGIL6	21.3.5.2	Cell wall organisation
2.33	2.26	11.39	Dm_00003975-RA	PG2	21.3.5.1.4	Cell wall organisation
4.64	2.42	60.30	Dm_00009785-RA	BBE8	50.1.1	Enzyme classif.oxidored.
1.69	9.28	30.02	Dm_00009021-RA	BBE21/OGOX2	50.1.1	Enzyme classif.oxidored.
4.32	0.87	17.42	Dm_00009800-RA	LAC7	50.1.10	Enzyme classif.oxidored.
1.59	3.81	11.45	Dm_00009799-RA	LAC7	50.1.10	Enzyme classif.oxidored.
-2.66	24.97	3.96	Dm_00001071-RA	sks17	50.1.10	Enzyme classif.oxidored.
3.75	4.61	61.94	Dm_00018023-RA	CYP76C4	50.1.13	Enzyme classif.oxidored.
2.45	2.28	12.44	Dm_00019675-RA	CYP71A26	50.1.13	Enzyme classif.oxidored.
1.57	22.46	66.62	Dm_00001604-RA	CYP76C4	50.1.13	Enzyme classif.oxidored.
-4.50	199.15	8.79	Dm_00010320-RA	CYP87A2	50.1.13	Enzyme classif.oxidored.
-2.25	16.81	3.52	Dm_00017809-RA	CYP72A15	50.1.13	Enzyme classif.oxidored.
-2.16	28.98	6.50	Dm_00001699-RA	CYP71A13	50.1.13	Enzyme classif.oxidored.
-1.51	43.65	15.29	Dm_00001695-RA	CYP71A22	50.1.13	Enzyme classif.oxidored.
-9.54	40.22	0.05	Dm_00010260-RA	ALDH3I1	50.1.2	Enzyme classif.oxidored.
3.55	3.05	35.67	Dm_00015273-RA	OMT1	50.2.1	Enzyme classif. transf.
1.70	7.42	24.15	Dm_00015011-RA	OMT1	50.2.1	Enzyme classif. transf.
-10.86	42.29	0.02	Dm_00011414-RA	OMT1	50.2.1	Enzyme classif.transf.
-6.92	37.60	0.31	Dm_00020937-RA	OMT1	50.2.1	Enzyme classif.transf.
5.00	1.21	38.72	Dm_00006793-RA	UGT74B1	50.2.4	Enzyme classif.transf.
3.59	0.85	10.17	Dm_00002050-RA	UGT88A1	50.2.4	Enzyme classif.transf.
-4.26	3949.82	205.95	Dm_00013957-RA	XTH6	50.2.4	Enzyme classif.transf.
-1.57	286.90	96.92	Dm_00002224-RA	HYR1	50.2.4	Enzyme classif.transf.
1.94	5.32	20.49	Dm_00004637-RA	Kin3	50.2.7	Enzyme classif.transf.
-1.51	91.36	32.10	Dm_00003819-RA	emb1067	50.2.7	Enzyme classif.transf.
4.08	1.08	18.30	Dm_00001180-RA	BGL2	50.3.2	Enzyme classif.hydrol.
2.15	4.37	19.39	Dm_00011309-RA	BGLU17	50.3.2	Enzyme classif.hydrol.
-2.31	103.76	20.96	Dm_00017887-RA	FUC1	50.3.2	Enzyme classif.hydrol.
-1.53	851.00	293.69	Dm_00010010-RA	CYN	50.4.2	Enzyme classif.lyases
4.30	6.50	127.75	Dm_00011727-RA	TRX1	10.6.1	Redox homeostasis
-9.21	221.28	0.37	Dm_00016566-RA	GPX6	10.4.2	Redox homeostasis
2.26	2.94	14.15	Dm_00001298-RA	GLDH	10.3.1.8	Redox homeostasis
-1.51	20.29	7.13	Dm_00006706-RA	PTAC3	15.6.1.2.2.1	RNA biosynthesis
-1.78	12.85	3.74	Dm_00007058-RA	BBX21	15.5.1.1	RNA biosynthesis
-11.40	38.47	0.00	Dm_00016753-RA	MYB88	15.5.2.1	RNA biosynthesis
2.03	3.58	14.74	Dm_00020377-RA	RL6	15.5.2.2	RNA biosynthesis
-1.79	26.47	7.67	Dm_00006932-RA	LBD37	15.5.24	RNA biosynthesis
2.15	6.86	30.40	Dm_00001350-RA	STZ	15.5.15	RNA biosynthesis
3.50	1.11	12.47	Dm_00015827-RA	WRKY41	15.5.22	RNA biosynthesis
1.93	6.22	23.59	Dm_00013547-RA	WRKY50	15.5.22	RNA biosynthesis

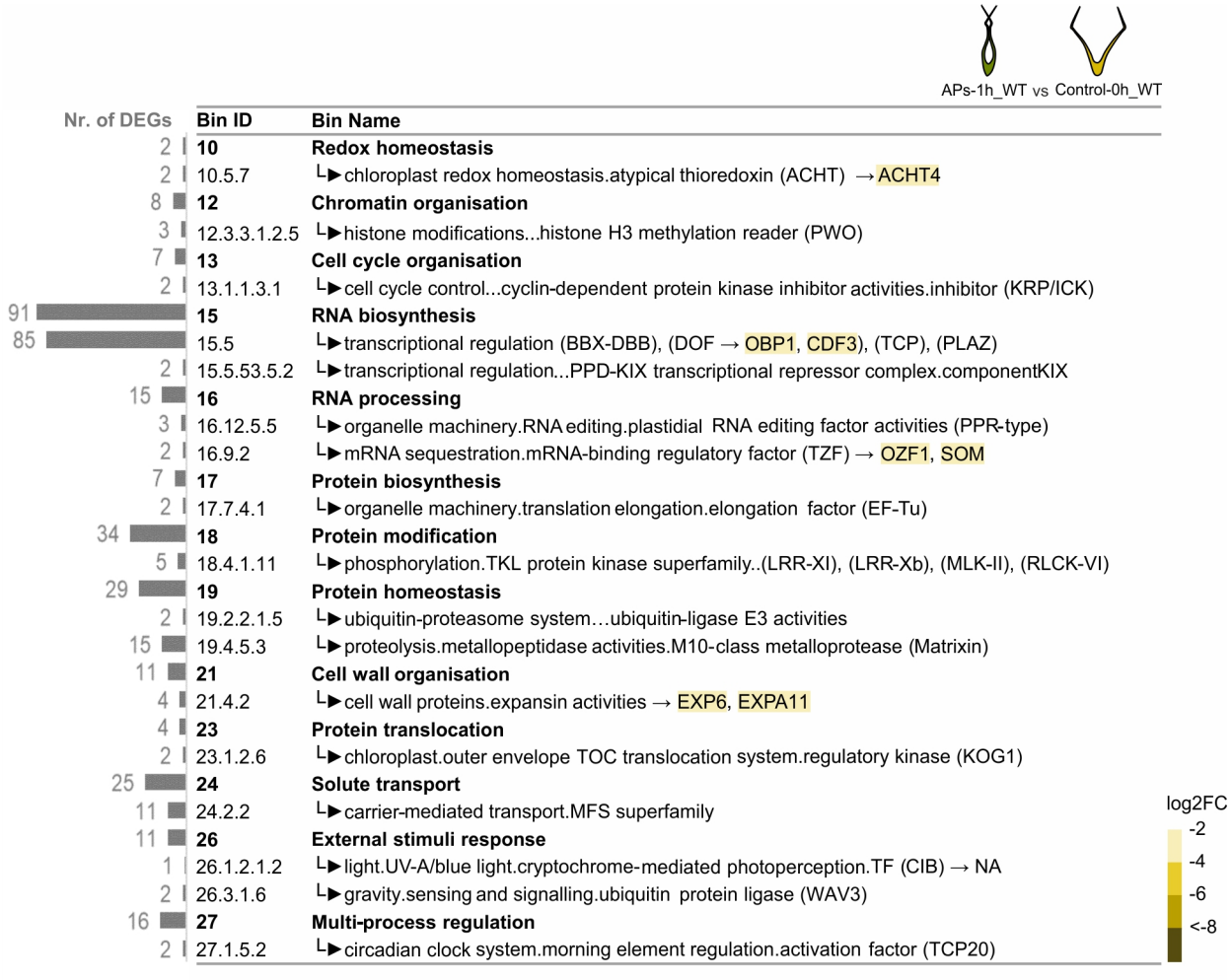

Figure 67: MapMan bin enrichment of downregulated DEGs between mechanostimulated WT and control WT traps. The number of DEGs belonging to each enriched bin is shown as a bar on the left side of the table. The DEGs with a $\log_2$FC value > 2 are shown as a heatmap. Bins that are not enriched in ERR upon mechanostimulation are marked in green text. NA = not annotated, DEGs = differentially expressed genes, FC = fold change.

Figure 68: GO-term enrichment treemap of upregulated unique DEGs upon mechanostimualtion in WT (A) and shared DEGs with ERR (B). GO-terms with BH-adj p value < 0.05 are considered enriched. Redundant GO-terms were reduced using the Revigo. The category marked in grey is found in (A) and not reflected in (B). GO = gene ontology.

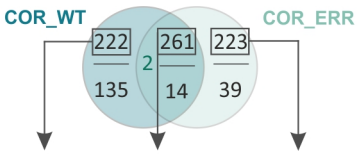

bin	name	up_COR_WT	up_COR_shared	up_COR_ERR
3	Carbohydrate metabolism	5	3	7
5	Lipid metabolism	5	7	4
11	Phytohormone action	4	10	9
15	RNA biosynthesis	26	60	18
15.5	RNA biosynthesis.transcriptional regulation	25	60	18
15.5.2	RNA biosynthesis.transcriptional regulation.MYB transcription factor superfamily	3	10	2
15.5.2.1	RNA biosynthesis.transcriptional regulation.MYB transcription factor superfamily.transcription factor (MYB)	3	7	1
15.5.3	RNA biosynthesis.transcriptional regulation.Homeobox transcription factor superfamily	0	3	6
15.5.7	RNA biosynthesis.transcriptional regulation.AP2/ERF transcription factor superfamily	4	11	3
15.5.7.2	RNA biosynthesis.transcriptional regulation.AP2/ERF transcription factor superfamily.transcription factor (DREB)	0	6	1
15.5.17	RNA biosynthesis.transcriptional regulation.transcription factor (NAC)	1	6	1
15.5.32	RNA biosynthesis.transcriptional regulation.transcription factor (bHLH)	3	7	1
18	Protein modification	11	16	12
18.4	Protein modification.phosphorylation	11	16	11
18.4.1	Protein modification.phosphorylation.TKL protein kinase superfamily	11	6	6
19	Protein homeostasis	8	16	9
19.2	Protein homeostasis.ubiquitin-proteasome system	2	9	1
19.2.2	Protein homeostasis.ubiquitin-proteasome system.ubiquitin-fold protein conjugation	2	9	1
19.2.2.8	Protein homeostasis.ubiquitin-proteasome system.ubiquitin-fold protein conjugation.Cullin-based ubiquitylation complexes	0	6	0
19.4	Protein homeostasis.proteolysis	6	7	6
20	Cytoskeleton organisation	1	2	6
21	Cell wall organisation	6	8	39
21.2	Cell wall organisation.hemicellulose	1	1	6
21.3	Cell wall organisation.pectin	3	3	19
21.3.2	Cell wall organisation.pectin.rhamnogalacturonan I	1	1	6
21.3.5	Cell wall organisation.pectin.modification and degradation	0	2	8
21.4	Cell wall organisation.cell wall proteins	0	4	9
21.4.1	Cell wall organisation.cell wall proteins.hydroxyproline-rich glycoprotein activities	0	4	8
21.4.1.1	Cell wall organisation.cell wall proteins.hydroxyproline-rich glycoprotein activities.arabinogalactan-protein (AGP) activities	0	3	7
21.4.1.1.3	Cell wall organisation.cell wall proteins.hydroxyproline-rich glycoprotein activities.arabinogalactan-protein (AGP) activities.fasciclin-type AGP (FLA)	0	1	7
24	Solute transport	16	11	10
24.2	Solute transport.carrier-mediated transport	13	7	6
26	External stimuli response	3	10	6
50	Enzyme classification	30	17	13
50.1	Enzyme classification.EC_1 oxidoreductases	7	7	5
50.1.13	Enzyme classification.EC_1 oxidoreductases.EC_1.14 oxidoreductase acting on paired donor with incorporation or reduction of molecular oxygen	2	6	2
50.2	Enzyme classification.EC_2 transferases	15	7	4
50.2.4	Enzyme classification.EC_2 transferases.EC_2.4 glycosyltransferase	11	5	2
50.3	Enzyme classification.EC_3 hydrolases	7	3	4
50.3.2	Enzyme classification.EC_3 hydrolases.EC_3.2 glycosylase	6	1	4

Figure 69: Number of upregulated DEGs upon COR in each MapMan bin of each double Venn diagram subset. Only bins that have a number of elements/DEGs > 5 in any of the subsets are shown.

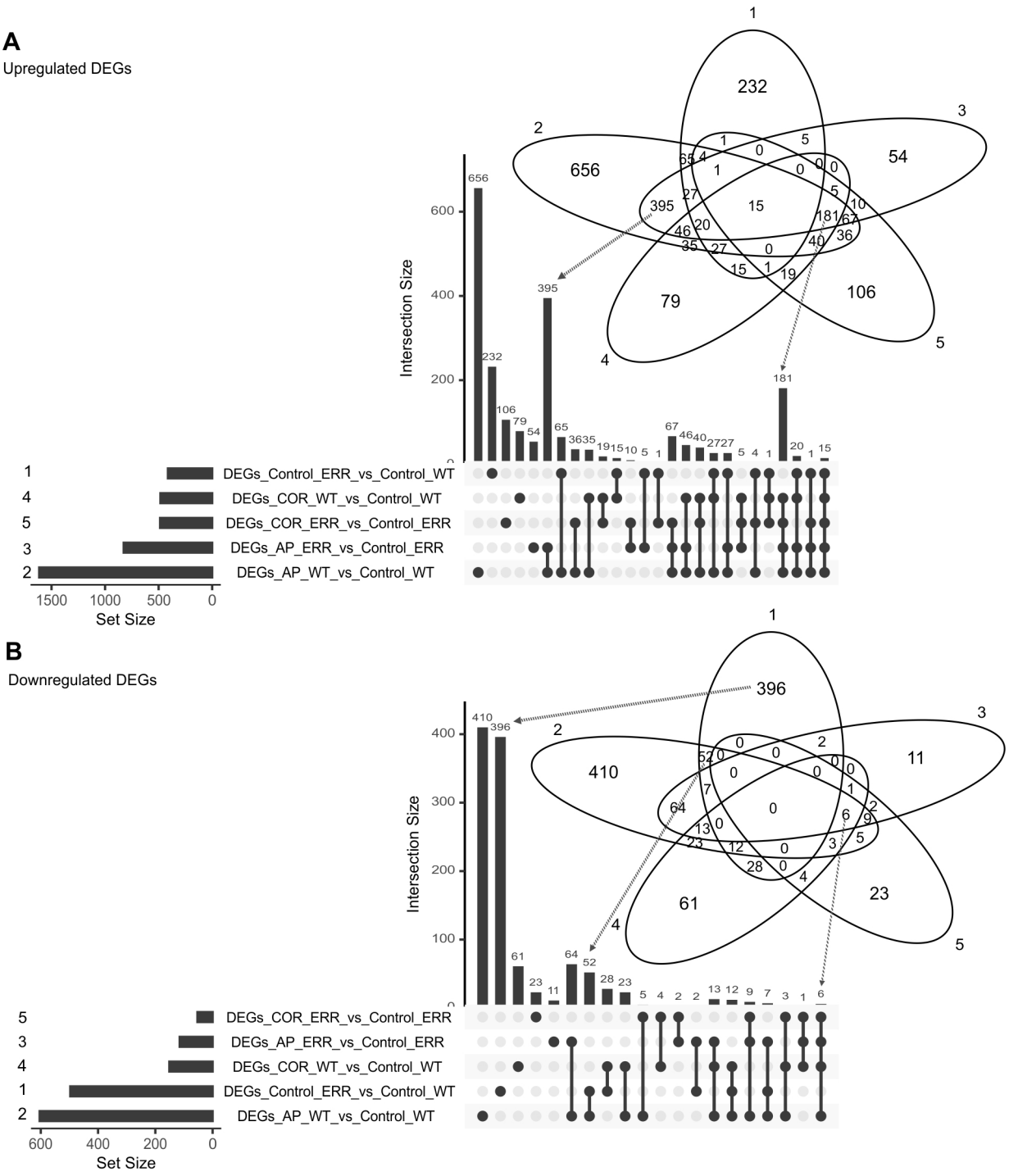

Figure 70: UpSet plot and Venn diagrams indicating the number of upregulated (A) and downregulated (B) DEGs within each of the interesection subsets when taking into account all pairwise comparisons used in this study.

Table 20: List of all DEGs mentioned in the text or in the figures together with log_2FC values of each pairwise comparison and FPKM expression values

Gene	DmID	Bin	Ct.ERR vs Ct.WT	AP.WT vs Ct.WT	AP.ERR vs Ct.ERR	COR.WT vs Ct.WT	COR.ERR vs Ct.ERR	Ct.WT	AP.WT	Ct.ERR	AP.ERR	COR.WT	COR.ERR
ABCB15	Dm_00010914-RA	24.1.3.1.1	NA	2.51	NA	NA	NA	3.91	22.39	5.00	7.52	3.72	4.70
ABCB19	Dm_00018388-RA	11.2.4.3	1.20	1.32	NA	1.37	NA	6.15	15.31	14.18	11.24	15.94	18.28
ABCB19	Dm_00018388-RA	24.1.3.1.1	1.20	1.32	NA	1.37	NA	6.15	15.31	14.18	11.24	15.94	18.28
ABR1	Dm_00017385-RA	15.5.7.1	NA	3.76	NA	NA	NA	0.91	12.38	0.75	1.60	0.69	0.67
ACA2	Dm_00006598-RA	24.1.2.2.2	-2.74	NA	NA	NA	NA	0.99	0.73	0.15	0.19	0.74	0.21
ACA2	Dm_00018589-RA	24.1.2.2.2	NA	2.16	1.69	NA	NA	31.56	141.19	37.92	122.03	33.84	40.31
AFB4	Dm_00015526-RA	19.2.2.8.1.4.6	NA	1.19	NA	NA	NA	31.84	72.52	39.87	46.12	30.92	30.75
AFB4	Dm_00015526-RA	11.2.2.1.1	NA	1.19	NA	NA	NA	31.84	72.52	39.87	46.12	30.92	30.75
AGD11	Dm_00005923-RA	35.1	NA	5.94	NA	NA	NA	0.40	25.27	0.00	1.72	0.12	0.03
AIB	Dm_00004196-RA	15.5.32	NA	4.74	3.78	3.86	3.61	10.13	271.04	9.43	129.20	146.67	115.06
AIB	Dm_00003237-RA	15.5.32	NA	4.50	3.66	3.65	4.12	7.72	174.99	6.43	81.36	97.14	111.37
ASG1	Dm_00001003-RA	35.2	NA	1.11	NA	NA	NA	44.52	95.95	52.22	91.75	53.30	57.15
ATL2	Dm_00016541-RA	19.2.2.1.5.3.3	NA	2.55	NA	NA	NA	13.80	80.40	24.71	41.79	24.78	42.56
ATL6	Dm_00002123-RA	19.2.2.1.5.3.3	1.23	2.59	NA	1.34	NA	6.71	40.41	15.76	31.26	16.99	15.98
ATL8	Dm_00000163-RA	19.2.2.1.5.3.3	NA	2.47	NA	NA	NA	23.33	129.48	21.93	41.44	25.25	29.42
BAG7	Dm_00012344-RA	35.1	NA	1.01	NA	NA	NA	47.79	96.51	35.43	53.33	48.97	38.33
BBE8	Dm_00009785-RA	50.1.1	4.64	NA	NA	2.49	NA	2.42	4.80	60.30	99.98	13.57	37.53
BBX21	Dm_00014316-RA	15.5.1.1	NA	-1.87	NA	NA	NA	14.97	4.00	14.77	9.71	12.80	12.95
BBX21	Dm_00007058-RA	15.5.1.1	-1.78	-1.49	NA	-1.43	NA	12.85	4.59	3.74	3.11	4.58	3.49
BCB	Dm_00005399-RA	35.1	2.48	4.80	NA	1.78	NA	4.92	136.95	27.42	65.66	16.90	28.49
BGL2	Dm_00001180-RA	50.3.2	4.08	4.15	NA	1.93	NA	1.08	19.12	18.30	30.66	4.08	23.01
BGLU17	Dm_00012465-RA	50.3.2	4.50	5.78	1.46	NA	NA	0.20	10.77	4.45	12.20	1.00	3.32
BGLU17	Dm_00011309-RA	50.3.2	2.15	NA	NA	NA	NA	4.37	7.97	19.39	19.39	5.04	20.93
BGLU17	Dm_00008253-RA	50.3.2	NA	NA	NA	NA	1.15	4.82	6.23	7.67	10.07	5.18	16.99
BGLU17	Dm_00018814-RA	50.3.2	-1.21	NA	NA	NA	NA	1673.77	2508.92	721.99	849.93	2269.13	874.23
BGLU17	Dm_00016946-RA	50.3.2	1.31	NA	NA	2.26	1.77	1.58	2.77	3.92	7.15	7.56	13.37
BGLU17	Dm_00008970-RA	50.3.2	-1.39	NA	NA	NA	NA	10.81	9.60	4.14	4.80	12.92	6.30
BME3	Dm_00008766-RA	15.5.1.3	NA	7.33	4.37	NA	1.25	0.47	76.33	0.82	17.09	0.83	1.97
BME3	Dm_00011203-RA	15.5.1.3	NA	3.81	2.08	NA	2.69	1.72	24.20	1.39	5.89	2.61	8.97
BPEp	Dm_00002860-RA	15.5.32	-1.18	3.11	1.43	1.53	2.83	5.22	45.10	2.32	6.26	15.13	16.48
BPEp	Dm_00002860-RA	26.1.2.1.2	-1.18	3.11	1.43	1.53	2.83	5.22	45.10	2.32	6.26	15.13	16.48
CBF1	Dm_00013892-RA	26.4.3.4.2	NA	9.18	6.32	8.91	7.85	0.18	104.91	0.38	30.07	87.32	86.95
CBF1	Dm_00012261-RA	15.5.7.2	NA	12.79	NA	NA	NA	0.00	49.78	1.24	3.24	0.86	0.52
CBF1	Dm_00012261-RA	26.4.3.4.2	NA	12.79	NA	NA	NA	0.00	49.78	1.24	3.24	0.86	0.52
CBF1	Dm_00013892-RA	15.5.7.2	NA	9.18	6.32	8.91	7.85	0.18	104.91	0.38	30.07	87.32	86.95
CBF4	Dm_00012260-RA	15.5.7.2	NA	11.06	8.81	3.65	3.76	0.54	1150.78	0.45	202.12	6.68	6.06
CBF4	Dm_00012260-RA	26.4.3.4.2	NA	11.06	8.81	3.65	3.76	0.54	1150.78	0.45	202.12	6.68	6.06
CBL1	Dm_00016099-RA	35.1	NA	2.46	1.26	NA	1.18	36.47	200.25	31.18	74.63	63.66	70.48
CBL10	Dm_00011526-RA	26.6.1.1.3	NA	2.23	1.35	1.89	1.00	18.03	84.80	21.54	54.79	66.88	43.12
CDI	Dm_00005783-RA	35.1	NA	1.69	NA	NA	NA	29.19	94.45	22.28	37.10	32.99	34.38
CDPK19	Dm_00009295-RA	18.4.5.4	NA	-1.13	NA	NA	NA	11.93	5.46	8.40	8.48	8.73	6.19
CKX5	Dm_00007779-RA	11.4.3.2	-5.32	3.91	6.38	-1.46	NA	2.30	34.38	0.06	4.78	0.84	0.12
CML42	Dm_00001554-RA	35.1	1.83	6.27	2.85	1.60	NA	3.21	248.19	11.41	82.18	9.66	12.26
CNGC8	Dm_00004597-RA	24.3.2.4	NA	2.35	NA	NA	NA	0.68	3.48	0.65	0.56	0.52	0.38
CP1	Dm_00015718-RA	35.1	NA	4.11	1.94	4.42	2.42	0.68	11.74	1.86	7.18	14.70	9.93
CPK1	Dm_00012895-RA	18.4.5.4	1.01	NA	NA	NA	NA	2.73	3.71	5.51	7.08	1.96	4.88
CPK16	Dm_00006184-RA	50.2.7	NA	2.52	1.59	NA	NA	21.49	122.97	41.55	124.92	28.63	40.64
CPK16	Dm_00016911-RA	18.4.5.4	NA	-1.23	NA	NA	NA	117.82	50.00	141.05	85.73	103.07	111.17
CPK7	Dm_00005101-RA	50.2.7	NA	-1.14	NA	NA	NA	69.58	31.50	95.35	59.66	58.05	61.61
CPK9	Dm_00000864-RA	18.4.5.4	NA	2.16	1.64	NA	NA	69.85	311.54	77.94	242.36	73.47	82.62
CRF10	Dm_00006739-RA	15.5.7.1	NA	4.46	2.40	2.64	2.42	25.18	556.02	37.96	200.18	156.54	202.92
CRK1	Dm_00001271-RA	18.4.5.5	NA	-1.01	NA	NA	NA	36.57	18.11	51.57	27.99	31.34	41.77
CSLD3	Dm_00007071-RA	21.2.3.1.1.2	NA	4.28	2.10	NA	NA	3.60	70.11	5.26	22.55	5.53	6.14
CSLD5	Dm_00020094-RA	21.2.3.1.1.2	NA	7.83	NA	NA	NA	0.00	1.18	0.02	0.35	0.02	0.03

Continued on next page

Table 20 – *Continued from previous page*

Gene	DmID	Bin	Ct.ERR vs Ct.WT	AP.WT vs Ct.WT	AP.ERR vs Ct.ERR	COR.WT vs Ct.WT	COR.ERR vs Ct.ERR	Ct.WT	AP.WT	Ct.ERR	AP.ERR	COR.WT	COR.ERR
CYN	Dm_00010010-RA	50.4.2	-1.53	NA	NA	NA	NA	851.00	768.55	293.69	261.46	678.12	239.21
CYP707A1	Dm_00018640-RA	11.1.3.2	3.08	NA	NA	NA	NA	0.90	1.50	7.61	9.55	1.40	7.12
CYP715A1	Dm_00013414-RA	50.1.13	NA	7.73	3.66	3.57	2.74	0.27	56.52	0.74	9.26	3.17	4.89
CYP71A13	Dm_00001699-RA	50.1.13	-2.16	-2.62	NA	NA	NA	28.98	4.77	6.50	10.87	24.68	5.20
CYP71A26	Dm_00019675-RA	50.1.13	2.45	2.22	NA	NA	NA	2.28	10.53	12.44	13.69	2.56	14.50
CYP71B35	Dm_00018034-RA	50.1.13	NA	2.04	NA	1.46	1.36	14.48	59.50	16.02	27.89	39.92	40.98
CYP72A15	Dm_00017809-RA	50.1.13	-2.25	NA	NA	NA	1.75	16.81	40.05	3.52	8.70	21.48	11.84
CYP76C4	Dm_00018023-RA	50.1.13	3.75	NA	NA	NA	NA	4.61	11.73	61.94	98.40	13.91	36.27
CYP76C4	Dm_00003959-RA	50.1.13	NA	11.59	7.13	8.82	7.85	0.03	92.86	0.07	10.20	13.65	16.87
CYP76C7	Dm_00010344-RA	50.1.13	4.55	3.47	NA	NA	NA	0.40	4.45	9.41	14.11	1.17	4.17
CYP76C7	Dm_00004650-RA	50.1.13	NA	11.25	7.67	9.80	8.32	0.10	259.67	0.22	45.28	95.18	70.91
CYP87A2	Dm_00010320-RA	50.1.13	-4.50	NA	1.06	NA	NA	199.15	185.29	8.79	18.37	179.41	15.77
CYP89A5	Dm_00015375-RA	50.1.13	NA	4.38	2.94	3.38	3.20	17.89	373.43	16.06	123.12	185.85	147.37
CYP94C1	Dm_00000775-RA	35.1	NA	1.69	NA	NA	NA	1.63	5.27	1.56	2.54	3.05	2.17
DEAR3	Dm_00002387-RA	15.5.7.2	NA	2.61	1.01	1.80	1.52	37.13	227.22	33.25	67.02	129.21	94.96
DEAR3	Dm_00013145-RA	15.5.7.2	NA	5.03	3.27	3.52	3.86	29.41	961.59	25.55	247.39	337.16	370.01
DMR6	Dm_00015415-RA	50.1.13	2.83	NA	NA	NA	NA	0.49	0.31	3.50	6.30	0.64	2.71
DREB1A	Dm_00003067-RA	15.5.7.2	NA	6.77	3.71	NA	NA	1.78	193.74	2.17	28.27	1.96	2.15
DREB1A	Dm_00010095-RA	26.4.3.4.2	NA	12.57	NA	12.80	11.79	0.00	40.01	0.00	1.50	46.91	21.16
DREB1A	Dm_00010095-RA	15.5.7.2	NA	12.57	NA	12.80	11.79	0.00	40.01	0.00	1.50	46.91	21.16
EBF1	Dm_00004169-RA	19.2.2.8.1.4.2	NA	1.10	NA	NA	NA	13.59	29.13	13.27	16.25	14.28	12.88
EBF1	Dm_00004169-RA	11.5.2.6	NA	1.10	NA	NA	NA	13.59	29.13	13.27	16.25	14.28	12.88
EBP	Dm_00020427-RA	15.5.7.1	NA	3.22	2.34	1.42	NA	61.02	568.02	61.60	312.35	163.60	119.11
ECA4	Dm_00009331-RA	24.1.2.2.1	NA	1.73	NA	NA	NA	12.71	41.99	18.45	21.20	13.98	11.88
EDA39	Dm_00003855-RA	35.1	1.27	4.45	1.73	NA	NA	9.93	217.83	23.97	79.41	16.12	19.27
EDR1	Dm_00000531-RA	18.4.1.30	NA	1.51	NA	NA	NA	14.15	40.26	15.06	25.80	12.89	14.47
ELP	Dm_00016399-RA	35.2	-2.16	1.11	NA	1.29	1.03	981.74	2114.64	219.01	419.03	2394.74	448.51
EP3	Dm_00000939-RA	35.1	3.02	3.43	NA	NA	NA	6.18	66.47	50.02	89.58	16.02	32.38
ERF12	Dm_00003851-RA	15.5.7.1	NA	5.54	2.43	1.85	3.10	1.53	71.20	1.88	10.12	5.56	16.10
ERF3	Dm_00005460-RA	15.5.7.1	NA	2.12	NA	NA	NA	67.22	291.61	67.25	127.74	94.06	84.84
ERF4	Dm_00003754-RA	15.5.7.1	NA	4.90	1.73	NA	NA	4.27	127.20	8.50	28.19	6.03	8.13
ERF4	Dm_00015937-RA	15.5.7.1	NA	4.76	3.61	NA	1.25	7.29	196.95	7.83	95.67	12.06	18.55
ERF4	Dm_00002282-RA	15.5.7.1	NA	1.25	NA	NA	NA	26.42	62.51	21.78	41.28	22.30	26.35
ERF4	Dm_00009654-RA	15.5.7.1	NA	1.64	NA	NA	NA	16.97	52.72	19.26	32.25	16.82	23.61
ERF9	Dm_00000724-RA	15.5.7.1	NA	5.49	2.59	NA	2.52	0.30	13.09	0.66	3.96	1.24	3.74
ESE1	Dm_00009378-RA	15.5.7.1	NA	2.54	NA	NA	NA	0.97	5.50	2.80	4.42	0.76	3.41
EXLA2	Dm_00003377-RA	21.4.2.2	-2.84	NA	1.03	NA	NA	464.11	717.01	64.99	133.05	351.70	90.08
EXLA2	Dm_00015175-RA	21.4.2.2	NA	1.03	NA	NA	NA	2.54	5.20	2.16	3.86	2.22	2.67
EXPA1	Dm_00010386-RA	21.4.2.1	NA	NA	NA	NA	-1.28	3.48	2.27	2.45	2.65	2.97	0.99
EXPA11	Dm_00000118-RA	21.4.2.1	NA	-2.02	-1.77	NA	NA	70.25	17.34	82.45	24.13	67.03	51.89
EXPA11	Dm_00001234-RA	21.4.2.1	-2.17	-1.34	NA	NA	NA	771.27	303.92	170.88	108.08	827.66	137.33
EXPA6	Dm_00003742-RA	21.4.2.1	-1.09	-2.04	NA	NA	NA	44.64	10.99	21.04	17.80	52.16	29.46
EXPA8	Dm_00017798-RA	21.4.2.1	NA	NA	-2.01	NA	NA	33.07	33.92	74.56	18.48	22.15	55.43
EXPB3	Dm_00003161-RA	21.4.2.3	NA	NA	NA	NA	2.41	12.19	14.34	5.21	5.62	18.95	27.70
FBL17	Dm_00017190-RA	19.2.2.8.1.4.6	NA	1.40	NA	NA	NA	1.64	4.40	2.82	3.02	1.49	1.88
FER	Dm_00000010-RA	18.4.1.16	NA	1.66	NA	NA	NA	52.84	166.78	71.20	117.82	56.69	72.05
FER	Dm_00000010-RA	11.10.2.4.2	NA	1.66	NA	NA	NA	52.84	166.78	71.20	117.82	56.69	72.05
FLA11	Dm_00006963-RA	21.4.1.1.3	NA	2.38	1.42	NA	1.65	1.33	6.95	0.88	2.34	0.64	2.72
FLA17	Dm_00011452-RA	21.4.1.1.3	NA	2.69	1.44	NA	1.01	20.78	134.40	20.73	56.41	23.95	41.85
FLA6	Dm_00010652-RA	21.4.1.1.3	NA	4.62	NA	NA	10.30	0.48	11.83	0.00	1.13	0.75	7.74
FLA7	Dm_00015199-RA	21.4.1.1.3	NA	7.16	5.33	2.08	2.80	2.70	387.66	2.36	94.71	11.43	16.48
FLS2	Dm_00000353-RA	26.8.1.1.1	NA	4.21	NA	NA	NA	3.60	66.62	3.91	8.00	3.84	3.52
FLS2	Dm_00000353-RA	18.4.1.12	NA	4.21	NA	NA	NA	3.60	66.62	3.91	8.00	3.84	3.52
FUC1	Dm_00017887-RA	50.3.2	-2.31	NA	NA	NA	NA	103.76	68.11	20.96	18.64	226.67	45.73
GALS1	Dm_00008334-RA	21.3.2.1.3	NA	1.61	NA	NA	2.28	4.77	14.64	4.81	12.52	12.78	23.34
GALS3	Dm_00017886-RA	21.3.2.1.3	NA	1.85	NA	1.16	1.44	23.14	83.57	25.53	42.49	51.83	69.32
GATA12	Dm_00011520-RA	15.5.1.3	NA	1.50	NA	NA	NA	24.48	69.39	22.89	34.15	24.52	32.95

Continued on next page

Table 20 – *Continued from previous page*

Gene	DmID	Bin	Ct.ERR vs Ct.WT	APWT vs Ct.WT	APERR vs Ct.ERR	COR.WT vs Ct.WT	COR.ERR vs Ct.ERR	Ct.WT	APWT	Ct.ERR	APERR	COR.WT	COR.ERR
GATA5	Dm_00009177-RA	15.5.1.3	NA	6.75	3.85	1.64	NA	1.96	210.31	3.26	46.99	6.06	4.77
GH9B5	Dm_00007715-RA	35.1	1.55	1.61	NA	NA	1.02	4.56	13.88	13.35	17.33	5.64	27.06
GLDH	Dm_00001298-RA	10.3.1.8	2.26	1.70	NA	2.31	NA	2.94	9.54	14.15	14.08	14.59	15.69
GLR2.1	Dm_00000700-RA	24.3.9	1.28	2.20	1.44	NA	NA	12.23	56.14	29.61	80.09	18.00	22.72
GLR2.8	Dm_00010360-RA	24.3.9	NA	3.10	NA	NA	NA	1.69	14.57	1.80	2.28	1.51	1.50
GLR3.4	Dm_00004609-RA	24.3.9	NA	-1.57	-1.32	NA	NA	113.75	38.38	149.34	59.96	94.48	115.67
GLR3.4	Dm_00011353-RA	24.3.9	NA	NA	NA	1.10	1.22	11.02	16.09	16.49	25.95	23.58	38.46
GOX1	Dm_00000331-RA	1.3.2	1.22	1.19	NA	NA	NA	3.23	7.29	7.51	9.49	3.75	6.71
GPX6	Dm_00011179-RA	10.4.2	-1.34	1.72	NA	NA	NA	34.47	112.93	13.60	18.11	39.92	11.93
GPX6	Dm_00016566-RA	10.4.2	-9.21	NA	NA	NA	NA	221.28	171.92	0.37	0.70	231.80	0.06
GRF8	Dm_00001479-RA	15.5.52.1	NA	1.61	NA	1.11	1.04	4.88	14.86	6.88	10.98	10.53	14.14
GRF9	Dm_00016844-RA	35.1	-1.03	-1.52	NA	NA	NA	53.95	18.53	26.39	26.60	36.27	23.68
HB22	Dm_00016472-RA	15.5.3.13	NA	2.94	NA	NA	NA	0.94	7.29	0.43	1.36	0.68	0.63
HERK1	Dm_00005767-RA	18.4.1.16	NA	2.10	NA	NA	NA	21.40	91.75	25.75	38.06	23.80	30.51
HERK1	Dm_00005767-RA	11.10.2.4.2	NA	2.10	NA	NA	NA	21.40	91.75	25.75	38.06	23.80	30.51
HEXO2	Dm_00007880-RA	18.1.1.7.1	NA	1.07	NA	NA	NA	10.51	22.20	16.92	16.40	11.90	14.57
HSP18.2	Dm_00009113-RA	35.1	NA	1.09	NA	NA	NA	51.32	109.19	41.85	78.61	64.77	62.77
HT1	Dm_00002595-RA	18.4.1.30	NA	1.01	NA	NA	NA	9.60	19.48	10.03	11.30	8.92	9.20
HTB1	Dm_00003386-RA	12.1.3	NA	1.12	NA	NA	NA	7.25	15.42	5.97	8.39	6.80	7.24
HTB4	Dm_00006856-RA	12.1.3	NA	1.75	NA	NA	NA	7.23	24.40	6.83	10.09	12.57	7.83
HYR1	Dm_00001100-RA	50.2.4	NA	1.44	NA	1.38	1.19	51.40	139.55	54.69	100.67	133.45	125.09
HYR1	Dm_00002224-RA	50.2.4	-1.57	-2.38	NA	NA	NA	286.90	55.36	96.92	61.55	193.40	66.18
ICE1	Dm_00000952-RA	15.5.32	NA	1.82	NA	NA	NA	24.97	88.45	24.36	32.82	27.05	19.38
ICE1	Dm_00000952-RA	26.4.3.4.1	NA	1.82	NA	NA	NA	24.97	88.45	24.36	32.82	27.05	19.38
IDD2	Dm_00001157-RA	15.5.15	NA	1.98	NA	NA	NA	27.16	107.49	42.44	57.64	32.19	44.16
IDD5	Dm_00020338-RA	15.5.15	NA	2.94	1.58	NA	NA	6.26	48.04	5.30	15.85	4.41	5.41
IQD19	Dm_00016508-RA	35.2	NA	1.54	NA	NA	NA	37.99	110.57	37.74	46.66	41.66	37.58
iqd2	Dm_00007194-RA	35.1	NA	1.83	NA	NA	NA	19.57	69.40	20.30	34.51	22.51	26.53
iqd2	Dm_00014543-RA	35.1	NA	1.25	1.10	NA	NA	20.38	48.49	31.84	68.07	23.39	24.27
IQD22	Dm_00013162-RA	35.2	1.89	3.76	1.36	1.28	NA	4.25	57.54	15.82	40.50	10.23	17.78
IRX1	Dm_00000667-RA	21.1.1.1.1	NA	-1.03	NA	NA	NA	9.57	4.67	4.92	4.31	7.05	5.63
IRX6	Dm_00017894-RA	21.1.2.2	NA	3.47	2.45	NA	1.87	0.75	8.41	0.51	2.78	0.91	1.88
IRX9	Dm_00005762-RA	21.2.2.1.3.1	-1.60	NA	NA	NA	NA	120.31	131.28	39.63	48.80	67.65	38.88
IRX9	Dm_00020340-RA	21.2.2.1.3.1	NA	NA	NA	2.21	NA	1.41	2.35	2.28	4.72	6.45	3.87
JAR1	Dm_00008505-RA	11.7.3.2	NA	4.00	1.53	NA	NA	39.35	629.31	33.42	96.74	49.82	26.48
JAZ1	Dm_00005123-RA	15.5.45	NA	4.65	3.84	3.69	4.31	55.47	1394.68	40.93	584.89	713.75	813.33
JAZ1	Dm_00005123-RA	11.7.2.1.2	NA	4.65	3.84	3.69	4.31	55.47	1394.68	40.93	584.89	713.75	813.33
JMT	Dm_00019652-RA	50.2.1	NA	1.59	NA	NA	NA	3.30	9.86	3.07	6.26	4.46	4.63
JMT	Dm_00019961-RA	50.2.1	NA	1.33	NA	NA	NA	31.43	78.62	27.77	48.61	30.49	34.56
LAC14	Dm_00017526-RA	50.1.10	NA	1.40	NA	NA	NA	3.23	8.50	3.81	6.49	4.46	5.32
LAC14	Dm_00016846-RA	50.1.10	7.58	NA	NA	NA	NA	0.03	0.07	4.95	5.49	0.30	4.93
LAC7	Dm_00009798-RA	50.1.10	NA	1.66	NA	NA	NA	9.50	30.05	15.86	28.80	13.52	14.99
LAC7	Dm_00009799-RA	50.1.10	1.59	NA	NA	1.53	NA	3.81	2.48	11.45	14.84	10.97	13.37
LAC7	Dm_00009800-RA	50.1.10	4.32	NA	NA	NA	NA	0.87	0.89	17.42	34.85	3.44	17.81
LBD37	Dm_00006932-RA	15.5.24	-1.79	3.08	2.64	2.98	2.72	26.47	224.04	7.67	47.94	209.28	50.33
LLG1	Dm_00010147-RA	11.10.2.4.3	NA	5.58	NA	NA	NA	0.34	16.20	0.22	3.03	1.58	0.85
LLG1	Dm_00001908-RA	11.10.2.4.3	NA	1.33	NA	NA	NA	27.22	68.00	36.86	50.68	31.29	37.96
LOX3	Dm_00015211-RA	11.7.1.2	NA	4.03	2.79	NA	NA	14.98	244.73	10.85	75.29	18.54	19.63
LRX2	Dm_00009341-RA	21.4.1.3.2	-2.31	NA	NA	NA	NA	0.95	0.55	0.19	0.15	0.41	0.17
LYK3	Dm_00005060-RA	18.4.1.21	NA	1.95	NA	NA	NA	3.74	14.56	4.21	5.67	5.34	6.75
LYK5	Dm_00018769-RA	26.9.1.1	NA	1.13	NA	NA	NA	17.66	38.58	18.24	27.46	19.40	16.35
LYK5	Dm_00018769-RA	18.4.1.21	NA	1.13	NA	NA	NA	17.66	38.58	18.24	27.46	19.40	16.35
MIOX1	Dm_00011008-RA	3.13.3.2.3	-1.79	2.23	NA	NA	1.04	23.06	107.99	6.66	13.31	23.24	13.69
MPK3	Dm_00006219-RA	13.4.4.1.4	NA	2.45	1.63	NA	NA	130.85	716.19	163.38	507.28	144.82	160.19
MPK3	Dm_00006219-RA	18.4.3.6	NA	2.45	1.63	NA	NA	130.85	716.19	163.38	507.28	144.82	160.19
MSL10	Dm_00009130-RA	24.3.5	1.91	NA	NA	NA	NA	0.60	0.57	2.25	1.34	0.84	2.18
MYB114	Dm_00020213-RA	15.5.2.1	NA	1.02	NA	NA	NA	9.11	18.61	8.96	10.28	7.77	10.46

Continued on next page

Table 20 – *Continued from previous page*

Gene	DmID	Bin	Ct.ERR vs Ct.WT	AP.WT vs Ct.WT	AP.ERR vs Ct.ERR	COR.WT vs Ct.WT	COR.ERR vs Ct.ERR	Ct.WT	AP.WT	Ct.ERR	AP.ERR	COR.WT	COR.ERR
MYB46	Dm_00018884-RA	15.5.2.1	NA	-1.34	NA	-1.59	NA	1.61	0.68	1.77	1.16	0.52	1.43
MYB5	Dm_00004200-RA	15.5.2.1	-1.17	-1.23	NA	NA	NA	34.59	14.90	15.38	15.19	17.95	20.00
MYB88	Dm_00016753-RA	15.5.2.1	-11.40	NA	NA	NA	NA	38.47	9.68	0.00	0.00	41.35	0.00
MYC2	Dm_00007573-RA	15.5.32	NA	2.01	2.14	3.16	4.11	1.03	4.12	0.53	2.34	9.25	9.11
NA	Dm_00000234-RA	35.1	NA	1.25	1.06	NA	1.58	10.22	24.02	7.16	14.90	18.33	21.37
NA	Dm_00000389-RA	35.1	NA	7.86	4.40	NA	NA	0.13	29.02	0.33	6.88	0.57	0.41
NA	Dm_00000418-RA	35.1	NA	3.11	1.50	1.05	1.54	15.20	131.59	12.93	36.60	31.54	37.55
NA	Dm_00000526-RA	35.2	NA	2.63	NA	NA	NA	2.26	14.02	0.68	3.29	1.67	0.75
NA	Dm_00001089-RA	24.3.15.1	-1.44	1.29	NA	NA	1.19	4.29	10.41	1.59	2.76	6.69	3.60
NA	Dm_00001167-RA	35.1	-1.26	NA	NA	NA	NA	121.66	127.03	50.64	71.08	83.62	54.88
NA	Dm_00001168-RA	35.1	-1.11	NA	1.48	NA	NA	7.14	6.96	3.30	9.20	4.47	3.40
NA	Dm_00001189-RA	35.1	1.46	3.08	1.42	NA	NA	10.72	90.35	29.49	78.77	14.75	35.77
NA	Dm_00001629-RA	35.1	NA	3.05	2.97	NA	NA	24.48	203.37	34.11	267.54	38.12	35.77
NA	Dm_00001947-RA	35.1	NA	2.16	1.74	NA	NA	1.97	8.58	1.23	4.10	1.12	1.60
NA	Dm_00003259-RA	27.2.7	NA	1.45	1.28	NA	NA	29.09	79.38	28.18	68.27	27.41	33.42
NA	Dm_00003515-RA	35.1	NA	2.12	1.29	NA	NA	11.89	51.59	21.65	52.98	13.09	20.76
NA	Dm_00003867-RA	35.1	1.01	NA	NA	NA	NA	29.83	46.20	60.20	51.02	30.02	46.65
NA	Dm_00004152-RA	35.1	NA	2.53	2.28	NA	NA	64.95	374.55	69.35	336.56	86.45	103.58
NA	Dm_00004720-RA	18.4.24.1.2.4	NA	1.67	1.15	NA	NA	19.44	61.69	26.96	59.75	19.85	27.78
NA	Dm_00009568-RA	35.1	NA	NA	1.30	NA	NA	2.27	1.88	1.73	4.26	1.81	2.82
NA	Dm_00009960-RA	35.1	NA	-1.14	NA	NA	NA	55.77	25.58	66.53	52.54	47.40	42.30
NA	Dm_00011215-RA	35.2	NA	5.71	1.45	NA	NA	0.61	32.05	4.54	12.39	2.01	6.48
NA	Dm_00011216-RA	35.1	1.60	5.24	1.83	1.52	1.14	2.04	76.53	6.17	21.90	5.75	13.48
NA	Dm_00012152-RA	35.1	NA	-1.55	NA	NA	NA	229.68	78.16	283.47	180.10	188.24	260.42
NA	Dm_00015225-RA	35.1	2.18	2.12	NA	NA	NA	11.24	48.58	50.74	62.35	14.71	34.51
NA	Dm_00015386-RA	24.3.15.1	1.20	5.22	2.74	3.13	2.61	17.38	649.24	40.01	266.93	151.75	243.73
NA	Dm_00018051-RA	35.1	NA	1.90	2.71	NA	NA	173.27	646.95	88.86	582.57	288.64	134.47
NA	Dm_00018647-RA	35.1	NA	5.80	2.04	1.15	NA	31.52	1755.74	59.15	243.37	69.81	81.17
NA	Dm_00018757-RA	24.2.9.1.4	NA	-1.26	NA	NA	NA	222.95	93.18	123.12	78.56	214.98	118.44
NA	Dm_00019071-RA	35.2	NA	1.94	1.45	2.18	1.62	12.53	48.15	17.74	48.50	56.85	54.59
NA	Dm_00000328-RA	19.2.2.8.1.4.6	NA	1.23	NA	NA	NA	46.16	108.47	39.44	74.78	61.72	48.54
NA	Dm_00000441-RA	24.2.2.15	NA	1.59	NA	NA	NA	137.11	411.90	191.74	361.64	197.17	255.63
NA	Dm_00000488-RA	18.4.1.21	NA	1.64	NA	NA	NA	9.38	29.01	13.26	24.92	11.43	13.89
NA	Dm_00001087-RA	19.2.2.1.5.3.2	NA	1.41	NA	NA	NA	24.54	65.09	32.89	63.31	27.70	40.67
NA	Dm_00001343-RA	12.1.3	NA	3.41	NA	NA	NA	0.72	7.54	0.57	0.68	0.92	1.00
NA	Dm_00002000-RA	19.2.2.1.5.3.4	NA	1.87	NA	NA	NA	45.40	166.33	45.94	89.07	47.61	50.18
NA	Dm_00002269-RA	15.5.38	NA	1.20	NA	NA	NA	1.72	3.88	1.58	1.88	1.42	2.19
NA	Dm_00002269-RA	18.4.24.2.7	NA	1.20	NA	NA	NA	1.72	3.88	1.58	1.88	1.42	2.19
NA	Dm_00002554-RA	11.10.2.4.1	NA	1.49	NA	NA	1.61	2.51	7.14	1.93	3.09	3.10	5.84
NA	Dm_00002777-RA	15.5.15	NA	1.24	NA	1.12	NA	6.70	15.84	7.37	9.91	14.53	8.33
NA	Dm_00003163-RA	24.2.2.1.7	NA	1.85	NA	NA	NA	2.75	9.86	1.76	3.17	2.80	2.20
NA	Dm_00003384-RA	15.5.15	NA	1.35	NA	NA	NA	4.85	12.37	5.41	4.85	3.94	5.35
NA	Dm_00003485-RA	15.5.15	NA	1.02	NA	NA	NA	12.94	26.36	14.72	17.41	9.67	11.42
NA	Dm_00003663-RA	19.2.2.1.5.3.3	2.07	1.77	NA	NA	NA	2.06	7.02	8.65	7.17	3.75	9.33
NA	Dm_00003955-RA	19.2.2.1.5.3.3	NA	1.52	NA	NA	NA	9.09	26.14	8.73	11.90	7.36	6.99
NA	Dm_00004377-RA	19.2.2.8.1.4.6	NA	1.19	NA	NA	NA	55.56	126.40	57.85	79.44	75.67	98.40
NA	Dm_00005904-RA	19.2.2.8.1.4.6	NA	1.39	NA	NA	NA	46.10	120.68	46.85	63.51	60.15	56.41
NA	Dm_00007038-RA	24.2.2.5	NA	1.06	NA	NA	NA	2.95	6.18	3.53	3.87	2.28	2.14
NA	Dm_00007814-RA	19.2.2.1.5.3.4	NA	1.49	NA	NA	NA	31.33	87.55	36.73	50.25	28.67	36.52
NA	Dm_00009379-RA	19.2.2.1.5.3.3	NA	2.42	NA	NA	NA	3.73	19.81	3.06	5.63	3.63	3.51
NA	Dm_00015468-RA	24.2.2.16	NA	1.29	NA	NA	NA	27.06	66.04	33.77	54.09	31.75	21.07
NA	Dm_00015541-RA	19.2.2.1.5.3.3	NA	1.28	NA	1.58	1.07	23.49	56.87	21.45	34.35	70.08	44.99
NA	Dm_00016050-RA	9.2.2.1.1.2	NA	1.92	NA	NA	NA	39.16	148.43	39.66	57.64	77.06	58.73
NA	Dm_00016050-RA	19.2.2.8.1.4.6	NA	1.92	NA	NA	NA	39.16	148.43	39.66	57.64	77.06	58.73
NA	Dm_00016319-RA	15.5.15	NA	6.61	NA	5.47	NA	0.39	38.28	2.45	4.92	17.44	6.64
NA	Dm_00018514-RA	19.2.2.8.1.1	NA	3.66	NA	NA	NA	0.98	12.35	0.41	0.94	1.60	0.43
NA	Dm_00019742-RA	15.5.15	NA	5.95	NA	NA	NA	0.31	19.14	0.98	2.90	0.24	1.35

Continued on next page

Table 20 – *Continued from previous page*

Gene	DmID	Bin	Ct.ERR vs Ct.WT	APWT vs Ct.WT	APERR vs Ct.ERR	COR.WT vs Ct.WT	COR.ERR vs Ct.ERR	Ct.WT	APWT	Ct.ERR	APERR	COR.WT	COR.ERR
NA	Dm_00020722-RA	19.2.2.1.5.3.3	NA	1.78	NA	NA	NA	33.83	116.20	45.05	86.77	49.44	44.71
NA	Dm_00003465-RA	18.4.1.12	2.99	4.42	1.53	1.89	NA	0.72	15.38	5.73	16.51	2.65	4.61
NA	Dm_00005888-RA	24.2.2.9	2.87	NA	NA	NA	NA	0.63	0.16	4.65	2.92	0.37	1.91
NA	Dm_00007893-RA	50.1.13	2.72	NA	NA	NA	NA	0.34	0.13	2.23	3.06	0.81	1.90
NA	Dm_00009633-RA	17.7.2.1.33	-2.24	-1.18	NA	NA	NA	40.36	17.95	8.51	7.05	32.95	12.26
NA	Dm_00012605-RA	50.1.13	3.07	NA	NA	NA	NA	4.90	14.04	41.17	76.48	17.62	44.40
NA	Dm_00015039-RA	50.1.10	3.34	2.79	NA	NA	NA	0.80	5.50	8.05	13.80	1.87	4.54
NA	Dm_00001597-RA	11.7.2.1.2	1.95	10.06	6.16	9.23	7.00	0.71	760.62	2.75	196.96	426.22	353.27
NA	Dm_00001597-RA	15.5.45	1.95	10.06	6.16	9.23	7.00	0.71	760.62	2.75	196.96	426.22	353.27
NA	Dm_00003954-RA	15.5.32	NA	5.28	3.09	NA	NA	6.98	271.75	5.09	43.37	7.63	7.66
NA	Dm_00016417-RA	15.5.7.1	NA	3.08	2.82	2.88	3.19	1.01	8.59	0.53	3.75	7.40	4.83
NA	Dm_00016707-RA	15.5.7.1	NA	3.35	1.70	2.30	2.39	4.72	47.95	3.90	12.68	23.19	20.30
NA	Dm_00000572-RA	35.2	NA	1.96	NA	1.31	NA	1.28	5.09	0.88	1.10	3.14	1.29
NA	Dm_00002770-RA	35.2	NA	1.08	NA	1.27	NA	4.19	9.04	7.89	9.77	10.10	5.99
NA	Dm_00006168-RA	35.2	NA	2.21	NA	NA	NA	11.80	54.85	13.15	19.26	17.90	11.64
NA	Dm_00007492-RA	35.2	NA	1.42	NA	NA	NA	3.02	8.17	5.24	2.25	2.12	2.20
NA	Dm_00007660-RA	35.2	NA	1.01	NA	NA	NA	2.93	6.04	2.13	3.62	2.58	3.99
NA	Dm_00014608-RA	35.2	NA	7.10	NA	NA	NA	0.08	10.28	0.11	0.70	0.18	0.23
NA	Dm_00018676-RA	35.2	NA	2.36	NA	NA	-4.05	5.13	26.31	10.25	2.80	6.98	0.56
NAS3	Dm_00001621-RA	25.4.3.1.1	-2.71	NA	NA	NA	NA	2.50	0.73	0.38	0.60	1.91	0.36
NGA1	Dm_00012161-RA	15.5.5.3	1.04	NA	NA	NA	NA	1.39	0.69	2.85	1.64	1.17	2.08
NGA1	Dm_00012404-RA	15.5.5.3	NA	1.99	NA	1.52	1.88	4.12	16.43	5.46	7.36	11.86	20.11
NIP1;2	Dm_00012214-RA	35.1	1.39	1.29	NA	1.52	NA	97.85	239.62	257.17	300.78	281.00	504.62
NPC2	Dm_00010906-RA	5.7.2.3.1	-6.95	NA	NA	NA	NA	1.96	3.70	0.02	0.04	2.94	0.03
NPG1	Dm_00019174-RA	35.1	1.41	NA	NA	NA	NA	0.46	0.85	1.23	1.79	0.97	1.26
NRT1:2	Dm_00019284-RA	24.2.2.9	NA	1.22	NA	NA	NA	10.26	23.91	5.92	6.26	18.00	11.67
NTT1	Dm_00018629-RA	24.2.2.14	NA	1.23	NA	NA	NA	23.34	54.66	33.67	59.15	46.31	37.78
OFP1	Dm_00000032-RA	15.5.37	NA	NA	NA	1.21	1.34	0.91	1.76	1.01	1.16	2.05	2.55
OFP1	Dm_00001581-RA	15.5.37	NA	1.57	NA	NA	NA	3.69	11.07	4.88	7.11	6.36	6.96
OMT1	Dm_00013653-RA	50.2.1	NA	NA	NA	NA	2.45	3.79	4.46	0.77	2.69	5.94	4.16
OMT1	Dm_00015011-RA	50.2.1	1.70	NA	NA	3.14	NA	7.42	15.41	24.15	32.57	65.41	16.06
OMT1	Dm_00020937-RA	50.2.1	-6.92	-3.27	NA	NA	NA	37.60	3.89	0.31	0.59	53.92	0.43
OMT1	Dm_00004560-RA	50.2.1	NA	NA	NA	3.25	NA	0.70	0.57	0.43	0.41	6.64	0.61
OMT1	Dm_00015273-RA	50.2.1	3.55	3.99	NA	NA	-1.89	3.05	48.48	35.67	41.62	6.05	9.64
OMT1	Dm_00011414-RA	50.2.1	-10.86	-5.41	NA	NA	NA	42.29	0.99	0.02	0.05	65.32	0.04
OMT1	Dm_00014254-RA	50.2.1	5.08	5.43	NA	NA	NA	0.17	7.55	5.88	9.29	0.74	1.92
OPR3	Dm_00019941-RA	50.1.3	NA	1.69	2.10	NA	NA	39.63	127.41	23.84	102.37	77.67	33.33
OPR3	Dm_00013518-RA	50.1.3	-1.62	NA	NA	NA	NA	8.80	9.91	2.86	2.27	6.72	2.97
OPT6	Dm_00003682-RA	24.2.10.2	1.71	1.34	NA	NA	NA	5.05	12.75	16.47	20.91	13.56	18.22
ORP3C	Dm_00003746-RA	5.8.1.1	NA	1.03	NA	NA	NA	108.19	221.73	108.70	185.00	110.64	102.31
OSCA1.2	Dm_00001755-RA	24.3.7	NA	1.68	NA	NA	NA	4.09	13.15	4.03	7.20	4.63	5.44
OSM34	Dm_00018459-RA	35.1	5.71	2.34	NA	2.04	NA	12.51	63.18	653.23	775.68	51.38	556.73
PAP1	Dm_00002987-RA	11.2.2.1.2	NA	1.62	NA	NA	NA	39.70	121.98	46.85	69.95	48.81	86.69
PAT1	Dm_00004119-RA	15.5.12	NA	2.61	1.44	1.83	NA	0.93	5.74	0.62	1.67	3.30	0.68
PAT1	Dm_00018068-RA	15.5.12	NA	3.60	2.18	NA	NA	14.23	173.05	16.99	77.23	25.23	32.89
PBP1	Dm_00009931-RA	35.1	NA	5.30	2.15	NA	NA	1.19	46.10	4.22	18.74	2.15	6.02
PDE149	Dm_00014784-RA	1.1.1.3.19	NA	1.18	NA	NA	NA	21.74	49.21	22.07	29.35	18.04	19.27
PGIP1	Dm_00012017-RA	26.8.3.4	NA	2.06	1.13	1.98	1.51	10.92	45.74	7.85	17.21	43.16	22.36
PGIP1	Dm_00017241-RA	26.8.3.4	NA	5.74	2.45	NA	2.05	6.59	352.96	12.73	69.77	16.64	52.54
PGIP1	Dm_00010364-RA	26.8.3.4	1.96	4.38	NA	NA	-1.52	10.34	214.88	40.22	73.98	25.00	14.00
PGIP1	Dm_00008634-RA	26.8.3.4	NA	NA	NA	1.28	NA	34.54	59.32	51.31	44.40	84.14	40.60
PGIP1	Dm_00008636-RA	26.8.3.4	NA	1.74	NA	NA	NA	15.21	50.94	20.15	46.72	27.05	15.59
PGIP1	Dm_00013133-RA	26.8.3.4	NA	2.77	NA	1.80	1.19	7.74	52.78	7.61	8.92	26.90	17.39
PIP5K4	Dm_00001283-RA	27.5.2.4	9.38	NA	NA	NA	NA	0.00	0.12	1.42	1.28	0.26	1.51
PIP5K4	Dm_00003119-RA	27.5.2.4	2.74	NA	NA	NA	NA	0.13	0.01	0.89	0.86	0.05	0.58
PLP6	Dm_00005025-RA	5.7.2.2.4	NA	1.21	NA	NA	1.33	2.57	5.88	2.73	5.14	2.33	6.88
PLP9	Dm_00020737-RA	5.7.2.2.4	NA	1.99	NA	NA	NA	0.81	3.24	0.49	1.34	1.04	1.41

Continued on next page

Table 20 – *Continued from previous page*

Gene	DmID	Bin	Ct.ERR vs Ct.WT	AP.WT vs Ct.WT	AP.ERR vs Ct.ERR	COR.WT vs Ct.WT	COR.ERR vs Ct.ERR	Ct.WT	AP.WT	Ct.ERR	AP.ERR	COR.WT	COR.ERR
PMT5	Dm_00015023-RA	24.2.2.1.7	NA	2.41	NA	1.53	NA	24.53	130.37	42.33	81.63	70.74	79.89
PMT5	Dm_00015738-RA	24.2.2.1.7	NA	1.89	NA	NA	NA	294.81	1095.58	300.14	551.87	537.09	350.03
PMT5	Dm_00001746-RA	24.2.2.1.7	NA	2.10	1.10	1.07	NA	48.85	209.66	91.56	196.11	102.55	95.95
PP2-A13	Dm_00018803-RA	19.2.2.8.1.4.6	NA	2.17	NA	1.47	2.25	28.43	128.06	23.40	46.50	78.85	111.38
PP2CG1	Dm_00016129-RA	18.4.24.2.7	NA	1.08	NA	NA	NA	33.11	69.96	31.23	45.27	34.18	45.45
PP2CG1	Dm_00016129-RA	15.5.38	NA	1.08	NA	NA	NA	33.11	69.96	31.23	45.27	34.18	45.45
PP2CG1	Dm_00020436-RA	18.4.24.2.7	NA	1.32	NA	NA	NA	61.62	153.92	55.66	72.76	63.01	66.49
PP2CG1	Dm_00020436-RA	15.5.38	NA	1.32	NA	NA	NA	61.62	153.92	55.66	72.76	63.01	66.49
PRB1	Dm_00019935-RA	35.1	NA	8.36	NA	NA	NA	0.08	24.98	0.17	0.93	1.94	2.60
PRP4	Dm_00019266-RA	35.1	-2.87	NA	NA	NA	4.14	25.32	78.15	3.46	13.86	16.57	61.09
PRX52	Dm_00009436-RA	35.1	NA	NA	NA	-3.68	NA	10.01	8.72	30.10	37.47	0.77	16.11
PRX52	Dm_00017284-RA	35.1	NA	NA	NA	-3.67	NA	4.10	3.11	8.84	7.82	0.32	3.94
PRX52	Dm_00016579-RA	35.1	NA	NA	NA	-1.56	NA	29.50	21.39	55.06	32.45	9.93	24.32
PRX52	Dm_00001327-RA	35.1	1.36	2.64	NA	NA	NA	4.53	28.31	11.62	17.78	6.82	9.48
PRX52	Dm_00000040-RA	35.1	-1.63	NA	NA	NA	NA	12.17	22.58	3.94	6.21	19.49	2.79
PRX52	Dm_00020250-RA	35.1	NA	NA	NA	NA	1.04	7.79	11.31	8.96	16.89	13.94	18.42
PS1	Dm_00016063-RA	13.3.5.6.2	-2.39	NA	NA	NA	NA	0.70	0.83	0.13	0.26	0.59	0.09
PTAC3	Dm_00006706-RA	15.6.1.2.2.1	-1.51	NA	NA	NA	NA	20.29	18.78	7.13	6.98	23.42	8.83
PTR1	Dm_00020039-RA	24.2.2.9	NA	8.92	NA	NA	8.50	0.02	7.98	0.00	0.30	0.65	0.99
PTR5	Dm_00018508-RA	24.2.2.9	NA	1.82	NA	NA	NA	29.46	104.06	31.11	58.91	37.64	38.86
PUB26	Dm_00004686-RA	35.1	NA	1.84	NA	NA	NA	27.49	98.52	40.46	63.00	41.02	51.03
PYR6	Dm_00013232-RA	6.2.3.1	-2.84	NA	NA	NA	NA	609.17	480.30	85.36	76.89	574.17	82.79
RALFL33	Dm_00000607-RA	11.10.2.4.1	NA	1.94	NA	NA	NA	3.20	12.18	2.78	6.08	1.69	2.73
RALFL33	Dm_00000608-RA	11.10.2.4.1	NA	2.06	1.28	NA	NA	288.12	1203.17	253.28	615.87	430.69	319.86
RAP2.11	Dm_00018650-RA	15.5.7.1	NA	5.89	4.24	NA	NA	0.17	10.37	0.34	6.33	0.16	0.40
RAP2.11	Dm_00018650-RA	26.9.1.7	NA	5.89	4.24	NA	NA	0.17	10.37	0.34	6.33	0.16	0.40
RAV1	Dm_00017712-RA	15.5.7.5	NA	2.00	NA	NA	NA	2.68	10.65	3.99	7.86	2.11	2.12
RAV1	Dm_00017712-RA	15.5.5.3	NA	2.00	NA	NA	NA	2.68	10.65	3.99	7.86	2.11	2.12
RBOHB	Dm_00000603-RA	10.1.1	NA	3.17	1.75	NA	NA	5.23	47.00	9.88	33.19	6.60	9.47
RGIL6	Dm_00008368-RA	21.3.5.2	-2.31	-2.93	-1.30	NA	NA	197.52	25.79	39.92	16.16	243.49	52.63
RLK	Dm_00002421-RA	18.4.1.3	NA	-1.09	NA	NA	NA	8.48	3.92	4.48	3.08	6.47	4.87
ROT3	Dm_00011590-RA	11.3.1.4	-1.30	NA	NA	NA	NA	14.42	13.13	5.85	5.57	14.67	6.68
RRTF1	Dm_00002642-RA	15.5.7.1	5.42	10.95	1.73	NA	-1.30	0.06	116.60	2.52	8.38	0.80	1.00
SAG12	Dm_00021072-RA	50.3.4	NA	8.94	NA	5.66	8.66	0.07	38.60	0.01	0.59	3.96	3.65
SAG12	Dm_00000680-RA	19.4.1.1	NA	NA	NA	5.73	NA	0.09	0.21	0.45	0.99	5.03	3.38
SAG12	Dm_00013767-RA	50.3.4	NA	NA	NA	8.60	NA	0.22	0.26	0.17	0.35	85.13	0.17
SAG12	Dm_00017323-RA	50.3.4	NA	11.57	8.34	8.43	10.23	0.06	190.96	0.02	5.43	21.76	20.16
SAG29	Dm_00000969-RA	24.2.6.1	2.03	1.74	NA	1.47	NA	8.19	27.51	33.42	24.46	22.76	43.73
SAH7	Dm_00008745-RA	35.1	NA	1.32	NA	NA	NA	515.47	1283.82	546.63	760.54	604.15	909.73
SBH1	Dm_00007811-RA	5.4.3	1.26	1.05	NA	NA	NA	25.94	53.32	62.20	86.26	43.23	48.59
SCL3	Dm_00009748-RA	15.5.12	NA	2.21	1.46	2.46	1.57	16.36	75.54	30.16	83.19	90.24	89.46
SCL3	Dm_00018549-RA	15.5.12	NA	1.53	NA	NA	NA	32.47	93.49	42.73	51.80	36.06	47.43
SCR	Dm_00004980-RA	15.5.12	NA	2.81	2.08	2.33	2.29	6.60	46.30	6.11	25.85	33.20	29.90
SCR	Dm_00004980-RA	26.3.1.5	NA	2.81	2.08	2.33	2.29	6.60	46.30	6.11	25.85	33.20	29.90
SIP3	Dm_00017137-RA	18.4.5.3	NA	3.00	2.70	1.98	2.75	102.66	824.01	109.52	709.61	405.66	734.43
SIP3	Dm_00018077-RA	18.4.5.3	NA	5.46	3.07	2.36	3.23	25.16	1103.97	15.63	130.88	128.87	146.50
sks5	Dm_00001251-RA	50.1.10	NA	1.50	NA	NA	1.88	43.76	123.83	66.37	122.08	52.08	244.86
SLT1	Dm_00019545-RA	35.2	NA	1.21	NA	1.27	1.07	51.77	120.10	48.63	88.65	125.17	102.17
SOS3	Dm_00000455-RA	26.6.1.1.1	NA	-1.08	NA	NA	NA	12.40	5.83	8.96	9.51	9.58	7.80
SR1	Dm_00001579-RA	18.4.5.3	NA	2.52	2.47	2.28	2.42	14.98	85.99	14.89	82.39	72.71	79.53
SR45	Dm_00009199-RA	17.3.1.2.1	-11.89	NA	NA	NA	NA	17.76	20.34	0.00	0.05	23.93	0.02
SRG1	Dm_00015296-RA	50.1.13	NA	2.35	NA	NA	NA	34.54	176.10	55.30	78.86	40.28	46.95
SRT1	Dm_00002675-RA	12.3.2.3	NA	1.25	NA	NA	NA	5.56	13.13	6.77	10.53	4.42	6.94
STOMAGEN	Dm_00019244-RA	11.10.2.3.1	-1.16	1.89	NA	NA	NA	30.75	114.32	13.75	18.53	60.16	30.64
STOP1	Dm_00016062-RA	15.5.15	NA	2.35	1.08	NA	NA	62.98	321.00	56.17	118.78	58.36	47.24
STP7	Dm_00011693-RA	24.2.2.1.6	NA	1.97	NA	NA	NA	28.32	111.01	36.33	72.19	43.49	47.45
STZ	Dm_00002355-RA	15.5.15	NA	2.68	NA	NA	NA	35.99	230.48	44.11	71.53	68.48	63.71

Continued on next page

Table 20 – *Continued from previous page*

Gene	DmID	Bin	Ct.ERR vs Ct.WT	APWT vs Ct.WT	APERR vs Ct.ERR	COR.WT vs Ct.WT	COR.ERR vs Ct.ERR	Ct.WT	APWT	Ct.ERR	APERR	COR.WT	COR.ERR
STZ	Dm_00009443-RA	15.5.15	NA	3.39	1.17	2.12	1.92	2.82	29.49	3.68	8.26	12.25	13.85
STZ	Dm_00001350-RA	15.5.15	2.15	5.64	1.69	2.44	NA	6.86	341.06	30.40	98.01	37.22	51.41
SUC2	Dm_00007651-RA	24.2.2.4	NA	5.39	NA	NA	NA	0.05	2.31	0.02	0.50	0.03	0.07
SUC2	Dm_00012178-RA	24.2.2.4	NA	5.14	NA	NA	NA	0.06	2.04	0.05	0.39	0.05	0.04
SWN	Dm_00006434-RA	12.3.3.3	-3.45	NA	NA	NA	NA	39.39	37.05	3.61	3.27	31.86	3.34
SYTA	Dm_00006459-RA	5.8.1.2	NA	1.91	NA	NA	NA	1.55	5.73	1.05	1.94	0.96	1.37
SYTC	Dm_00009767-RA	35.1	NA	-1.02	NA	NA	NA	12.71	6.24	8.53	5.11	8.59	9.75
TBL27	Dm_00005821-RA	21.2.1.2.2	-9.14	-2.30	NA	NA	NA	1.71	0.34	0.00	0.00	1.17	0.00
TCH2	Dm_00020642-RA	35.1	NA	3.03	2.91	NA	NA	58.81	480.35	55.29	415.81	113.71	99.91
TCH4	Dm_00002331-RA	50.2.4	NA	2.47	1.73	NA	NA	26.83	149.15	27.56	91.72	30.91	54.76
TDF1	Dm_00019455-RA	15.5.2.1	-7.01	NA	NA	NA	NA	6.05	1.88	0.05	0.09	1.33	0.00
TEM1	Dm_00008858-RA	15.5.5.3	NA	2.53	NA	NA	NA	1.53	8.86	0.50	1.00	2.03	1.19
TEM1	Dm_00008858-RA	15.5.7.5	NA	2.53	NA	NA	NA	1.53	8.86	0.50	1.00	2.03	1.19
THE1	Dm_00021083-RA	18.4.1.16	NA	5.64	1.69	NA	1.36	0.36	17.81	0.68	2.19	0.14	1.74
THE1	Dm_00018125-RA	11.10.2.4.2	NA	2.39	NA	NA	NA	2.50	13.08	3.86	4.15	2.11	4.29
THE1	Dm_00021083-RA	11.10.2.4.2	NA	5.64	1.69	NA	1.36	0.36	17.81	0.68	2.19	0.14	1.74
THE1	Dm_00018125-RA	18.4.1.16	NA	2.39	NA	NA	NA	2.50	13.08	3.86	4.15	2.11	4.29
TMKL1	Dm_00000931-RA	18.4.1.3	-2.71	NA	NA	NA	NA	1.49	0.83	0.23	0.34	1.10	0.42
TMT2	Dm_00002276-RA	24.2.2.1.4	1.30	1.59	NA	NA	NA	3.03	9.08	7.49	10.76	1.98	5.70
TPPJ	Dm_00009919-RA	3.3.2	2.97	2.81	NA	2.70	NA	0.25	1.71	1.93	1.67	1.59	1.05
TPPJ	Dm_00014335-RA	3.3.2	1.31	1.38	NA	NA	NA	6.32	16.33	15.66	23.24	7.31	15.97
TPS11	Dm_00004433-RA	50.2.4	NA	2.66	2.05	1.32	NA	3.89	24.61	3.78	15.67	9.68	5.32
TPS7	Dm_00001335-RA	50.2.4	NA	6.27	4.16	4.14	4.46	1.46	113.11	1.94	34.71	25.79	42.54
TPS7	Dm_00005597-RA	50.2.4	NA	6.85	4.81	1.59	1.86	0.47	54.86	0.69	19.21	1.45	2.48
TPS9	Dm_00010742-RA	50.2.4	NA	2.14	1.40	1.38	NA	16.05	70.61	22.25	58.73	41.80	42.22
TRIP-1	Dm_00016365-RA	35.1	-1.31	1.11	NA	NA	NA	129.52	279.14	52.32	73.35	182.82	45.04
TRX1	Dm_00011727-RA	18.7.2	4.30	4.16	NA	NA	NA	6.50	115.85	127.75	121.06	13.84	123.93
TRX1	Dm_00011727-RA	10.6.1	4.30	4.16	NA	NA	NA	6.50	115.85	127.75	121.06	13.84	123.93
TSD2	Dm_00011202-RA	35.1	1.02	1.83	NA	NA	NA	38.06	135.50	77.04	126.33	22.79	82.61
TT10	Dm_00010771-RA	50.1.10	3.13	NA	NA	NA	NA	0.33	0.44	2.88	1.19	0.14	2.71
TT4	Dm_00000436-RA	9.2.2.1.1.1	NA	1.43	NA	NA	1.92	0.60	1.64	0.38	1.20	1.40	1.43
UFO	Dm_00010490-RA	19.2.2.8.1.4.3	NA	9.06	NA	NA	NA	0.00	1.86	0.03	0.04	0.00	0.03
UGT76E11	Dm_00002935-RA	50.2.4	NA	2.71	1.41	1.90	1.57	14.85	96.93	15.05	40.10	55.29	44.62
UGT78D2	Dm_00019388-RA	50.2.4	-1.46	3.02	1.81	1.55	2.85	4.41	35.67	1.60	5.60	12.98	11.55
VAMP724	Dm_00005459-RA	22.7.5.1	NA	1.39	NA	NA	NA	3.50	9.27	5.57	9.26	2.45	5.62
WAVE2	Dm_00002303-RA	20.2.2.2.4	NA	1.83	NA	NA	NA	3.20	11.39	4.87	6.63	2.59	6.15
WRKY33	Dm_00000052-RA	26.8.3.3.1	2.36	4.44	1.29	1.46	NA	0.23	4.90	1.17	2.85	0.63	1.21
WRKY33	Dm_00000052-RA	15.5.22	2.36	4.44	1.29	1.46	NA	0.23	4.90	1.17	2.85	0.63	1.21
WRKY41	Dm_00015827-RA	15.5.22	3.50	7.02	2.81	2.25	NA	1.11	142.69	12.47	87.35	5.20	15.13
WRKY50	Dm_00013547-RA	15.5.22	1.93	1.71	NA	NA	NA	6.22	20.31	23.59	40.30	11.01	20.44
WRKY7	Dm_00002377-RA	15.5.22	NA	1.44	NA	NA	NA	75.33	204.39	58.82	116.00	55.78	83.77
XTH15	Dm_00002549-RA	50.2.4	6.70	11.21	3.38	8.04	NA	0.02	46.91	2.07	21.50	5.21	12.15
XTH15	Dm_00011577-RA	50.2.4	NA	NA	NA	7.22	NA	0.02	1.50	0.03	0.59	2.94	0.71
XTH2	Dm_00018539-RA	50.2.4	NA	3.22	1.68	1.69	NA	9.94	92.91	19.47	62.19	32.06	43.83
XTH25	Dm_00001319-RA	50.2.4	2.25	10.52	4.65	3.68	NA	1.56	2300.55	7.43	187.11	19.99	14.73
XTH26	Dm_00005775-RA	50.2.4	NA	4.06	NA	NA	NA	0.25	4.23	0.15	0.20	0.23	0.09
XTH33	Dm_00009369-RA	50.2.4	NA	1.32	NA	NA	NA	17.78	44.31	18.93	21.75	12.33	21.80
XTH6	Dm_00013957-RA	50.2.4	-4.26	-2.17	-1.50	NA	NA	3949.82	875.83	205.95	72.94	5042.06	292.16
XTH8	Dm_00005513-RA	50.2.4	NA	1.80	1.04	NA	1.74	14.50	50.58	11.82	24.37	8.64	39.40
XTR6	Dm_00004862-RA	50.2.4	NA	3.99	2.60	NA	2.79	103.93	1646.67	131.72	797.20	303.42	911.11
XTR6	Dm_00000624-RA	50.2.4	NA	10.19	4.30	3.08	NA	0.45	518.59	1.50	29.33	3.77	1.64
XTR6	Dm_00000758-RA	50.2.4	NA	1.64	NA	-1.02	NA	8.68	27.14	15.33	13.48	4.26	14.14
XYL1	Dm_00006740-RA	21.2.1.2.5	-1.05	NA	NA	NA	1.53	35.79	41.43	17.27	27.11	63.44	49.77
YUC10	Dm_00015384-RA	11.2.1.1.2	NA	1.73	NA	NA	NA	2.42	8.16	2.84	3.31	4.46	2.84
YUC3	Dm_00006573-RA	11.2.1.1.2	NA	2.45	NA	NA	NA	0.65	3.48	0.53	1.63	1.15	1.34
YUC4	Dm_00015597-RA	11.2.1.1.2	NA	2.52	NA	NA	NA	4.79	27.51	7.53	7.29	4.50	6.44
YUC5	Dm_00000941-RA	11.2.1.1.2	-9.36	4.36	9.72	NA	NA	4.76	97.71	0.01	6.14	4.39	0.00

Continued on next page

Table 20 – *Continued from previous page*

Gene	DmID	Bin	Ct.ERR vs Ct.WT	AP.WT vs Ct.WT	AP.ERR vs Ct.ERR	COR.WT vs Ct.WT	COR.ERR vs Ct.ERR	Ct.WT	AP.WT	Ct.ERR	AP.ERR	COR.WT	COR.ERR
YUC5	Dm_00004943-RA	11.2.1.1.2	NA	2.41	1.05	NA	NA	9.46	50.59	7.38	15.24	12.09	9.55
YUC7	Dm_00014743-RA	11.2.1.1.2	NA	2.75	NA	NA	NA	0.48	3.20	0.49	1.53	1.68	1.15
ZAT6	Dm_00018833-RA	15.5.15	NA	4.92	2.24	3.81	4.40	0.94	28.54	0.61	2.89	13.25	12.82
ZAT7	Dm_00004769-RA	15.5.15	NA	4.36	NA	NA	NA	3.33	68.32	9.68	20.08	5.07	8.34
ZEU1	Dm_00014908-RA	6.3.2.3	-7.44	NA	NA	NA	NA	8.23	8.89	0.05	0.04	5.97	0.03
ZFP4	Dm_00000374-RA	15.5.15	NA	1.39	NA	1.86	1.57	4.64	12.24	7.57	10.57	16.93	22.47
ZIP2	Dm_00009891-RA	24.2.11.1	-2.25	-3.45	NA	NA	NA	1.81	0.19	0.38	0.40	3.35	0.67
ZIP7	Dm_00017331-RA	24.2.11.1	-2.13	2.82	2.74	1.70	NA	3.63	25.66	0.83	5.55	11.78	1.34

Publication List

Sönke Scherzer, Shouguang Huang, Anda Iosip, Ines Fuchs, Ken Yokawa, Khaled AS AL-Rasheid, Manfred Heckmann, and Rainer Hedrich. **Ether anesthetics obstructs touch-induced trigger hair calcium-electrical signals preventing excitation of the Venus flytrap**. *Scientific Reports*, 12(1):1–10, 2022.

Anda L Iosip, Jennifer Böhm, Sönke Scherzer, Khaled AS Al-Rasheid, Ingo Dreyer, Jörg Schultz, Dirk Becker, Ines Kreuzer, and Rainer Hedrich. **The Venus flytrap trigger hair-specific potassium channel KDM1 can re-establish the K^+ gradient required for hapto-electric signaling**. *PLoS Biology*, 18(12):e3000964, 2020.

Gergo Palfalvi, Thomas Hackl, Niklas Terhoeven, Tomoko F Shibata, Tomoaki Nishiyama, Markus Ankenbrand, Dirk Becker, Frank Förster, Matthias Freund, Anda Iosip, Ines Kreuzer, Franziska Saul, Chiharu Kamida, Kenji Fukushima, Shuji Shigenobu, Yosuke Tamada, Lubomir Adamec, Yoshikazu Hoshi, Kunihiko Ueda, Traud Winkelmann, Jörg Fuchs, Ingo Schubert, Rainer Schwacke, Khaled Al-Rasheid, Jörg Schultz, Mitsuyasu Hasebe, Rainer Hedrich. **Genomes of the Venus flytrap and close relatives unveil the roots of plant carnivory**. *Current Biology*, 30(12):23122320, 2020.

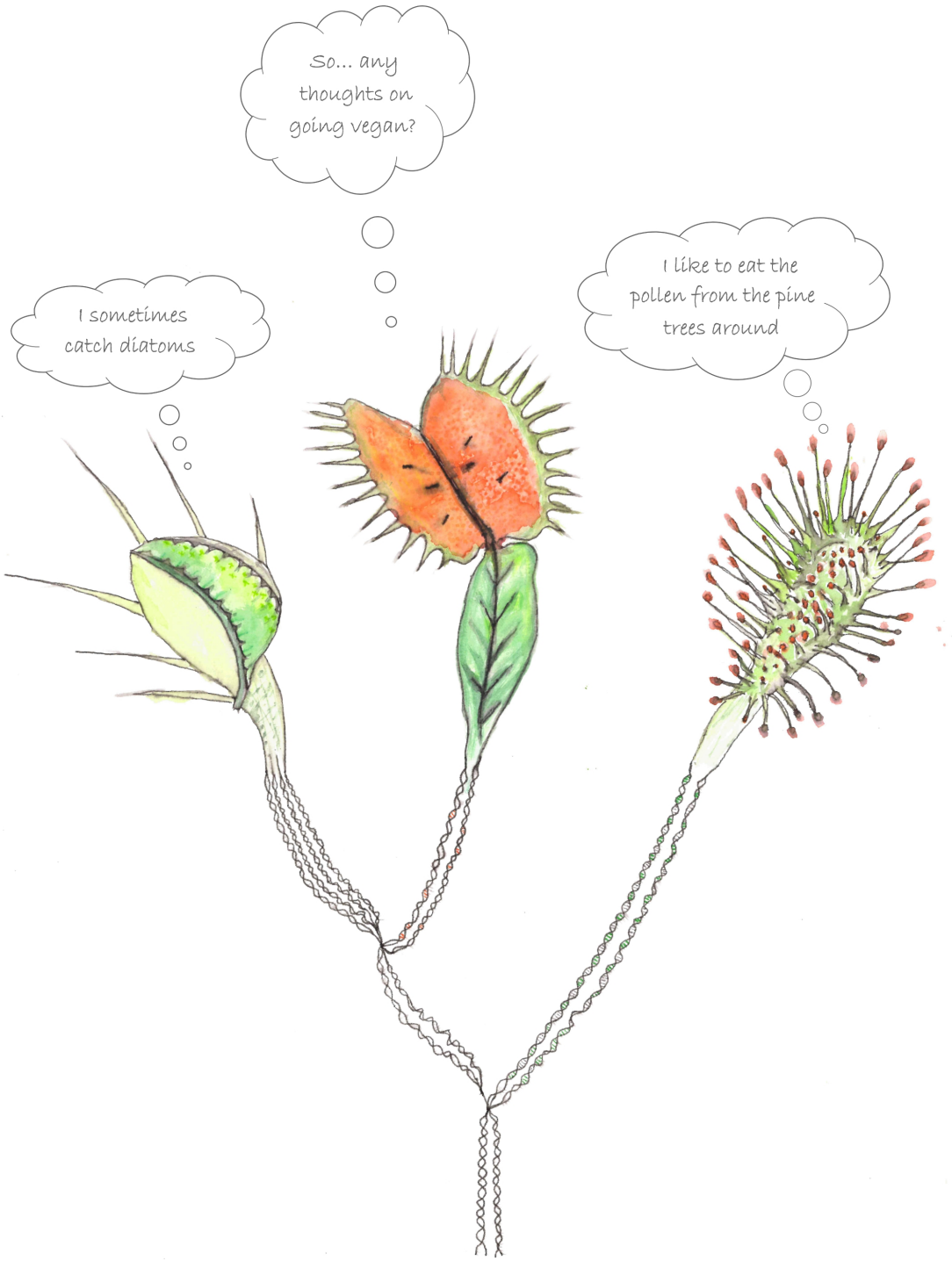
So... any thoughts on going vegan?
I sometimes catch diatoms
I like to eat the pollen from the pine trees around